The Preferred Retinal Locus in Macular Degeneration: Relating Structure and Function

By

Arun Kumar Krishnan, B.S. Optom.

DISSERTATION

In partial satisfaction of the requirements for the degree of

DOCTOR OF PHILOSOPHY

in

PHYSIOLOGICAL OPTICS

Presented to the Graduate Faculty of the

College of Optometry
University of Houston

May 2016

Approved:

_____
Harold E. Bedell, Ph.D. (Chair)

_____
Ronald S. Harwerth, O.D., Ph.D.

_____
Scott B. Stevenson, Ph.D.

_____
Nimesh B. Patel, O.D., Ph.D.

_____
Susana T.L. Chung, O.D., Ph.D.

Dedication

To all the visually challenged role models across the globe who inspire and motivate many researchers, clinicians and humans like me

Acknowledgments

First and foremost, my sincere and heartiest thanks to my mentor, Harold E Bedell for all the guidance, support, motivation, time and help since the day I met him. My PhD journey was guided in the right course chiefly by him and if not for him, my PhD life would have been a void. I would also extend my thanks to Laura J Frishman for her sustained guidance and support during the entire length of my graduate studies at University of Houston. I would also like to thank my other committee members, Ronald S Harwerth, Scott B Stevenson, Nimesh B Patel, and Susana T.L. Chung for their invaluable inputs to my dissertation study, timely advice, guidance and encouragement. I would like to thank for all the help and support from Hope M Queener, Julia S Benoit and Joshua D Pratt at the University of Houston, College of Optometry (UHCO). A special mention to all the staff at the UHCO-library and the audio-visual department for their support and willingness to help when needed.

The study wouldn't have been possible without the constant support and assistance from the optometrists and personnel at the Center for sight enhancement at the UHCO. Specifically, my sincere gratitude to Drs. Swati Modi, Nicole Hooper, Jenifer Tasca, Ana Perez, Thien Tran, Lisa Kamino and all the training student interns. To all my dedicated and passionate subjects, those with central vision loss and those with normal vision; I wish to express my heartfelt thanks.

Finally, I would also like to acknowledge the grant support by the core grant P30 EY07551 (UHCO) and other grants including the UHCO-SVGR, Minnie-Flaura Turner

fund for visually impaired research, Fight-for Sight summer student fellowship, AAO-ARVO travel fellowship and the ARVO publication grant.

I wish to recognize all my previous teachers and mentors who have inspired me at various stages of my life. If not for my alma-maters ‘Vivekananda Vidyalaya’ and ‘Elite School of Optometry’, I would have never made it to the graduate program in vision science. Thanks to ‘Sankara Nethralaya’ and family for giving me a good platform to hone my clinical skills. A special mention to all the alumnus of Elite School who have inspired and continue to inspire many students like me to pursue the path of research.

I am very grateful to my family and relatives, especially my parents and my sister, and I can’t imagine a day in my life without them. Very lucky to have friends (both here and back home) and peers who have motivated, inspired and supported me throughout my life and career. Houston has been my second home and has given me several acquaintances and friends, some of whom are the reason why I always felt like in home, though away from home. Thanks to my extended family comprising of cricket, badminton, photography, hiking and tennis buddies, room-mates and many others who gave me another world to live outside the academic walls.

I surrender to the omnipresent for bestowing this life and the opportunity to serve the humanity.

The Preferred Retinal Locus in Macular Degeneration:

Relating Structure and Function

By

Arun Kumar Krishnan, B.S. Optom.

DISSERTATION

In partial satisfaction of the requirements for the degree of

DOCTOR OF PHILOSOPHY

in

PHYSIOLOGICAL OPTICS

Presented to the Graduate Faculty of the

College of Optometry
University of Houston

May 2016

General Abstract

Purpose: Central field loss (CFL) that ensues from macular degeneration can impact many activities of daily living, including reading, in both younger (as in Stargardt disease, STGD) and older (age-related macular degeneration, AMD) subjects. Subjects with CFL typically choose a non-central retinal location, called the preferred retinal locus (PRL) for fixation. This dissertation aims to understand and relate functional and structural changes within the PRL.

Methods: Preliminary studies determined the effectiveness of the MP-1 microperimeter (a) to compensate for excessively unstable fixational eye movements (FEMs), such as occur in subjects with CFL, and (b) to accurately register the retinal test locations on baseline and subsequent automated follow-up testing. Subsequently, the following functional measures were obtained for 29 subjects with bilateral CFL: (a) reading performance using hand-held MNRead charts and LCD-displayed MP1 Read charts, (b) contrast-detection thresholds using the Freiburg acuity test, (c) fixation stability on 3-letter words, measured as bivariate contour ellipse areas (BCEAs) with the MP-1, (d) sensitivity in the central visual field determined with a standard 10-2 threshold grid, and (e) fine-grained sensitivity within the word-fixation PRL for supra-threshold 13x13 arc min spots. Spectral-domain optical coherence tomography (SD-OCT) was used to assess structural characteristics of the PRL, specifically, thickness ratios for the retinal pigment epithelium - Bruch's membrane complex (RPE-BM), the photoreceptor and outer nuclear layer (PL), and the total retina layers (TRL) between PRL locations where test spots were and were

not consistently detected. Finally, 8 younger (< 35 years) and 8 older (>50 years) naive subjects with normal vision read high and low contrast sentences presented one word at a time at the fovea and 5 and 10° in the inferior field. Random 13x13 arc min blocks corresponding to 0-78% of the text area were set to the background luminance to simulate retinal micro-scotomas (MSs) and a staircase algorithm estimated the threshold reading rate.

Results: The MP-1 compensated ~90% of the experimentally induced increase in FEMs and the average registration error was ~8 arc min. The maximum reading speed of subjects with CFL correlated poorly with contrast thresholds, BCEA, PRL eccentricity, median sensitivity around the PRL and all retinal thickness ratios. Twenty-two of 29 subjects with CFL (AMD: 8/10 subjects; STGD: 10/12 subjects) exhibited one or more MSs, defined as local regions of insensitivity for supra-threshold targets within the PRL. Although the average percentage of MSs was similar in the cohorts with AMD (25.4%) and STGD (20.3%), reading speed was significantly faster in STGD than AMD subjects. Average thickness ratios for RPE-BM, PL and TRL were 0.97, 0.84 and 0.86 respectively in the AMD cohort and 0.97, 0.77 and 0.89 respectively in the STGD cohort. Only TRL in subjects with AMD differed significantly from 1. In normally-sighted subjects, log reading rate decreased significantly with decreasing contrast and increasing age, eccentricity, and density of element-deletions. For a given eccentricity and contrast, a higher density of element-deletions maximally affected the older subjects.

Conclusion: The compensation of the MP-1 for excessive FEMs and the registration between retinal test locations during baseline and follow-up testing are sufficient to assess

functional changes within local retinal regions in subjects with CFL. MSs exist within the PRL of a high proportion of subjects with CFL, but are not strongly associated with structural changes determined using SD-OCT. Based on a simulation in normally-sighted subjects, we expect impact of MSs on reading to be greater for older than younger subjects with CFL.

Table of Contents

List of Figures

List of Tables

1. CHAPTER I: General Introduction

Contributing Author:

Harold Bedell, PhD

1.1 Introduction

Humans like other living creatures are largely reliant on their eyesight to perform many daily activities. Starting from grooming, cooking, walking or driving to reading, writing, working on personal displays, watching or playing a sport, enjoying nature and the diversity of flora and fauna, it is a real challenge to perform these tasks without vision. Unfortunately, some individuals are either born with impaired vision or develop visual impairment as they grow old. Irrespective of the eye condition that causes visual impairment, the World Health Organization estimated in 2010 that around 285 million people worldwide are visually impaired (Pascolini & Mariotti, 2011; Visual impairment and blindness. (2014, August). Retreived from http://www.who.int/mediacentre/factsheets/fs282/en/). Given that almost all the causes of visual impairment (except refractive error and cataract, the leading causes) are irreversible and incurable, the visual rehabilitation and training of affected individuals to optimally use their residual vision is pivotal. This dissertation research is intended to provide insight into the characteristics of central vision loss and its compensation.

1.2 Prevalence and the Need

Central vision loss (CVL) ensues from irreversible damage to the photoreceptors in the central macular region of the retina. Some of the common causes include macular degeneration (both juvenile as in Stargardt disease (STGD), Best disease and age-related), rod and cone dystrophies, macular holes, and myopic macular degeneration. Age-related macular degeneration (AMD) is one of the leading causes of CVL and is a leading cause

of vision loss in the U.S, next only to diabetic retinopathy and glaucoma. In 2010, the National institute of Health estimated that ~2.1% (i.e. around 2.1 million) of all adults over age of 50 in the U.S had AMD. This estimate is expected to more than double to ~5.4 million by 2050 (NEI: Age related macular degeneration, Retreived from https://nei.nih.gov/eyedata/amd). Due to its high prevalence, AMD is the most investigated of the various diseases that cause CVL. However, genetic conditions like Stargardt disease or photoreceptor dystrophies can occur early in the life and hence can be potentially more disabling.

1.3 The New Locus of Fixation

Like many other neural elements, the photoreceptors in the human retina don't regenerate. Research to regenerate damaged or lost photoreceptors and rewire their connections within the retina and to the visual cortex, although ongoing, has a long way to go. The results of gene therapy, stem cell therapy, retinal prostheses and very recently even a retinal transplant are encouraging but certainly not ready for large-scale implementation. As of today, the main mode of arresting the vision loss in patients with macular degeneration is by injecting anti-growth factors that inhibit the growth of abnormal new blood vessels in the retina and choroid (American Academy of Ophthalmology - Retina/Vitreous Panel, 2015). But this treatment is applicable to only a small proportion of the individuals with CVL. For many other conditions, the best available management is low-vision care and training in the use of a non-foveal (non-central) retinal region to perform most visual functions. The preferred retinal locus (PRL), referred to previously as

the ‘pseudo-fovea’ or ‘fixation locus’ (Timberlake et al., 1986; Whittaker, Budd, & Cummings, 1988), is the non-foveal retinal region that an individual with central vision loss uses to perform visual activities. It has been more than 3 decades since Timberlake, Mainster, Webb, Hughes, & Trempe (1982) mapped the location of a small number of patients’ PRL in their fundus images. In spite of numerous subsequent research studies on patients with CVL, understanding of the development, use and function of PRL is far from complete.

1.4 Deficits in CVL

The PRL is generally located near the edge of the central area of atrophy, especially in individuals with AMD (Timberlake et al., 1986; Whittaker et al., 1988). In other conditions that produce CVL, like in STGD, the PRL can be located further away from the atrophy margins (Rohrschneider et al., 2008; Sunness, Applegate, Haselwood, & Rubin, 1996). Some reports (Maia-lopes et al., 2008; Sunness et al., 1996) hinted that sub clinical pathology can exist adjacent to atrophic regions in CVL, while others pointed to functional deficits outside the affected macula (Hogg & Chakravarthy, 2006; Winther & Frisen, 2015). Some of the deficits that are known to exist in individuals with CVL (like in AMD) include sub-normal reading speed, distance and near visual acuities, contrast sensitivity, dark adaptation, glare recovery, and flicker sensitivity. (Hogg & Chakravarthy, 2006). Given that PRL is the region used for performing day-to-day visual activities and that most individuals with CVL learn to consistently use a single PRL for a given task (Crossland, Crabb, & Rubin, 2011; Fletcher & Schuchard, 1997), it is crucial to know whether changes

in local sensitivity exist in and around the PRL. If areas of reduced sensitivity occur at the PRL, they may help to explain the reported deficits in visual performance, especially related to reading and slowed visual processing. (Cheong, Legge, Lawrence, Cheung, & Ruff, 2007)

1.5 Aims

The broad aim of this dissertation research is to probe the PRL region for sensitivity deficits, in a bid to offer an explanation for some of the reading deficits experienced by individuals with CVL (Legge, Rubin, Pelli, & Schleske, 1985; Rayner & Bertera, 1979; Sunness, Applegate, Haselwood, & Rubin, 1996). Difficulties in reading and recognition of faces are some of the most common complaints in individuals with low vision (Bullimore, Bailey, & Wacker, 1991; Elliott et al., 1997). We hypothesize that local sensitivity changes (which we will designate as micro-scotomas, MSs) can occur outside the region of central atrophy in individuals with CVL and, that when the PRL includes such MSs, reading performance can be adversely impacted.

In the past, the terms eccentric fixation and eccentric viewing sometimes have been used interchangeably. We prefer to use the term eccentric viewing because the report by White & Bedell, (1990) suggested that a complete rereferencing of eye movements to the PRL is uncommon and is certainly not the norm. Eccentric viewing (EV) training is undertaken by low vision specialists and occupational therapists to help subjects with CVL to identify and use a consistent and stable PRL. EV training involves mapping the patient's central scotoma, creating scotoma awareness (Fletcher, Schuchard, & Renninger, 2012)

and training either with an easy-to-understand technique like a clock dial or using bio-feedback training with a micro-perimeter (Vukicevic, Le, & Baglin, 2010). We propose that for successful EV training and rehabilitation, both the central scotoma and the PRL have to be accurately mapped (e.g., with a micro-perimeter, if available) and the PRL region has to be screened for the presence and locations of MSs.

1.6 Organization of the Dissertation

In **CHAPTER II**, we report on the capabilities of a commercially available micro-perimeter (NIDEK MP-1) to undertake a detailed mapping of the PRL in patients with CVL. A micro-perimeter can be an effective tool to assess CVL as it is capable of compensating, at least partly, for the increased magnitude of fixational eye movements that is commonly associated with AMD/STGD (Kumar & Chung, 2014; Reinhard et al., 2007; Whittaker, Budd, & Cummings, 1988). Monitoring the CVL over time requires accurate registration of fundus images across successive test sessions, to ensure that the same retinal regions are tested at baseline and during automated follow-up testing. The second chapter assesses quantitatively the MP-1's capability to compensate for the increased magnitude of fixational eye movements that occur in patients with CVL (Kumar & Chung, 2014; Reinhard et al., 2007) and the accuracy of the MP-1 in registering baseline and follow-up fundus images. We report on the accuracy of compensation for excessive fixational eye movements in cohorts of younger and older subjects with normal vision and on the accuracy of fundus-image registration from cohorts of subjects with normal vision and in subjects with CVL. The assessment of the MP-1's performance is pivotal for assessing

functional changes at the PRL that are assessed in Chapter 3. Thus, the first chapter lays the necessary groundwork for the next chapter.

CHAPTER III, relates functional and structural changes in the outer retina at the PRL region in subjects with CVL (AMD, STGD and others). The functional tests that were performed are the following: an assessment of reading speed with MN Read charts, the determination of contrast thresholds with the Freiburg visual acuity test (FrACT, Bach, 1996) and using the micro-perimetry capability of the MP-1, and mapping the retinal location and the extent of fixational eye movements with the MP-1. Blue fundus auto-fluorescence imaging and spectral domain optical coherence tomography (SD-OCT, Spectralis) were used to obtain structural images of the outer retinal layers of both the PRL and the damaged macular region of patients with CVL. We report that localized regions outside the area of central atrophy can exhibit sub-normal sensitivity. After performing affine transformation to register the fundus images from the MP-1 and Spectralis instruments, locations within the PRL that either had MSs or were free from MSs were identified and the retinal layers were segmented. Although several types of structural changes were noted, the correlation between structural and functional changes was far from perfect.

In **CHAPTER IV**, we describe the impact of simulated scotomas on both foveal and peripheral reading. Random blocks of pixels (elements) within the words of a sentence were deleted to simulate retinal MSs and rapid serial visual presentation (RSVP) reading speed was assessed in cohorts of younger and older subjects with normal vision. This

experiment illustrates the impact on reading speed of having scattered MSs over an extended region in either the central or the peripheral retina. In addition to deleting the elements, the impact of contrast loss was explored and a linear mixed-effects model was used to predict the subjects' RSVP reading speed. This chapter also discusses the applicability of the results to page-mode reading and in subjects with CVL.

Taken together the findings of the chapters II – IV provide more insight into the characteristics of the PRL, both in subjects with AMD and STGD. We anticipated that these 2 groups would behave differently and our results provide limited support for this prediction. A final summary in **CHAPTER V** discusses the applicability and relevance of our findings, shortcomings of our approaches and future directions of this line of research. Relevant calculations, images and supplementary data are provided as **APPENDICES** at the end of this dissertation.

All studies and testing reported in this dissertation were performed after the Committee for the Protection of Human Subjects at the University of Houston reviewed and approved the protocol, "Micro-scotomas around the preferred retinal locus and visual performance" (7/9/12 - 5/18/16).

2. CHAPTER II: Compensation for excessive fixational unsteadiness and accuracy of image registration during follow-up testing by the NIDEK MP-1 microperimeter

Contributing Author:

Harold Bedell, PhD

2.1 Abstract

Purpose: To investigate the a) accuracy of compensation for excessive fixational eye movements (FEMs) and b) registration accuracy of infrared (IR) images during follow-up testing with a NIDEK MP-1 microperimeter in cohorts of subjects with normal vision and subjects with central field loss (CFL).

Methods: Sensitivity across vertical and horizontal optic disc margins was tested using NIDEK MP-1 in 11 subjects with normal vision while they fixated on a small cross and a 10-deg circular target. An additive variance model based on cumulative Gaussian fits to sensitivity profiles was used to determine percent compensation for the increased fixational variability while fixating the larger target. Supra-threshold screening was performed at a randomly chosen non-foveal location in another cohort of 11 normally-sighted subjects and at the preferred retinal locus of 4 subjects with bilateral CFL. Offset of perimetric test points between a baseline and follow-up test on the same day was determined.

Results: The large circular fixation target successfully generated an increase in normal FEMs, ~88 ±18 % and 92 ±9 % of which were compensated on average by MP-1 in the vertical and horizontal directions, respectively. Registration accuracy of MP-1 for follow-up testing had an average registration error <~2 IR-image pixels (8 arc min) in both cohorts.

Conclusions: The NIDEK MP-1 microperimeter can reliably compensate for the increased variability of FEMs such as those seen in patients with CFL and registers IR fundus images to ~8 arc min between initial and follow-up testing. These qualities are important for employing the MP-1 to assess and follow functional changes in patients with CFL.

2.2 Introduction

Fundus-correlated perimetry or micro-perimetry has been used extensively in the past decade for various eye disorders including macular degeneration, (Rohrschneider, 2007; Rohrschneider et al., 2008) diabetic retinopathy, (Vujosevic et al., 2006) glaucoma (Lima et al., 2010) and macular hole (Richter-Mueksch et al., 2007). The Scanning Laser Ophthalmoscope (SLO, Rodenstock, Germany), which preceded the current generation of micro-perimeters, is no longer commercially available and is gradually becoming obsolete primarily due to additional features and algorithms for automated testing that are available in modern day micro-perimeters. Although the NIDEK MP-1 microperimeter was one of the first commercially available micro-perimeters, Timberlake et al. demonstrated the idea of fundus-correlated perimetry roughly 2 decades before the MP-1's introduction in 2002 (Timberlake, Mainster, Webb, Hughes, & Trempe, 1982).

Since their introduction, micro-perimeters have evolved rapidly and the modern day instruments also can include high-resolution retinal imaging in the form of Optical coherence tomography (e.g.: OPTOS OCT-SLO). The NIDEK MP-1 microperimeter is not an SLO and has a built-in liquid crystal display (6.5", 640 x 480 pixels), on which visual stimuli are displayed in optical conjugacy with the IR camera CCD sensor (768 x 576 pixels) (Midena, Radin, & Convento, 2006). The MP-1 also has a built-in color camera that is capable of acquiring high-resolution (1392 x 1038 pixels) flash photographs of the retina, which can be registered later with the low-resolution native IR images.

The primary advantage of micro-perimeters over an SLO is the automated eye tracking that enables rapid online compensation for patients' fixational eye movements (FEMs). Compensation for FEMs is especially important when testing the sensitivity of patients with unsteady fixation, such as those with central field loss (CFL), to ensure that the perimetric targets are presented at or close to the intended retinal locations. Proper alignment of the perimetric targets with respect to a patient's retina is critical for correlating sensitivity losses with observable structural changes in the retina. The MP-1 tracks a region of interest (ROI, 128 x 128 pixels) once every 40 ms and evaluates the X and Y shifts, relative to a previously acquired baseline frame (Midena et al., 2006; Rohrschneider, 2007). The only available published information about the accuracy of eye tracking comes from Midena et al, (2006) who reported a mean tracking accuracy of 4.9 arc min along both vertical and horizontal axes. Unfortunately, these authors reported just the numerical results, and details such as the test population and strategy for determining tracking accuracy are unknown.

Automated follow-up testing is another important feature of modern day micro-perimeters that is not available with an SLO. Repeated testing of the identical retinal locations in a given subject is pivotal for tracking disease progression and for assessing the efficacy of treatment intervention. To conduct follow-up testing at the same retinal locations, the MP-1 registers 2 ROIs each in the baseline and follow-up IR images. However, only sparse information exists about the registration accuracy between baseline and follow-up testing. Again Midena et al, (2006) provided the only report, where the average distance (in 22 subjects, using a 45-stimulus grid) between corresponding points

examined in 2 sessions 1 week apart, was 8.9±3.9 arc min. As Midena et al. used color fundus images to assess registration, rather than the native IR MP-1 images, the error reported presumably includes any mis-registration between the IR and color fundus images.

The motivation for the current study is as follows. The widespread use of micro-perimeters like the MP-1 warrants better understanding of their primary capabilities, namely the accuracy with which fixational eye movements are compensated and the accuracy of registration of the IR images between baseline and follow-up testing. As noted above, the descriptive literature regarding the above-mentioned capabilities is meager. In this study, we used the MP-1 to investigate the accuracy of compensation for excessive FEMs, such as those that characterize patients with central field loss, (Timberlake et al., 1986; White & Bedell, 1990) and the registration accuracy for pairs of IR images acquired during baseline and follow up testing.

2.3 Methods

All testing was performed in a semi-dark room using the NIDEK MP-1 micro-perimeter (NIDEK Technologies SRL, Padova, Italy, Reference Software Version 1.6.0). Normally-sighted subjects were recruited from among the faculty, staff and students of the University of Houston, College of Optometry (UHCO) and subjects with bilateral central field loss were recruited from the Center for Sight Enhancement at UHCO. Subjects were compensated in part for their time. The study protocol was approved by the committee for protection of human subjects at the University of Houston and all subjects provided written

informed consent before participating. Before testing, each subject was provided with a few minutes to adapt to the dim illumination of the examination room.

2.3.1 Experiment 1: Compensation for Increased FEMs

Eleven subjects with self-reports of normal vision (7 younger, < 35 years; 4 older, 50-70 years) were recruited. One eye was selected at random for testing and the other eye was occluded with a black patch. In the 4 older subjects the pupil was dilated with 1% Tropicamide to enable better imaging of the fundus. Dilation was deemed unnecessary for the younger subjects. In separate testing sessions the subject was instructed to fixate at the center of a 1-deg (size of each arm) red cross or at the center of a 10-deg radius red circle (Fig. 1), upon which fixation was expected to be substantially less stable. (Sansbury, Skavenski, Haddad, & Steinman, 1973; Steinman, 1965; Thaler, Schütz, Goodale, & Gegenfurtner, 2013) The cross fixation target, which is the default fixation target in the MP-1, was presented first for 9 of the 11 subjects. At the beginning of each test session a well-focused IR image of the fundus (768 x 576 pixels) was frozen, and a ROI that was rich in features such as blood vessels or a part of the disk margin was chosen for tracking. The location of the fixation stimulus was adjusted to place the optic disc within the central 1/3rd of the MP-1 screen.

The MP-1 reports a ‘goodness’ index for potential ROIs that ranges from 0 to 10+. In this study the goodness index of the ROI always exceeded 3.0. A custom 15x2 grid of Goldmann size II spots (nominal diameter = 13 arc min, separation = 6 arc min) was placed to straddle either the vertical (superior or inferior) or the horizontal temporal optic disc

margin for sensitivity testing (Fig. 1). In all subjects, sensitivity across the temporal disc margin was tested first. Detection thresholds were determined for each spot in the grid using a 4-2-1 thresholding strategy that varied the test-spot luminance within the range 0-20 dB (i.e., 127 – 2.54 cd/m^2) (NIDEK Technologies, 2010). Test spots were flashed one at a time for 200 ms on the 1.27 cd/m^2 uniform white background of the micro-perimeter LCD screen. The subject indicated when a test spot was visible by pressing the hand-held response button.

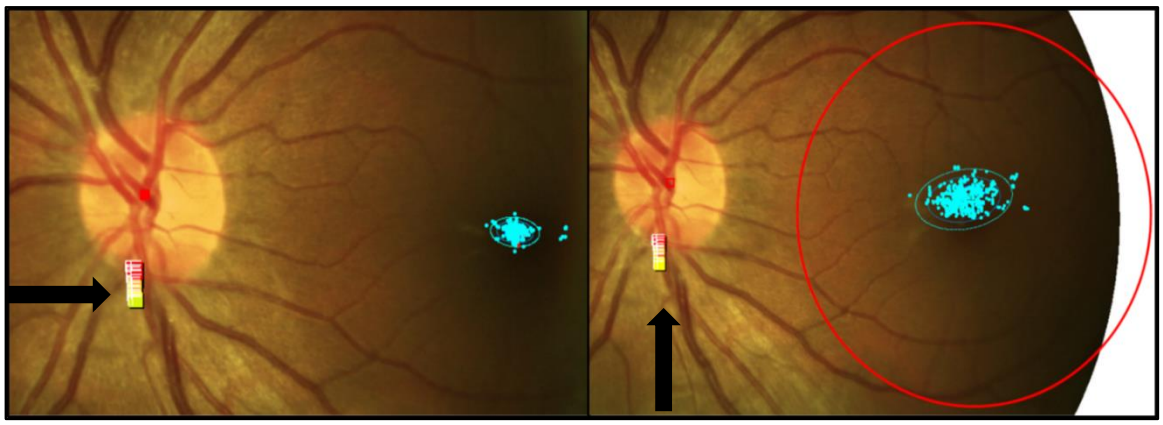

Figure 2-1 Sensitivity Testing Across Disc Margins

Color fundus test images from sensitivity testing across the vertical (inferior, black arrows) optic disc margin using a 1-deg cross fixation target (left) and a 10-deg circular fixation target (right) of representative young normal subject, S3. The 1 standard deviation (SD, blue) and 2 SD (light blue) bivariate contour ellipses (BCEs) fit to the fixation data are obscured by the cyan fixation samples. The 3 SD ellipses (encompassing 99.6% of the fixation samples) are visible (cyan). Based on offline computations, the 1 SD BCE Area $_{cross}$ = 0.36 deg^2 and BCE Area $_{circle}$ = 2.91 deg^2.

The overall test duration was contingent on the subject's fixation stability and sensitivity to the test spots. In general, the cross fixation condition was completed in less time (~3-6 min) than the circle fixation condition (~7-10 min). The MP-1 provides the option of pausing the test and breaks were provided as needed. A high-resolution (1392 x 1038 pixels) color fundus image was obtained at the end of all testing, and the automated inbuilt registration tool of the MP-1 was used to register the color and IR images. The text files containing the locations of the fixation target during testing (in degrees X, Y referred to top-left corner of the IR image) and perimetric sensitivity data were exported and analyzed offline using MS-Excel (2010) and custom MATLAB (R2007b) codes. In this study we didn't employ methods based on kernel density estimation such as 'equidensity line' as proposed by Castet and Crossland for fixation points that are not normally distributed (Castet & Crossland, 2012). Bivariate contour ellipses (BCEs) were fit to the X and Y data points during fixation (5000-10,000 test points per condition), after filtering out the ±3 SD outliers and the potential losses of tracking during blinks and large saccades. The computed bivariate contour ellipse areas (BCEAs) were similar to the BCEA values reported by the software of the MP-1 (**Figure 2-1**)

The sensitivity at each pair of adjacent grid locations parallel to the local orientation of disc margin was averaged. Up to 15 such sensitivity values arrayed perpendicular to the disc margin formed the sensitivity profile. Cumulative Gaussian curves were fit by probit analysis to the psychophysical (PSY) sensitivity profiles using custom software that returned the slope (inverse SD) and half-maximum (mean) (**Figure 2-2**). It is worth noting that the probit regression generally fits the probability, y. However,

the data in our case are the normalized maximum sensitivities (and is not proportions). Thus, a probit fit is perhaps not appropriate and other sigmoid functions could have been employed. But for a first degree of approximation, the probit fits adequately represent the data and describe the profile of sensitivity change across the disc margins.

The SD corresponding to the sensitivity profile during fixation with the circular fixation target was assumed to reflect two sources of variance: (1) the gradient of sensitivity across the vertical or horizontal disk margin (i.e., smoothing of disc borders, (Bek & Lund-Andersen, 1989)) during fixation on the cross target and (2) the increase in variability produced by failure of the MP-1 to compensate completely for the increased variability of fixation in the meridian orthogonal to the disk margin when using the circle compared to the cross fixation target. An additive variance model was used to predict the increase in fixational variability with the use of the circular fixation target. (**Figure 2-3**).

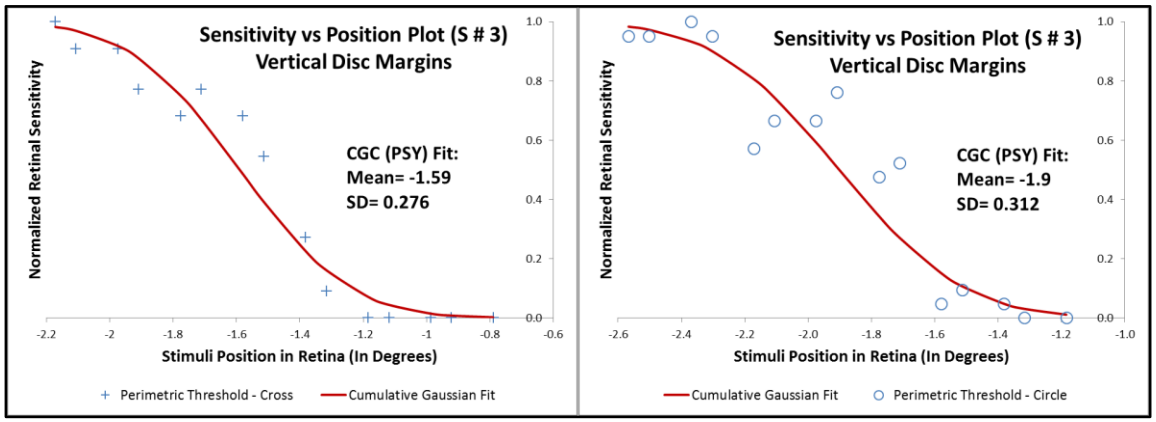

Figure 2-2 Cumulative Gaussian Curve Fit

Cumulative Gaussian curves [CGC (PSY)] fit by probit analysis for fixation on a

cross (left) and at the center of a 10-deg circular target (right) for subject S3. The variances (square of the SD of the probit fit) are: 0.076 and 0.097 respectively.

$$\text{Model Predicted Variance (PSY fit for Circle Fixation Target)}$$

$$= \text{Variance of PSY fit for Sensitivity Testing with Cross Taget}$$

$$+ \text{ Added Fixation Variance}$$

Added Fixation Variance = Fixation Variance Circle - Fixation Variance Cross

The percent compensation by the MP-1 for the increase in fixational eye movements when fixating the circle stimulus was calculated as follows:

$$\text{Percent Compensation (Increase in FEMs for Fixation on Circle Target)}$$

$$= 100 * \frac{\{\text{Predicted } \Delta \text{ in PSY SD} - \text{ Actual } \Delta \text{ in PSY SD}\}}{\text{Predicted } \Delta \text{ in PSY SD}}$$

Where, Predicted Δ in PSY SD = Model Predicted PSY SD_{Circle} - PSY SD_{Cross}

Actual Δ in PSY SD = PSY SD_{Circle} – PSY SD_{Cross}

If the actual Δ in PSY SD is negative, the % Compensation is more than 100, which is not plausible and hence such values are set to 100%.

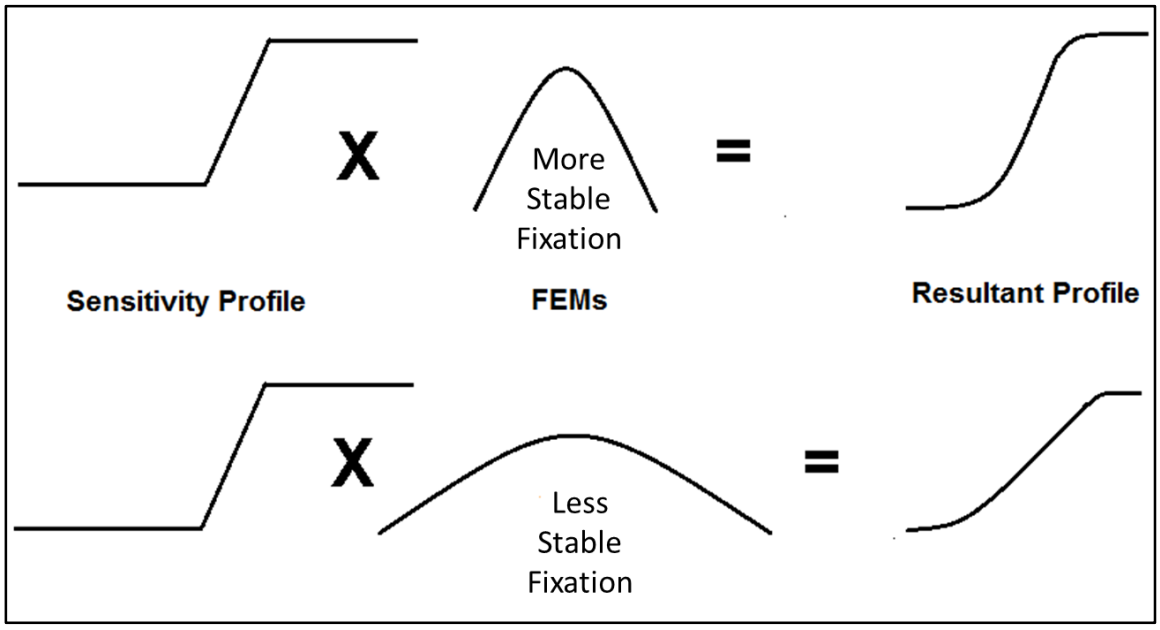

Figure 2-3 Additive Variance Model

An illustration to describe the expected consequence of fixational eye movements (FEMs) on the slope of the sensitivity profile across the optic disc margin. As the SD of FEMs increases, the slope of the resultant sensitivity profile becomes shallower. Note that in this illustration the S-shaped sensitivity profile during fixation on the cross target is approximated as a ramp function. FEMs are shown to be normally distributed and the resultant sensitivity profile is fit with a cumulative Gaussian.

2.3.2 Experiment 2: Registration Accuracy

Sensitivity at a non-foveal region was assessed using the MP-1 in 11 subjects with normal central vision (6 younger, < 35 years; 5 older, >50 years) and 4 subjects with CFL

(2 AMD, 2STGD, refer to **Appendix 6.2** in page157 and **Table 3-1** for more details) secondary to macular degeneration. The pupil of the preferred eye was dilated in all 15 subjects with 1% Tropicamide and subjects fixated with this eye at the center of a 10-deg radius circular target. For subjects with normal central vision, a custom square grid (6 x 6, 1.2 deg) of 36 points was manually placed at an extra-foveal location (eccentricity range: 5 - 15 deg), usually straddling a blood vessel (**Figure 2-4**), to assess the sensitivity to Goldmann size II spots.

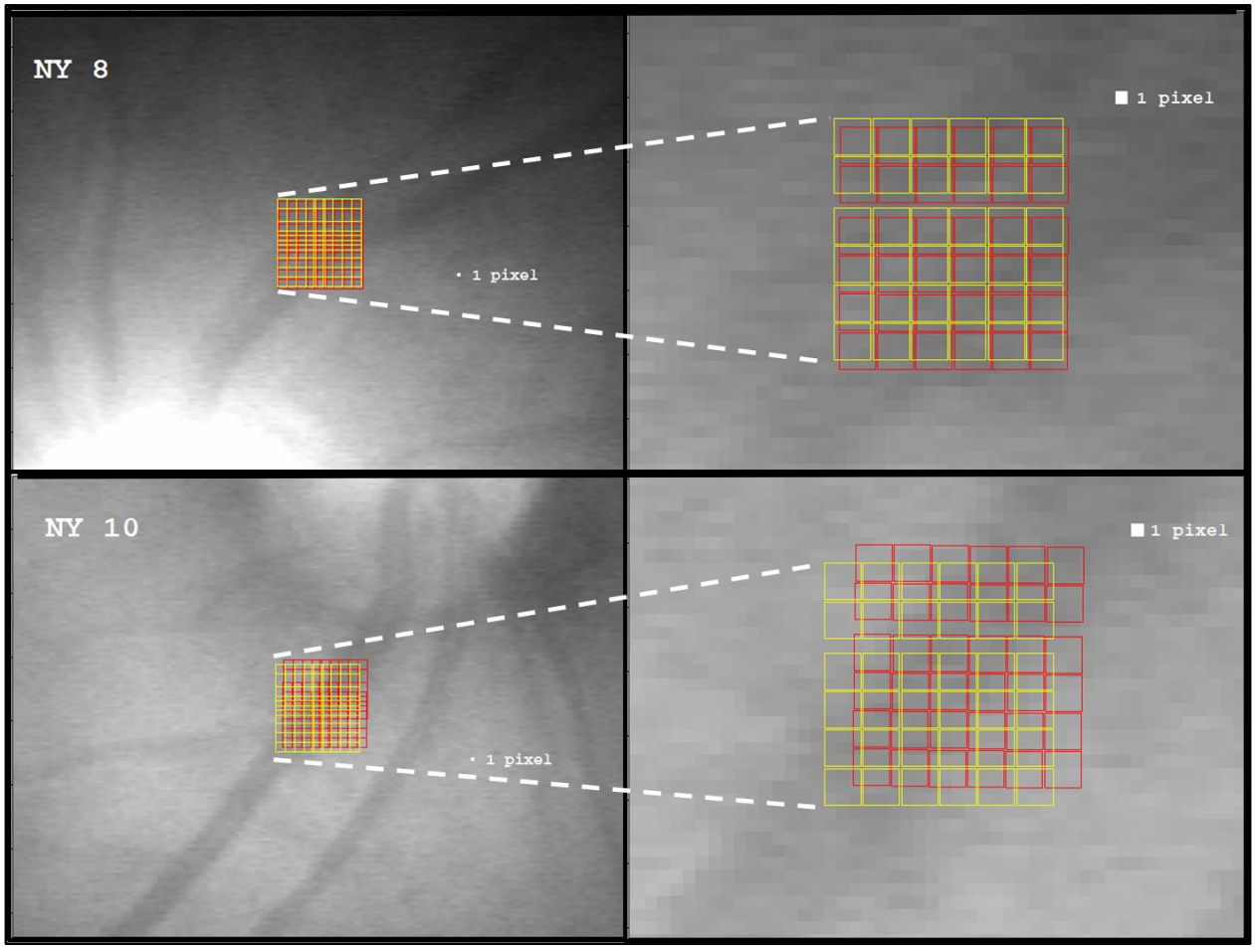

Figure 2-4 Test Grid: Sensitivity Testing – Subject with Normal Vision

Test grid (6x6 array, spacing = 0.2˚) placed at a non-foveal location in younger subjects with normal vision, NY8 (median registration error, top) and NY10 (largest registration error, bottom). Testing was done with the medium IR-illumination level. Yellow squares indicate the grid position during baseline testing; red squares indicate the position during follow-up testing. In the panels to the right, the test grid is zoomed to show the offset details. ***Note:*** *The magnitude of the registration error with respect to size of a single IR-image pixel (~4 arc min). After registration, the grids were replotted on the baseline IR image using a custom MATLAB program.*

The MP-1's IR illuminance can be adjusted between nominal settings of 0 - 160. (NIDEK Technologies, 2010) To determine to what extent the registration accuracy depends on the IR illuminance we chose a 'low' IR setting (<=20) that resulted in weak illumination and low contrast of the IR image, a 'medium' IR setting (20-30) that evenly illuminated the fundus, and a 'high' IR setting (>30) that resulted in a visible shimmer due to saturation of many pixels in the center of the IR fundus image. **(**Figure 2-5**)**

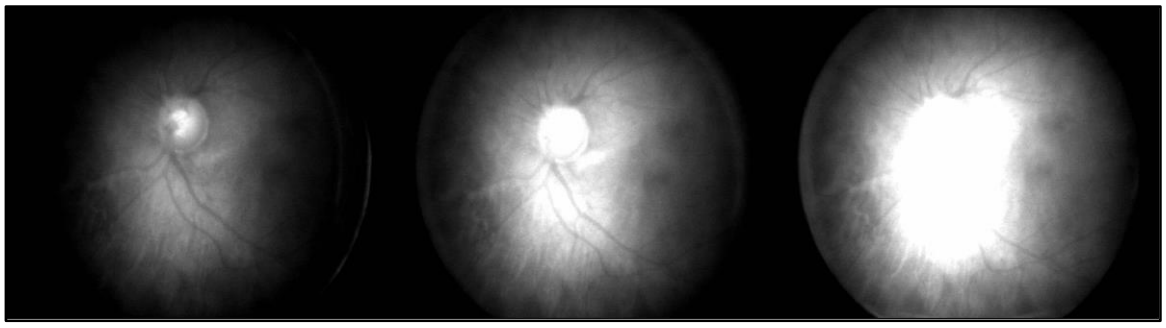

Figure 2-5 Levels of IR Illumination

Montage of IR images (Subject NY 7) returned by the MP-1. Shown above (from L

to R) are the images obtained using three IR illuminance settings 'Low', 'Medium' and 'High' in this normal subject.

In subjects with CFL, a custom grid of 40-70 points corresponding to the 2-D extent of the 1 or 2 SD BCE, was centered on the word-fixation PRL (**Figure 2-6**). The latter was determined as the median of three BCE's obtained during fixation on a three-letter word set at the critical print size, determined using a printed MN read chart (Mansfield, Legge, Luebker, & Cunningham, 1994). Subjects fixated at the center of a red circle that was adjusted to be larger than the long axis of the BCE (See **Figure 2-6**). In both subject cohorts, conventional thresholding was replaced by a screening procedure that quickly estimated the detectability of an array of supra-threshold stimulus. For the normal cohort, a stimulus intensity of either 7 or 10 dB was chosen arbitrarily. For subjects with CFL, the median sensitivity of test points around the PRL was calculated from a baseline 10-2 test and two luminance levels corresponding to (1) 5 dB above the median sensitivity and (2) the brightest level produced by the instrument (0 dB) were used for testing. In the normally-sighted subjects, a pair of tests (baseline and follow-up) was performed at each IR-illumination setting using the 'follow-up' test option of the MP-1. In the cohort with CFL, only one pair of baseline and follow-up tests was performed for each test spot intensity using the 'medium' IR setting of the MP-1. Follow-up testing was performed in all subjects on the same day, immediately after the baseline tests.

The text file containing the perimetry test data and the bitmap IR fundus images were exported from the MP-1. The text file contained: a) Degree to pixel conversion factor,

b) Custom grid center coordinates, in deg, referenced to the top-left corner of the IR image and c) X and Y stimuli coordinates referenced to the center of the custom grid, all of which are required for offline image analysis. A Generalized Dual Bootstrap – Iterative Closest Point (GDB-ICP) algorithm, (Yang, Stewart, Sofka, & Tsai, 2007) was used for the offline registration of the baseline and follow-up IR images. A 2-D affine transformation was used to register the follow-up image with respect to the baseline image. For each pair of tests, the registration returned by the GDB-ICP algorithm was confirmed to exhibit minimal apparent motion when the pair of (nominally aligned) images was flickered alternately. The affine coefficients returned by the GDB-ICP algorithm were then used to transform the locations of the perimetric test points during follow-up testing. Both the transformed test points (X_F, Y_F) from the follow-up image and the baseline test points (X_B, Y_B) were plotted on the baseline IR image and the mean absolute position difference ($|X_B - X_F|$ and $|Y_B - Y_F|$) between corresponding test points was designated the average absolute registration offset.

$$\text{Average Absolute Offset} = \Sigma|X_B - X_F|/N; \Sigma|Y_B - Y_F|/N$$

Where, X_B, Y_B, X_F and Y_F = X and Y coordinates of test points in baseline testing and follow-up testing respectively.

N= Number of test points in the sampling array.

2.4 Results

2.4.1 Experiment 1: Compensation for Increased FEMs

As anticipated, fixation by the normally-sighted subjects at the center of the 10° circle target increased the variability of fixational eye movements. The mean BCEA for the 11 subjects increased ~10-fold compared to fixation on the cross target**.** Specifically, the mean (±SD) BCEAs for fixation on the cross and circle targets were 0.39±0.37 and 3.16±2.28 deg^2 and 0.21±0.14 and 2.36±0.91 deg^2 for testing across the vertical and horizontal disc margins, respectively. The average computed compensation by the MP-1 was 88.11 ± 18.02% and 91.78 ± 9.12% for the increase in vertical (V) and horizontal (H) components of fixation instability, i.e., during testing across the vertical and horizontal disk margins, respectively (See **Table 2-1 and Table 2-2**).

Subject #	PSY Fit SD	PSY Fit SD	Fixn. SD_Y	Fixn. SD_Y	Model Pred. SD Circle	Actual Δ in PSY SD	Pred. Δ SD	Final %Comp. (Δ SD)	Uncompensated FEMs
Younger (<35Yrs.)	Cross	Circle	Cross (deg)	Circle (deg)				Value > 100 = 100%	(arc min)
S1	0.291	0.340	0.230	1.124	1.138	0.049	0.847	94.215	5.173
S2	0.252	0.328	0.153	0.542	0.577	0.076	0.326	76.732	9.047
S3	0.276	0.312	0.203	0.487	0.522	0.036	0.246	85.348	4.163
S4	0.130	0.244	0.181	0.735	0.724	0.114	0.594	80.806	10.630
S5	0.283	0.239	0.153	0.387	0.455	-0.044	0.172	100.000	0.000
S6	0.115	0.236	0.105	0.314	0.317	0.121	0.202	40.164	12.506
S7	0.197	0.178	0.557	0.419	0.311	-0.019	0.001	100.000	0.000
Older (>60Yrs.)									
S8	0.015	0.067	0.068	0.667	0.664	0.052	0.649	91.928	4.837
S9	0.402	0.389	0.182	0.482	0.601	-0.013	0.199	100.000	0.000
S10	0.199	0.009	0.246	0.453	0.429	-0.190	0.230	100.000	0.000
S11	0.214	0.170	0.120	0.815	0.834	-0.044	0.620	100.000	0.000
							Mean	**88.109**	**4.214**
							SD	**18.022**	**4.726**
							Median	**94.215**	**4.163**

Table 2-1 Precision of FEMs Compensation: Vertical Disc Margins

Results based on cumulative Gaussian curve (PSY) fits for all subjects, for testing across the vertical disc margin. Note that model prediction in column 6 is based on the additive variance model described in the text. In column 9, note that >100% compensation

is not possible, thus the maximum value of % Compensation was set at 100%.

The fixation stability of the younger normal group for the two fixation targets (in deg^2, Mean ±SD, Cross: 0.34 ±0.34 and Circle: 2.52 ±2.02) was not significantly different from the older normal group (Cross: 0.24 ±0.18 and Circle: 3.19 ±1.11 deg^2; 2-tailed t (20) = -0.27, p= 0.39 for the cross and t (20) = -0.46, p= 0.33 for the circle fixation target). Further, the percent compensation of the younger normal group (Mean ±SD, 86.94 ±15.9) was not significantly different from the older normal group (Mean ±SD, 95.7 ±8.38; 2-tailed t (19) = -1.24 and p= 0.12). For both groups of normally-sighted subjects, the mean uncompensated component of the added fixational variability was 4.2 and 3.8 minutes of arc, respectively, in the vertical and horizontal directions.

Subject #	PSY Fit SD	PSY Fit SD	Fixn. SD_X	Fixn. SD_X	Model Pred. SD Circle	Actual Δ in PSY SD	Pred. Δ SD	Final %Comp. (Δ SD)	Uncompensated FEMs
Younger (<35Yrs.)	Cross	Circle	Cross (deg)	Circle (deg)				Value > 100 = 100%	(arc min)
S1	0.381	0.259	0.316	0.769	0.798	-0.122	0.417	100.000	0.000
S2	0.143	0.215	0.139	0.451	0.452	0.073	0.309	76.526	7.326
S3	0.146	0.210	0.131	0.695	0.698	0.064	0.552	88.378	6.553
S4	0.105	0.130	0.204	0.689	0.666	0.025	0.561	95.562	2.152
S5	0.108	0.132	0.130	0.495	0.489	0.024	0.381	93.786	2.268
S6	0.213	0.215	0.096	0.508	0.542	0.002	0.329	99.544	0.188
S7	0.208	0.283	0.227	0.749	0.743	0.074	0.535	86.087	7.253
Older (>60Yrs.)									
S8	0.154	0.144	0.146	0.583	0.585	-0.010	0.431	100.000	0.000
S9	***	***	0.195	1.150	NA	NA	NA	NA	NA
S10	0.248	0.203	0.287	0.653	0.637	-0.045	0.389	100.000	0.000
S11	0.018	0.165	0.149	0.700	0.684	0.147	0.666	77.956	12.137
							Mean	**91.784**	**3.788**
							SD	**9.123**	**4.254**
							Median	**94.674**	**2.210**

Table 2-2 Precision of FEMs Compensation: Horizontal Disc Margins

*Same as Table 2-1, except that the data represent testing across the horizontal optic disc margin. [******* Represents insufficient data, as the test grid did not straddle the horizontal disc margin.]*

2.4.2 Experiment 2: Registration Accuracy

The average (±SD) X and Y offsets in arc min were respectively: 4.43 ±3.29 and 3.66 ±2.37 for the low IR setting, 2.45 ±2.55 and 3.3 ±2.25 for the medium IR setting, and 4.23 ±4.22 and 3.9 ±2.85 for the high IR setting. **Figure 2-4**, shows the registration errors for 2 representative normally-sighted subjects, NY8 and NY10, during testing at the medium IR setting. Across all of the normally-sighted subjects, the overall average Pythagorean registration offsets ($\sqrt{X2+ Y2}$) were not significantly different ($P> 0.05$) for the low (L), medium (M) and high (H) IR settings (2 tailed paired t-tests: L vs. M: $p = 0.12$; M vs. H: $p = 0.3$; L vs. H: $p = 0.97$).

The average (±SD) registration errors for testing in CFL subjects (tested only at the medium IR setting) were 8.14 ±5.19 and 5.21 ±2.9 arc min respectively in the X and Y directions. **Figure 2-6** shows the test grid and the registration error from a representative CFL subject, MD2b. The Pythagorean offsets were not significantly larger (2-tailed t-test, $t (15) = -1.86$ and $p=0.082$) for the CFL compared to the normally-sighted subjects.

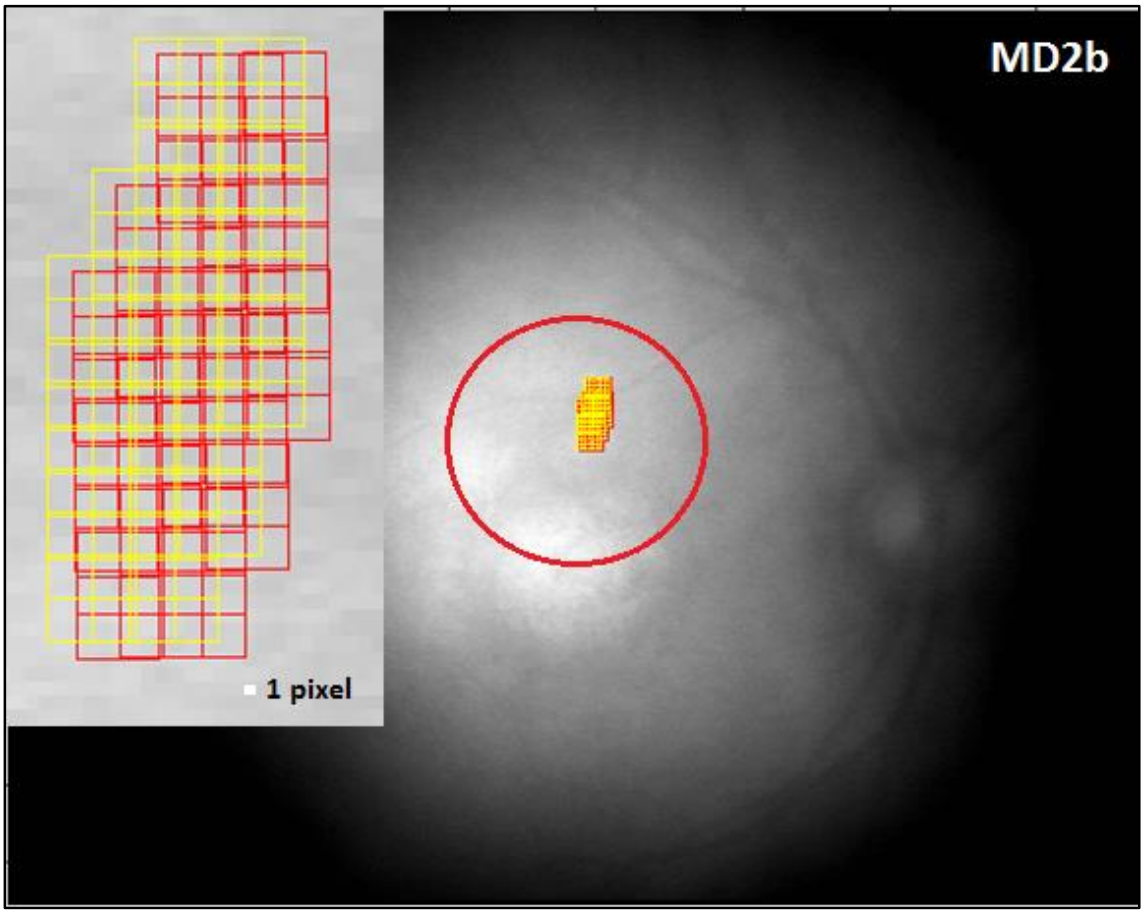

Figure 2-6 Test Grid: Sensitivity Testing - CFL Subject

Test grid of 50 points (0.2˚ apart) centered on the word-fixation PRL (2SD BCE) of a representative subject with CFL, MD2b, who exhibited the median registration error. In the inset, the test grid is zoomed to show the offset details (Note that the grids in ***Figure 2-4*** *are zoomed to a different scale). The red fixation circle shown here was added and test grid was replotted to the IR image.*

2.5 Discussion

We assessed the compensation for excessive fixation instability and the registration accuracy between baseline and follow-up testing of a commercially available NIDEK MP-1 microperimeter. Reports suggest that the narrower dynamic range of MP-1, i.e., 2 log units vs. 5 log units in a Humphrey Field Analyzer, can limit its use to quantify defects that are too severe or too subtle due to floor and ceiling effects (Acton, Smith, Greenberg, & Greenstein, 2012; Chen et al., 2009). To partly overcome these limitations, Seiple et al. (2012), used a smaller target size (Goldmann Size I) to extend the range of useable stimulus intensities. Further, some of the newer micro-perimeters have a wider dynamic range than the MP-1, e.g., the MAIA has a range of ~4 log units. Assessing the retinal sensitivity thresholds with microperimetry can take significantly longer time than testing with standard automated perimetry (Acton, Smith, et al., 2012; Springer, Bültmann, Völcker, & Rohrschneider, 2005) or using scanning-laser-ophthalmoscope perimetry (Rohrschneider, Springer, Bültmann, & Völcker, 2005). Nevertheless, the merits of precise automated real-time fundus tracking and image registration outweigh the above limitations.

2.5.1 Fixation Stability and FEMs

In older normal adults, measures of visual fixational stability have been shown to be similar to those of younger adults (Kosnik, Fikre, & Sekuler, 1986). In our study, the fixation stability of older normally-sighted subjects on cross and circular targets was not significantly different from that of younger normally-sighted subjects. Bellmann et al., (2004) showed that the BCEA during fixation in a cohort of subjects with late-stage AMD

was roughly 10 times larger than that of age-matched controls. In particular, the average (±SD) BCEA in their cohort of 12 AMD subjects, for the target that fostered the greatest stability (1° letter 'x') was reported to be 3.35 ±0.071 deg^2. The average BCEA in our cohort of 11 normally-sighted subjects, when fixating at the center of a 10-deg circular target was similar (3.12 ±1.93 deg^2). The large difference in standard deviations between the two studies is likely to result from an arithmetic error, as the SD value in min arc^2 that is listed by Bellmann et al (2004) is unrealistically small. The BCEA for fixation on the cross targets (vertical margins) was 0.39±0.37 deg^2. The fact that the SD is the roughly the same size as the mean suggests that our data was significantly skewed (Range SD_y for Cross from Col. 4 of **Table 2-1** is: 0.068 – 0.557°).

FEMs and their magnitude have been investigated widely since 19th century (Cherici, Kuang, Poletti, & Rucci, 2012; Helmholtz, 1925; Martinez-Conde, Macknik, & Hubel, 2004). The flicks (micro-saccades) of normally-sighted subjects are usually in the range of 1-20 arc min and drifts are usually up to 6 arc min in amplitude (Ditchburn & Ginsborg, 1953). A Goldmann III target, the most commonly used size for perimetric testing, has a diameter of 26 min arc and the standard grid of the Humphrey 10-2 pattern samples retinal locations every 2 deg. For this target size and sampling density, a retinal position error of a few min arc is tolerable and it is therefore not a big problem if normal fixational variability is either uncompensated or only partly compensated, because the retinal locations of each perimetric test stimuli will be within a few min arc of the intended retinal location. Even for a Goldmann II target, which has a nominal diameter of 13 min arc, an error in the target's retinal location equal to the fixation SD (~5-10 arc min) still

allows some part of the target to remain at the intended retinal location. On the other hand, when testing patients whose BCEAs are 10 times larger than normal (and even larger in some patients with CFL), the locations of perimetric test targets can deviate substantially more (e.g., a factor of $\sqrt{10}$) from the intended retinal location if these patients' FEMs remain uncompensated.

Our simulation of the fixation instability of patients with CFL is based on the results of Sansbury et al. (1973) who demonstrated that the fixation stability of normally-sighted subjects deteriorates with the size of the fixation target. In their study, the worsening of fixation for large targets was associated with an increase in the size of both saccades and inter-saccadic drifts. On the other hand, in a cohort of subjects with macular disease, Kumar and Chung (2014) concluded that it was the amplitude of micro-saccades that mainly contributed to the increased variability of these subjects' FEMs compared to normally-sighted subjects. So, although the simulation in our study quantitatively mimics the FEMs in CFL, it may not be qualitatively the same.

The histology and structure of the region around the optic disc margins has received much attention in the past few decades primarily due to changes like peri-papillary atrophy that can be associated with conditions like glaucoma or myopia (Jonas, Budde, & Panda-Jonas, 1999). That said, it is worth noting that none of our subjects (both younger and older) had any visible atrophic changes near the disc margins. Whereas the temporal and nasal disc margins have received much attention, the changes in retinal histology in the superior and inferior disc margins are largely unknown (Fantes & Anderson, 1989). This is

primarily due to presence of major blood vessels near the vertical margins. The latter also made the positioning of test grid difficult in some of our subjects. Fantes and Anderson (1989) using histologic sections, classified the peri-papillary anatomic arrangement into 4 non-mutually exclusive categories. They report that nearly all disc margins have a flange of sclera around the entire circumference and this flange separates the choroid from optic nerve head tissue. Also, there is a gradual depigmentation of RPE as the disc is approached.

More recently, Lee et al. (2010) used high resolution in-vivo imaging to document the tapering configuration of retinal layers at the edge of the optic disc. They report that the photoreceptor layers and the retinal pigment epithelium terminated with-in the area of the peri-papillary atrophy. In eyes without the atrophy, the density of the photoreceptor layer generally reduced gradually till the disc margins were approached. The regions around the disc margins can exhibit a wide array of changes and these changes in retinal structure could be very different across subjects. However, these shouldn't influence our results or the interpretation of these results as we report compensation for each subject individually. Also by probing a similar (if not exactly the same) region in the 2 fixation conditions, we eliminate the influence of the structural changes in retina. We used a cumulative Gaussian fit (sigmoid function) with varying slopes to approximate the sensitivity profile across the disc margins, and given the evidence of changes in retinal layers (specifically RPE and photoreceptors) near the disc margins, the fit describes the profile adequately. However, any non-linear fit could be used to describe the sensitivity changes. In this study we chose to use the cumulative Gaussian chiefly because we modeled

the FEMs to be normally distributed. When the distribution of FEMs is not normal, this model may be less applicable.

2.5.2 Registration Accuracy

In a cohort of 10 subjects with AMD and 12 normally-sighted subjects, Midena et al. (2006) manually identified the same 2 anatomical landmarks in a pair of color fundus images during perimetric testing. A 45-stimulus grid (Goldmann Size III) was used to assess retinal sensitivity and follow-up testing was done after 1 week, at which time all of the stimulus coordinates were re-referenced with respect to the previously identified retinal landmarks. Midena et al. then calculated the retinal Pythagorean distance between each of the corresponding 45 test stimuli on the initial and follow-up tests. The average (±SD) Pythagorean distance was 8.9 ± 3.9 arc min, which is larger than the mean offset value of 4.4 ±3.0 arc min that we obtained for normally-sighted subjects. In closer agreement with the value reported by Midena et al., the Pythagorean offsets for our CFL subjects averaged 10.1 ± 5.1 arc min. The discrepancy may be attributable to differences in the methods employed for aligning the test image pairs, whereas the discrepancy in registration accuracy between our normal and CFL subjects may be explained by the ROI goodness index that is contingent on the shape and contrast of the retinal features selected. Thus, it will be a worthwhile future endeavor to explore the role of the ROI goodness index in registration accuracy.

2.5.3 Limitations of the Study

The software version (1.6.0) of MP-1 used in our study, doesn't allow the use of 2 different fixation targets during the automated 'follow-up' testing. The 'follow-up test option' of MP-1 registers images from 2 test sessions and ensures the same retinal region can be tested, which was desired in our first experiment that assessed sensitivity across disc margins. Thus, we could only manually and visually align the test locations between the 2 fixation conditions. The BCEAs reported here are computed from fixation sampled for the entire duration of perimetric testing, corresponding to several minutes, as opposed to the widely used approach of sampling fixation for only ~15 - 30 seconds (Amore et al., 2013; Bedell et al., 2015; Bellmann et al., 2004). An increase in sampling time would be expected to result in larger BCEAs (Longhin et al., 2013). Also, the assumption that fixational eye movements are normally distributed, which underlies the construction of BCEs, may not be valid in some subjects. More specifically, the distribution of fixational eye movements in patients with AMD may differ from the distribution of fixation in normal eyes, even when the range of fixational eye movements is scaled appropriately. Therefore, extending the current results to the testing of patients with CFL needs caution especially because of the small number of CFL subjects in this study.

Absolute Compensation of FEMs: We investigated only the compensation by the MP-1 for an *increase* from the normal amplitude (cross condition) of FEMs and not the absolute (normal + increased fixational instability) percent compensation of FEMs by the MP-1. Two likely limiting scenarios are: (1) the MP-1 compensates normal fixational variability

in the same percentage as the added fixational variability that is observed when using a large circular target, or (2) the MP-1 does not compensate for the normal variability of FEMs (i.e., when viewing the cross target) at all. In our study, the average SDs in the vertical and horizontal directions during fixation on the cross target were 12.0 and 10.8 arc min. Therefore, for the scenario that assumes the same percent compensation for normal and excessive FEMs, the absolute uncompensated FEMs would be ~5 arc min both the vertical (4.2 + 0.12 x 12 arc min = 5.6 arc min) and horizontal (3.8 + 0.08 x 10.8 arc min = 4.7 arc min) directions. On the other hand, if normal fixational variability is not compensated at all, then the magnitude of uncompensated FEMs would be (SQRT (4.2^2 + 12^2) = SQRT (162) =) 12.7 arc min vertically and (SQRT (3.8^2 + 10.8^2) = SQRT (131) =) 11.5 arc min horizontally.

To assess the registration accuracy, we compared the default semi-automated registration of the MP-1 (based on a normalized gray scale correlation of features at the chosen ROIs) to a fully automated dual-bootstrapping algorithm. A possible mis-registration by the MP-1 of test targets with respect to the fundus image has been reported previously (Woods, Vera-Diaz, Lichtenstein, & Peli, 2007). It should be noted that the MP-1 performs image registration and computes test point locations on line in a short span of time (usually <5 sec), as opposed to the GDB-ICP algorithm, which requires extensive off-line computations. We performed the baseline and follow-up testing on the same day and on cohorts of subjects with stable CFL or normal vision. Provided that stable, feature-rich ROIs can be selected from the fundus images during both the baseline and following-up

testing, our expectation is that the registration accuracy should not be affected by the time to follow-up or by disease progression.

2.6 Conclusions

The study examined the accuracy of the MP-1 microperimeter for compensating the increase in fixational eye movements that occurs in patients with CFL and for registering the IR fundus images between baseline to follow-up testing. The results indicate that the MP-1 compensates for ~90% of the increased in fixational eye movements that is expected in patients with CFL and that the image registration is accurate to ~2 pixels (8 arc min). Consideration of these values is necessary when the MP-1 is employed to characterize and follow various eye conditions longitudinally, including CFL secondary to macular degeneration.

2.7 Acknowledgments

We thank Josh Pratt for allowing us to use his custom MATLAB code for fixation analysis. Hope Queener and Scott Stevenson provided valuable input regarding the fitting of cumulative Gaussians to the distributions of FEMs. Julia Benoit and 2 anonymous reviewers for their inputs on the MP-1 system, the appropriateness of probit analysis. We thank all of our motivated study subjects and patients with CFL for their participation as well as the optometrists of the Center for Sight Enhancement at UHCO, specifically Drs. Modi and Hooper, for their help in identifying prospective study subjects.

3. CHAPTER III: Relating functional and structural changes at the preferred retinal locus of subjects with bilateral central field loss

Contributing Author:

Harold Bedell, PhD and Nimesh Patel, OD, PhD

3.1 Introduction

Age-related macular degeneration (AMD) is among the most common cause of permanent visual impairment in developed countries like the USA, accounting for more than 54% of all vision loss in the white population (Smith et al., 2001). Juvenile macular degeneration, a term that includes conditions like Stargardt disease (STGD), Best disease, and fundus flavimaculatus, is similar in pathophysiology to the dry type of AMD, in that a gradual vision loss results from pigment epithelial changes and photo-receptor degeneration and/or loss (Facts About Stargardt Disease. (April 2015). Retrieved from https://nei.nih.gov/health/stargardt/star_facts).

Early AMD manifests with a variety of retinal findings including hard and soft drusen, localized pigment alterations in the retinal pigment epithelium, and loss of the foveal light reflex. The etiology of AMD is multi-factorial. It includes environmental (smoking, low dietary intake of anti-oxidants) and genetic (CFH polymorphism) factors aside from ageing (de Jong, 2006). Development of a neo-vascular membrane (CNV) and/or fluid accumulation are classic findings in the wet type of AMD, as opposed to a geographic atrophy (GA) in the dry type. CNV, if left untreated, can progress to legal blindness within months, whereas the progression in dry AMD is usually slow, and is known to impact retinal regions outside the macula (de Jong, 2006). In fact, the rod photoreceptors in the parafovea (1-3mm from fovea) are affected first and are more vulnerable than foveal cones to degenerative changes in both the early and late stages of age-related maculopathy (Curcio, Owsley, & Jackson, 2000; Owsley et al., 2000).

Although the central field loss is irreversible, most late stage patients with either the dry or the wet type of AMD retain ambulatory vision, due to remaining peripheral visual sensitivity (de Jong, 2006). Treatment is usually preventive and includes laser photo-coagulation, anti–VEGF injections (in wet AMD), anti-oxidant supplements and modification of risk factors (Lim, Mitchell, Seddon, Holz, & Wong, 2012).

STGD (also referred to as Stargardt macular degeneration) is a genetically inherited outer retinal disorder that affects about 1 in 8,000 to 10,000 individuals (Stargardt macular degeneration. (May, 2016). Retrieved from https://ghr.nlm.nih.gov/condition/stargardt-macular-degeneration). The most common reason for STGD is a mutation in the ABCA4 gene (ATP-binding cassette subfamily A member 4) that is responsible for removing the photo-transduction metabolite N-retinylidene-PE. The ABCA4 protein is specific to the retina and is located in the outer segment discs of the photoreceptors. The defective ABCA4 gene prevents the ABCA4 protein from clearing N-retinylidene-PE, the accumulation of which results in a buildup of lipofuscin that eventually damages the photoreceptors and the surrounding retinal cells. Interestingly, Curcio et al. (2001) reported that the site of rod loss in the early AMD is about 1-2 mm from foveal center (not related to the site of highest rod density), and was not related to lipofuscin accumulation. Unlike STGD, numerous models and theories have been proposed to explain the changes in both wet and dry AMD. The consensus as of today lists drusen and hyper-pigmentation of RPE as the initial insult in dry AMD, whereas insult to chorio-capillaries could potentially trigger the wet form of AMD (Ambati & Fowler, 2012).

3.1.1 Central Field Loss and Fixation Stability

Visual acuity is considered to be a poor indicator of early AMD, not only because it is impacted only after considerable changes have occurred already in the retina, but also because acuity does not completely reflect the challenges faced by patients in tasks like face recognition, text reading, mobility, and orientation (Legge, Rubin, Pelli, & Schleske, 1985). In a retrospective study of the patients who sought rehabilitation services in a veteran affairs clinic, Schuchard et al. found that ~90% of cases had bilateral central scotomas secondary to AMD (Schuchard, Naseer, & De Castro, 1999). Although the disease can be asymmetrical, involvement of both eyes makes it difficult to perform many visual tasks. Fixation frequently is compromised in patients with AMD, leading to an increase in fixational eye movements and excessive variability (Kumar & Chung, 2014; Reinhard et al., 2007; Timberlake et al., 1986). Bivariate Contour Ellipse Area (BCEA) is one of several metrics that describe fixation stability, taking into account the scatter of fixation along both the major and minor ellipse axes and the correlation between the values along these two axes (Steinman, 1965; Timberlake et al., 2005).

3.1.2 Preferred Retinal Locus

Most subjects develop an adaptive strategy to compensate for the central field loss (CFL), in which they use a non-central, relatively healthy retinal area near the margin of the scotoma for fixation. This non central retinal locus or fixation area is called the ‘Preferred Retinal Locus’ (PRL) (Timberlake et al., 1986). The PRL is chosen such that it is away from the central area of obvious retinal damage but it can be surrounded by regions

of reduced sensitivity, perhaps due to changes associated with macular degeneration (Cideciyan et al., 2005; Maia-lopes et al., 2008; Rogala et al., 2015). The location of the PRL varies a lot among subjects and primarily depends on the scotoma size and shape (Fletcher & Schuchard, 1997). Shima et al. reported that the location of the PRL in group of 15 subjects with AMD didn't coincide the retinal location of highest sensitivity (Shima, Markowitz, & Reyes, 2010).

Studies have consistently documented that the PRL is located further away from the edge of the central-retinal degeneration in eyes with JMD than AMD. For example, Rohrschneider et al. documented a clear patch of viable retina between the PRL and the central area of degeneration in JMD (Rohrschneider et al., 2008). In AMD the PRL is located invariably near the edge of the central scotoma, but can shift more peripherally as the degeneration engulfs greater regions of central retina (Fujita & Yuzawa, 2003). Fletcher et al., in their study of 825 patients with low vision, found that roughly 1 in 6 patients have their PRL surrounded by dense scotomas, constraining the usefulness of the PRL for many visual tasks (Fletcher & Schuchard, 1997; Fletcher, Schuchard, & Gale, 1999). Crossland et al. concluded that patients who are not aware that they are using a PRL read more quickly than those who are conscious of using a non-central retinal locus (Crossland, Culham, Kabanarou, & Rubin, 2005). On the other hand, Fletcher et al. (2012) reported that some awareness of the central scotoma in subjects with AMD tends to improve the reading accuracy. A small proportion of subjects with long standing macular degeneration may progress from a strategy of eccentric viewing to develop a locus of eccentric fixation,

wherein the oculomotor reference or fixation center shifts from the dysfunctional fovea to a healthier eccentric region (Von Noorden & Mackensen, 1962; White & Bedell, 1990).

3.1.3 Functional Deficits in AMD and STGD

The ability to discriminate orientation and shape can be impacted very early in the course of AMD, and hyperacuity tests have been proposed as a screening test for macular disease (Bressler & PHP-Research-Group, 2005; Hogg & Chakravarthy, 2006; Wang, Wilson, Locke, & Edwards, 2002). Visual field testing is one of the frequently-performed clinical tests in AMD. Midena et al reported that functional abnormalities are present in eyes with macular drusen, although the drusen may not directly cause a reduction in sensitivity (Midena et al., 2007). These authors also opined that testing sensitivity in the central visual field is a reliable, easy to administer, and relatively quick way to understand the disease. Retinal degeneration in patients with AMD is not restricted to the macula but is usually more widespread, and it is now known that even normal appearing retinal regions can have deficits in various visual functions like dark adaptation, spatial contrast sensitivity and flicker sensitivity (Curcio et al., 2000; Hogg & Chakravarthy, 2006; Rogala et al., 2015). Some types of functional testing like flicker thresholds and photo stress recovery (Dimitrov et al., 2011) or dark adaptation (Jackson et al., 2014) have been reported recently to have the capability to diagnose some of the earliest changes in AMD. There have been conflicting reports about whether visual sensitivity is impaired over retinal regions with drusen, although concurrence exists that field losses exist over areas of pigment epithelial

atrophy in AMD subjects (Iwama et al., 2010; Midena et al., 2007; Rohrschneider et al., 2008)

STGD primarily impacts the macular cones (and secondarily the rod system) and subjects can exhibit reduced foveal and extrafoveal focal electroretinograms, reduced pigment density, delayed bleaching adaptation and prolongation of rod dark adaptation, especially the later segment of rod recovery (Fishman, Farbman, & Alexander, 1991; Scullica & Falsini, 2001). Sunness & Steiner (2008), reported that retinal areas that have a uniform loss of auto-fluorescence (AF) are very likely to have dense scotomas. They also concluded that lesions observed in fundus photography or AF imaging may not directly correlate with the size and location of the dense scotoma. More recently, Parodi et al. (2015) used near-infrared AF to image 27 patients with STGD. They reported that eyes with foveal hyper-AF had better acuity, better mean sensitivity within the central 2° retinal regions, and better preservation of the outer retinal layers as observed with optical coherence tomography (OCT) imaging.

3.1.4 Reading and Contrast Sensitivity

Reading and contrast deficits in patients with central vision loss will be dealt with in greater detail in the fourth chapter and only a brief overview is provided here. Legge and his colleagues were one of the first groups to document a subnormal (~5x slower) reading speed in subjects with bilateral CFL (Legge et al., 1985). The visual-field deficits in AMD and STGD are only compounded by an associated loss in contrast sensitivity (Kleiner, Enger, & Fine, 1988; Ortiz, Jiménez, Pérez-ocón, & Castro, 2010). When studying the role

of contrast in low-vision subjects, Rubin and Legge (1989) concluded that visually impaired subjects act as 'contrast attenuators', and if text contrast is appropriately scaled for the reduction in contrast sensitivity, the effect of contrast on reading is similar to that seen in normally sighted subjects. Chung, Mansfield, & Legge (1998) explored reading performance in normal peripheral vision (up to 20 deg) and reported that the reading speed varies with eccentricity even after scaling for the print size. They inferred that the print size of the words is not the only limitation on reading with peripheral retina. A study that assessed word reading in normal peripheral vision using Rapid Serial Visual Presentation (RSVP) after scaling for font size, showed that reading rates are consistently better than those observed in AMD subjects (Rubin & Turano, 1994)

Reading difficulties are one of the most common complaints in CFL patients, and hence low vision management has been biased to cater to this need (Elliott et al., 1997). In evaluating the results of low vision rehabilitation, reading speed is more informative than visual acuity, as reading is much more demanding than identifying a small number of letters on the acuity chart. Subjects with STGD read consistently better than those with AMD. Legge, Ross, Isenberg, & LaMay (1992) assessed reading speed using MNRead sentences in a cohort of subjects with AMD, STGD and other types of CFL and found that for a given acuity the average reading speed of the STGD subjects was ~2 times better than that of AMD subjects. Fixation instability, a reduction in the number of characters that can be recognized in one glance (the visual span), and slower temporal processing are three factors proposed to explain the subnormal reading performance in established CFL subjects with

stable PRLs (Cheong et al., 2008; Cheong, Legge, Lawrence, Cheung, & Ruff, 2007). However, none of these factors provides a complete explanation.

Legge and Kersten (1987) used contrast increment thresholds to obtain the contrast discrimination functions in nasal (up to 10 deg) and temporal retina (up to 20 deg) of 2 subjects with normal vision. They concluded that when scaled with the local contrast sensitivity function the contrast discrimination functions were both qualitatively and quantitatively similar in central and peripheral vision. Ortiz et al. (2010) plotted the contrast sensitivity function in 25 AMD patients and aside from the expected lowering of the high spatial frequency cut-off, a significant difference from subjects with normal vision was found for low and mid spatial frequencies ranging from 0.6 - 8.2 cycles per degree. Recently, Chung and Legge (2016) compared the contrast sensitivity functions (CSFs) in normally-sighted and low-vision subjects. They report that the CSFs in low-vision subjects can be approximated by the CSF from normally-sighted subjects that is shifted along both the log-spatial frequency and log-contrast sensitivity axes. The shifting accounts for the impaired acuity and contrast sensitivity of the low-vision subjects. As a last comment on contrast and reading, Seiple, Holopigian, Szlyk, & Greenstein (1995) investigated the impact of random element loss on supra-threshold letter identification and reported that at higher levels of element dropout reduced luminance and contrast can combine to decrease the accuracy of letter identification. Extending these results to subjects with CFL, if the PRL has considerable loses in sensitivity (akin to random element loss) along with a co-existing impairment of contrast sensitivity, letter identification and hence reading would be expected to be impacted negatively. Recently Winther & Frisen (2015) reported that

rarebit testing using receptive field-size microdots can reveal 'hidden' deficits in macular disease. Specifically, the subjects with AMD required a higher number of rarebit elements per character segment to identify digits that were ~20/200 in size.

3.1.5 Micro-perimetry

The problems of testing patients with variable and often non-central fixation are minimized by the Nidek MP-1 micro-perimeter, which can compensate largely for fixational eye movements and present targets reliably to specific regions of the retina, such that retinal sensitivity changes can be followed over the course of the disease and its treatment (Midena, Radin, & Convento, 2006). Micro-perimeters have been used increasingly in the recent past to assess a variety of retinal conditions, including AMD. Dinc, Yenerel, Gorgun, & Oncel (2008) concluded that micro-perimetry is a safe, non-invasive diagnostic procedure that is effective in detecting early function loss in the macula of subjects with AMD. Because much of the inherent fixation instability of eyes with AMD can be compensated by the instrument, the results are expected to be more reliable than those of conventional perimetry (Midena et al., 2006). Hartmann et al. (2011) used scanning-laser-ophthalmoscope-based microperimetry to assess sensitivity over drusen in a cohort of dry AMD subjects. They reported good correlation between drusen volume and retinal sensitivity. White-yellowish fish-tail like spots (flecks) are usually noted in STGD and Verdina et al. (2012) reported that the hyper-AF flecks are associated with a significant reduction of visual sensitivity (in MP-1 testing) and alteration of the photoreceptor layer in OCT imaging. Several other groups investigated sensitivity in eyes with AMD in retinal

regions with pigmentary changes, drusen, and with demonstrated abnormal AF, but the crucial region around PRL has not received sufficient attention (Iwama et al., 2010; Edoardo Midena et al., 2007; Rogala et al., 2015; Sulzbacher et al., 2012; Yehoshua & Rosenfeld, 2012).

3.1.6 Structural Imaging of the Retina

High resolution tomographic imaging of the macula has been shown to provide crucial details for diagnosing, monitoring and managing many central retinal disorders including macular degeneration. Specifically, Yehoshua & Rosenfeld (2012) emphasized the utility of Spectral Domain Optical Coherence Tomography (SD-OCT) in imaging both drusen and geographic atrophy, the two classic retinal features of a dry AMD. The robust algorithms included for the analysis of OCT images provide an option for reliably quantifying the volume and area of these retinal changes. Morphologic alterations of the retinal pigment epithelium (RPE) and other outer retinal layers can be determined by SD-OCT and several studies in the past decade have documented these alterations (Acton, Theodore Smith, Hood, & Greenstein, 2012; Fleckenstein et al., 2008; Schuman et al., 2009; Sulzbacher et al., 2012). Outer retinal layer changes, like distinct thickening of the external limiting membrane and accumulation of reflective deposits in the outer nuclear layer (Lee et al., 2014), have also been documented in STGD. In a cohort of subjects with retinal degeneration caused by ABCA4 mutation, Huang et al (2014) reported that extensive thinning of the photoreceptor layer can be associated with inner retinal changes like thickening of the inner nuclear layer, perhaps due to retinal remodeling.

Many of the studies cited above employed different segmentation techniques, including manual segmentation, to mark the boundaries of desired retinal layers. Some of the most commonly reported automated segmentation techniques use the shortest-path approach based on graph theory (Chiu et al., 2012; Garvin et al., 2009). Although some segmentation algorithms are available for free download and limited use (Human and Murine Retinal OCT Analysis and Display. (September 2014). Retrieved from https://www.iibi.uiowa.edu/content/iowa-reference-algorithms-human-and-murine-oct-retinal-layer-analysis-and-display), we chose to segment the retinal layers manually in the study described here. This was primarily because of the diverse changes that are seen in the retinas of CFL subjects and the greater accuracy that can be achieved by manual segmentation in the presence of pathologies. Manual segmentation was feasible because the number of OCT scans that was segmented was relatively small (~10-30 scans per subject).

Landa, Su, Garcia, Seiple, & Rosen (2011) showed that the retinal sensitivities assessed by microperimetry correlated well with the integrity of the IS-OS junctional layer in both dry and wet forms of AMD. Acton et al. (2012) reported significant thinning of the photoreceptor layer and thickening of the RPE that was associated with visual field defects found during 10-2 testing using a MP-1 in a cohort of subjects with early AMD. However, the studies in the literature don't probe the region of PRL locally. Conventional visual-field testing has a sampling density of 2 deg, whereas the region of PRL is often <2deg wide (mean = 0.66 deg to 1.24 deg, calculated as the circle diameter from reported BCEA values

of 0.08 log deg^2 for word fixation (Bedell et al., 2015) and 3.09 log arc min^2 for fixation on faces (Seiple, Rosen, & Garcia, 2013)).

Although not strictly a structural assessment, many investigators in the past decade have documented a wide spectrum of changes in the AF patterns of patients with CFL. Bindewald et al. (2005) classified AF changes in AMD subjects into 8 phenotypic patterns including focal, reticular and speckled patterns. They also discussed the poor correlation of AF changes with visible fundus lesions. Nevertheless, the origin of AF is thought to be due to lipofuscin (LF) in the RPE which, when accumulated in excess, can damage both the RPE and nearby retinal cells (Dorey, Wu, Ebenstein, Garsd, & Weiter, 1989). In a seminal study, Dorey et al. (1989) counted the numbers of RPE and photoreceptor cells and measured LF fluorescence (at 470 nm, with excitation at 365nm) at 6 sites in the central and peripheral retina. They reported that the number of photoreceptors per RPE cell was higher where LF levels were elevated. They supposed that increased LF levels (due to factors including environmental and genetic, as in STGD) may increase the risk of degeneration of RPE and/or photoreceptor cells. Lastly, Smith et al. (2006) reported that a focal increase in AF co-localized with soft drusen and areas of hyper pigmentation in subjects with early AMD. On the other hand, in eyes with advanced atrophic AMD, the increased AF was dispersed and was noted in areas adjacent to drusen or GA.

3.1.7 Why Probe the Local Changes at the PRL?

The visual span is the region around fixation within which characters of given size can be resolved (Dockeray, 1910; Legge, Ahn, Klitz, & Luebker, 1997; Legge, Mansfield,

& Chung, 2001). Beyond the boundary dictated by the visual span (usually specified as a number of letters and dependent on letter size and presentation type) letters are no longer recognizable. In the retinal periphery, the visual span is reduced jointly by a decrease in visual acuity (so that letters need to be larger to resolvable) and an increase in crowding (Legge et al., 2001). The perceptual span, which is usually bigger than the visual span, can extend up to 5 deg in the reading direction during a fixation (Trauzettel-Klosinski, 2011). Thus, if the PRL is surrounded by areas of micro-scotoma then, not only is the available visual field reduced, but the extension of the perceptual span in the direction of reading may be reduced or nullified. These considerations provide the rationale for probing visual sensitivity specifically in the vicinity of the PRL. It is worth noting that in this study we probed only the region of the PRL (~1 - 3°) for sensitivity changes and so have no evidence whether the losses in sensitivity are sufficiently widespread to extend beyond the PRL (i.e., to include the perceptual span region). Nevertheless, in the next chapter on reading with simulated scotomas we demonstrate the impact of random element deletions, for words that occupy wider regions in peripheral retina.

When text is obscured partially by one or more micro-scotomas, an obvious reaction is to shift the text to another retinal region. If a patient's PRL is known to include areas of reduced sensitivity (micro-scotomas), then training to use a different PRL, where sensitivity is more homogeneous, may be fruitful. In subjects with macular degeneration, Cheong et al. (2007) documented longer temporal thresholds for letter recognition than age-matched controls at the same retinal eccentricity. They ruled out crowding as a contributing factor and suggested that this deficit is secondary to distortions of the sampled

image that result from concomitant pathology in the peripheral retina and/or to fixation instability. As indicated briefly above, SD-OCT imaging studies have provided crucial insights in various forms and stages of AMD and juvenile macular degeneration. The current study aims to relate the outer retinal structure to local sensitivity losses and is expected to provide better understanding of the characteristics of a critical region of the retina - the fixation PRL.

Documenting and relating SD-OCT changes around the PRL to retinal sensitivity as determined perimetrically is pivotal because SD-OCT is a lot quicker to perform than microperimetry and could therefore serve as a surrogate indicator for designating an appropriate PRL for visual rehabilitation. We propose to detect regions of reduced sensitivity (i.e., micro-scotomas - MSs) in the vicinity of the PRL in subjects with bilateral central field loss, and relate them to structural abnormalities in the same retinal region, as revealed by SD-OCT imaging. Mapping the MSs of subjects with AMD is expected to benefit visual rehabilitation, as patients can be trained to use an area of non-central retina (Shima et al., 2010) with few or no MSs as the PRL for essential visual tasks like reading and facial recognition.

3.2 Methods

Twenty-nine subjects (Age range: 17-89 years, Median: 57 years, See **Table 3-1**) with bilateral CFL due to conditions like age-related macular degeneration, Stargardt disease, cone dystrophy etc. were recruited from the Center for Sight Enhancement at the University Eye Institute, University of Houston. The study protocol was reviewed by the

Committee for the Protection of Human Subjects at the University of Houston and all the subjects provided written informed consent (or assent along with parental consent) before participating. Subjects were compensated in part for their time and participation. Most of the testing and all the outcome measures reported in this study are for the eye with better corrected distance visual acuity (BCVA) or for the preferred eye (determined as the eye that subjects didn't close when asked to close one eye) if acuity in the two eyes was equal. During testing, the non-participating eye was occluded with an eye patch. A NIDEK MP-1 microperimeter (S/W Version: 1.7, NIDEK Inc., Padova, Italy) was used both to assess fixation and for visual-field testing. Except for a reading assessment that was performed using MNRead charts *(*Lighthouse Low Vision Products*)*, all testing on both study visits was done after pupillary dilation using 1% Tropicamide and/or 2.5% Phyenylephrine. The two study visits were at least a week (Range: 1-27 weeks) apart. Details regarding the various test procedures are given below, in the order of testing.

3.2.1 Reading Assessment

Hand-held MNRead charts (Charts 1 and 3, Precision Vision, IL) with black text printed on a uniform white background were held by an examiner in front of the subject's tested eye at the preferred test distance (the distance at which the chart title was clear to the subject with their near prescription, if any; range: 16-40 cm) and viewing angle. Each chart has a total of 19 sentences (acuity range: 1.3 to -0.5 logMAR when tested at 40 cm) and each sentence comprises 60 characters printed in 3 lines. The test required 2 examiners. Examiner 1 had the scoring key to evaluate reading accuracy and a stopwatch

to record the time taken (in seconds) to read each sentence. Examiner 2 was responsible for holding the chart at the appropriate distance and position. The subjects always read from chart 1 first and the sentence to be tested, as well as all smaller sentences, were covered with a sheet of blank paper until examiner 1 instructed the other to reveal it. The uncovering of each sentence as the subjects read eliminated any preview benefit and reduced the possibility of confusion. Subjects were repeatedly encouraged to correct any errors and guess the words when necessary. It was stressed that both speed and accuracy were important. Testing began after confirming the chart was evenly illuminated ($L_{Avg} \approx$ 63 cd/m^2) by normal overhead room illumination. Subjects wore their habitual near correction, if any, or a +2.50D near addition (stronger additions for closer distances) and read the sentences aloud. The reading acuity (RA) in logMAR was determined from the number of sentences ('Sentences' in the formula below) that could be read without making significant errors (MNRead brochure, Light house). When necessary, the RA was corrected for reading at a non-standard viewing distance and for missed words. The critical print size (CPS, in logMAR) was calculated as the smallest print that could be read at maximum speed, also accounting for a non-standard reading distance when applicable. The assessment was repeated immediately using a second MNRead chart and the reported RA, CPS and maximum reading speed (in words per minute, WPM) are the average of the 2 recordings. The reading speed and RA were calculated as:

$$Reading\ Speed\ (WPM)$$

$$= \frac{60 \times (10 - Number\ of\ Words\ Missed)}{Time\ taken\ (in\ \ s)}$$

$$Reading\ Acuity\ (RA)$$

$$= 1.4 - (Sentences\ \times 0.1) - (errors\ \times 0.01)$$

S. NO	Subject Code	Diagnosis	Age (Years)	Gender	Follow up Time (Weeks)
1	S1	AMD	68	M	20.1
2	S2	AMD	77	M	1.4
3	S3	STGD	50	M	2.4
4	S4	STGD	20	M	2.0
5	S5	Cone Rod Dystrophy	56	F	6.3
6	S6	STGD	32	M	7.9
7	S7	Plaquenil Maculopathy	63	F	4.0
8	S8	Cone Rod Dystrophy	44	M	1.0
9	S9	STGD	30	F	1.0
10	S10	AMD	69	M	7.6
11	S11	Macular Hole	84	F	2.6
12	S12	STGD	45	F	10.0
13	S14	STGD	31	M	1.0
14	S15	STGD	37	F	7.7

15	S16	AMD	85	F	3.3
16	S18	STGD	42	F	27.7
17	S19	AMD	73	M	2.3
18	S20	Plaquenil Maculopathy	62	F	4.7
19	S22	STGD	57	F	13.6
20	S23	AMD	89	F	7.1
21	S25	Myopic Macular Degeneration	57	F	1.0
22	S26	STGD	50	F	4.1
23	S27	AMD	88	M	2.0
24	S28	AMD	78	F	5.3
25	S29	AMD	80	M	1.0
26	S30	STGD	58	F	4.7
27	S31	STGD	17	M	2.3
28	S32	AMD	76	M	0.9
29	S33	Cone Dystrophy	39	F	0.1
		Median	**57**	**Min.**	**0.1**
		Mean	**57.1**	**Max.**	**27.7**
		SD	**20.8**		

Table 3-1 Demographics of Subjects

Details and demographics of all 29 (16 females) study subjects. AMD is age-related macular degeneration and STGD is Stargardt disease. The age of the subject on the first visit is reported here. Four more subjects were able to make it only for the first study visit

and hence did not complete the study. None of the findings from those 4 subjects are reported.

3.2.2 Freiburg Visual Acuity Testing (FrACT) - Contrast

"FrACT" is a computer based program that uses a psychometric method (bracketing threshold strategy, in this study) combined with anti-aliasing and dithering to provide automated, self-paced measurement of visual acuity, contrast sensitivity and Vernier acuity (Bach, 1996). The program is available as freeware (Freiburg Vision Test ('FrACT'), by Prof. Michael Bach. (February 2016), Retrieved from http://www.michaelbach.de/fract/index.html) and has been widely used in the vision science literature (Mcculloch et al., 2011; Plank et al., 2014). FrACT software (Ver. 3.9) was installed on a personal laptop (Thinkpad Edge 14", Intel HD Graphics) and the LCD display was gamma corrected using a Minolta LS-100 photometer (See **Appendix 6.1** for more details). FrACT contrast testing was performed under standard room illumination. The subject sat at 50 cm with the test eye aligned (other eye patched) to the center of the display. The task was to report the orientation of single Landolt C (sized either 50 or 100 arc min ≈ 20/200 or 20/400) that appeared at the center of the display with a fixed size but a contrast that varied from trial to trial. The default size of the Landolt C was 20/200 (which is larger than BCVA for most subjects) and was increased to 20/400 only when the former size was not recognizable at high contrast. Subjects were encouraged to adopt their preferred eye and head positions and report the orientation of the C within the 30 s duration

of each trial. If the subject did not respond within 30 s, the C disappeared from the screen and the program recorded the response as incorrect. The subject's response was registered by the examiner using the keyboard arrow keys and an auditory beep provided immediate feedback about the correctness of each response. The values reported in this study are the average of the Weber threshold contrasts, obtained on 2 successive sessions of 24 trials each.

3.2.3 Fixation Testing

The word-fixation PRL for a 3-letter word sized at each subject's CPS (based on the outcome of MN Read testing) was assessed using a Nidek MP-1 microperimeter. Subjects were instructed to use their preferred eye and viewing position to a) ensure that the whole word was visible and clear and if so b) fixate at the central letter of a 3-letter word (See **Figure 3-1**) presented on the uniform white background of the MP-1's LCD display. These instructions were repeated continuously during the fixation assessment. Note that in spite of the repeated instructions the subjects could potentially fixate at other locations, such as the top (and not center) of the middle letter or on the last letter. Unfortunately, there is no way to confirm where the subjects were really looking. However, for the accurate estimation of the PRL, it is crucial that subjects were looking at the desired portion of the relatively large fixation targets.

A reference infrared (IR) illuminated image was captured by the built-in IR sensitive camera (768 x 576 pixels) of the MP-1 at the start of the fixation testing. The examiner then selected a feature-rich region of interest (ROI, 128 x 128 pixels), such as a

blood vessel crossing or part of the disc/atrophy margin on the frozen reference image. The ROI was tracked at a sampling rate of 25 Hz (40 ms) during the fixation testing. The MP-1 first referenced the center of the fixation target to the top-left corner of the reference IR-image and after the start of the live fixation recording, the coordinates of the center of the fixation target were computed (once every 40ms) based on the X and Y shifts of the selected ROI. Fixation was usually recorded for a duration of approximately 30 seconds (Range: 12-55 Seconds). Three assessments of fixation were obtained successively and the fixation files were exported to compute the bivariate contour ellipse area (BCEA). The latter was calculated, after filtering outliers (±3 SD, to eliminate data points potentially collected when MP-1 lost tracking of the ROI or from periods before and after blinking), using the following formula (Timberlake 2005):

$$\text{BCEA} = \pi \, \chi^2 \, \sigma_x \, \sigma_y \sqrt{(1 - \rho^2)}$$

where, χ^2 is the value of the chi-square distribution with 2 degrees of freedom for a probability of 68, 95 or 99% (corresponding to ±1, ±2 or ±3 SDs), σ_x, σ_y are the standard deviations of the distribution of fixation positions in the X and Y meridians, and ρ is the Pearson correlation coefficient between the set of recorded X and Y values. The MP-1's exported fixation file provides a degrees-to-pixel conversion factor (1° ≈ 15.19 pixels) and the X and Y coordinates (in deg, referenced to the top-left corner of the 768 x 576 pixel IR image) of the retinal locations at which the center of the fixation target was imaged during each fixation sample. BCEA values that were computed offline using a custom MATLAB

(R2007a/R2014a - MathWorks, Natick, MA) program agreed well with the values returned by the MP-1's software.

The datum recorded for each subject's median BCEA from the three successive fixation tests and the retinal region corresponding to this contour ellipse were used to perform sensitivity screening on the second study visit. During fixation testing, a transparent plastic sheet was placed over the output display of the MP-1 and the locations of the word-fixation PRL as well as retinal features like blood vessels and the margins of the optic disc and macular scar were marked. This transparency was used during the second study visit to help center the test grid at the location of the PRL.

The repeatability of positioning the test array using the transparency was assessed by placing a 9x9 test grid, 6 times at an IR image location designated as the word-fixation PRL. Based on the transparencies that had the PRL marking of 4 CVL subjects (S18,19,22 and 28), the grids were centered on a standard IR image that was captured with lens cap on and without positioning any subject in front of eyepiece. The average of the SD's of the X and Y locations of the center of the grid was: ~ 1.1 pixel (range: 0.52 - 1.64).

Eccentricity of the PRL: The distance of the center of the PRL with median BCEA from the center of the optic disc was measured using the overlay grid option of the MP-1. The MP-1 overlays a circular grid centered on the PRL center, and two experimenters (HEB and AKK) marked the mutually agreed location of optic disc center on the MP-1's computer display. A ruler was then placed vertically and horizontally from the marked disc center to read the eccentricity of the disc center from the center of the PRL. Using the

reported normative values of the foveal center from the center of the optic disc (15.5° temporal and 1.5° inferior from the optic disc center, according to Rohrschneider at al., 2004), and the Pythagorean theorem, the radial eccentricity of the PRL (in degrees) from presumed foveal location was calculated.

3.2.4 Central Visual Field Testing

After fixation testing, central retinal sensitivity in the better (test) eye of each subject was assessed using a standard Humphrey 10-2 grid (68 points, 2° apart, 4-2-1 thresholding). Goldmann size II spots (square of nominal side 13 arc min) with a luminance ranging from 0 to 20 dB (127 to 2.54 cd/m^2) were presented on a white background of 1.27 cd/m^2 (4 apostilbs). Subjects were instructed regarding the test procedures, method of responding, and the need to maintain stable fixation on the fixation target (1-3° red cross). Testing began after the subjects had adapted for at least 15 minutes to the dimly lit examination room, as performed in other studies (Longhin et al., 2013; Midena, Vujosevic, & Cavarzeran, 2010). After ensuring adequate pupillary dilation, the MP-1 was positioned to provide the best focused and uniformly illuminated IR retinal image, after adjusting the IR power and internal refractive-error correction (when applicable). A retinal ROI (128 x 128 pixels) rich in details and with a ROI index of at least 2.5 (range in our subjects: 2.5 – 8.0) was chosen from an IR image that was frozen during fixation with the previously determined PRL. The MP-1 automatically centers the 10-2 test grid based on the subject's fixation locus during the initial few seconds (2-5 sec) of field testing. Consequently, the

center of the test grid need not coincide exactly with the word-fixation PRL that was documented during fixation testing.

Field testing usually required 10-30 minutes to complete, including rest breaks. The MP-1 provides an option to automatically or manually register the IR-test image with a color fundus image (1392 x 1038 pixels) that can be acquired at the end of the field testing (See **Figure 3-1**). This proprietary automatic registration appears to be based on a cross-correlation technique and requires the selection of 2 feature-rich ROIs in both the IR and color fundus images. Automatic image registration was attempted in all subjects; if the automatic registration procedure failed then a manual registration (which required manual marking of 2 retinal landmarks) was performed. The word-fixation PRL was located in the registered color fundus image and the median sensitivity of the 4 – 6 test locations surrounding the PRL was used to determine the luminance of the supra-threshold screening targets described in the next section. The 10-2 testing confirmed the presence of CFL in the test eye of each subject included in the study.

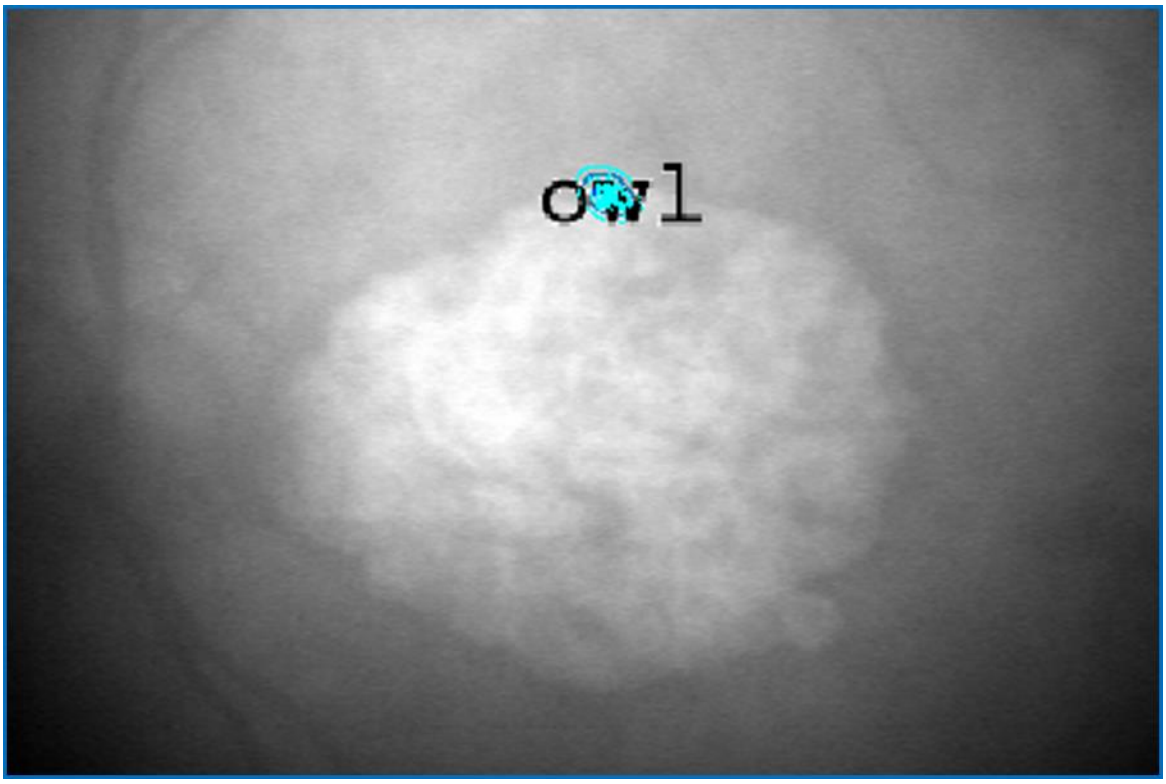
owl

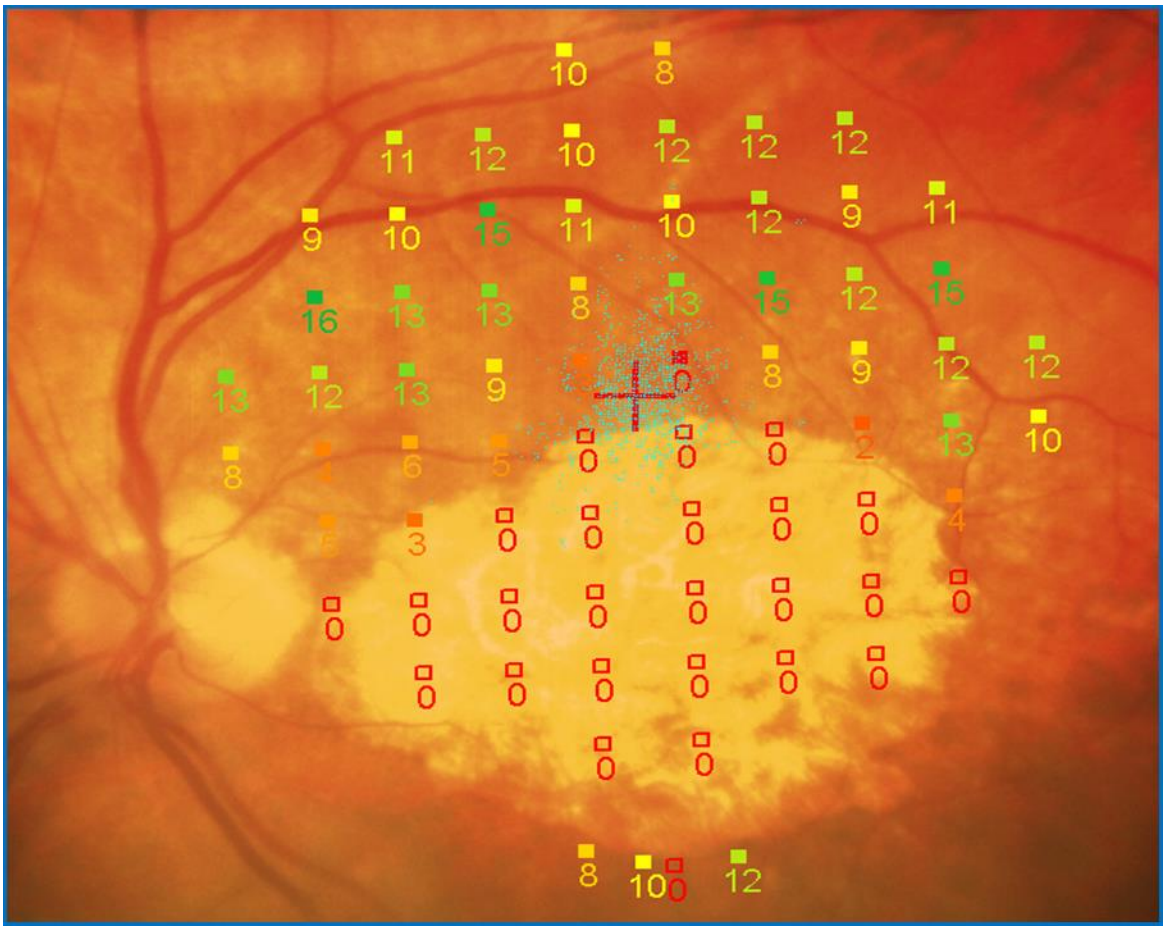

Figure 3-1 Fixation and 10-2 Testing with MP-1

Fixation testing (IR image on the top) to determine the word-fixation PRL and the 10-2 perimetric testing (color fundus image on the bottom) for the same subject S10.

Note that in the top image, the word is flipped vertically (in the retinal view, the word would be inverted) to illustrate the field view. The word-fixation PRL (enclosed by the 3SD cyan BCE in the IR-image), roughly coincides in location with the cross-fixation PRL (center of the cloud of cyan dots) during perimetric testing in this subject with AMD.

It is paradoxical that some subjects in our study (like S10) chose to position the

word at a retinal location with a surrounding sensitivity of 0dB. A possible explanation is that the large high-contrast words are more visible than the small 0dB test spots due to spatial summation. Also, it should be noted that the 0dB in MP-1 is 400 asb (127 cd/m^2) and is therefore not as bright as targets presented in the Humphrey visual field analyzer with 0db = 10,000 asb (3185 cd/m^2).

Aside from the standard 68 test locations that comprise the 10-2 grid, the MP-1 allows testing of more locations (like 4 locations near the bottom edge of the atrophic region) at the end of testing. Greater scatter of the fixation dots in the color fundus image than in the IR image is attributed to the substantially longer duration of perimetric testing than word fixation (Longhin et al., 2013).

A screening test (6 x 6° grid, 36 locations 1° apart) with 0 dB spots was implemented on the second study visit to confirm the presence of CFL in the non-tested (worse) eye. This testing revealed that all of our subjects had a region of 'absolute' scotoma in the non-preferred eye.

3.2.5 Supra-threshold Sensitivity Screening

Supra-threshold screening to detect micro-scotomas (MSs) was performed using Goldmann size II targets (13 arc min nominal, maximum L_{Spot} =127 cd/m^2, L_{BG} = 1.27 cd/m^2) with a center-to-center spacing of either 12 or 18 arc min (0.2 or 0.3 deg) in a grid region centered on the word-fixation PRL (See **Figure 3-2**). We prefer to refer the regions within the PRL at which test spots were consistently not detected as a 'micro-scotomas' a)

as the Goldmann size II spots that we employed are half the diameter of the conventional size III (26 arc min) spots and b) because of the high sampling density that was used. A custom MATLAB code was used to densely sample sensitivity within the word-fixation PRL (number of locations range: 23-94). The sampling density (0.2 or 0.3 deg center-to-center) and size of the ellipse (1 or 2SD) sampled was chosen so as to minimize the overall test duration (usually 10-20 min) and, hence, avoid fatigue. Thus, the supra-threshold screening grid used for each subject was unique. The grid was manually positioned to span the word-fixation PRL, using the landmarks recorded on the plastic transparency during visit 1 as a guide. The grid pattern was designed using the 'pattern editor' option of the MP-1 and, in separate screening tests, the luminance of the test spots was set to one of 2 luminance levels.

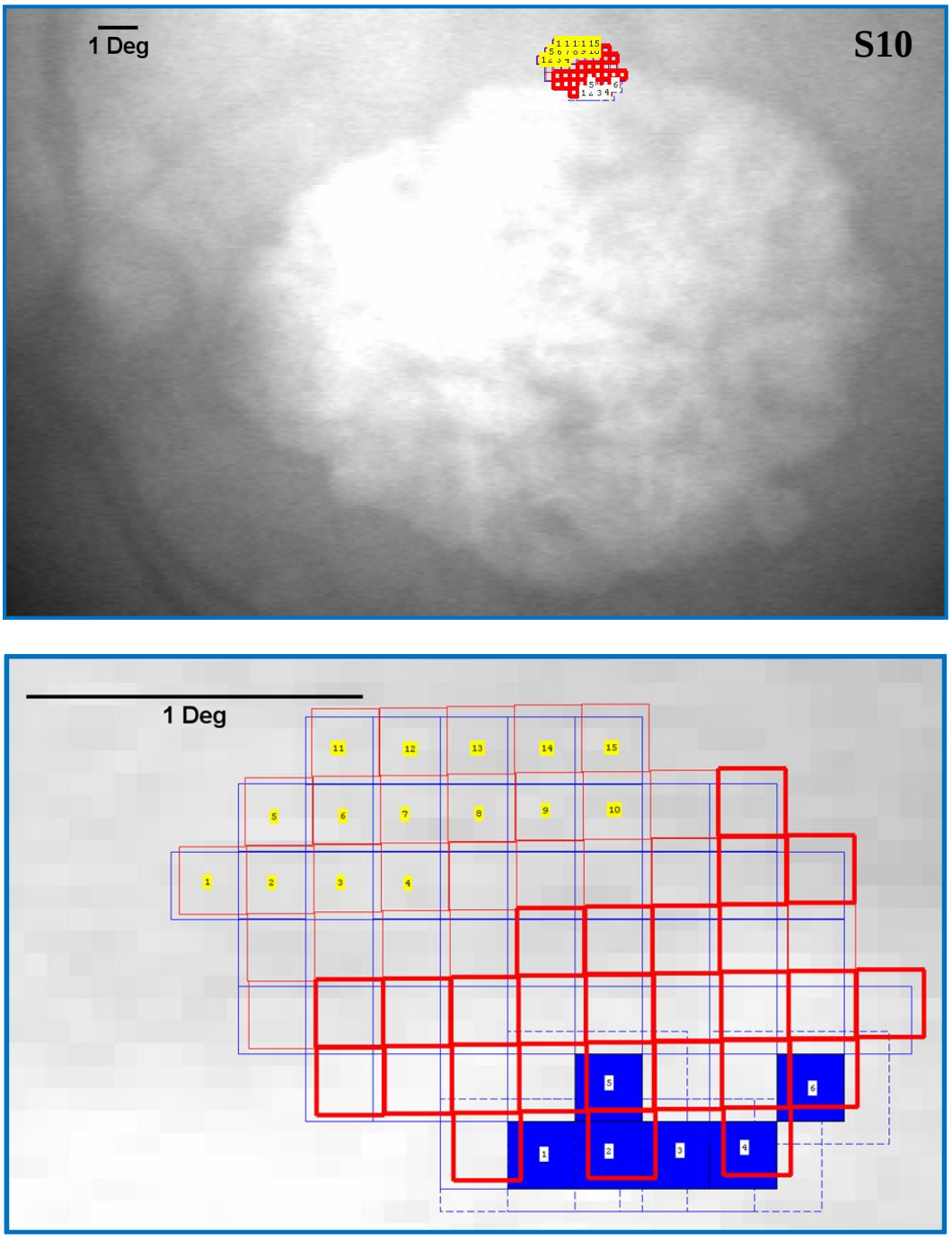

Figure 3-2 Screening the Word-Fixation PRL

The supra-threshold screening of the word-fixation PRL in subject S10. The customized grid that was centered on the word-fixation PRL (top image) is zoomed to show the details (bottom image). In the zoomed image, the blue unfilled squares are from test 1 (Filled blue squares are the locations of test spots not detected on test 1, shown along with 8x5 pixel overlap regions - blue dashed lines) and the red unfilled squares are from test 2 (thick red squares are the locations of test spots not detected on test 2). There were 6 MSs, defined as overlapping locations at which a test spot was detected on neither test 1 or test 2 (labeled 1-6 in the bottom panel) and 15 locations that were labeled nonMSs (overlapping locations at which test spots were detected on both test 1 and test 2, labeled in yellow) in this subject.

All subjects were screened using the brightest (0 dB) test spots available and locations at which these 0 dB targets were not detected were designated 'absolute scotomas.' 'Step size' is an option that the MP-1 provides for 'semi-automatic' testing and all the testing reported here for supra-threshold screening was done using this option. Step size dictates the subsequent stimulus luminance when a test spot of the initial luminance value is seen by the subject. For example, if the observer detected a test spot that was initially 0 dB and the step size was 5 dB, the luminance of the next stimulus presented to the same retinal location would be +5 dB, and so on. If 10-2 central-field testing indicated that the median sensitivity (of 4 or 6 locations) around the PRL was ≥8 dB, test spots of a second, lower luminance level (5 dB brighter than median sensitivity; maximum luminance

= 3 dB; range across subjects: 3-7 dB) was chosen to screen the PRL for 'relative' scotomas. For example, if 10-2 testing revealed a median sensitivity around the PRL of 12 dB, then the lower luminance level used to probe for 'relative' scotomas was 12 - 5 = 7 dB (Also see **Appendix 6.18**). However, only the retinal locations with 'absolute' scotomas (0 dB test spot not seen) were included in the analysis to relate functional and structural changes within the PRL. This is primarily because the sensitivity measured at the PRL was not high enough in all subjects for 'relative' scotomas to be assessed. Irrespective of the number of luminance levels tested, testing at each test-spot luminance was repeated at each grid location once using the 'follow-up' test option of MP-1.

Follow-up testing immediately followed the initial, baseline testing. Before a follow-up test begins, the MP-1 requires the examiner to select 2 ROIs in the retinal image captured during the second (follow-up) screening test. The MP-1 uses these ROIs to register the IR image pairs from the initial and follow-up testing automatically. Unlike the registration of the IR and color image pair following 10-2 testing, automatic registration of the IR image pairs from the initial and follow-up tests never failed. Following IR-to-IR image registration, the MP-1 automatically placed the supra-threshold grid at the same retinal location as during the initial test. The registration accuracy of the MP-1 for follow-up testing was evaluated and reported previously (CHAPTER II) to be within ~2 pixels in subjects with CFL when using a medium level of IR intensity to illuminate the fundus.

3.2.6 Image Registration: IR-MP-1 Images

A Generalized Dual Boot strap – Iterative Closest Point (GDB-ICP, Yang et al., 2007) algorithm was used offline to register IR image pairs, and the retinal locations of the first and second supra-threshold screening grids, during baseline and follow-up testing. Briefly, the GDB-ICP extracts and matches key points to create a local transformation, which expands progressively to include the entire overlap region between images. This method of offline registration is different and is more computationally intensive than the in-built ROI-based registration of the MP-1. The accuracy of the algorithm-based registration was confirmed visually by observing minimum flicker when the two images were alternated rapidly. The 2-D affine coefficients returned by the GDB-ICP algorithm were used to transform and re-plot the locations of the test points during follow-up testing onto the baseline IR image. (See Figure 3-2– zoomed IR images). A rectangular overlap region (8 x 5 pixels, determined from the mean ± SD registration error, CHAPTER II (Also see **Appendix 6.2**)), was drawn around each 'absolute' scotoma (0 dB test spot not seen) that was found during baseline testing. An 'absolute' scotoma detected during follow-up testing was considered to overlap with a baseline scotoma if the follow-up scotoma fell within the rectangular region of overlap. Only those locations that had overlapping 'absolute' MSs (0 dB not seen on both baseline and follow-up tests) and regions that demonstrated no MS on both tests were used in the analysis to relate functional sensitivity results to structural changes in the outer retina.

3.2.7 Reading Assessment within the MP-1

Calibration of Sentences: A corpus of 40 MNRead like sentences (provided by Drs. S. Mansfeld and G. Legge) were constructed in 4 lines each of 14-point Courier font using Photoshop (CS6, Adobe Systems Inc. San Jose, CA). Black letters on a white background were designed on a 640 x 480-pixel canvas (matching the resolution of LCD display of the MP-1), saved as bitmap (.bmp) images, and later uploaded to the MP-1 system.

To calibrate the letter size of the text presented in the MP-1, a mirror inclined at a 45° angle was used to present the reflected image of a laptop screen at an optical distance of 114 cm to the left eye of 2 subjects with normal vision. The laptop displayed a black lowercase 'x' rendered in Courier font on a white background, using the MS-Word (Microsoft, Redmond, WA) program. Black-on-white MNRead-like sentences were viewed simultaneously by the right eye on the LCD screen of the Nidek MP-1. The x-height of the character viewed by the left eye was then adjusted by changing the font size in MS Word until the observer reported equal letter heights. This dichoptic image-size matching was done with natural pupils, in a dimly-lit room. This step allowed us to obtain a relation between the Courier font sizes in point notation (both in Photoshop and MS Word) and the x-height (expressed in logMAR) of the text displayed on the MP-1's LCD display. Using this relation, 5 sets of 8 sentences with font sizes ranging from 1.3 to 0.6 logMAR (20/400 - 20/80) were designed in Photoshop and imported to the MP-1.

The accuracy of calibration was confirmed for all 8 sizes of sentences, again using dichoptic image size matching by the same 2 subjects. The lower acuity limit (≈20/80) of

the sentences that can be displayed within the MP-1 is contingent on the resolution of the LCD display. We refer to the calibrated MNRead like sentences that were displayed using the MP-1 as MP-1 Read sentences. The primary advantage of using the MP-1 for reading assessment is the opportunity to visualize the retinal region used for the reading task. The MP-1 provides an option to record the IR image during reading, but we chose not to record as our priority was to accurately measure MP-1 Read reading speed.

MP-1 Read Assessment: Reading assessment using MP-1 Read sentences was done in 26 of the 29 subjects after supra-threshold screening and after a couple of practice trials to demonstrate the reading task. As during MNRead testing, the instructions stressed that speed and accuracy were equally important and subjects were encouraged to correct any errors and guess at words when unsure. To begin each reading trial, the subject fixated on a cross target. After a ready signal from the subject, the fixation cross was replaced by a MP-1 Read sentence. Subjects read the sentences orally, with their chin resting on the MP-1 chinrest and made eye movements as necessary. A stopwatch recorded the time taken (in s) to read each sentence. Testing always began with a 20/400 sentence and each time the subject successfully read a sentence the font size was decreased. All the reading measures reported here are the average of 2 measurements using 2 randomly chosen sets of MP-1 Read sentences. The CPS and RA were calculated in the same way as during MNRead assessment, except that no correction for working distance was necessary and, for RA, there was no discounting for missed words. As during MNRead testing, the maximum reading speed was the best attainable reading speed.

3.2.8 Structural Imaging of the Retina

The structure of the outer retina was imaged using the high resolution (Axial resolution ~7µm optical) imaging capabilities of a Spectral-Domain Optical Coherence Tomography (SD-OCT, Spectralis HRA+OCT; Heidelberg Engineering, Heidelberg, Germany). Subjects were seated comfortably while chin and forehead rests stabilized the head. Subjects fixated (usually with their PRL) on a central bright spot and were encouraged to blink normally throughout the testing. A high-density (B-scans ~60µ apart) raster scan at the 'high-resolution' setting was used to image the central retinal region including the PRL and the atrophic macular region. The Automatic Real Time (ART) mode was turned on and a B-Scan averaging of 9 frames was used to enhance the signal-to-noise ratio of the OCT scans. When time permitted, fundus auto-fluorescence imaging (blue-FAF, $\lambda = 488$ nm) imaging was obtained after OCT imaging was completed. The Spectralis instrument provides an option to export '.vol' files containing all the scan details and images for further analysis. A custom MATLAB code was used to extract the B-Scans (496 x 768 or 496 x 1024 pixels), the high resolution confocal scanning laser ophthalmoscope (cSLO) image (1536 x 1536 pixels) and relevant scan details like scan start and end locations, pixel width and pixel height of both the OCT and the SLO image, and the distance between adjacent B-scans (all values in mm). The blue FAF images (1536 x 1536 pixels) were exported separately as a .png file.

Relating Function to Structure: The IR image coordinates of overlapping 'absolute' MS locations determined during baseline and follow-up testing were affine transformed to SLO

image coordinates using control-point tool matching in MATLAB. The latter involved manually marking 6 pairs of landmarks in each MP1 IR image and Spectralis SLO image. The landmarks usually selected were blood vessel crossings, regions of atrophy, and sections of the optic disc margin (See **Figure 3-3**). Like the IR-IR image pair registration for follow-up testing with the MP-1, the registration accuracy of the affine transformed MP-1 IR-image and the SLO image was always confirmed by alternatively flickering the image pairs. In addition, for a random subset of image pairs (4 pairs for IR-SLO and 4 other pairs for IR-IR follow-up testing registration) the registration accuracy was quantified using a psychophysical method of constant stimuli. A set of 7 known image offsets, ±2, 4, 6 and 0 pixels were used to introduce a horizontal or vertical shift in one of the registered image pairs and the author reported the perceived direction of image shift. Each image shift was presented multiple times, in random order. A cumulative Gaussian curve was fit using a curve-fitting program (Psych-Fit), which returned the slope and bias for the fit. After inspecting the fit, the absolute bias (in pixels) was converted to arc min using the appropriate degree-to-pixel conversion factors of 15.19 pixels/deg for MP-1 IR images and 51.2 pixels/deg for Spectralis SLO images. The variances of the bias for IR-IR and IR-SLO registration were respectively: 1.29 and 1.67 arc min^2 in the horizontal direction and 4.53 and 0.85 arc min^2 in the vertical direction. The variance from uncompensated fixational eye movements, (reported in Chapter 2 on the accuracy of compensation by the MP-1 for fixational eye movements in normally-sighted subjects) was 18.06 and 22.37 arc min, respectively, in the horizontal and vertical directions. By adding the 2 sources of variance, namely, the variability from uncompensated fixational eye movements and from

registration error, we calculated the effective target size of a 13 arc min, size II, spot, which represents our region of interest, to be approximately 17.4 arc mins (horizontally), or ≈14 pixels in the OCT image. (See **Appendix 6.5**)

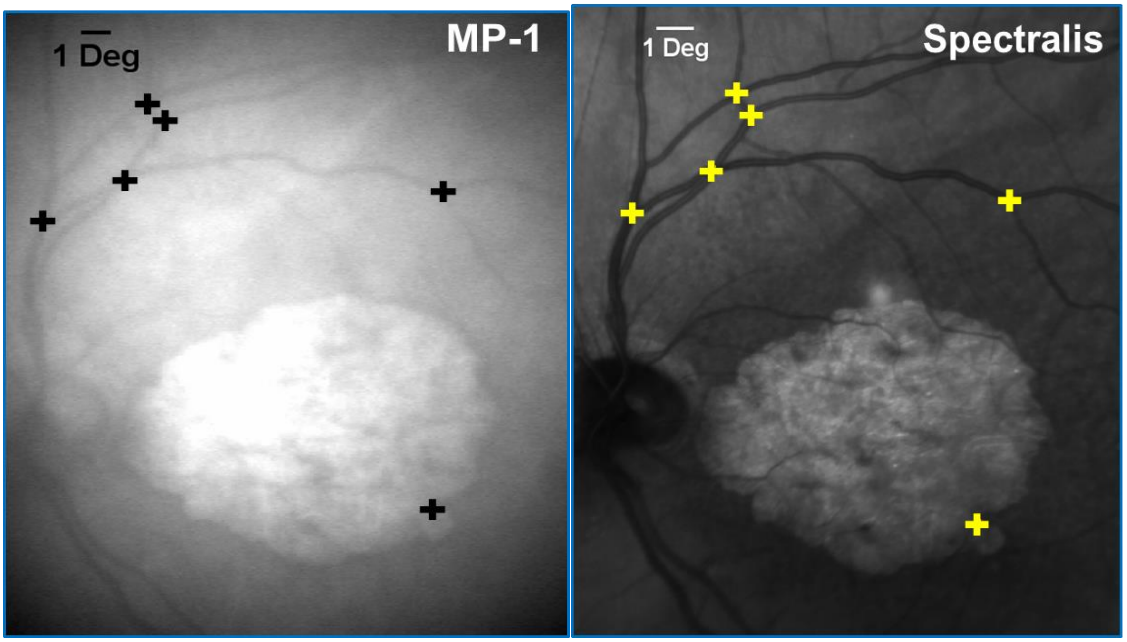

Figure 3-3 Image Registration Using 'Control point tool'

Registering the image pairs using MATLAB control point tool in subject S10 with AMD. Six corresponding retinal landmarks (like a vessel crossing, atrophy or disc margins) were manually marked. Cross marks shown on the IR-MP-1 image (left) and the cSLO Spectralis image (right) are enlarged for demonstration.

Manual Segmentation of Retinal Layers: All segmentation of the subjects' OCT images was done by one of the authors (AKK), using a custom MATLAB program originally

developed by Dr. Nimesh B. Patel for segmenting the inner retinal layers. Segmentation was performed using a personal laptop display (Lenovo Z70, Intel HD Graphics 5500/NVIDIA GeForce 840M) and an external mouse. A brief summary of the steps involved in the manual segmentation is provided here.

ROIs, 14 pixels wide, in each B-Scan of interest that either corresponded to a location with overlapping 'absolute' MSs (henceforth, 'MSlocn') or no MS on both supra-threshold screening tests (henceforth, 'nonMSlocn') were manually segmented. The steps involved in segmentation are listed here:

- The B-Scan image (496 x 154 pixels) was cropped to only include the 14-pixel ROI and a padding zone (5x ROI on each side). The padding zone helped the segmenter to get a better understanding of the overall contour of the retinal layers.
- When executed, the program presented both MSlocn and nonMSlocn scans from a given subject and hence they were segmented in the same session on the same day.
- No information regarding the subject or the origin of the scan (i.e., from a MS or non-MS location) was available to the segmenter.
- The segmenter manually traced the boundaries of 4 retinal layers, namely:
  1. The outer margin of the Retinal Pigment Epithelium – Bruch's Membrane complex (RPE – BM)
  2. The inner margin of the RPE

3. The inner margin of the Photoreceptor Nuclear layer or the Outer Nuclear layer (ONL)
4. The Internal Limiting Membrane (ILM)

- To begin marking a layer, the segmenter depressed the left mouse button and moved the cursor over the appropriate locations on the image. Tracking continued until the segmenter released the mouse button.
- A continuous line was drawn as the cursor moved over the screen. The segmenter could release the cursor at any time during active tracking and click at desired locations on the image to revise the marking.
- The segmentation always started with the junction between the RPE-BM (layer 1) and proceeded sequentially until the ILM (layer 4) was reached.
- When segmentation of all scans from a given subject was complete, the program returned three thickness (3x14 matrix) values namely: *RPE-BM, PL, and TR* (see formulas below).
- The average thickness over the 14-pixel ROI region (from the step above) was computed for all 3 layers (3x1 matrix) and for each scan (See **Appendix 6.4** and **Figure 3-4**).
- Then for each subject, the 3 layer thicknesses (in pixels) for all the scans corresponding to MSlocn and nonMSlocn were separately averaged and the ratios, average MSlocn thickness / average nonMSlocn thickness, were calculated. It should be noted that the

numbers of MSlocn and nonMSlocn for a given subject were not necessarily similar (see **Table 3-3).**

$$RPE\ Thickness\ (RPE - BM)$$
$$= RPE\ Outer\ Margin\ (Layer\ 1) - RPE\ Innner\ Margin\ (Layer\ 2)$$

$$Overall\ Photoreceptor\ Layer\ Thickness\ (PL)$$
$$= RPE\ Inner\ Margin\ (Layer\ 2) - ONL\ Inner\ Margin\ (Layer\ 3)$$

$$Total\ Retinal\ Thickness\ (TR) = \ RPE\ Outer\ Margin\ (Layer\ 1) - ILM\ (Layer\ 4)$$

$$MS{:}\ NonMS\ Thickness\ Ratio\ for\ \boldsymbol{Each\ Subject}\ (RPE - BM\ , PL\ , TR\ )$$
$$= \frac{Average\ Thickness\ of\ a\ Layer\ from\ all\ \boldsymbol{MSlocn}\ scans}{Average\ Thickness\ of\ a\ Layer\ from\ all\ \boldsymbol{nonMSlocn}\ scans}$$

Rules for Segmentation: Initial ground rules for segmenting each layer were set and a subset (~5%) of the scans were segmented by the author (AKK). This initial segmentation was verified for accuracy by another experienced segmenter (NBP). The final segmentation of all ROIs began only after weeks of pilot segmentation. The outer margin of the RPE/BM (Layer 1) was always marked to include the BM complex, even at locations that had classic sub-RPE drusen or a pigment epithelial detachment (Refer to **Appendix 6.6**). Similarly, if the usually distinct hyper-reflective layer of the photoreceptor inner and outer segments was in contact with the RPE and could not be delineated, then marking of the inner margin of the RPE included this layer. Any drusen-like hyper reflective clumping/elevation was considered as a part of the RPE, as long as it was continuous and was attached to the RPE layer. There were instances when marking of the RPE margin was challenging, as when a

ROI was within an area of geographic atrophy where the RPE was very thin or non-existent, and the increased hyper reflectivity of choroid made the margin identification tricky. The segmenter marked any continuous hyper-reflective band of remnant pixels as RPE. The marking of the inner margin of the ONL (Layer 3, green trace in **Figure** 3-4) was toughest of all in our subjects and was usually guided by the boundaries of the hypo-reflective space of the nuclear layer. There were a wide variety of changes ranging from local thinning, indistinct margins, and accumulation of migrated RPE/drusenoid materials to the total absence of the ONL. When in doubt, the segmenter followed the contour of the RPE as a guide and any migrated RPE material was segmented to be within the PL boundary. Marking the ILM (Layer 4, purple trace) was straight forward. When an epi-retinal membrane was present, it was excluded as a part of the retina. (See **Appendix 6.6** for few representative examples of segmentation)

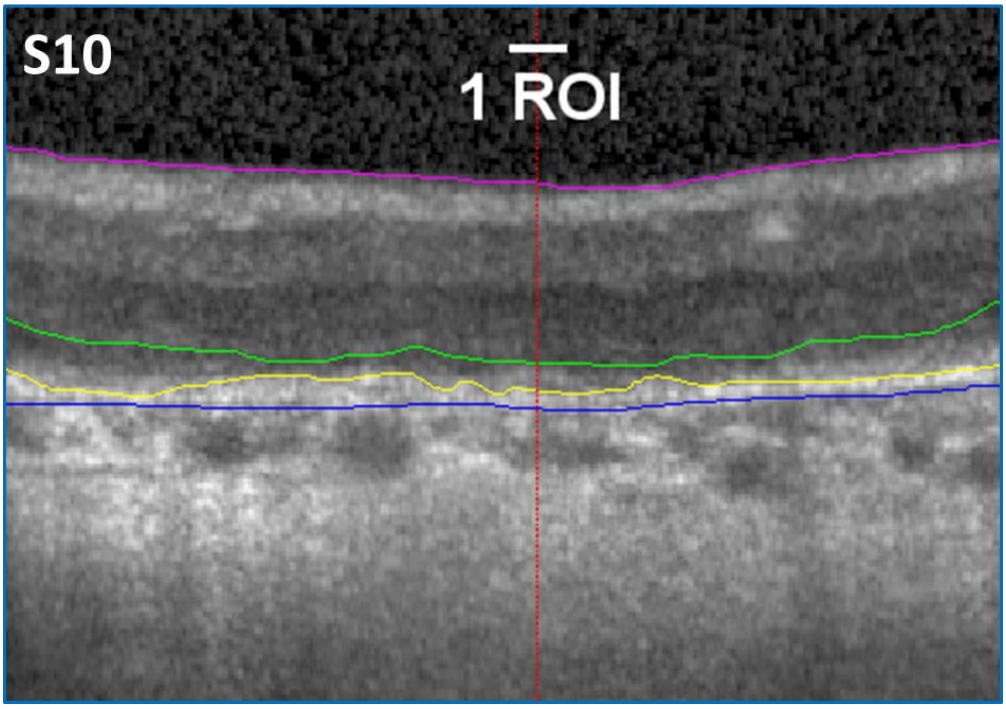

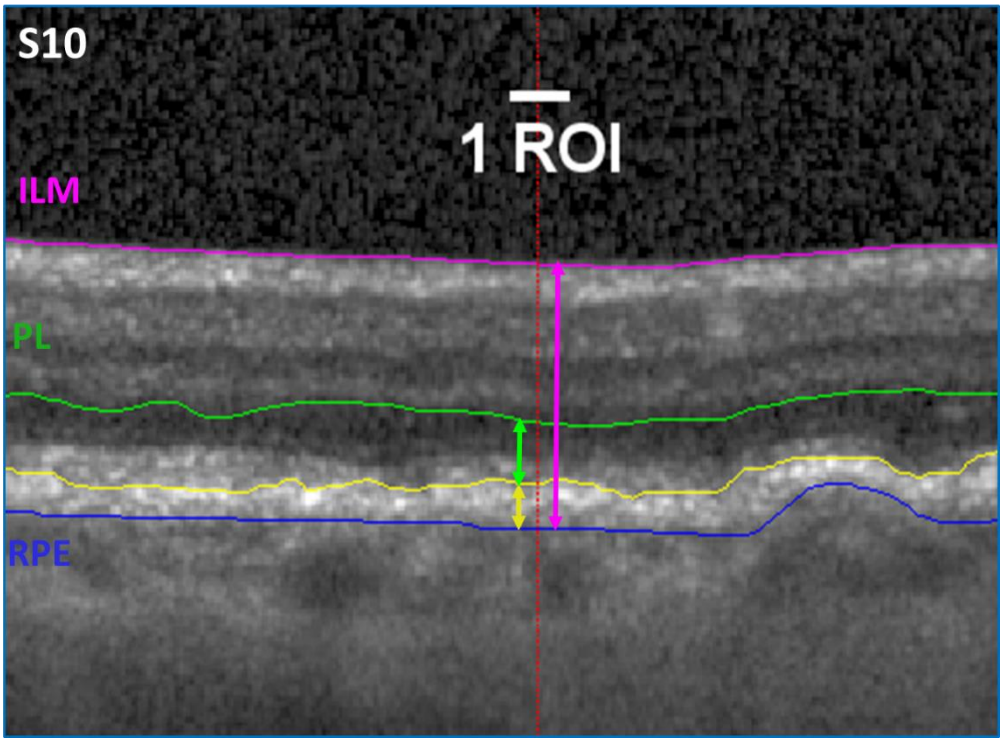

Figure 3-4 Manual Segmentation of OCT Scan

The segmentation of the outer retinal layers by manually tracing the boundary margins, in a representative subject (S10) with AMD. Four boundaries that were marked in all the scan from MS location (top image) and nonMS location (bottom image) are shown in different colors. Note that the segmentation was performed on a region (496 x 154 pixels) wider than that of the ROI (the red vertical line in each image passes through the center of the ROI that was ~14 pixels wide). Note that for the MS/nonMS ratios, the overall photoreceptor layer thickness (receptor + nuclear layer, green arrow) was used and the RPE boundaries included the Bruch's membrane complex (yellow arrow).

Post-Segmentation Analysis: MS / NonMS thickness ratios using the formula listed above were computed for the RPE, the whole photoreceptor layer, and for the total retina. The details of the retinal layers were very poor in one subject (S16) due to bad image quality and were excluded from the OCT analysis. For the 7 subjects (2 AMD, 2 Stargardt, 3 other forms of CFL) who didn't exhibit any MSs within the PRL only the nonMSlocn scans were analyzed. MS / NonMS ratios could not be computed in this subset of subjects. The 6 subjects (2 AMD, 3 STGD, and 1 other CFL) who had MSs within the PRL but no nonMSlocns were matched by diagnosis and eccentricity of the PRL to another subject who exhibited a non-zero number of nonMSlocns and ratios (average MSlocn layer thickness / average nonMSlocn layer thickness) were computed based on this match. Finally, the 28 subjects were classified into two groups namely: 1) CFL due to AMD or Stargardt disease and 2) other forms of CFL. Thickness ratios were analyzed separately for the 2 groups. In group 1, a sub-analysis between the subjects with AMD and Stargardt disease also was done.

Qualitative Grading of the Region of Interest: All the MS and nonMS location scans, especially the 14-pixel region ROI was graded for the presence of outer retinal changes like: Druse(n), RPE atrophy (with or without choroidal hypertrophy), discontinuous/absent/abnormal IS-OS junction line (2^{nd} hyper reflective band above the RPE band), absent/abnormal external limiting membrane (ELM, third hyper reflective thin band above IS-OS). The author (AKK) did all the grading, and was masked to the origin of the scans (MS/nonMS location). When the presence of abnormality was inconclusive, the author always classified the scans as normal. For a given subject the sum of total

number of abnormalities in both MS and NonMS locations were calculated and a sign test was used to test for significant differences.

Analysis of Blue-FAF Images: Blue-FAF imaging was performed in only 22 of the 29 subjects. After excluding one image due to poor quality, the remaining 21 images were analyzed. The coordinates of each subject's MP1 IR image (obtained during fixation testing and representing the median BCEA) were affine transformed to blue FAF-SLO image coordinates using the control point tool in MATLAB (See the section, "Relating Structure to Function," above). Each subject's 3 SD fixation ellipse was also transformed and plotted on the SLO image (See **Figure 3-5**). Two graders (AKK and NBP) independently graded the region inside this ellipse as either abnormal (Hyper/hypo fluorescent) or having normal fluorescence. When a heterogeneous fixation ellipse could not be assigned to a single category, it was assigned to 2 categories that best represented the fluorescence within sub-regions of the ellipse (e.g., Hypo-Normal, Hypo-Hyper, etc.).

Quantitative Analysis: The blue-FAF SLO images sometimes had speckle noise at the edges and always included a default white scale bar. To eliminate these artifacts (See **Figure 3-5**), a 50-pixel thick border was removed from all the 4 sides of the SLO image and only the central 1436 x 1436 pixels was used for the quantitative analysis. The maximum (Max I) and minimum (Min I) intensity within this central region was very different across the 21 images analyzed. Across subjects, the Max I and Min I ranged, respectively, from 129 - 255 and from 1 – 35. Although this wide range of luminance values

could result partly from the diversity in the subjects' auto-fluorescent changes, differences in retinal illumination across subjects also had to be considered.

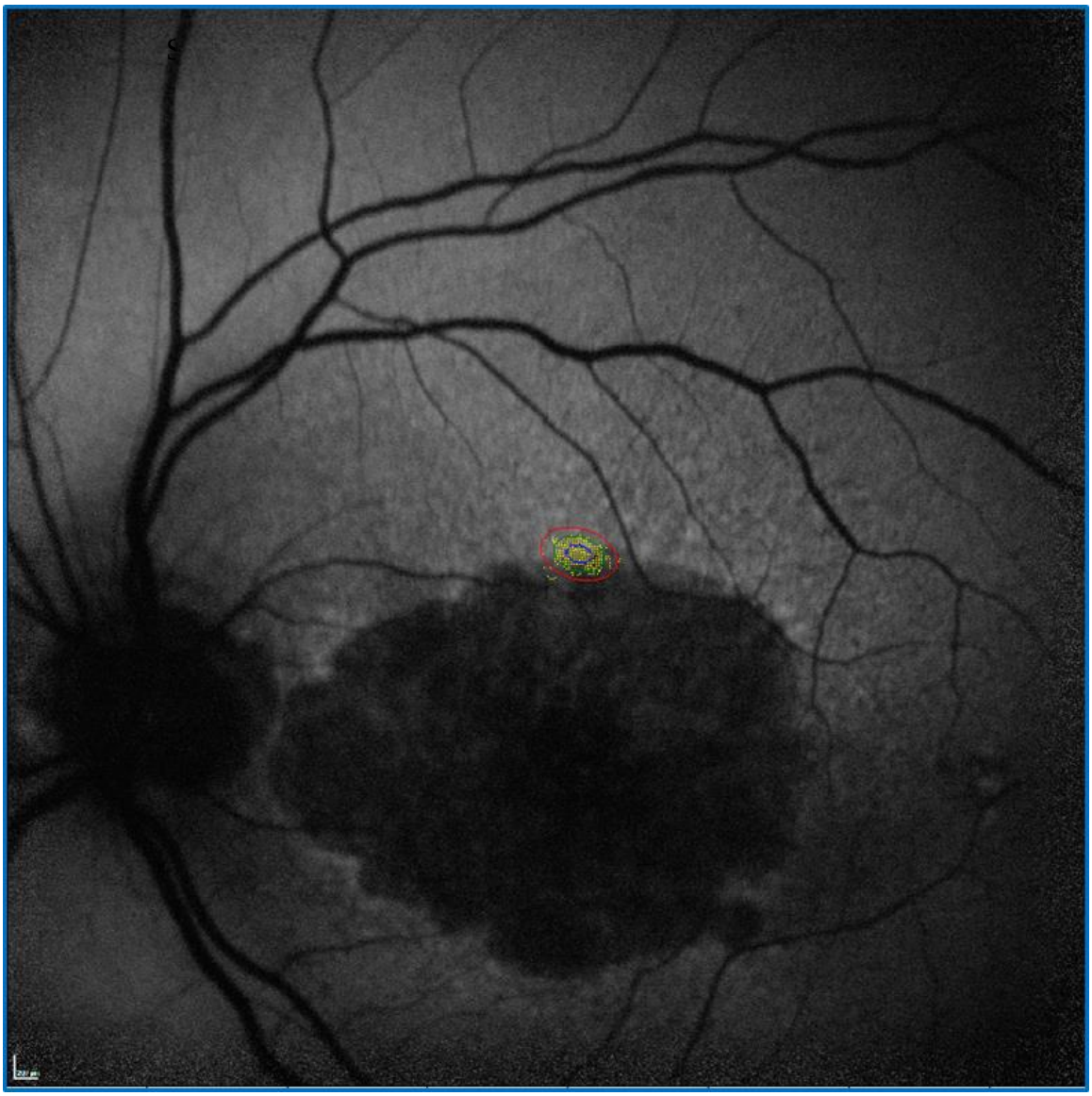

Figure 3-5 Blue FAF imaging with Fixation Ellipses

The blue FAF image obtained using CSLO of Spectralis in subject S10 with AMD. The 3 SD BCE at the word fixation PRL was plotted on this image after manual image registration using the MATLAB control point tool. The autofluorescence over the 3 SD BCE region (enclosed by the red ellipse) was quantified after normalizing the intensity. Note the white scale bar (bottom left, 200µm) and speckle noise on the image borders, both of which were excluded from the analysis.

The wide range across subjects of blue-FAF image intensities was also observed within the 3 SD BCE region. The average intensity values of all pixels (range: ~2000 - 72,000) within the 3 SD ellipse region ranged from ~29 - 178. To account for these across-subject differences in pixel intensities, the average intensity with in the 3SD BCE was normalized to range from 0 (New Min I) to 255 (New Max I). This normalization was based on the Max I and Min I of the larger 1436 x 1436 image region for each subject, and was calculated as:

$$Normalized\ Intensity\ (I_N) = \left(I_{Avg} - Min\ I\right) \times \frac{New\ Max\ I - New\ Min\ I}{Max\ I - Min\ I} + New\ Min\ I$$

Where,

$$Average\ Raw\ Intensity\ (I_{Avg}) = Average\ of\ all\ pixels\ inside\ the\ 3SD\ ellipse\ region$$

$$I_N < Q_1 \rightarrow Hypo\ Fluorescent;\ I_N > Q_3 \rightarrow Hyper\ Fluorescent$$

The normalized intensity (I_N) values of the different subjects ranged from ~14 – 178. Based on whether or not they fell below the first quartile (Q_1), above the third quartile (Q_3), or between the first and third quartiles, the values of I_N were categorized as hypo-fluorescent, hyper-fluorescent or normal, as shown above. For values of I_N that ranged potentially from 0 – 255, the first and third quartiles were: 63.75 (Q_1) and 191.25(Q_3).

Because the qualitative grading of the 2 graders was not always concordant, only the normalized intensity values of FAF intensity within the PRL, determined using the quantitative analysis described in this section, were compared to the subjects' functional measures of reading and contrast sensitivity.

3.3 Results

As in the Methods section, the results are presented here in the order of testing. The reading assessment measures between the MP1 Read and MNRead testing correlated well (See **Figure 3-6**; r= +0.847 for maximum reading speed and r = +0.772 for reading acuity). The CPS and the reading acuity estimated from the MN-Read assessment had a good correlation (r = +0.83, See **Appendix 6.12**). However, the correlation between the FrACT contrast thresholds and the reading measures (MNRead) was poor (r = -0.126 for maximum reading speed and r = +0.027 for reading acuity). **Table 3-2** summarizes the results from the reading and contrast sensitivity assessments.

Three fixation assessments were done successively in each subject and the median bivariate contour ellipse area (BCEA, refer to **Appendix 6.8** for the BCEA determined for each individual test) correlated poorly with the radial eccentricity of the word-fixation PRL

(r=+0.231, see **Figure 3-7**). **Appendix 6.8** also lists the CPS used during the fixation assessments for each subject. Across subjects, the average (±SD) sensitivity of the 4-6 test locations around the word-fixation PRL from 10-2 testing using the MP-1 was 4.93 ± 4.73 dB.

On average 51 locations (Range: 23-94, see **Table 3-3**) around the word-fixation PRL were screened for MSs. The number of locations that had MSs (number of MS locations, **Table 3-3**) and the number of nonMS locations varied widely across our subjects (Refer to **Appendix 6.4**, for MS plots for all of the subjects). Except for few subjects who had roughly similar numbers of MS and nonMS locations (e.g.: S3, S12), the majority of our subjects had a biased distribution of MS and nonMS locations. It was surprising to note that the prevalence of MSs within the PRL was similar for the subjects with AMD (8/10 subjects) and STGD (10/12 subjects) and that average %MSs was similar across the 3 CFL groups (AMD: 25.4%, STGD: 20.3% and Misc. CFL: 27.1%).

Although the OCT imaging was performed on all 29 study subjects, structure-function comparisons were possible only in 21 subjects (7 subjects with 0 overlapping MSs in the PRL and 1 subject with poor OCT scan quality were excluded). In each of these 21 subjects, B-scans corresponding to all the MS and nonMS locations (ROI ≈ 14 pixels) were segmented separately and the average MS/nonMS thickness ratios of the three layers of interest (RPE-BM, overall photoreceptor layer (PL) and the total retinal thickness) are listed in **Table 3-4.** (Refer to **Appendix 6.7** for SDs and a complete listing of the layer thicknesses and ratios for each layer in all 21 subjects). Blue fundus auto-fluorescence

imaging could be completed only in 22 of the 29 subjects. The results of the quantitative AF grading are provided in last column of **Table 3-4** (also see **Table 3-5**). The qualitative grading of blue AF images by the 2 examiners disagreed for 11 of the 21 subjects and hence we interpret the AF results using only the quantitative scores.

Reading performance assessed using the MNRead charts didn't correlate well with the MS/nonMS ratios determined for any of the 3 retinal layers (See **Figure 3-8**). The maximum reading speed didn't correlate well with functional measures like PRL eccentricity (r= -0.232) or BCEA (r= -0.197, Refer to **Appendix 6.9** and **6.10** for plots). The MNRead reading acuity had a significant positive correlation (r = +0.383) with the eccentricity of the word-fixation PRL (Refer to **Appendix 6.11** for the plot).

The qualitative grading of the ROI for presence of outer retinal changes was performed in 17 subjects with AMD or STGD (and who had MSs in the PRL). In the ROI corresponding to a MSlocn, ≈ 8, 49, 93 and 87% of the 237 locations had drusen, RPE thinning, abnormal IS-OS junction and abnormal ELM respectively. The corresponding numbers for the nonMSlocn were: 12, 1, 51 and 43% of 181 locations graded. Sign tests comparing the MS and nonMSlocn for each of these 4 OCT changes, were not significant ($p>0.05$) due to presence of numerous comparisons that were tied.

A theme that has been investigated widely in the past that we set out to explore is the difference between the age-related and juvenile forms of macular degeneration. We divided our subjects into the three cohorts based on their diagnosis (AMD, STGD and miscellaneous CFL) and compared the structural and functional measures (see **Table 3-6**).

The STGD group (n=12) had the best maximum MNRead reading speed. Maximum reading speed was significantly faster in STGD than the AMD group (p=0.012) and marginally faster than in the miscellaneous CFL group (p=0.056, also see **Table 3-6**). None of the other differences between the groups achieved statistical significance (see **Table 3-7**).

The relationships between functional measures and the maximum reading speed for all the CFL subjects (n=22 for FrACT contrast testing and n=29 for retinal sensitivity) are shown in **Figure 3-9** and **Figure 3-10**. Neither the FrACT contrast thresholds (see **Figure 3-11**) nor the median sensitivity around the PRL (see **Figure 3-12**) correlated significantly with the maximum reading speed achieved during MNRead testing, either in the CFL subjects as a group or in any diagnostic subgroup. We also related the median retinal sensitivity measured using the MP-1 around the PRL and FrACT contrast thresholds in 28 subjects (S4, outlier removed for all FrACT-related analyses) and found a weak non-significant negative correlation (r=-0.204, p = 0.362; see **Figure 3-13**). As a last analysis, we explored the relation between the maximum reading speed and subject's age. As anticipated the reading performance declined with age, but the effect didn't reach statistical significance. (See **Figure 3-14**).

		Reading Measures				**FrACT Threshold**
Subject Code	**Diagnosis**	**MN Read Max. Reading Speed**	**MP1 Read Max. Reading Speed**	**Reading Acuity MN Read**	**Reading Acuity MP1 Read**	**Weber Contrast**

		wpm	wpm	(logMAR)	(logMAR)	% (-ve)
S1	AMD	111.1	125.11	0.3	0.6	9.219
S2	AMD	126.45	115.39	0.65	0.7	16.815
S3	STGD	72.2	82.52	0.96	0.9	11.359
S4	STGD	144.6	149.46	0.805	0.7	70.226
S5	Cone-Rod	80	130.21	1.01	0.8	25.773
S6	STGD	169.75	109.61	0.72	0.7	21.679
S7	Plaq. Mac	64.2	–	1.055	–	–
S8	Cone-Rod	43.8	70.24	0.585	0.6	33.208
S9	STGD	45.75	45.25	1.01	1	15.039
S10	AMD	91.1	66.63	0.805	0.8	10.956
S11	Mac. Hole	144.75	120	0.69	0.7	9.017
S12	STGD	27.75	53.95	1.1	1	16.655
S14	STGD	182.4	154.25	0.88	0.7	6.205
S15	STGD	181.1	139.44	0.82	0.9	–
S16	AMD	17.6	20.29	1.3	1.2	–
S18	STGD	185.72	–	0.82	–	5.398
S19	AMD	53.8	62.32	0.7	0.8	–
S20	Plaq. Mac	65.34	40.21	0.8	0.9	–
S22	STGD	99.73	–	1.035	–	6.430
S23	AMD	90.71	85.35	0.515	0.7	10.902
S25	Myopic	83.87	21.13	0.76	0.7	6.029
S26	STGD	132.24	80.38	0.76	0.7	25.847
S27	AMD	54.74	34.6	0.925	0.8	10.921

S28	AMD	75.01	31.52	0.74	0.75	16.359
S29	AMD	70.22	35.25	0.59	0.9	13.875
S30	STGD	174.6	131.79	0.93	0.8	28.3
S31	STGD	237.28	215.56	0.65	0.7	12.879
S32	AMD	93.002	43.4	0.78	0.7	12.792
S33	Cone Dys	142.52	93.71	0.68	0.75	–

Table 3-2 Results: Reading and Contrast Assessment

FrACT contrast thresholds and MP1 Read assessment couldn't be completed in all subjects, whereas all subjects completed the MNRead reading assessment. All of the values reported here are the average of 2 estimates.

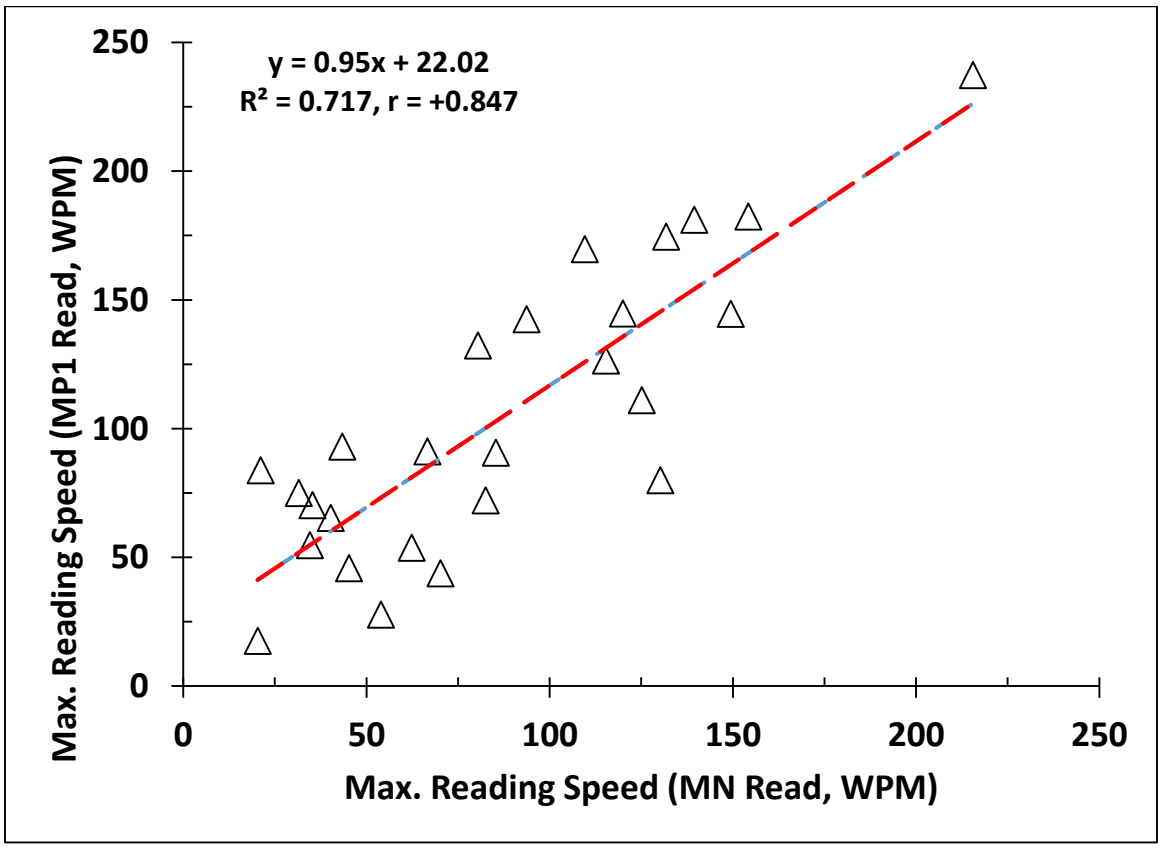

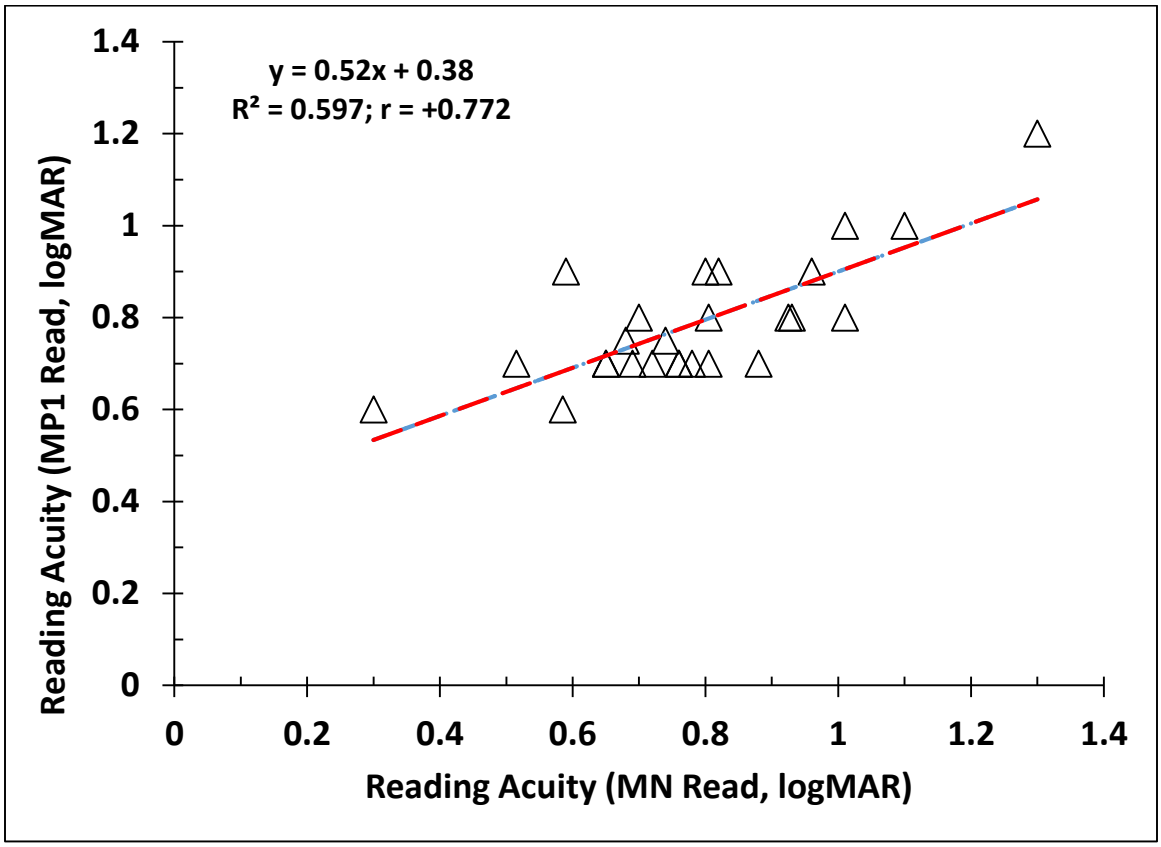

Figure 3-6 MP1 Read vs MN Read

Relation between the reading measures obtained using the MNRead and MP1 Read testing. The two measures of reading speed (r=+0.847, t (24) = 7.80, p=5x10^{-8}) and the two measures of reading acuity (r=+0.772, t (24) = 5.957, p=3.8x10^{-6}) were significantly correlated.

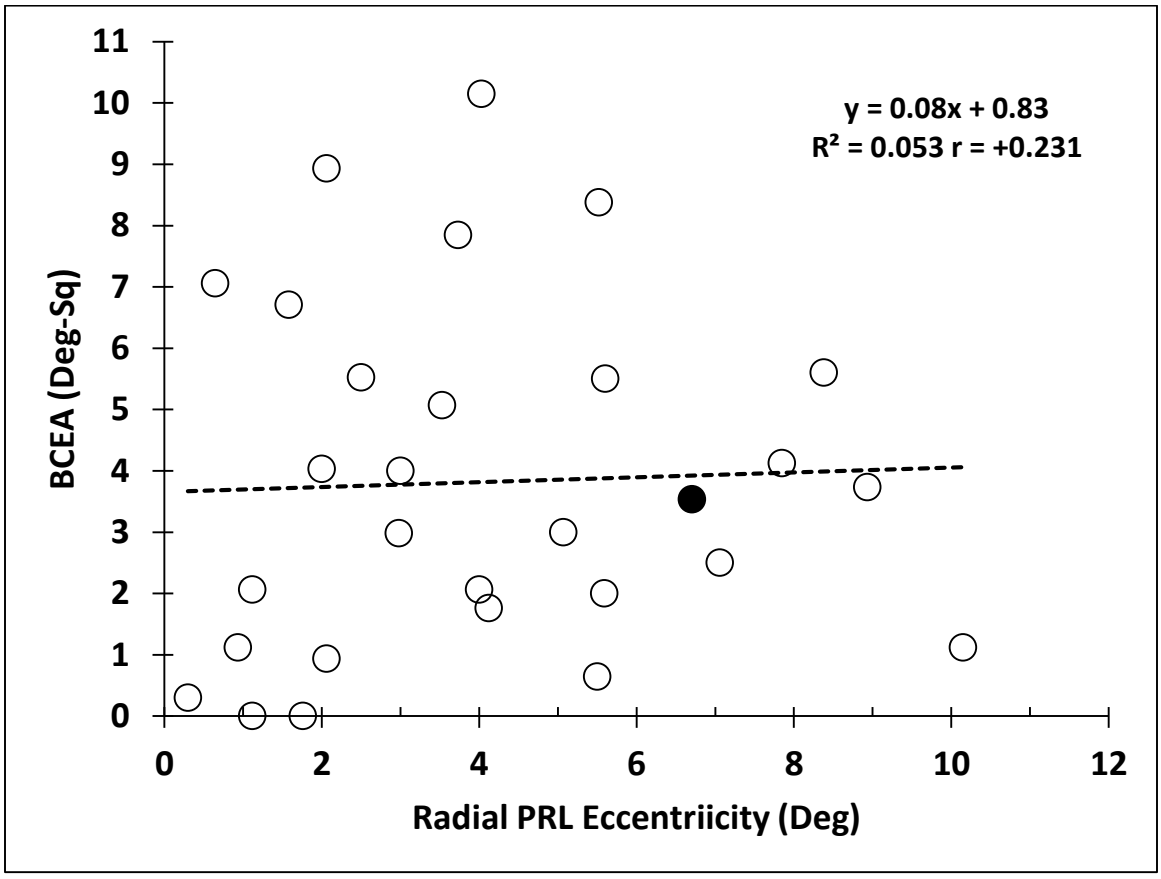

Figure 3-7 BCEA vs PRL Eccentricity

Scatter plot of the 1 SD bivariate contour ellipse area (BCEA, median of 3 fixation tests; refer to ***Appendix 6.8****), determined during word fixation in the MP-1, as a function of the radial eccentricity of the PRL. The PRL eccentricity was measured as the Pythagorean distance from the estimated location of the residual fovea, determined using the standard values from 104 normally-sighted subjects reported by Rohrschnieder et al. (2004). Refer to* ***Appendix 6.16*** *for the list of PRL meridians and polar angle. The correlation between BCEA and PRL is low (+0.231) and became worse (+0.141) when the outlier (S20, filled black circle) was removed (t (26) = 1.21, p = 0.24, without the outlier).*

Subject Code	Diagnosis	Median Sensitivity	Total Locations	Number of MS Locations	Number of nonMS locations	% MS
		(around PRL from 10-2 testing, in dB)	**(Tested in Screening)**	**(0 dB missed on both tests)**		
S1	AMD	0	28	0	6	0.00
S2	AMD	2.5	67	6	36	8.96
S10	AMD	0	55	6	15	10.91
S16	AMD	0	33	25	0	75.76
S19	AMD	6.5	67	0	23	0.00
S23	AMD	5.5	77	6	2	7.79
S27	AMD	2	39	13	0	33.33
S28	AMD	0	62	29	1	46.77
S29	AMD	0	73	49	0	67.12
S32	AMD	4	62	2	29	3.23
	N	**10**				
	Mean	**2.05**	**56.30**	**13.60**	**11.20**	**25.39**
	SD	**2.51**	**17.15**	**15.98**	**13.65**	**28.61**
	Median	**1**	**62**	**6**	**4**	**9.93**
S3	STGD	12.5	73	7	10	9.59
S4	STGD	8	50	3	11	6.00
S6	STGD	8	33	1	15	3.03
S9	STGD	0	37	22	0	59.46

S12	STGD	10	36	5	5	13.89
S14	STGD	14.5	23	0	23	0.00
S15	STGD	13	41	2	21	4.88
S18	STGD	8.5	57	1	16	1.75
S22	STGD	0	57	44	0	77.19
S26	STGD	0	62	39	0	62.90
S30	STGD	3	31	0	31	0.00
S31	STGD	2.5	44	2	20	4.55
	N	**12**				
	Mean	**6.67**	**45.33**	**10.50**	**12.67**	**20.27**
	SD	**5.37**	**14.68**	**15.70**	**10.15**	**28.44**
	Median	**8**	**43**	**3**	**13**	**5.44**
S5	Cone Rod Dys.	10	67	0	61	0.00
S7	Plaq.Maculopathy	5	37	0	37	0.00
S8	Cone Rod Dys.	0	41	25	1	60.98
S11	Macular Hole	8.5	29	12	0	41.38
S20	Plaq.Maculopathy	8	94	34	15	36.17
S25	Myopic Mac Deg	0	37	19	1	51.35
S33	Cone Dys.	11	56	0	50	0.00
	N	**7**				
	Mean	**6.07**	**51.57**	**12.86**	**23.57**	**27.13**
	SD	**4.55**	**22.74**	**13.72**	**25.59**	**26.54**
	Median	**8**	**41**	**12**	**15**	**36.17**

Table 3-3 Results: Supra-threshold Screening

Results from the functional sensitivity testing using the NIDEK MP-1 are listed here. The third column reports the median sensitivity of the 4 to 6 test points located around the word-fixation PRL, from 10-2 testing (with nominal Goldmann size II spots and a 4-2-1 thresholding strategy). Note that the numbers of MS and NonMS locations were identified manually using a MATLAB program, after defining an overlap region (8x5 pixels) around the MS locations identified on test -1.

Note that the mean % of MSs is approximately the same in the 3 diagnostic groups (20 - 27% MSs). Also refer to ***Appendix 6.14*** *for a scatter-plot on %MSs vs Age. The % of subjects with AMD and STGD who exhibit MSs in the PRL is about the same (8/10 vs. 10/12). The subject codes for seven subjects (2AMD, 2STGD, 3 other CFL) who were found to have no MSs and 1 subject with poor OCT imaging (S16) are shown in bold and are underlined. Interestingly, subject S1 whose median sensitivity around PRL was 0, had no MSs in the screening. This is because the number of missed targets in test #1 was 0. Although S1 failed to detect 6 targets in test # 2, the number of overlapping missed targets was 0. Also see* ***Appendix 6.3*** *that lists the number of targets missed in each test session for all subjects and* ***Appendix 6.15*** *for a scatter-plot on BCEA vs % MSs.*

	MS : NonMS Ratios			**Blue FAF Grading**
Subject Code	**RPE-BM**	**Overall Photoreceptor (PL)**	**Total Retinal**	**(Quantitative)**
S2	1.060	1.379	0.813	–
S3	0.885	0.891	0.983	Normal
S4	1.106	0.992	1.002	–

S6	0.810	0.881	0.987	Abnormal
S9*	1.205	0.540	0.905	Normal
S10	0.458	0.592	0.904	Normal
S12	0.753	0.563	0.911	Normal
S15	1.397	1.277	1.078	Abnormal
S18	0.987	1.331	1.014	Normal
S22*	0.490	0.287	0.765	Normal
S23	1.092	1.019	0.854	Normal
S26*	0.958	0.433	0.445	–
S27*	0.883	0.927	0.681	–
S28	1.628	0.318	0.967	Abnormal
S29*	0.384	0.651	0.820	Normal
S31	1.073	0.525	0.840	Normal
S32	1.279	0.969	1.009	Abnormal
S8	1.144	0.685	1.257	–
S11*	0.898	0.306	0.899	Abnormal
S20	1.080	0.387	0.891	Normal
S25	0.442	1.858	0.818	Normal

Table 3-4 Thickness Ratios from OCT Imaging

Average retinal layer thickness ratios in ROIs corresponding to MS and NonMS locations in 21 (of the total 29) subjects who had MSs. The top portion of the table reports

the findings from subjects diagnosed with either AMD or STGD. The 4 subjects in the bottom portion of the table had other diagnoses. Note that subjects who had 0 nonMS location from ***Table 3-3*** *are marked with an asterisk (*) and thickness ratios were computed using the data of a subject with CFL matched for diagnosis, PRL eccentricity and age. (Also refer to* ***Appendix 6.7*** *that provides the individual layer thicknesses and the SDs of the thickness ratios for all subjects)*

Five subjects whose total thickness ratios are >1 are underlined. The last column lists the grades based on the quantitative assessment of normalized intensity values at the PRL from blue fundus autofluorescence images. Subjects for whom autofluorescence grades could not be assigned are marked with a '– '.

Subject Code	**Qualitative Score**	**Quantitative Score**	**Agreement**		**Qualitative Score**	**Quantitative Score**	**Agreement**
	NBP	**(from normalized intensity)**	**1= YES 0 = NO**		**AKK**	**(from normalized intensity)**	**1= YES 0 = NO**
S1	Abnormal	Abnormal	1		Abnormal	Abnormal	1
S3	N	N	1		N	N	1
S6	N	Abnormal	0		Abnormal	Abnormal	1
S9	N	N	1		Abnormal	N	0
S10	Abnormal	N	0		N	N	1
S11	Abnormal	Abnormal	1		Abnormal	Abnormal	1
S12	Abnormal	N	0		N	N	1
S14	N	N	1		N	N	1

S16	Abnormal	Abnormal	1		Abnormal	Abnormal	1
S18	Abnormal	N	0		N	N	1
S19	Abnormal	Abnormal	1		Abnormal	Abnormal	1
S20	Abnormal	N	0		Abnormal	N	0
S22	Abnormal	N	0		Abnormal	N	0
S25	Abnormal	N	0		Abnormal	N	0
S28	Abnormal	Abnormal	1		Abnormal	Abnormal	1
S29	Abnormal	N	0		N	N	1
S30	Abnormal	N	0		N	N	1
S31	Abnormal	N	0		Abnormal	N	0
S32	N	Abnormal	0		N	Abnormal	0
S33	N	N	1		N	N	1
S15	Abnormal	Abnormal	1		N	Abnormal	0
S23	–	N	–		–	N	–
Total N	**Count Abnormal**	**Count Abnormal**	**Total Agreement**		**Count Abnormal**	**Count Abnormal**	**Total Agreement**
22	**15**	**9**	**10**		**11**	**9**	**14**

Table 3-5 Results: Blue FAF Imaging

*The results of qualitative grading of blue fundus autofluorescence images in the region of the PRL. The grades determined independently by 2 examiners (NBP, AKK) are listed here. Note that the number of abnormal regions based on qualitative grading was more than that based on quantitative grading (column 3 and also in **Table 3-4**). Because*

of the lack of consensus between the graders, only the results from quantitative grading are used to interpret the autofluorescence findings. Neither grader could provide grades for S23 because of poor image quality.

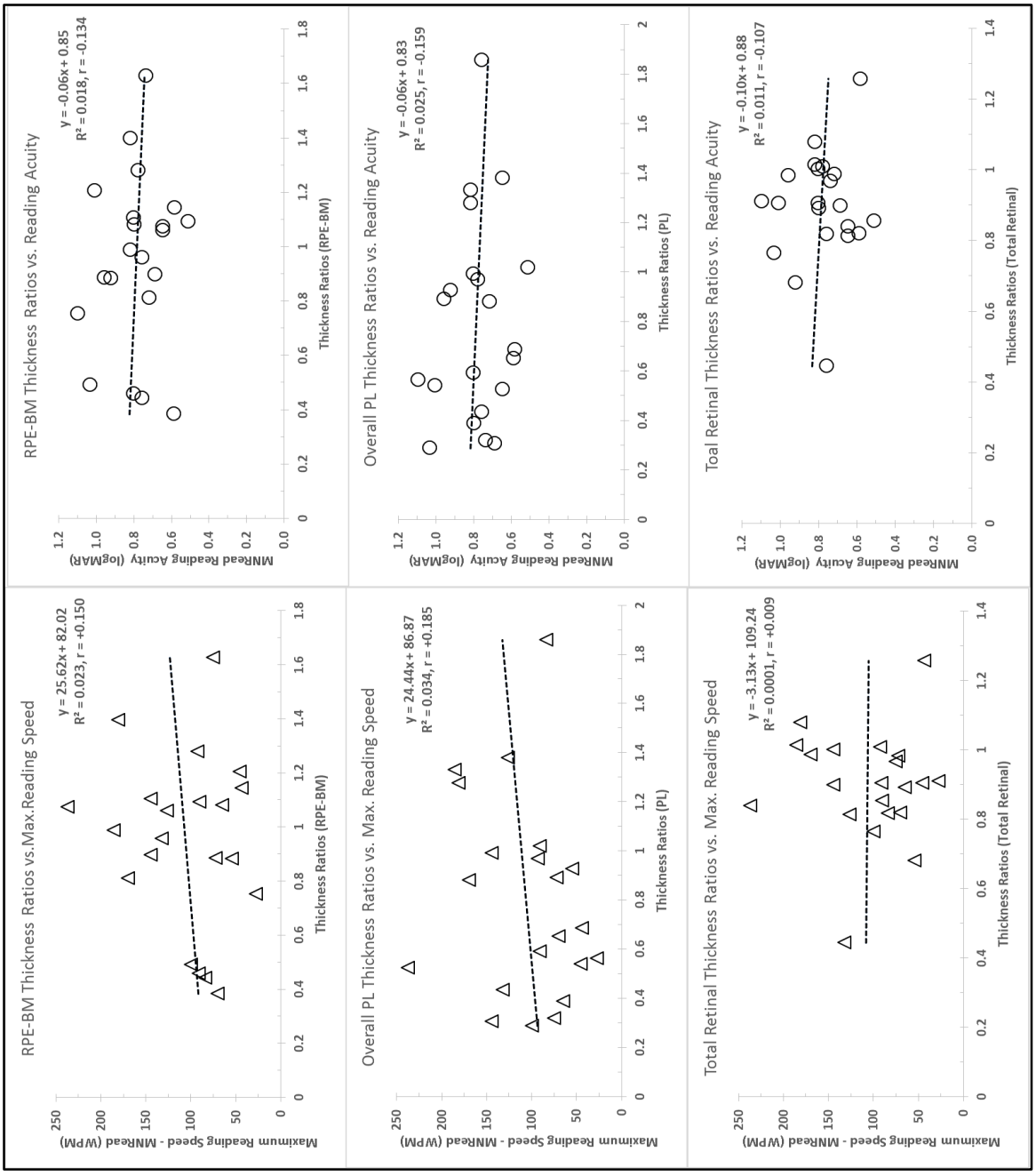

Figure 3-8 Reading vs Thickness Ratios of Layers

Scatter plots of maximum reading speed (left column) and reading acuity (right column) from the MNRead assessment, as a function of average MS / nonMS thickness

ratios (RPE-BM, top row; overall photoreceptor layer (PL), middle row, and total retinal thickness, bottom row). The correlations were poor and non-significant.

Subject Code	**Diagnosis**	**1 SD BCEA**	**MNRead Max. Reading Speed**	**Reading Acuity**	**MS/nonMS Thickness Ratios**			**Blue FAF Grading**
		(deg-sq.)	**(wpm)**	**(logMAR)**	**RPE-BM**	**PL**	**Total Retina**	**(Quantitative)**
S1	AMD	0.20	111.1	0.30	–	–	–	–
S2	AMD	2.31	126.5	0.65	1.06	1.38	0.81	–
S10	AMD	0.66	91.1	0.81	0.46	0.59	0.90	Normal
S16	AMD	1.12	17.6	1.30	–	–	–	–
S19	AMD	2.58	53.8	0.70	–	–	–	–
S23	AMD	1.05	90.7	0.52	1.09	1.02	0.85	Normal
S27	AMD	0.45	54.7	0.93	0.88	0.93	0.68	–
S28	AMD	0.76	75.0	0.74	1.63	0.32	0.97	Abnormal
S29	AMD	0.98	70.2	0.59	0.38	0.65	0.82	Normal
S32	AMD	1.96	93.0	0.78	1.28	0.97	1.01	Abnormal
Total N	**Mean**	**1.21**	**78.4**	**0.73**	**0.97**	**0.84**	**0.86**	**Abnormal: Normal**
10	**SD**	**0.81**	**31.3**	**0.26**	**0.44**	**0.35**	**0.11**	**2:3**
S3	STGD	1.31	72.2	0.96	0.88	0.89	0.98	Normal
S4	STGD	0.57	144.6	0.81	1.11	0.99	1.00	–

S6	STGD	0.34	169.8	0.72	0.81	0.88	0.99	Abnormal
S9	STGD	1.16	45.8	1.01	1.20	0.54	0.90	Normal
S12	STGD	1.10	27.8	1.10	0.75	0.56	0.91	Normal
S14	STGD	0.30	182.4	0.88	–	–	–	–
S15	STGD	0.46	181.1	0.82	1.40	1.28	1.08	Abnormal
S18	STGD	1.97	185.7	0.82	0.99	1.33	1.01	Normal
S22	STGD	2.07	99.7	1.04	0.49	0.29	0.76	Normal
S26	STGD	0.89	132.2	0.76	0.96	0.43	0.44	–
S30	STGD	0.97	174.6	0.93	–	–	–	–
S31	STGD	0.48	237.3	0.65	1.07	0.52	0.84	Normal
Total N	**Mean**	**0.97**	**137.8**	**0.87**	**0.97**	**0.77**	**0.89**	**Abnormal: Normal**
12	**SD**	**0.60**	**63.9**	**0.14**	**0.25**	**0.36**	**0.18**	**2:6**
S5	CRD	0.85	80.0	1.01	–	–	–	–
S7	Plaq. Mac	1.01	64.2	1.06	–	–	–	–
S8	CRD	0.25	43.8	0.59	1.14	0.69	1.26	–
S11	Mac Hole	0.82	144.8	0.69	0.90	0.31	0.90	Abnormal
S20	Plaq. Mac	4.40	65.3	0.80	1.08	0.39	0.89	Normal
S25	Myopic Mac	0.41	83.9	0.76	0.44	1.86	0.82	Normal
S33	Cone Dys	1.86	142.5	0.68	–	–	–	–
Total N	**Mean**	**1.37**	**89.2**	**0.80**	**0.89**	**0.81**	**0.97**	**Abnormal: Normal**
7	**SD**	**1.43**	**39.4**	**0.17**	**0.32**	**0.72**	**0.20**	**1:2**

Table 3-6 Reading vs OCT Measures

*Structural and functional measures are grouped according to diagnosis for comparison. Except for reading speed none of the differences are significant. The between-group difference in reading speed is highlighted in **Table 3-7**. It is interesting that a higher proportion of STGD subjects than AMD subjects exhibit normal AF at the PRL. Unfortunately, the numbers are too small to make a statistical comparison. The significance of the differences between the cohorts is shown in **Table 3-7.***

Comparison	MN Read Max Reading Speed	Reading Acuity	1 SD BCEA	% MS	MS/nonMS Thickness Ratios		
(2 tailed t-test, p values)					RPE-BM	PL	Total Retina
AMD vs STGD	**0.012**	0.144	0.449	0.680	0.989	0.715	0.690
AMD vs Misc. CFL	0.557	0.541	0.791	0.899	0.742	0.947	0.392
STGD vs Misc. CFL	**0.056**	0.339	0.501	0.606	0.689	0.926	0.548

Table 3-7 Significance Testing: Reading vs Thickness Ratios

Probability values (p) of the observed differences between the subject cohorts for various comparisons. Note that of all comparisons only 2 of them are significant (highlighted in bold and underlined). There is no correction for multiple comparisons.

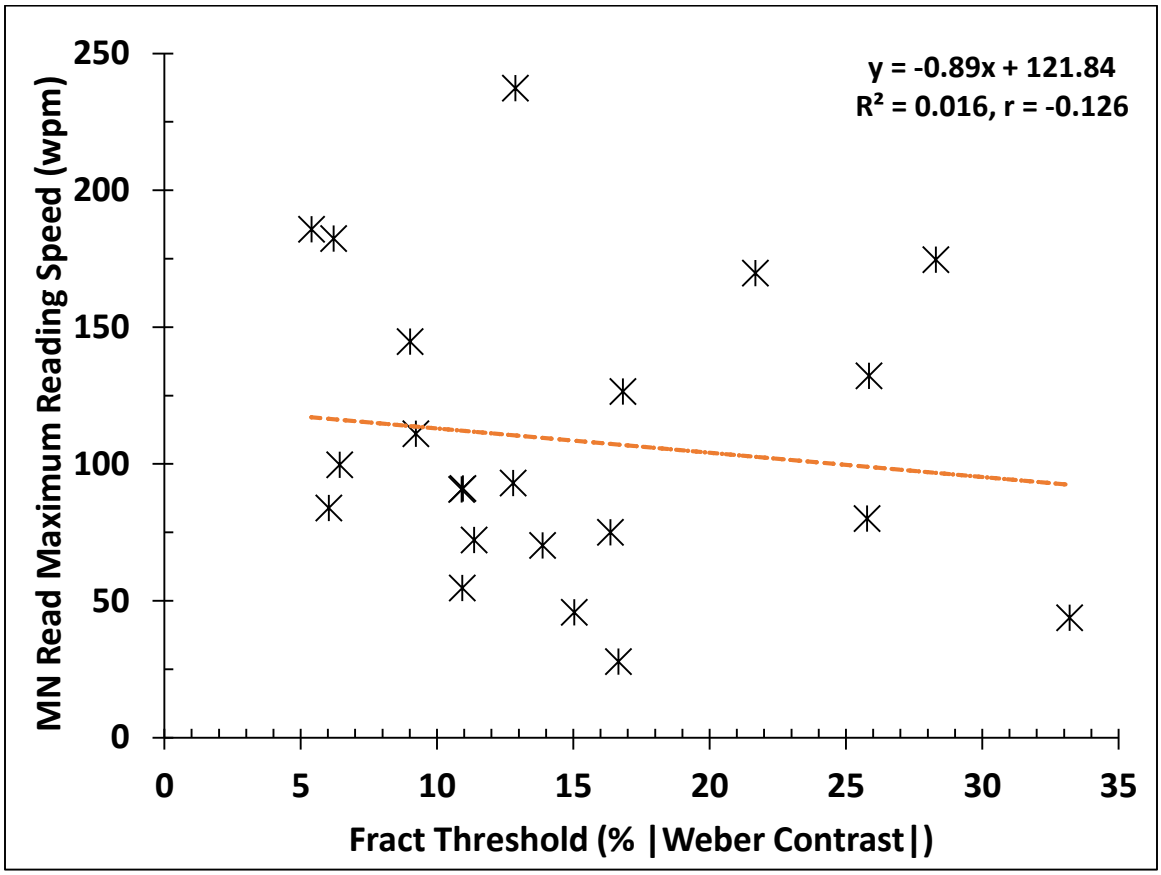

Figure 3-9 Reading vs Contrast Testing

Scatterplot of maximum reading speed during MNRead chart testing vs. the FrACT contrast threshold for all CFL subjects (N=22, as FrACT testing could not be completed for 6 CFL subjects; in addition, data for S4 omitted). The correlation was negative but non-significant (r= - 0.126; t (20) = 0.5703, p = 0.575).

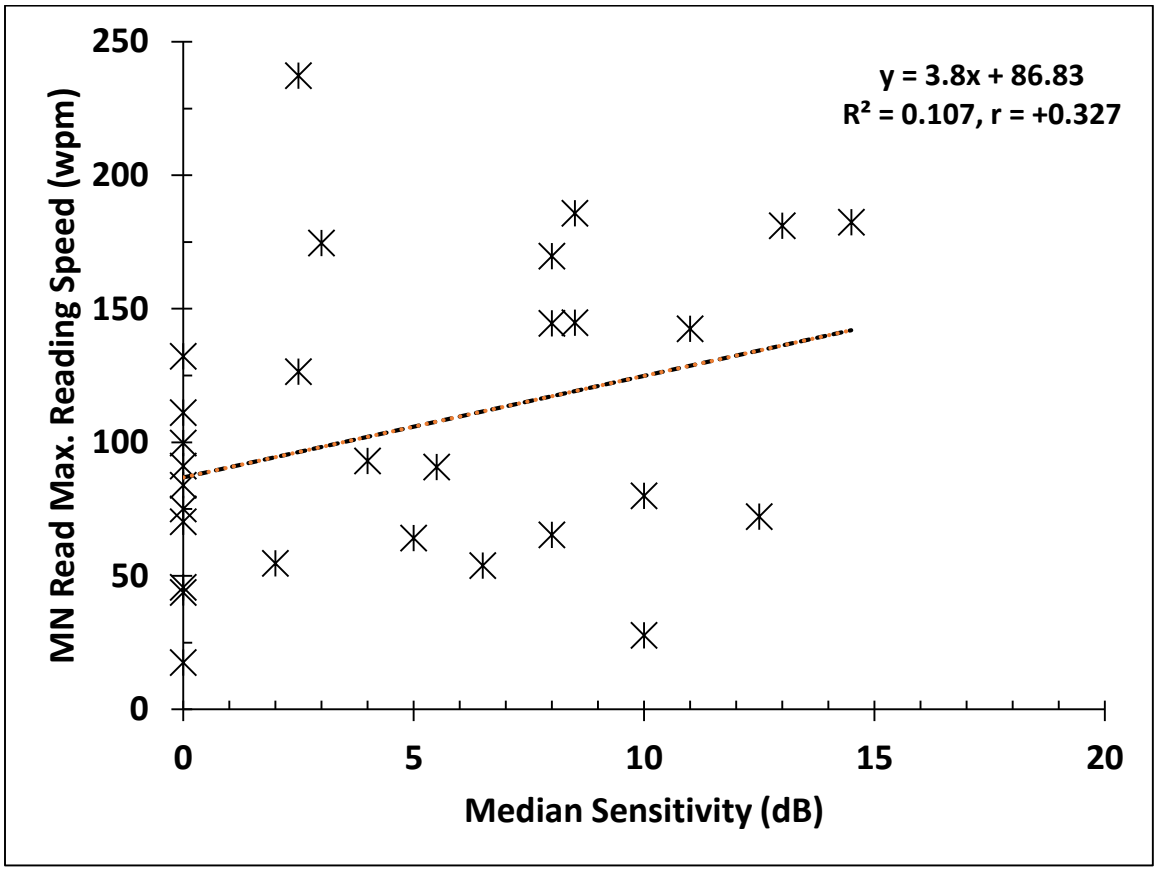

Figure 3-10 Reading vs Central Retinal Sensitivity

Scatterplot showing the relationship between the median sensitivity around the word-fixation PRL from 10-2 testing (Goldmann size II spots) and MNRead maximum reading speed in all 29 CFL subjects. The low correlation approached significance (t (27) = 1.798, p = 0.083). Note that many subjects (n=10) had a median sensitivity around the PRL equal to zero, suggesting that the PRL was surrounded by region of very poor sensitivity.

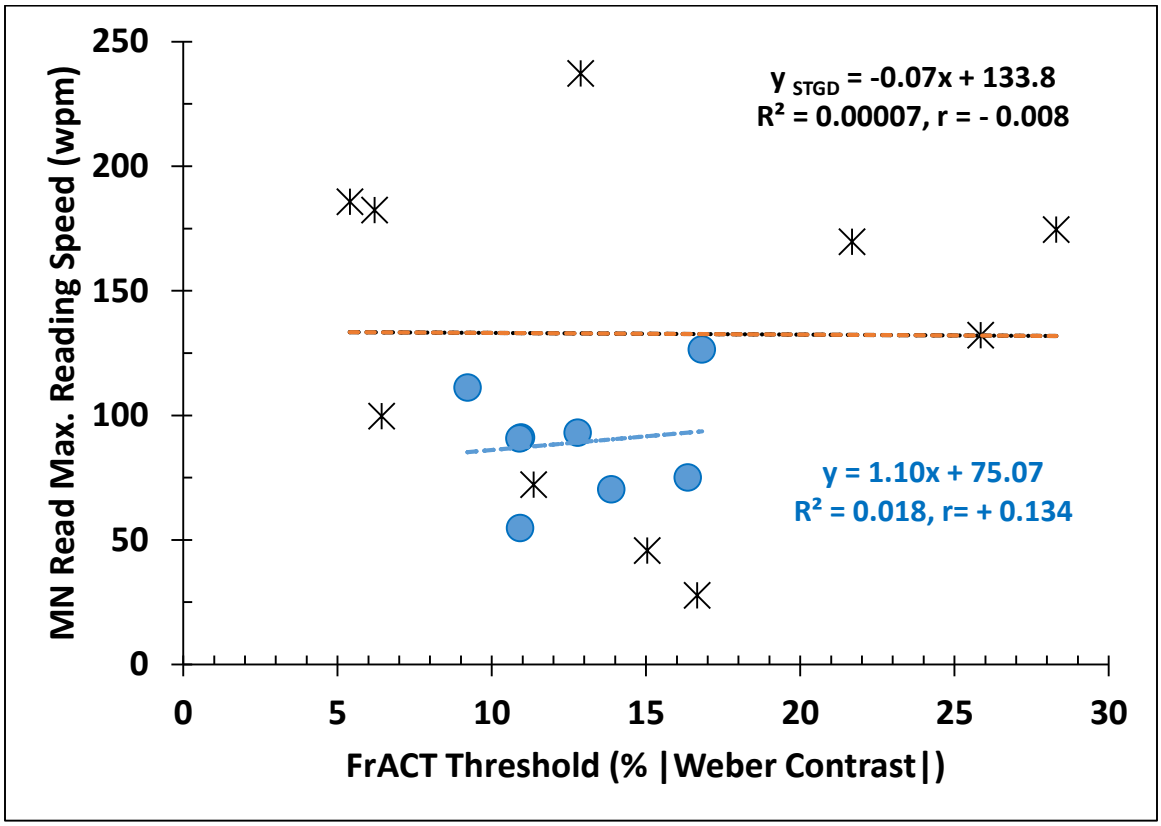

Figure 3-11 Reading vs Contrast Testing (AMD-STGD)

Scatterplot of maximum reading speed in MNRead chart testing vs. FrACT contrast thresholds for the AMD cohort (n= 8, blue circles) and for the STGD cohort (n=10, black asterisks). Reading speed is expected to decrease as the FrACT threshold increases. Neither the correlation (r=+0.134) in the AMD group or the STGD cohort is significant. An outlying data point from subject S4 (STGD, see ***Table 3-2****) was not included in the plot.*

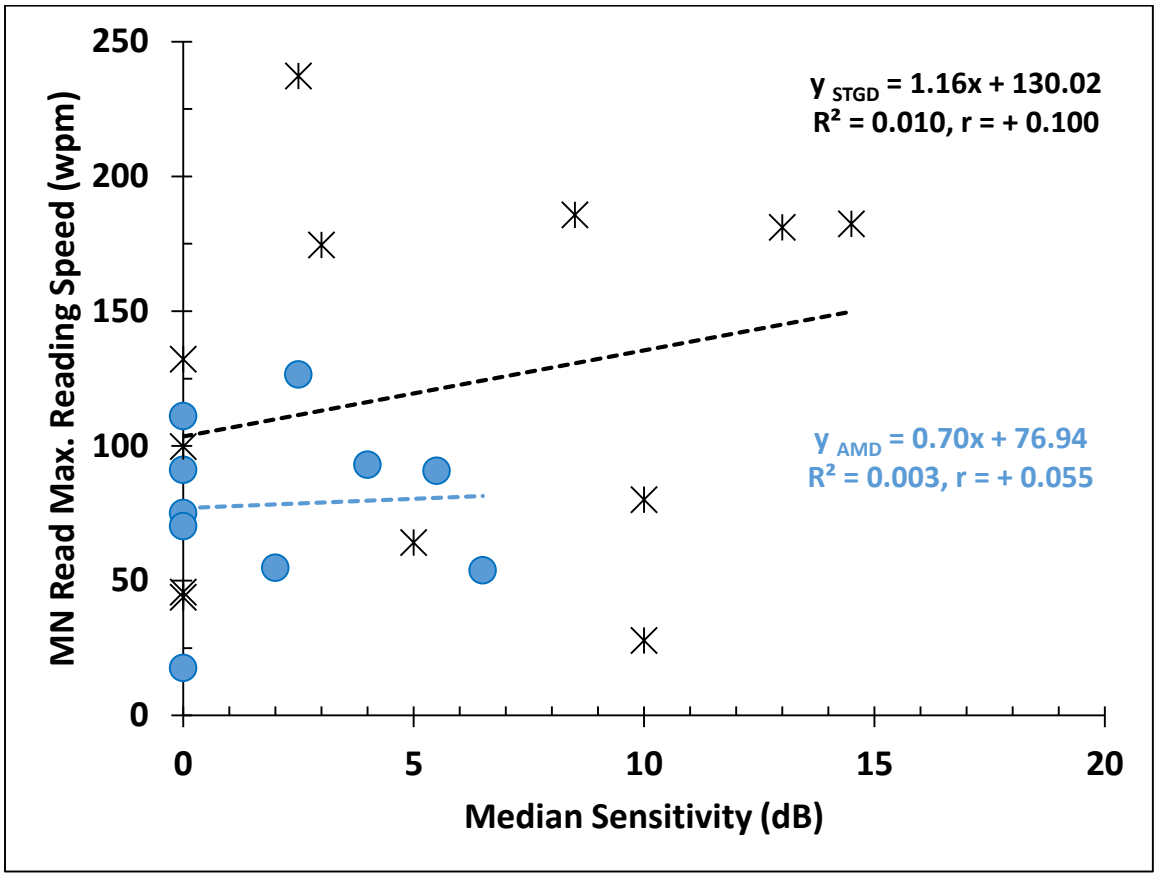

Figure 3-12 Reading vs Central Retinal Sensitivity (AMD-STGD)

Scatterplot showing the relationship between median sensitivity around the word-fixation PRL from 10-2 testing (Goldmann size II spots) and MNRead maximum reading speed. Symbols designating subjects with AMD and STGD are as in Figure 4. Correlations were very low and not significant in both the cohorts (AMD: t (8) = 0.155, p = 0.881 and STGD: t (10) = 0.318, p = 0.757).

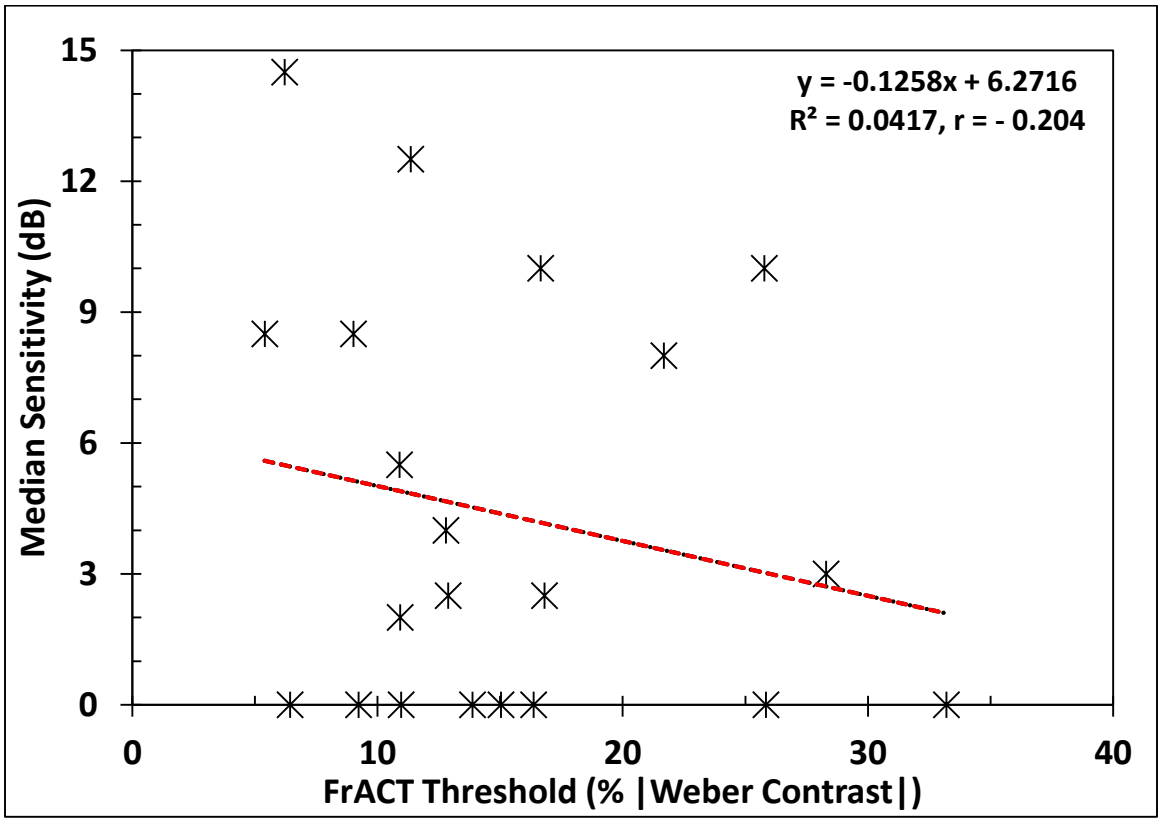

Figure 3-13 Central Retinal Sensitivity vs Contrast Testing

Scatterplot relating FrACT contrast thresholds and the median retinal sensitivity around the PRL (from 10-2 testing) for all 28 CFL subjects (data for S4 excluded, as an outlier). Although the relationship is negative as expected, the FrACT contrast threshold explains only ~4% of the variance in median sensitivity and the low correlation was not significant (r= - 0.204; t (20) = 0.933, p = 0.362).

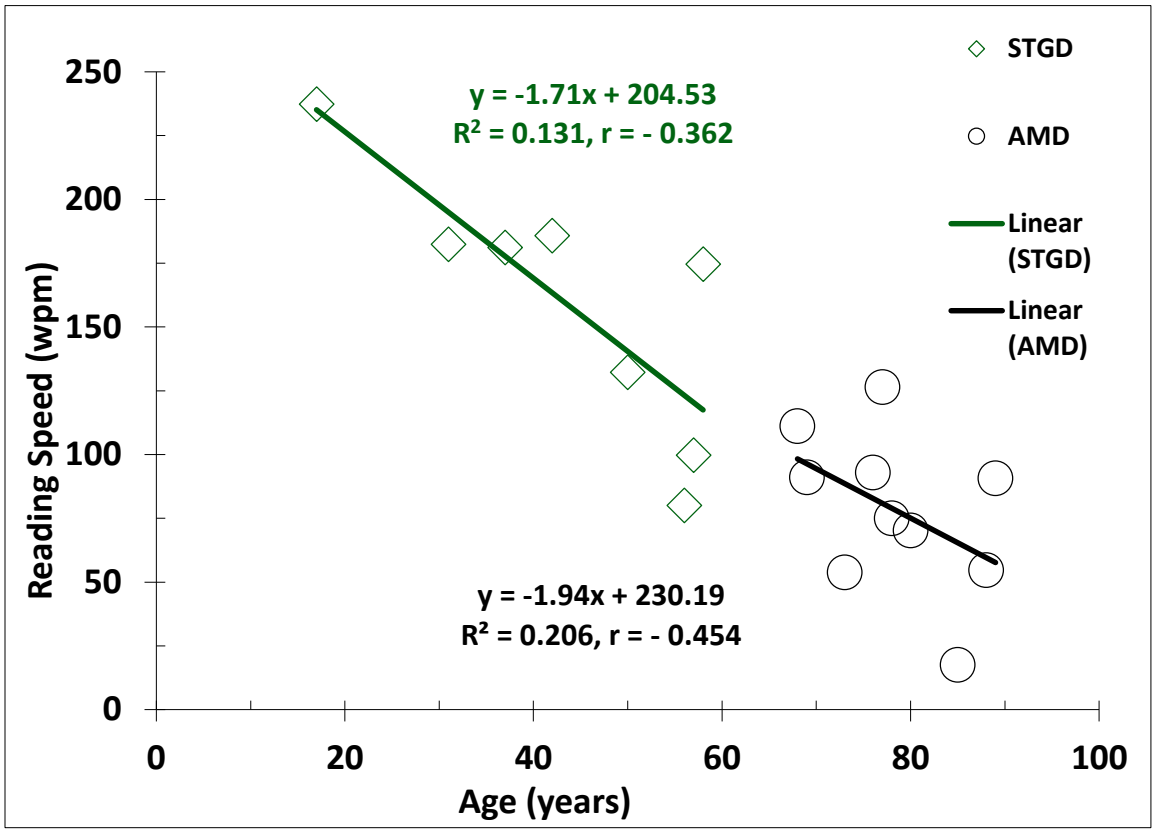

Figure 3-14 Reading vs Age (AMD-STGD)

Scatterplot relating MN Read maximum reading speed and the age of CFL subjects. Note that the age explains ~13 and 21% of variance in reading speed in subjects with STGD and AMD, respectively. It was interesting to find that the slope of the fitted lines was similar across subject groups. The correlation between reading speed and age was negative, but not significant in either group. (AMD: t (8) = 1.44, p = 0.188 and STGD: t (10) = 1.23, p = 0.248). Also refer to ***Appendix 6.13*** *for a scatterplot with all 29 subjects pooled.*

3.4 Discussion

Reading performance in CFL subjects has been assessed in the past using various methods including unrelated words, paragraphs, MNRead charts, RSVP sentences, etc. In this study, we assessed the reading speed with MP1 Read sentences that are similar to MNRead charts but constructed in 4 lines. The MP1 Read sentences, though similar to MNRead sentences in terms of word content and text difficulty, were presented on a uniform white background (127 cd/m^2) on the LCD display of the NIDEK MP-1 microperimeter. Fixation testing using various micro-perimeters including MP-1 has been reported widely. However, this study is perhaps the first to report the use of the MP-1 in assessing the reading speed and reading acuities. Reading sentences on a display with a limited field of view, during head restraint and with pupillary dilatation can be very different from the regular assessment using the hand-held externally illuminated MNRead charts.

However, the correlation between these two dissimilar testing modalities was good (>0.7) for both reading acuity and reading speed. The advantage of using the MP-1 (which is at least 100 times costlier than other standard methods) instead of or in addition to the MNRead assessment is the availability of a retinal view to allow monitoring of the retinal locus used for reading. The MP-1 allows the examiner to freeze an image and therefore plot the locus of fixation points to know the reading PRL and the trajectory of eye movements (subject to a temporal sampling limitation). However, when we projected sentences in the MP-1 to record the reading speed, it was not feasible to achieve proper

subject alignment and focus, freeze the IR fundus image and choose a ROI for image tracking, and only then start the timer for reading assessment. For this reason, we chose not to track the fundus during reading with the MP-1. Nevertheless, we confirmed in all of our study subjects that the retinal region used to sequentially position each word of the MP1 Read sentence was roughly similar to the word-fixation PRL.

Contrast sensitivity thresholds were assessed using the FrACT program, which displayed 'C' optotypes of different contrast in 4 orientations to estimate Weber contrast thresholds. The test is different from chart-based testing (like Pelli-Robson or Regan, (Pelli & Robson, 1988; Regan & Neima, 1983)) that employs letters or sentences of varying contrast. FrACT testing is relatively quick (as a run can be completed in about 10 minutes including training), has been reported widely in the literature, and is available for use anywhere after proper calibration of the display. It is worth noting that although the retinal location that was used for identifying the low-contrast 'Cs' in the FrACT test is unknown, we presume the locus was the same as the word-fixation PRL. The poor correlation between the FrACT contrast thresholds and the reading measures perhaps demonstrates that reading is influenced by many factors in addition to contrast sensitivity. Fixation stability assessed using BCEA had a poor and insignificant correlation with the eccentricity of the PRL. This surprising finding is perhaps due to the diverse nature of subjects, with varying duration of CFL in our study. Several studies report a significant correlation between the PRL eccentricity and the fixation stability (Nguyen-Tri et al., 2016, Bedell et al., 2015, Reinhard et al., 2007, Timberlake et al., 2005). The range of BCEA values reported here is similar to other studies of patients with CFL (Bedell et al., 2015; Longhin

et al., 2013; Macedo, Crossland, & Rubin, 2011; Seiple et al., 2013). As speculated previously by others, it is plausible that the duration and stability of CFL has a bearing on the fixational stability (Crossland et al., 2005; White & Bedell, 1990).

Most of the subjects in our study had a clear dominance/preference to one eye due to considerable inter-ocular differences in acuity and/or extent of macular degeneration. Recall that the CFL in the worse eye was confirmed by screening the central 6° of the visual field. All of our assessments were monocular and so may not reflect the real-world situation, which is almost always binocular. Many eye-trackers don't offer the option of binocular evaluation but recently, an optical attachment that attaches to an SLO was demonstrated (Timberlake & Ward, 2013) to be effective in imaging the both the eyes simultaneously. The location of the PRL, which can be different across tasks, can potentially vary between monocular and binocular viewing especially when the central visual loss is symmetrical. Wiecek et al. (2015) reported a binocular micro-perimetry system employing eye tracking and stereo shutter glasses that reliably mapped the location of simulated scotomas in normally-sighted subjects. Thus with these new technologies, it will be interesting to explore the binocular development of the PRL especially in individuals with progressive and symmetric CFL.

The novel finding that micro-scotomas occur frequently within the PRL of subjects with CFL can perhaps explain some aspects of the reading deficits in these subjects. In our cohort of 28 subjects (1 excluded for poor OCT image quality), 7 subjects didn't exhibit any MSs, whereas the remaining 21 subjects were determined to have MSs at an average

of ~25% of the sampled PRL locations. The peripheral retinal locations of a cohort of 8 subjects with normal vision (**Appendix 6.17**) was screened for MSs using a high density grid and 0 dB test spots. The screening confirmed that local defects don't exist in normal peripheral retina. This lends more credence to the finding of MSs in the PRL of CFL subjects.

The distribution of %MSs was very similar across our subject cohorts. Because of the various reports (Crossland et al., 2005; Timberlake et al., 1986, 2005) that suggested that the PRL in AMD is usually located at the atrophy margin, we anticipated that the AMD cohort would have a higher % of MSs than, for example subjects with STGD. Unfortunately, we didn't demarcate the edges of atrophy in our subjects and in fact such demarcation can be difficult in non-AMD subjects where the atrophy margins are not very conspicuous. But using the absolute scotomas in 10-2 testing as the guide for the margins of atrophy, 9 of the 10 AMD subjects had the PRL at the edge of the atrophic area, whereas only 4 of the 12 STGD subjects located their PRL adjacent to the atrophic margin.

One explanation for the apparently similar mean %MSs in the three cohorts is that our region-of-overlap criterion for undetected target locations on tests 1 and 2 was perhaps excessively large, and so some of the MSs classified on the basis of overlapping missed test spots were not necessarily overlapping. In seven subjects (3 AMD, 3 STGD, 1 with macular hole) there were no locations within the PRL that did *not* exhibit MSs. On the other hand, two of the subjects with AMD, two of the subjects with STGD and two subjects with other etiologies of CFL had no MS locations within the PRL. Despite the fact that

most subjects with STGD adopt a PRL that is remote from the visible margin of the atrophic macula, the high prevalence of MSs in these subjects leads us to speculate that in the majority of subjects with STGD retinal function at the PRL is abnormal.

Despite similar proportions of MSs, subjects with STGD had significantly faster reading speeds than subjects with AMD. This difference in reading speed has been reported previously (e.g., Legge et al., 1992). One possible contribution to this difference is the age difference between the AMD and STGD subjects in our cohorts (mean ages: 39 vs. 78 years), as the maximum reading speed is known to decrease with age (Legge et al., 1992). In the next chapter, we assess reading of sequentially flashed words in the presence of varying percentages of simulated MSs, and show that the influence of these simulated MSs is more profound in older compared to younger subjects with normal vision. However, in our cohorts of subjects with CFL, the presence of MSs didn't seem to influence reading performance as anticipated.

The prevalence of structural retinal changes was not significantly different between MS and nonMS locations in our subjects with CFL. This outcome has several possible explanations, like difficulty in accurately segmenting the OCT scans with alterations in outer retinal layers such as drusen or RPE loss (which would increase the variability of measured layer thicknesses), errors in image registration and hence in the definition of MS and nonMS ROIs and, lastly, that changes in function might precede observable structural changes in the retina. We believe that the chief reason for the discordance between the functional and structural estimates could be the noise associated with the process of manual

segmentation. Although the segmenter (AKK) did consult and confirm the results of segmentation with an experienced segmenter (NBP), the skill of manual segmentation has a potential to improve as more scans with pathology are segmented.

AF imaging indicated that 9 of the 22 PRLs assessed exhibited abnormal levels of fluorescence. Although agreement between quantitative and qualitative grading of the AF images was weak, this relatively new imaging modality provides supplemental evidence for localized retinal changes within the PRL. Together with the high prevalence of MSs within the PRL, there appears to be adequate evidence that the PRL can include local areas with both functional and structural abnormalities. However, the significance of these abnormalities and their possible extent beyond the region of PRL need to be explored. The changes that we observed within the PRL are only a small piece of the puzzle called reading.

3.5 Conclusions

The word-fixation PRL in subjects with macular degeneration (AMD, STGD and other subjects with CFL) can include local regions of sensitivity loss, or micro-scotomas. These micro-scotomas correlate poorly with changes in retinal structure detected by SD-OCT and with auto-fluorescence, suggesting that functional deficits at the PRL may often precede the structural changes. Probing the PRL and the region surrounding the PRL, including the margin of the central atrophic region, has the potential to improve the selection and training of patients' eccentric viewing loci.

4. CHAPTER IV: Impact of simulated micro-scotomas on reading performance in central and peripheral retina

Contributing Authors:

Hope Queener, M.S, Scott B Stevenson, PhD, Julia S Benoit, PhD and Harold Bedell, PhD

4.1 Abstract

Subjects with central field loss typically fixate with a non-foveal preferred retinal locus, which can include areas of localized sensitivity loss, or micro-scotomas. In this study, we introduced randomly located element deletions to simulate micro-scotomas at the fovea and in the peripheral retina to assess their impact on rapid-serial-visual-presentation (RSVP) reading speed. Eight younger (< 35 years old) and 8 older (> 50 years old) naïve subjects with normal vision monocularly read high and low contrast words, presented at or above the critical print size at the fovea and at 5 and 10 deg in the inferior visual field. MNRead sentences and sentences taken from novels were presented in RSVP format. Randomly distributed 13 x 13 arc min blocks corresponding to 0-78% of the text area were set to the background luminance to simulate micro-scotomas. A staircase algorithm estimated maximum reading speed from the threshold exposure duration for each combination of retinal eccentricity, contrast and element-deletion density in both age groups. Log_{10}RSVP reading rate decreased significantly with element-deletion density and eccentricity. Across conditions, reading speed was slower with low contrast text and faster in younger subjects with normal vision. For a given eccentricity and contrast, a higher density of random element losses maximally affected older subjects with normal vision. These outcomes may explain some of the reading deficits observed in older subjects with central field loss.

4.2 Introduction

Reading is one of the many day-to-day activities that is both visual and cognitive. Vision and its role in reading have been investigated for more than a century (e.g., Huey, 1900). Seminal works by researchers such as Dockeray (1910), Taylor (1965), and Rayner (1975)) were instrumental in formulating the concept of the perceptual/visual span, i.e., the 12 – 15-character area from which a reader acquires information during a single fixation during page reading. Bouma (1973) was one of the first to report that the initial and final letters contribute more substantially than interior letters to word recognition. His studies confirmed a right field advantage for peripheral word recognition and showed that the extent of 'visual interference' or crowding, is more or less a constant fraction (~0.5) of target eccentricity. Today, we know that crowding represents a bottleneck for object recognition in the peripheral retina, although with reference to lexical processing, central and peripheral vision are qualitatively similar (Pelli et al., 2007). In the past few decades, the task of reading in altered visual conditions, as in subjects with real (McMahon, Hansen, & Viana, 1991) or simulated (Fine & Rubin, 1999) vision loss or with involuntary nystagmus eye movements (Thomas et al., 2011; Woo & Bedell, 2006), has received increased attention.

Legge and his colleagues (Legge, Rubin, Pelli, & Schleske, 1985) were one of the first groups to demonstrate a subnormal (~5x slower) reading speed in subjects with bilateral central vision loss (CVL). Conditions like age-related macular degeneration (AMD) and Stargardt disease are common causes of CVL and visual impairment, which is

only compounded by an associated loss in contrast sensitivity (Kleiner, Enger, & Fine, 1988; Ortiz, Jiménez, Pérez-ocón, & Castro, 2010). By studying the role of contrast in low-vision subjects, Rubin & Legge (1989) concluded that visually impaired subjects act as 'contrast attenuators', and if text contrast is appropriately scaled for the reduction in contrast sensitivity, the effect of contrast on reading is similar to that seen in subjects with normal vision. Many subjects with CVL compensate for their loss of central vision by choosing an eccentric viewing locus or, sometimes, multiple eccentric loci for performing day-to-day activities including reading and facial recognition (Macedo et al., 2011; Sullivan, Jovancevic-misic, Hayhoe, & Sterns, 2008; Timberlake et al., 1986). Reading with CVL has been investigated extensively but the non-central viewing locus itself has not received much attention. Recently, the non-central viewing locus was shown in many subjects with CVL to include regions of localized retinal-sensitivity loss, i.e., micro-scotomas (MSs) (Krishnan & Bedell, 2014; Winther & Frisen, 2015).

4.2.1 The RSVP Paradigm

Altered programming and execution of saccadic eye movements (Frost, 1976), fixation instability (Falkenberg et al., 2007; Whittaker et al., 1988a) and extensive crowding (Levi, 2008) are some of the factors that impact performance when individuals are required to read text using a peripheral (non-foveal) retinal location. Rapid Serial Visual Presentation (RSVP) is a paradigm that sequentially presents either the individual letters of a word or the words of a sentence, one at a time, at a given location to minimize the need for saccadic eye movements. This paradigm has been used in several studies of

reading (some in subjects with central field loss, e.g., Rubin & Turano, 1994) for more than half a century (Sperling, 1960). Forster (1970) used sentences of varying complexity, with and without scrambling the word order and identified factors such as word length, visual storage and information loss during transfer to short term memory that impact the speed and accuracy of RSVP reading. Juola, Ward, & Mcnamara (1982) reported that comprehension was similar in conventional page (paragraph) reading and RSVP reading over a range of text difficulties. Rubin & Turano (1994) showed a clear benefit of the RSVP paradigm (~4 times) in terms of reading speed compared to conventional page reading, and concluded that saccadic eye movements impose an upper limit on conventional reading speed. The same authors also investigated RSVP reading in 14 subjects with dense CVL. Although the RSVP paradigm was successful in minimizing the need for saccades, the CVL subjects still required longer word durations to read than non-CVL subjects. Rubin and Turano suggested that the peripheral retina includes a severe bottleneck that limits the ability to decode patterns, such as those required in reading. More recently, Yu, Cheung, Legge, & Chung (2007) reported that in subjects with normal vision the magnitude of improvement with RSVP reading was only about 1.4x faster than normal (flashcard) reading for various conditions of print size and letter spacing.

4.2.2 Simulated Scotomas and Visual Performance

In a study that investigated the impact of simulated scotomas on letter identification, Seiple, Holopigian, Szlyk, & Greenstein (1995) blanked randomly selected pixels to mimic the sampling-element loss that can happen in retinal diseases like retinitis

pigmentosa. Pixels were blanked throughout a rectangular area (20x27 arc min), and the letters were mapped to the center of this area. The luminance of the blanked pixels was set equal to the surround and, interestingly, even high levels (~80%) of pixel blanking didn't affect performance. Geller, Paul, & Green (1992) reported a similar finding when subjects were asked to identify the orientation of high contrast square-wave gratings at or below the Nyquist frequency limit with different levels of stimulus degradation, produced by removing various percentages of the array elements. However, the above-mentioned studies assessed the impact of stimulus degradation only on foveal performance for letter or grating identification.

Levi, Sharma, & Klein (1997) investigated the number of stimulus samples needed for pattern identification. Of the 17 Gabor features that formed an E shape, about 40-50% were required at the fovea to achieve a threshold level of correct performance; however, the number of samples required to reach the identification threshold at 5 and 10 deg in the inferior field was ~70%. Winther & Frisen (2015) used segmented digits (acuity equivalent of 20/200) that were formed by tiny 'rarebits' (0.5 arc min diameter) to assess macular deficits in subjects with CVL secondary to AMD. The median number of rarebits per character stroke required to read the briefly presented (150 ms) digits was 3, 5 and 30 in normal, dry AMD and wet AMD groups respectively. These results indirectly support the idea that subjects with CVL can have MSs that necessitate a greater number of rarebits per stroke to construct legible test digits.

To understand the adaptation of oculomotor system to simulated CVL, Kwon, Nandy, & Tjan (2013) simulated a 10-deg circular disc-like scotoma with distinct edges in a cohort of 6 younger subjects with normal vision. The authors reported rapid development of a preferred retinal locus with re-referencing of saccades to a non-foveal location and interpreted their findings to suggest a flexible and adaptive oculomotor system. Unlike the sharp-edged scotoma employed by Kwon et al., Walsh & Liu (2014) assessed the impact of both sharp- and gradual-edged scotomas on a visual search task. The sharp-edged scotoma resulted in a more consistent use of a single peripheral location (called the preferred retinal locus, PRL) than the gradual-edged scotoma. These results suggest that scotoma awareness, which is reduced for a gradual-edged scotoma, plays an important role in adaptation to CVL (Goodrich, 1977). Lastly, Liu & White (2010) used random local degradation of texture patterns to assess the impact of this manipulation on texture discrimination in young and elderly subjects with normal vision and in patients with early AMD. They reported a reduction in performance and reduced tolerance to stimulus degradation with early AMD.

We hypothesize that scattered MSs in the region of the PRL will degrade visual stimuli, such as the words in a sentence and, potentially, exert a negative impact on reading performance. Although high densities of simulated MSs are required to degrade foveal letter recognition or orientation discrimination (Geller et al., 1992; W Seiple et al., 1995), an outcome measure such as reading speed might disrupted more readily by MSs, especially for text presented in the retinal periphery. Because of their small size, MSs at

the PRL are likely to remain imperceptible and, hence it might be difficult for patients with CVL to adapt to their presence.

4.2.3 Motivation and Predictions

The demonstration that MSs occur within the PRL of many subjects with CVL (Krishnan & Bedell, 2014) leads to the question of the impact of these MSs on visual performance. In particular, the influence of pixel deletion(s) for words presented in the retinal periphery has not received much attention in the vision science literature. To address this issue, in the current study we evaluated the impact of simulated MSs on foveal and non-foveal reading rates. By simulating MSs with and without a simulated contrast sensitivity loss while assessing RSVP reading speed in both younger and older subjects, we sought to better anticipate and explain the functional reading loss in patients with CVL. Because the areas of missing information produced by random element deletion are tiny and scattered across a region of the visual field we expected their influence to be more akin to a gradual- than a sharp-edged scotoma. For this reason, and because we varied the locations of the MSs from trial to trial, we would not expect subjects with normal vision to adapt to this manipulation during the course of the experiment. Further, as the simulated MSs should be less perceptible for words of low compared to high contrast, we anticipated that the impact of random-element deletion would be more severe when subjects attempted to read low compared to high contrast text.

4.3 Methods

Sixteen naive subjects with normal vision (8 younger, <35 years; 8 older, >50 years) were recruited from among the faculty, staff and students of the University of Houston, College of Optometry. The study protocol was approved by the committee for the protection of human subjects at the University of Houston and all subjects provided written informed consent before participating. Subjects were compensated in part for their time and participation. Each observer's preferred eye (determined as the eye that subjects didn't close when asked to close one eye) was chosen for testing and the other eye was occluded with a black opaque patch. Six of the 8 older subjects wore their habitual correction (progressive lenses or trifocal contact lenses), which was appropriate for the two testing distances of 35 and 57 cm used for reading in this study. The other 2 older subjects read with a near correction that was appropriate for 35 cm and rejected a reduced reading addition for 57 cm. Testing was done under normal room illumination with natural undilated pupils. A chin and a forehead rest were used to stabilize the observer's head. The reading material used in this study included 60-character MNRead (Mansfield et al., 1994) sentences (provided by Drs. Steve Mansfield and Gordon Legge) and 53 ± 8 character sentences, taken from novels (provided by Dr. Susana Chung, c.f., Chung, Mansfield, & Legge, 1998). Words were presented in lower case, except for the first letter of the word that began each sentence and the first letter of proper nouns.

A 21" flat Sony Trinitron (model GDM-F520, resolution of 1600 x 1200 pixels) CRT was used to display the test stimuli at a refresh rate of 85 Hz. The test stimuli were

designed using the Psychophysics Toolbox -3 (Brainard, 1997; Kleiner et al., 2007)) that interfaces between MATLAB R2014a (MathWorks, Natick, MA, USA) and the computer hardware used. The test area comprised 1280 x 1024 pixels and subtended 36° x 29° at the 57 cm viewing distance (1 pixel subtended ~1.7 arc min). The luminance of the dark Courier font letters and the uniform white background ($L_{BG} \approx 113$ cd/m^2) was assessed using a Minolta LS-100 luminance meter. Testing using letters with high (> -90%) and low Weber contrast (≈ -10%) was performed in 2 different sessions. During the study, the examiner sat next to the subject and monitored his or her fixation visually. Trials that were observed to include a vertical saccade were discarded and re-run immediately.

4.3.1 Pilot Testing for Reading Acuity

In a pilot study involving 5 young naïve subjects with normal vision (ages: 23-31 years), the word reading acuity was estimated at the fovea (E0) and at 5 and 10 deg (E5 and E10) in the inferior visual field. Subjects fixated on a 1-deg cross (turned off during foveal testing) and randomly selected words of 5-10 letters sampled from the sentence pool described above were displayed at various sizes (acuity range: 20/800 - 20/20 in 0.1 logMAR steps) to determine the reading acuity, defined as the smallest letter size at which words could be read correctly. Testing was repeated thrice for each subject, using both high and low contrast words at eccentricities E0, E5, and E10. The critical print size (CPS) was specified as 4 lines larger than the reading acuity, i.e., CPS = mean logMAR reading acuity + 0.4 (Cacho, Dickinson, Smith, & Harper, 2010; Chung et al., 1998). In the main experiment, the x-height (height of the lowercase x, c.f., Mansfield et al., 1994) of the

presented text at each eccentricity was equal to the average CPS as determined in the pilot study, with the exception of high-contrast testing at the fovea where the x-height was set larger (x-height = logMAR reading acuity + 0.7). Larger letters were used in the high contrast foveal condition to prevent the individual 13 x 13 arc min element-deletions (see below) from obscuring entire letters.

4.3.2 RSVP Testing for Reading Speed

Simulation of Micro-scotomas and Fixational Jitter

At each eccentricity tested (E0, E5 and E10) the words of a randomly selected sentence from the sentence pool were presented sequentially, one at a time. As noted above, when the text was presented at E5 and E10, the experimenter monitored the subjects to ensure that fixation on the fixation cross was maintained. The unaided eye can usually detect an eye movement that is larger than 1° (Yarbus, 1967).

Each presented word was centered both horizontally and vertically within a rectangular RSVP window (**Figure 4-1**, right), which itself was at the center of the Sony CRT screen. In different conditions, randomly distributed 13 x 13 arc min blocks (chosen to match the size of the stimuli used previously to map MSs in patients with CVL by Krishnan & Bedell, 2014) corresponding to 0, 13, 26,…,78% of the RSVP window were set to the background luminance (gray scale = 255) to simulate the influence of localized MSs (**Figure 4-2**). The step size of 13% was chosen to ensure adequate sampling of range of the MS densities from 0 to 75% and is not related to the block size of 13 arc min. To simulate the influence of fixational eye movements, the location of all of the element-

deletions was jittered (SDx, SDy = 0.3 deg) in tandem during the presentation of the successive words in each sentence. Both the locations of the element-deletions within the RSVP window and the jitter to simulate the effect of fixational eye movements varied from sentence to sentence.

RSVP Window

The RSVP window, excluding a surrounding padding area, was 13 letter characters wide and 2 characters high. The surrounding padding area (±0.9 deg) was included to accommodate the word-to-word jitter that was introduced in the location of the MSs. The RSVP window size was contingent on the text x-height (window height = 2*(x-height)) and so was different for the 3 eccentricities tested. A fixation cross was present throughout testing, except for testing at E0. Vertical markers (**Figure 4-1**, right), which helped the subjects to direct their attention to the appropriate location on the CRT screen for words at eccentricities, E5 and E10 stayed on the screen only during the presentation. The attention markers appeared with onset of the first word and disappeared simultaneously with offset of last word in each sentence. The height of the attention markers was set equal to one x-height and the vertical center-to-center distance between each word and surrounding markers was set to 3 times the x-height. These values were so chosen to avoid any undue interference between the attention markers and the margins of the RSVP window.

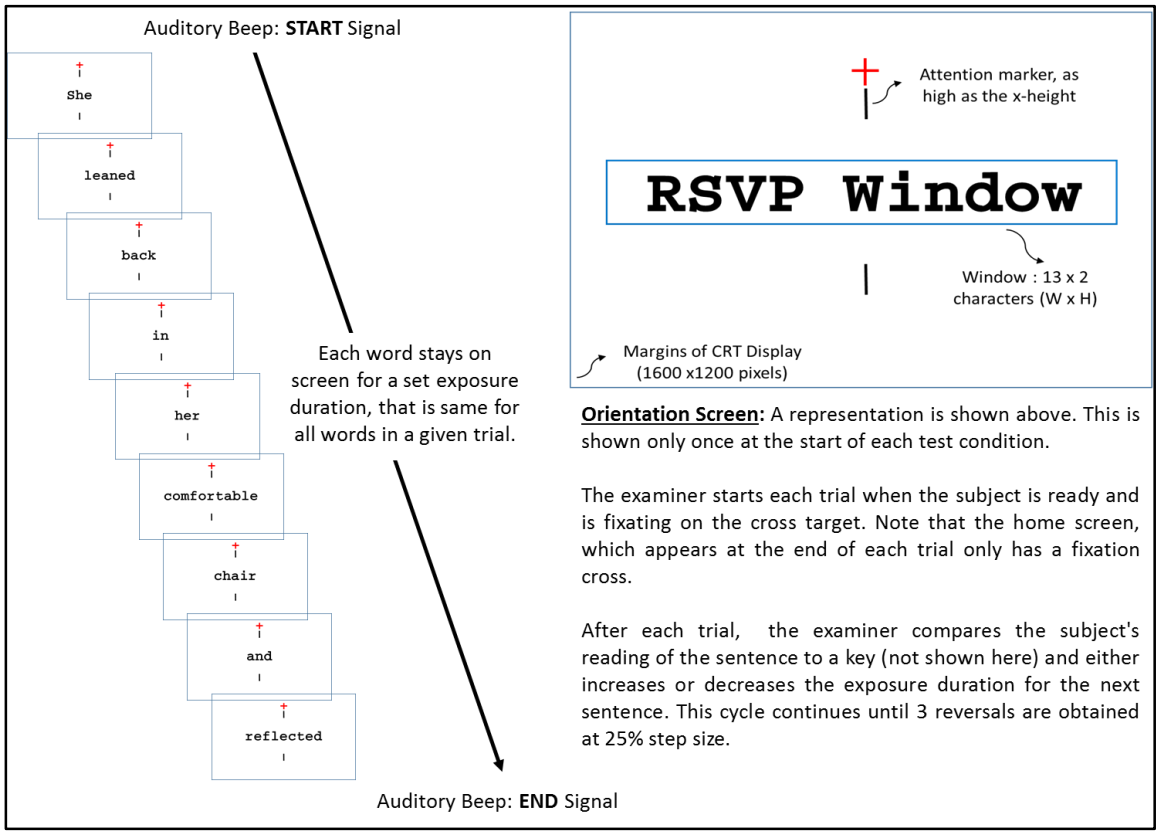

Figure 4-1 Illustration of RSVP Testing

***On the left**, a representation of the sequence of words of a sentence during the assessment of RSVP reading speed using high-contrast text, for an eccentricity of 5 deg in the inferior visual field (E5). The red fixation cross and the vertical attention markers stayed on the screen throughout each trial. **On the right,** the orientation screen is enlarged to show details. Note that the margin of the RSVP window was not visible during testing (See **Figure 4-2**). The padding area (empty white space inside the RSVP window) that surrounds the word in both the horizontal and vertical directions allows for simulated fixational jitter of the element-deletion locations.*

Reading Speed Assessment

After about 15 minutes of demonstration, training and practice with the RSVP reading task, assessment began either at E5 or E10, chosen randomly across subjects. The chosen condition was always followed by testing at the fovea and then at the third, remaining eccentricity. For the subjects who participated in testing using both high and low contrast text, the high contrast condition was always done first. An auditory beep signaled the start and the end of each trial and the subjects either read the words as they appeared sequentially on the screen or read the whole sentence after all the words had appeared (**Figure 4-1** left). There was no time limit to respond and subjects were encouraged frequently to guess and to make corrections if deemed necessary.

Individual sentences were shown just once to each observer. Following the observer's response on each trial, the whole sentence was displayed on the screen to provide immediate feedback. Presenting the entire sentence on the CRT also helped the examiner to score the subject's response to each sentence as either correct (read all of the words correctly; the addition of extra words aside from the words that constituted the sentence was not penalized) or incorrect (missed one or more words). The examiner recorded the score using either the 'up' or 'down' arrow key, which increased or decreased the exposure duration of each word on the following trial. The different levels of element deletion were tested in ascending order, starting from 0% to 39%, and to 52% (shown in **Figure 4-2**), 65% and 78%, if reading was still possible. We didn't randomize the order of element deletion and chose to test in the ascending order to eventually prepare subjects for

the most severe condition with maximum element deletion. In testing that is already demanding for several reasons including the brief presentation durations, eccentric viewing, and the requirement to recall words in order, the ascending order of testing helped motivate the subjects, but might have inflated the reading speeds at higher element-deletion densities.

A staircase algorithm estimated the threshold exposure duration for each combination of retinal eccentricity, letter contrast and element deletion. The exposure duration of each word changed in gross steps of 50% until the occurrence of the first staircase reversal, after which a step size of 25% was used to define 3 more reversals. For each condition tested, the reading speed in words per minute (wpm) was determined for each subject from the threshold exposure duration, as shown below.

$$Exposure\ Duration\ (ms)$$

$$= Number\ of\ frames\ \times \frac{1000}{Frame\ Rate(Hz)}$$

$$Threshold\ Exposure\ Duration\ (ms)$$

$$= Arithmetic\ Mean\ of\ last\ 3\ Staircase\ Reversals$$

$$RSVP\ Reading\ Speed\ (wpm)$$

$$= \frac{60{,}000}{Threshold\ Exposure\ Duration\ (ms)}$$

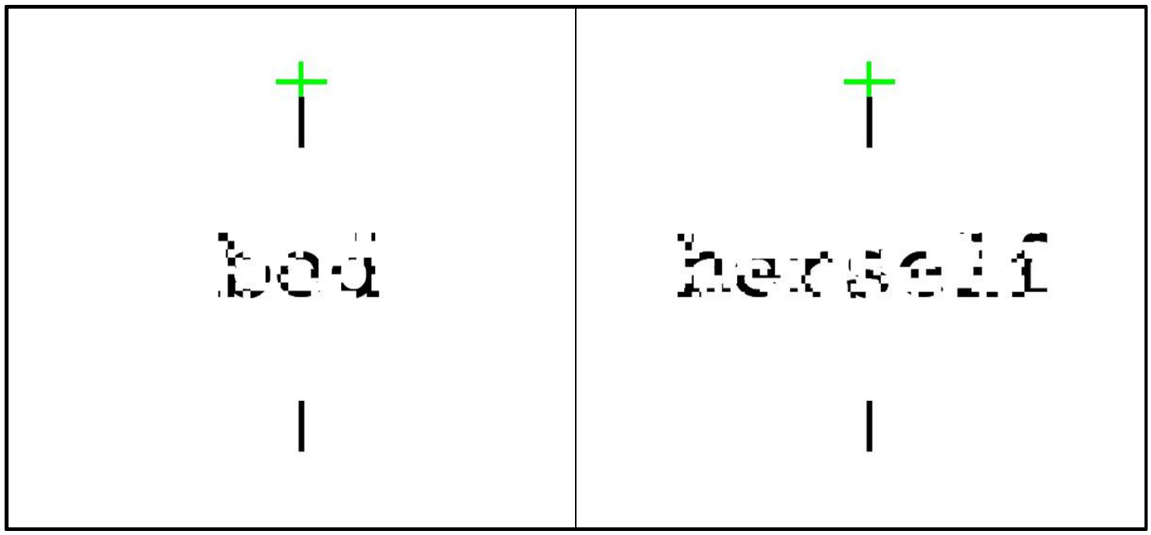

Figure 4-2 Screenshot of Simulated Micro-scotomas

A cropped image showing the central portion of the screen during RSVP testing. The example shows high-contrast words at E5 (x-height = 1.2 logMAR) and at an element-deletion density of 52%. The red fixation cross in ***Figure 4-1*** *turned green during testing and along with the vertical attention markers, stayed on the screen throughout each trial. Note how the same element-deletion density can have a different impact on legibility depending on number of letters in the word and the locations of the deleted elements in the window. As seen here, the RSVP window margins were not visible during testing.*

4.3.3 Data Analysis

A linear mixed modeling approach (Bagiella, Sloan, & Heitjan, 2000) was used to assess the effect of simulated % element-deletion on the $\log_{10}$RSVP reading speed. Reading rate is expressed throughout as base $\log_{10}$ wpm to approximately equalize variances across conditions. The effect of element-deletion density was modeled in the presence of

interacting independent variables of age group, contrast and eccentricity. The mixed effects model allows analysis of an imbalanced repeated-measures data set like ours (as all subjects could not successfully read text at all levels of simulated element-deletion density) and makes the best use of the available data. We deemed this analysis preferable to ANOVA, in which missing data points from one or more subjects require the data of all subjects in the specified treatment condition to be discarded.

To examine the relationship between element-deletion density and the $\log_{10}$RSVP reading speed we ran a mixed effects linear regression analysis using PROC MIXED in *SAS 9.2* (SAS Institute, Cary, NC) to control for the within-subjects nature of the study design while handling missing data. A random effect for subject with a variance component structure was specified and the residual correlation was modeled specifying an unstructured covariance structure. We were also interested in the effects of contrast, eccentricity, and age on mean reading speed and how these factors affected the relationship between element-deletion density and log RSVP reading speed. Therefore, fixed effects included within-subject variables element-deletion density as a continuous variable, repeated factors contrast (2 levels: high, low) and eccentricity (3 levels: 0, 5, 10) and between-individual factor age (2 levels: younger, older) in addition to interaction terms. We checked the interaction terms, beginning with the full model including the highest order terms, and removed non-significant interaction terms to simplify the model, while also aiming for a reduced Akaike information criteria (AIC). A residual analysis was used to evaluate the fit of the final model. The parameter estimates for the main effects and

interaction terms included in the final model are presented in **Table 4-1** along with p-values based on the *t* statistic.

4.4 Results

In the preliminary experiment, the average CPSs for E0, E5 and E10 were 0.4, 1.2 and 1.7 logMAR respectively, for high contrast words and 0.7, 1.2 and 1.7 logMAR for low contrast words. For RSVP testing with high contrast words and no random element-deletions (0% MS), the average (±SD) reading speeds in $\log_{10}$ wpm (wpm given in parenthesis) at the fovea were: 2.87±0.12 (743.2) and 2.77±0.16 (584.1) for the younger and older subjects, respectively. The corresponding values for testing with low contrast words were: 2.69±0.08 (492.4) and 2.49±0.13 (310.8).

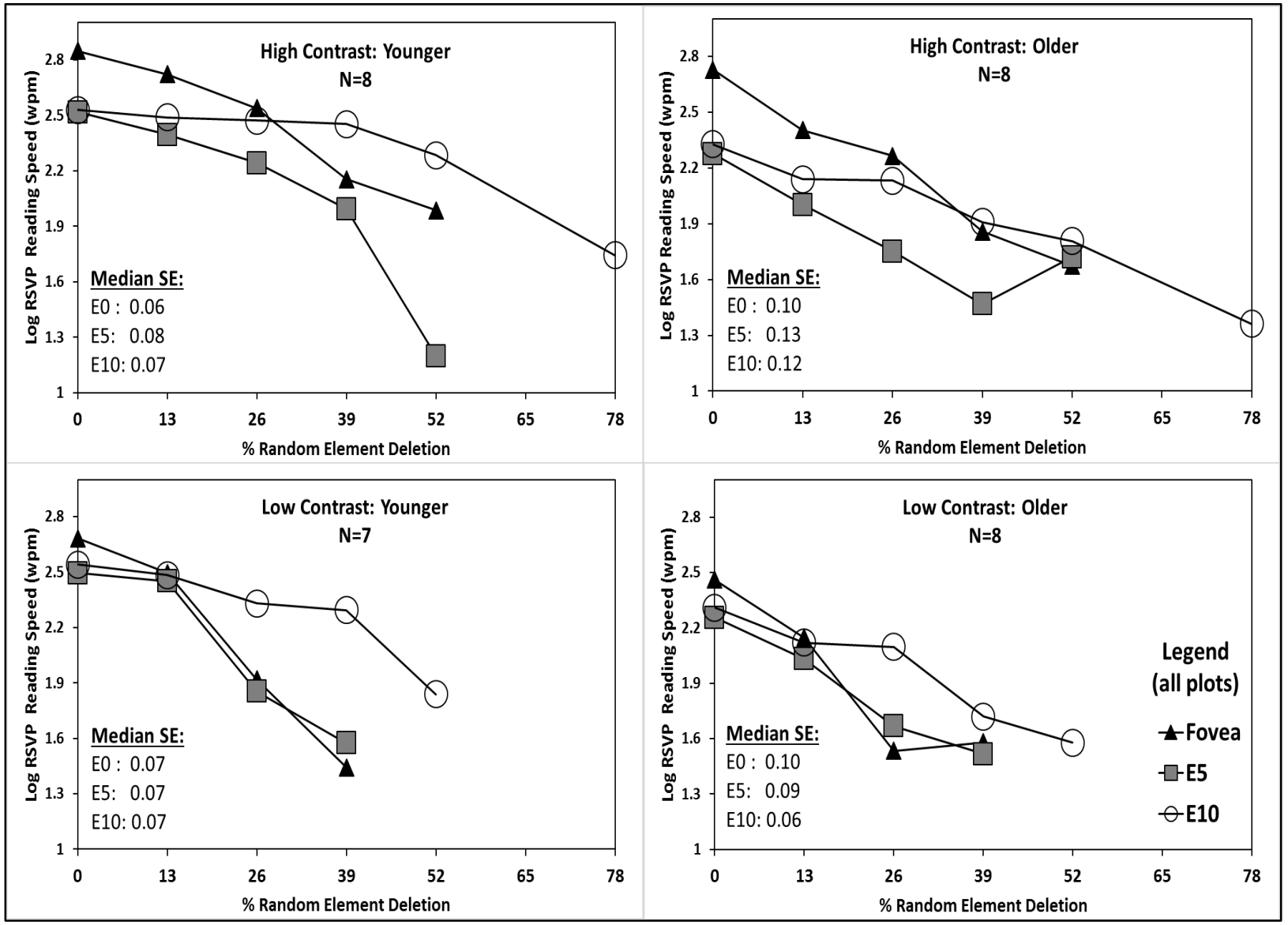
High Contrast: Younger
N=8
Log RSVP Reading Speed (wpm)
% Random Element Deletion
Median SE:
E0 : 0.06
E5: 0.08
E10: 0.07
High Contrast: Older
N=8
Median SE:
E0 : 0.10
E5: 0.13
E10: 0.12
Low Contrast: Younger
N=7
Median SE:
E0 : 0.07
E5: 0.07
E10: 0.07
Low Contrast: Older
N=8
Median SE:
E0 : 0.10
E5: 0.09
E10: 0.06
Legend
(all plots)
Fovea
E5
E10

Figure 4-3 Reading vs Element-Deletion Density

Log RSVP reading speeds (in wpm) as a function of % element-deletion density for high (top row) and low contrast text (bottom row) in younger (left column) and older (right column) subjects. Note that testing for >39% simulated element-deletion density for low and >52% for high contrast words was possible only at an eccentricity of 10 deg (E10).

Not all subjects could be tested for the highest element-deletion density and hence the reading speed for the highest element-deletion density at E5 (HC-Older) and E0 (LC-Older) were more variable and less reliable. The median standard error (SE, across element-deletion densities) is provided as an inset in each panel for each eccentricity.

As shown in **Figure 4-3**, log RSVP reading rate decreases significantly with the simulated element-deletion density ($b = -0.025$, $p<0.0001$, also see **Table 4-1**) and eccentricity (E5: $b = -0.43$, $p<0.0001$, E10: $b = -0.402$, $p<0.0001$). The expected reading speed was lower ($10^{0.305} \approx 2x$) for the low contrast text and was higher ($10^{0.259} \approx 1.8x$) in the younger subjects with normal vision. The intercept value of 2.742 ($10^{2.74} \approx 552$ wpm) represents the model-predicted mean log RSVP reading speed for the foveal testing of older subjects, with high contrast words (Reference condition, see **Table 4-1**) at 0% element-deletion density.

The slopes (across both the contrast and age groups) of the linear fit were significantly different between the eccentricities E0 vs. E10 ($t(89.4) = 8.3$, $p<0.0001$) and E5 vs. E10 ($t(74.4) = 6.8$, $p<0.001$). However, the fitted slopes for E0 vs. E5 were not significantly different ($t(55.25) = 1.19$, $p=0.24$, Also refer to **Figure 4-4**). The 2-way

interactions that were significant ($p<0.05$) are %Element-deletion x eccentricity, %Element-deletion x contrast, and contrast x eccentricity (from type 3 tests of fixed effects, not shown here). The relationship between element-deletion density and reading speed is significantly modified by eccentricity (E10 vs. E0, b=0.014, P<0.0001), age (younger vs. older b=0.004, p=0.0274), and contrast (low vs. high, -0.005, p=0.0059, also see **Table 4-1**).

Effect	Estimate (SE)	Pr >|t|
Fixed Effects		
Intercept	2.742 (0.07)	<.0001
Contrast: Low	-0.305 (0.06)	<.0001
Age: Younger	0.259 (0.09)	0.0107
MS Density	-0.0247 (0.001)	<.0001
Eccentricity: E5	-0.43 (0.06)	<.0001
Eccentricity: E10	-0.402 (0.06)	<.0001
Interactions		
MS Density * Eccentricity (E5)	0.002 (0.002)	0.2708
MS Density * Eccentricity (E10)	0.014 (0.002)	<.0001
MS Density * Age (Younger)	0.004 (0.002)	0.0274
MS Density * Contrast (Low)	-0.005 (0.002)	0.0059
Contrast (Low) * Eccentricity (E5)	0.327 (0.069)	<.0001
Contrast (Low) * Eccentricity (E10)	0.325 (0.06)	<.0001

Table 4-1 Maximum Likelihood Parameter Estimates from the Model

Maximum likelihood parameter estimates of log RSVP reading speed (wpm) for the linear mixed effects model. The second column lists the estimate and standard error (SE) of the fixed-effect parameters. The parameter estimates are for comparison with the arbitrarily chosen reference condition of: high contrast, older age group and E0 (fovea).

4.5 Discussion

Our study demonstrates that simulated MSs impact RSVP reading performance both in the central and peripheral retina. Although this is not surprising, it is worth noting that the impact was persistent even after scaling the word size to be equal to the CPS at each eccentricity. When compare to the study by Seiple et al (1995) on letter identification our plots don't show a plateau region and a steep decline. This was true for both contrast levels and age groups, and it is likely due to the unlimited viewing time that was available to subjects in letter identification study. In our study, our subject's task was to read both as accurately and as fast as possible and hence even a small percentage of element deletions can have an impact on reading speed. Recall that the element size was 13 arc min here vs 0.5 arc min in the study by Seiple et al (1995). With an increase in element size, even a small % of element deletion can impact performance.

In a retrospective study of 82 subjects with central scotoma who were referred for low vision rehabilitation, Fletcher et al. (1999) reported an average CPS of 1.20 logMAR (0.6 (10^{th} percentile) – 1.8 (90^{th} percentile). Cacho et al. (2010) from a study on 243 subjects with AMD, report an average CPS of 1.43 logMAR (Range: 0.54-2.20). Thus, the

x-height of the words used in our study at 5 and 10 deg in the inferior visual field is either at or above the average CPS for CVL subjects.

The choice of CPS at each eccentricity might explain the similar reading speeds (**Figure 4-3**) for E5 and E10 for 0% element deletion condition. Chung et al. (1998) investigated the effect of print size on reading speed in normal peripheral vision. The two-line fits for the plots of reading speed (wpm) as a function of print size (deg), have an ascending limb with a slope that varies across subjects and a plateau region (Refer to Figure. 3 in Chung et al. 1998). In our testing, the CPS used for E5 might be lower than the plateau for some subjects, so that the CPS used perhaps fell on the ascending limb region of the 2-line model fit by Chung et al.

We report that the average reading speed for testing at E10 was always higher than testing at E5. Though counter-intuitive, this can be explained by the larger size of words for testing at E10. The larger the CPS, the bigger the words and the RSVP window and, hence, lower the impact of % element deletion. Recall that for simulating MSs by element deletion, we set the luminance of a specific percentage of the whole RSVP window to background luminance. This percentage was not a fraction of the character height but rather the whole window. The foveal reading speed for high and low contrast words were not very different in both younger and older normal cohorts. This is perhaps because the Weber contrast of the low contrast words (10%) was either close or above the critical contrast for foveal reading. The latter is defined as the lowest text contrast that could still support maximum reading speed (Chung & Tjan, 2010; Legge, Rubin, & Luebker, 1987).

Impaired reading performance for low contrast words is not novel (Legge & Kersten, 1987), but it may help to explain the interaction of scattered sensitivity losses (from MSs) with impaired contrast sensitivity, such as those seen in some individuals with CVL secondary to macular degeneration (Rubin & Legge, 1989). Taken together, our findings shed light on the reading deficits in individuals with CVL. The greater the eccentricity of the PRL, the greater the number of MSs, and the more contrast sensitivity is impaired, the slower should be the reading speed. Because the RSVP mode of text presentation minimizes the need for reading eye movements, the impact of MSs on real-world page reading by subjects with CVL can potentially be more detrimental than shown by our results.

Of the several interactions noted, two of them stand out and warrant comment. In addition to an overall slower reading rate in the older- compared to the younger-subject group (**Table 4-1**, $p < 0.0107$), the reading speed of the older subjects dropped slightly but significantly faster as the density of random element-deletions increased (**Table 4-1**, $b= 0.004$, $p=0.0274$). Both the slower overall reading speed as well as the more deleterious impact of random localized sensitivity losses in the older compared to younger subjects might result from altered high-level visual processing (such as visual memory) in the older age cohort. Along a similar line, the significant interaction between element-deletion density and contrast is interesting. With other factors being the same, reading speed fell more quickly with the density of random element-deletion ($b= -0.005$, $p=0.0059$) for low than high contrast text. One way to interpret this interaction is that, by setting small regions of the text to the background luminance, the introduction of random element-deletions can

effectively reduce the local contrast. Rubin & Legge (1989) reported a rapid reduction in reading speed for contrasts below the critical contrast, defined as the lowest text contrast that could still support maximum reading speed. Because the contrast "reserve" is smaller for low- compared to high-contrast text, a reduction of the effective contrast that results from random element-deletions would be expected to exert a greater influence on reading speed for low-contrast words.

Although we simulated an influence of fixational eye movements on successively presented words by jittering the locations of the random element-deletions *en bloc* both horizontally and vertically, the fixational eye movements made by subjects with CVL may differ quantitatively from this simulation. For example, Kumar & Chung (2014) reported that the median amplitude of slow fixational drifts in 16 subjects with macular disease (mean age ~75 years) was ~14 arc min, almost twice that of older subjects with normal vision. The authors also reported that the median amplitude of micro-saccade was ~53 arc min in subjects with macular disease, approximately 3.5 times larger than age-matched subjects with normal vision.

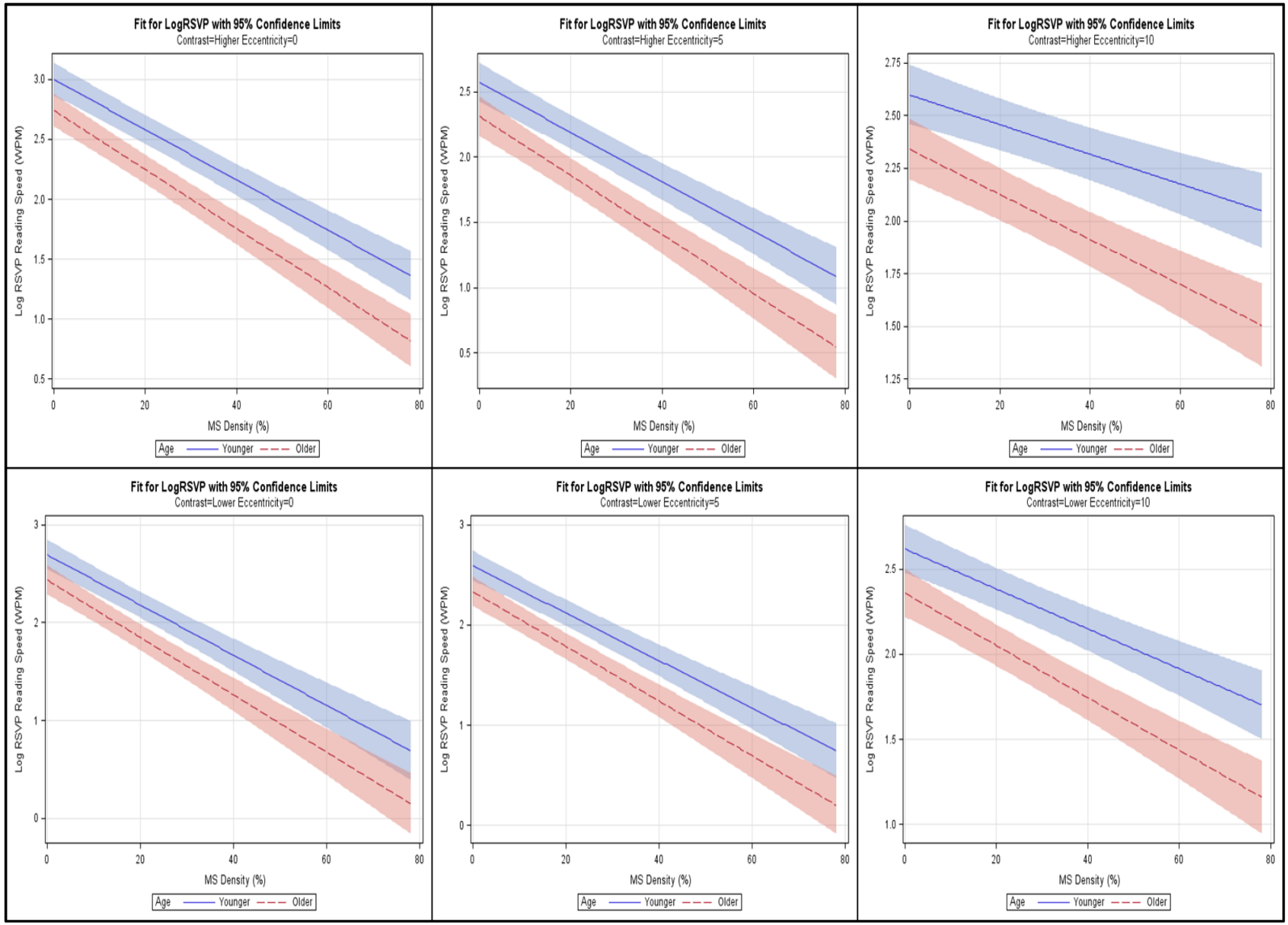
Fit for LogRSVP with 95% Confidence Limits
Contrast=Higher Eccentricity=0
Log RSVP Reading Speed (WPM)
MS Density (%)
Age Younger Older
Fit for LogRSVP with 95% Confidence Limits
Contrast=Higher Eccentricity=5
Log RSVP Reading Speed (WPM)
MS Density (%)
Age Younger Older
Fit for LogRSVP with 95% Confidence Limits
Contrast=Higher Eccentricity=10
Log RSVP Reading Speed (WPM)
MS Density (%)
Age Younger Older
Fit for LogRSVP with 95% Confidence Limits
Contrast=Lower Eccentricity=0
Log RSVP Reading Speed (WPM)
MS Density (%)
Age Younger Older
Fit for LogRSVP with 95% Confidence Limits
Contrast=Lower Eccentricity=5
Log RSVP Reading Speed (WPM)
MS Density (%)
Age Younger Older
Fit for LogRSVP with 95% Confidence Limits
Contrast=Lower Eccentricity=10
Log RSVP Reading Speed (WPM)
MS Density (%)
Age Younger Older

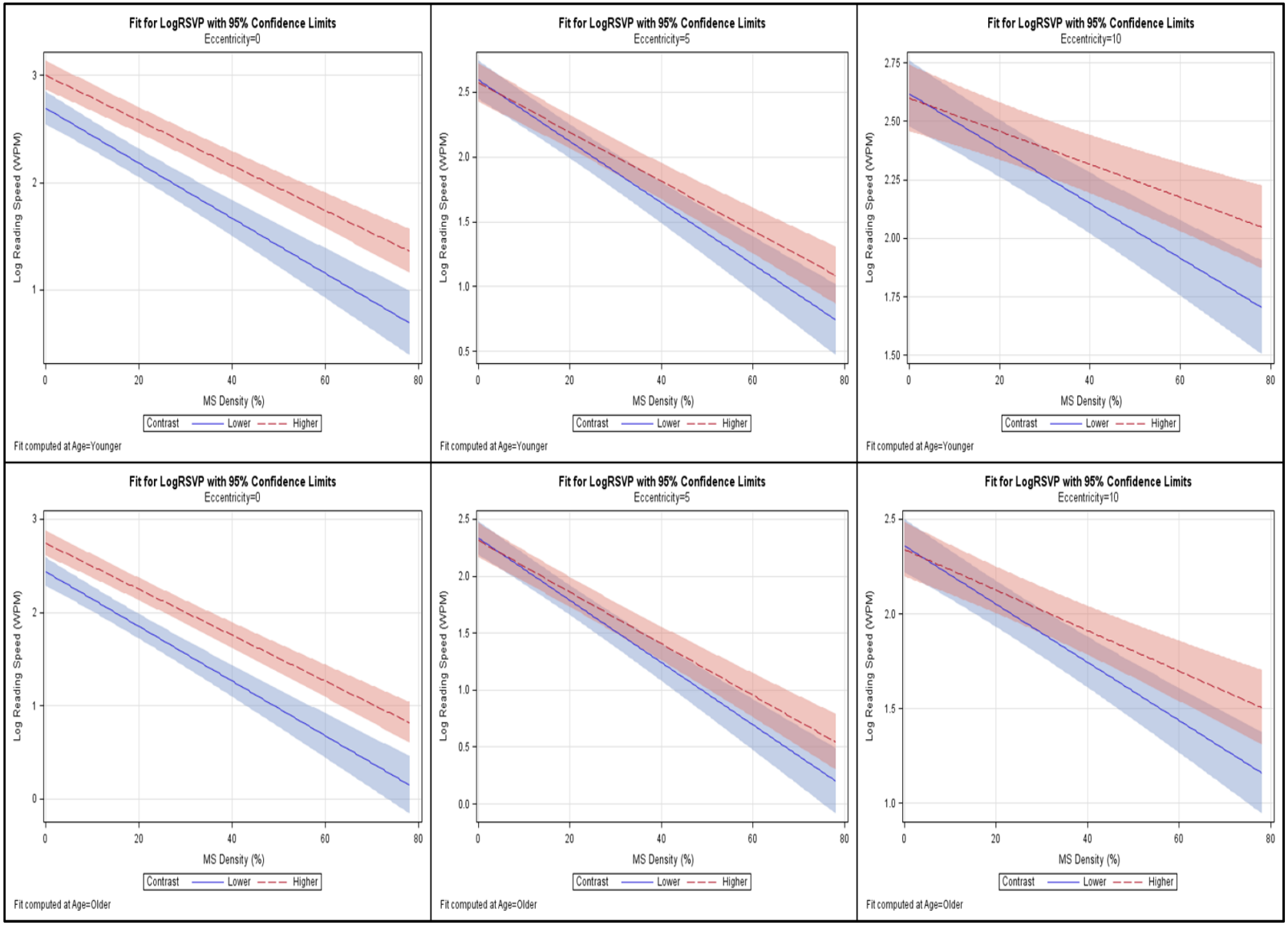
Fit for LogRSVP with 95% Confidence Limits
Eccentricity=0
Log Reading Speed (VVPM)
MS Density (%)
Contrast Lower Higher
Fit computed at Age=Younger
Fit for LogRSVP with 95% Confidence Limits
Eccentricity=5
Log Reading Speed (VVPM)
MS Density (%)
Contrast Lower Higher
Fit computed at Age=Younger
Fit for LogRSVP with 95% Confidence Limits
Eccentricity=10
Log Reading Speed (VVPM)
MS Density (%)
Contrast Lower Higher
Fit computed at Age=Younger
Fit for LogRSVP with 95% Confidence Limits
Eccentricity=0
Log Reading Speed (VVPM)
MS Density (%)
Contrast Lower Higher
Fit computed at Age=Older
Fit for LogRSVP with 95% Confidence Limits
Eccentricity=5
Log Reading Speed (VVPM)
MS Density (%)
Contrast Lower Higher
Fit computed at Age=Older
Fit for LogRSVP with 95% Confidence Limits
Eccentricity=10
Log Reading Speed (VVPM)
MS Density (%)
Contrast Lower Higher
Fit computed at Age=Older

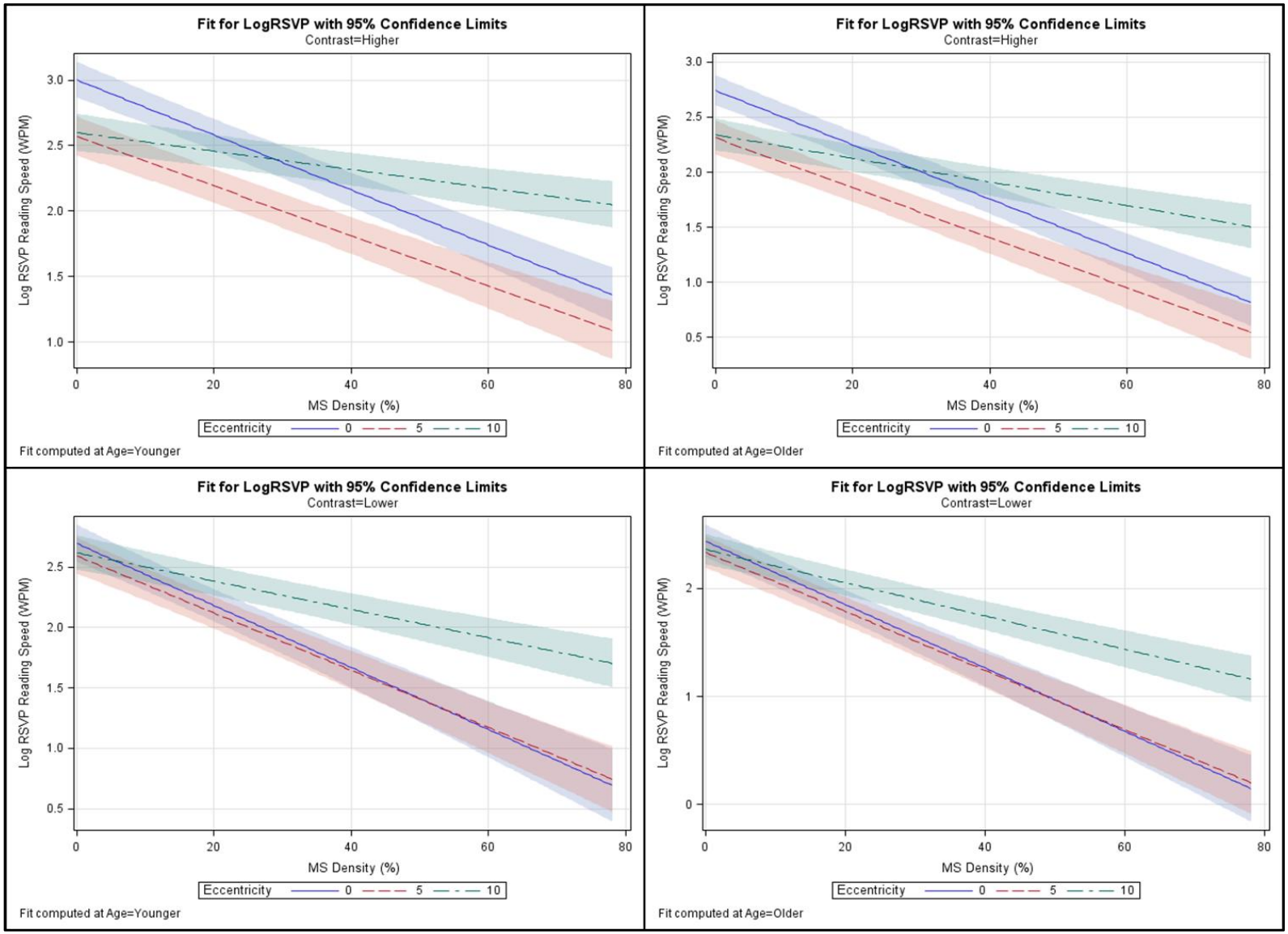
Fit for LogRSVP with 95% Confidence Limits
Contrast=Higher
Log RSVP Reading Speed (WPM)
MS Density (%)
Eccentricity 0 5 10
Fit computed at Age=Younger
Fit for LogRSVP with 95% Confidence Limits
Contrast=Higher
Log RSVP Reading Speed (WPM)
MS Density (%)
Eccentricity 0 5 10
Fit computed at Age=Older
Fit for LogRSVP with 95% Confidence Limits
Contrast=Lower
Log RSVP Reading Speed (WPM)
MS Density (%)
Eccentricity 0 5 10
Fit computed at Age=Younger
Fit for LogRSVP with 95% Confidence Limits
Contrast=Lower
Log RSVP Reading Speed (WPM)
MS Density (%)
Eccentricity 0 5 10
Fit computed at Age=Older

Figure 4-4 Interaction of Various Factors

The linear fits from the mixed-effects model, with random element-deletion density (Shown in figure as micro-scotoma- MS density) on the X-axis and the predicted log_{10} reading speed on the Y-axis. The shaded region represents the 95% confidence limits. Plots, in the order as they are listed, A) Plots illustrating the interaction of age group and element-deletion density on log_{10} reading speed. B) Illustrates the interaction of contrast and element-deletion density on log_{10} reading speed and C) illustrates the interaction of eccentricity and element-deletion density on log reading speed. Note that C) is the model fit to the plot of raw data in ***Figure 4-3***

Scherlen, Bernard, Calabrese, & Castet (2008) assessed page-mode reading in 7 subjects with normal vision in the presence of a simulated artificial scotoma (6 or 10 deg in diameter) that was filled with upper-case X characters and concluded that the number of saccades and the mean fixation duration are the primary factors that influence reading speed. The authors suggested that when the visual encoding of text becomes more difficult, more saccades are required within a given region of text in order for word identification to occur. This interpretation is consistent with work by Deubel, Schneider, & Bridgeman (2002), who reported that when visual encoding is degraded the efficiency of trans-saccadic integration of information is reduced.

Both fixation duration and number of fixations can influence the reading speed. Calabrese et al. (2014) investigated the eye movements in subjects with macular degeneration, while reading sequentially presented meaningful sentences. They report that

the total number of fixations (and not fixation duration) fully mediated the effect of reduced reading speed with the mean number of letters traversed per forward saccade. However, Loftus et al. (1992) reported that the degradation of visual input (like for instance, by decreasing contrast) potentially necessitates an increase in fixation duration thereby slowing the reading speed. In our study, the RSVP paradigm minimizes the need for saccades across words of a sentence and the need for encoding the relative spatial locations of text across eye movements. However, the degradation of the text that is produced by random element-deletions may interfere with the integration of information at low, and perhaps also at high levels of visual processing.

Rayner, Pollatsek, & Schotter (2012) compared template and feature models of word recognition during reading. In template models, visual input is compared to the memory representations of various objects (templates) and the best matching template is perceived as the object. On the other hand, feature models posit that recognition occurs based on the individual elements that constitute the object (like the combination of strokes that form a letter and/or the letters that comprise a word). Irrespective of which type of model is correct, the degradation produced by random element-deletions can impact recognition and reading performance, either because missing areas of the stimulus make template matching difficult or because the individual features that comprise letters and words are distorted or degraded.

McMahon, Hansen & Viana (1991) described reading as a complex process requiring visual resolution, stable images, accurate saccades, word encoding, lexical

assessment, and short and long term memory. The last aspect of this process perhaps needs mention, as in our study the subjects verbalized words as they appeared on the computer monitor, following the end of trial, or a mixture of both. The degraded visual stimuli that we used in our study could either have less or more impact during page-mode reading. The argument in favor of less impact is that during page reading, one may have a preview benefit from text that does not suffer from element deletions and perhaps a reduced need to store the visual input in memory. On the other hand, the text degraded by random element-deletions can potentially have an adverse impact on eye movements and the fact that page mode reading requires efficient eye movements, argues for a greater impact of element-deletion on page mode reading.

The random element-deletions that we employed in this study assume random sensitivity losses, spanning a considerable portion of the central or the peripheral retina. It may be that such random losses don't occur in subjects with CVL, whose sensitivity losses (even outside the large clinically documented central scotoma) may be more clustered and restricted only to specific regions in the vicinity of the PRL. As a logical extension of the current study, it would be interesting to use maps of the MSs determined over an extended retinal region surrounding the PRL in subjects with CVL to simulate vision loss and assess reading speed in subjects with normal vision.

4.6 Conclusions

RSVP reading rate in both the central and peripheral retina is influenced by the density of random element losses, age, word eccentricity, and contrast. For a given

eccentricity and contrast, higher densities of random element loss maximally affected older subjects with normal vision. This may partly explain the subnormal reading performance in older subjects with bilateral CVL, when they use a retinal location that can include local areas with sub-clinical local sensitivity losses. The results presented here indicate that scattered sensitivity losses, in conjunction with co-existing changes in contrast sensitivity in areas outside the region of central field loss, should exert a negative impact on reading speed.

5. CHAPTER V: Overall Summary

Contributing Author:

Harold Bedell, PhD

5.1 Summary

The primary aim of this dissertation study is to understand central field loss (CFL) and the associated deficits in reading performance. To assess the functional changes that happen in CFL, we needed to make sure that the commercial MP-1 micro-perimeter is capable of correcting for subjects' eye movements and does testing at known retinal locations as claimed. The results from the study discussed in CHAPTER II (**Page 1**) confirmed that the NIDEK MP-1 micro-perimeter compensates for ~90% of the increase in fixational eye movements that is expected in patients with CFL and that image registration on repeated testing is accurate to ~2 pixels (8 arc min). Both these capabilities are crucial for following-up subjects with CFL. With this information, we screened the word-fixation preferred retinal locus (PRL) for local sensitivity loses in CHAPTER III **(Page 38**). The results indicate that the PRL in subjects with macular degeneration often includes local regions of sensitivity loss, or micro-scotomas. These micro-scotomas correlate poorly with changes in retinal structure detected by SD-OCT and with increases or reductions in retinal auto-fluorescence. The local defects found within PRL can be detected by a functional screening, but it remains to be seen if these local defects have significant consequences for reading, or other day-to-day activities, in patients with CFL. To understand the impact of local sensitivity defects we simulated micro-scotomas in subjects with normal vision in CHAPTER IV (**Page 116**). We report that the reading speed for sequentially presented words of a sentence is influenced by the density of random element losses (micro-scotomas), age, word eccentricity, and contrast. For a given

eccentricity and contrast, higher densities of random-element loss maximally affected older subjects with normal vision. Combining the studies, we now know that MP-1 can detect local sensitivity changes within PRL in subjects with CFL but that these local changes poorly explain the deficits in reading performance seen in subjects with CFL.

Local sensitivity changes within PRL have not been explored in the past. Many previous researchers explored the margins of geographic atrophy and local changes in both structure and function at the sites of drusen or RPE atrophy (Fleckenstein et al., 2008; Iwama et al., 2010; Sulzbacher et al., 2012; Janet S Sunness & Steiner, 2008). Although the PRL in many subjects with CFL appears relatively normal, our results indicate that it typically is not. It remains to be seen if the extent of the sensitivity losses evolves over the course of time.

5.2 Limitations of the Study and Scope

Several limitations have been listed in the individual chapters but some of the key potential shortcomings of this work are reiterated here. The region of word-fixation PRL is usually small (~ 1-3 deg in extent). Although reading involves sequential placement of words at the PRL, regions outside the PRL can also contribute to reading. For instance, a preview benefit (akin to the perceptual span) exists in patients with CFL (Legge et al., 2001; Trauzettel-Klosinski, 2011) and is likely to be sub served by regions outside the PRL. Having mirco-scotomas at the PRL could degrade textual information locally and thereby slow the reading speed by necessitating an increase in fixation duration, or the impact of localized micro-scotomas on reading might be mitigated by top-down influences

on the recognition of words (Rayner et al., 2012). In our simulation study we assumed that local sensitivity losses at the PRL occur also in wider regions of the peripheral retina in subjects with CFL. However, this supposition may not be entirely true.

When assessing the accuracy of eye movement compensation by MP-1 we used a large circular target, which led to an increase in the fixational eye movements (FEMs) of subjects with normal vision. Although compensation by the MP-1 was good, we aren't sure if the simulation using normally-sighted subjects best represents the FEMs in subjects with CFL. It is possible that the MP-1 performs more poorly than indicated by our simulations in patients with real CFL and, if so, the sensitivity estimates that we obtained in Chapter III need to be interpreted with caution. Less complete compensation of FEMs in subjects with CFL could explain the imperfect overlap of the local defects detected on successive supra-threshold screening tests (**CHAPTER III**). Although we used screening to quickly detect locations with reduced sensitivity (and minimize subject fatigue), one might use a thresholding paradigm to get a more reliable measure of sensitivity changes. Thresholds could be extended to regions beyond the PRL, including the estimated extent of the perceptual span (~5 deg or 15 letters to the right of fixation (Legge et al., 1997; Trauzettel-Klosinski, 2011)). The dense sampling that we employed may represent overkill, and a grid that samples the PRL at 0.5 deg intervals in conjunction with a thresholding algorithm may provide more useful and reliable functional information. To compare local sensitivity changes at the PRL to reading speed, we assumed that the word-fixation PRL is the same as the reading PRL, which need not always be true (Crossland, Crabb, & Rubin, 2011;

Sullivan et al., 2008). Also, the reading PRL may not always be described adequately as a single retinal location.

The NIDEK MP-1 microperimeter used in this study, was one of the first commercially available micro-perimeter to perform a fundus correlated perimetry. Since its introduction in the last decade, many micro-perimeters have become available (e.g., OPTOS OCT/SLO, MAIA). Some of the recent micro-perimeters use a scanning laser ophthalmoscope to scan and image the retina and by its very nature of image acquisition, the image resolution is far superior than that of IR-video camera based system like MP-1. About 2-3 micro-saccades per s (median: 2.48/s, with increased amplitude in macular disease) are observed in individuals with macular disease (Kumar & Chung, 2014). Assuming a micro-saccade amplitude of 1°, we know from the human main-sequence plot that the time duration for such a FEM will be ~20 ms. The time required for the MP-1 to detect and correct for an eye movement should be at least one frame (or 40 ms, 25 Hz). If so, then the likelihood that a micro-saccade occurs and is not corrected is approximately equal to the duration of 1 frame (40 ms) divided by the average interval between micro-saccades (1000/2.48 = ~400 ms). Hence, the probability of an uncorrected micro-saccade is roughly 40/400 = 10%. The likelihood that micro-saccades will be uncorrected during both of the presentations of a screening target at (nominally) the same retinal location on the baseline and follow-up tests is 0.1 * 0.1 = 1%.

On a different note, no information is available regarding the system time lag between the computation of ROI shift and the final adjustment of the stimulus. This is

pivotal given that the computations of cross-correlation over ROI can be intensive and the eventual adjustment of the projection system to offset the eye movement can potentially be delayed. Aside from this, there also could be delay associated with the update rate of the MP-1's LCD display. We assume that the overall error/lag due to these factors are minimal, especially the errors produced in falsely detecting or not detecting targets at the same test location on both the baseline and follow-up tests are minimal.

Although manual segmentation works best for retinal images that include pathologies like drusen or RPE thinning, the inconsistencies in criteria used by a segmenter could influence the thickness results. Compared to the affine approach used here, a quadratic transformation might better register the pairs of fundus images from two different imaging devices, especially when probing changes over a local region of the retina. We began this study with an aim of having 15 subjects with AMD and 15 with STGD, but in the end we recruited 29 subjects including several with CFL due to causes other than AMD or STGD. Even in these 29 subjects, the distribution of micro-scotomas (MSs) was not uniform within subject groups. To make better comparisons based on locations that had MS vs. nonMS locations as well as between them, it would be worthwhile to obtain measurements on larger numbers of subjects, specifically with diagnoses of AMD and STGD, to better describe the distribution of MSs.

5.3 Clinical Implications

First and foremost, screening the PRL for local sensitivity changes can provide a better understanding of the extent of the retinal changes produced by disease. When the

PRL is not yet established fully, screening the candidate retinal regions should help patients to make a better selection of their PRL location. We propose that a microperimeter-based fixation assessment and PRL screening when coupled with conventional eccentric viewing training (that demonstrates the subject with CFL his or her visual potential) could permit better rehabilitation of subjects with CFL. The presence of MSs in the PRL may represent a sign of an impending spread of atrophic changes or disease progression. For clinics that have access to micro-perimeter, then aside from fixation and sensitivity assessment, performing a reading assessment using material similar to our MP Read sentences can supplement traditional reading.

6. APPENDICES

6.1 Gamma Correction for Contrast Testing

CHAPTER III refers to contrast sensitivity assessment using FrACT testing. For contrast testing to be accurate the display has to be corrected for any non-linearity in output intensity. We displayed a square patch (designed in Microsoft PowerPoint) set at various RGB values (0-255), which occupied more than 75% of the Lenovo ThinkPad Display (Intel HD Graphics). The luminance of this patch was measured in a totally dark room (illuminated only by the light from the display that was being calibrated) using a Minolta LS-100 photometer, held steady by a tripod at ~1m distance from the center of the display. The average values from at least 2 readings are displayed in the plot below. A gamma value of 2.8 made the relationship between the RGB value and Luminance nearly linear (Fit Slope of 0.82 and Fit R-Sq = 0.99). During the FrACT assessment reported in this study, the Gamma was set to this value.

Gamma = 1	**L1**	**L2**	**L3**	**Average L**	**Gamma= 2.8**	**L1**	**L2**	**Average L**
(Default Setting)				**(cd/m^2)**	**(Graphics Settings)**			**(cd/m^2)**
RGB Value								
0	**0.41**	**0.39**	**0.39**	**0.39**		**0.26**	**0.25**	**0.25**
32	**3.05**	**3.00**	**2.99**	**3.01**		**28.80**	**28.82**	**28.81**
64	**9.18**	**9.15**	**9.08**	**9.14**		**51.93**	**51.99**	**51.96**
128	**37.97**	**37.91**	**37.77**	**37.88**		**97.46**	**97.49**	**97.48**
196	**100.70**	**100.60**	**100.50**	**100.60**		**151.90**	**151.90**	**151.90**
255	**213.80**	**213.90**	**214.00**	**213.90**		**214.10**	**214.10**	**214.10**

L = Luminance of a square patch of set RGB value. The listed values are for a Gamma of 1 (default) and Gamma of 2.8. The value of 2.8 is not arbitrary and was obtained after trial and error. The plot below shows the non-linear output intensity for the default setting and the nearly linear output after the Gamma correction by setting the Gamma slider in the Intel graphics settings panel to 2.8.

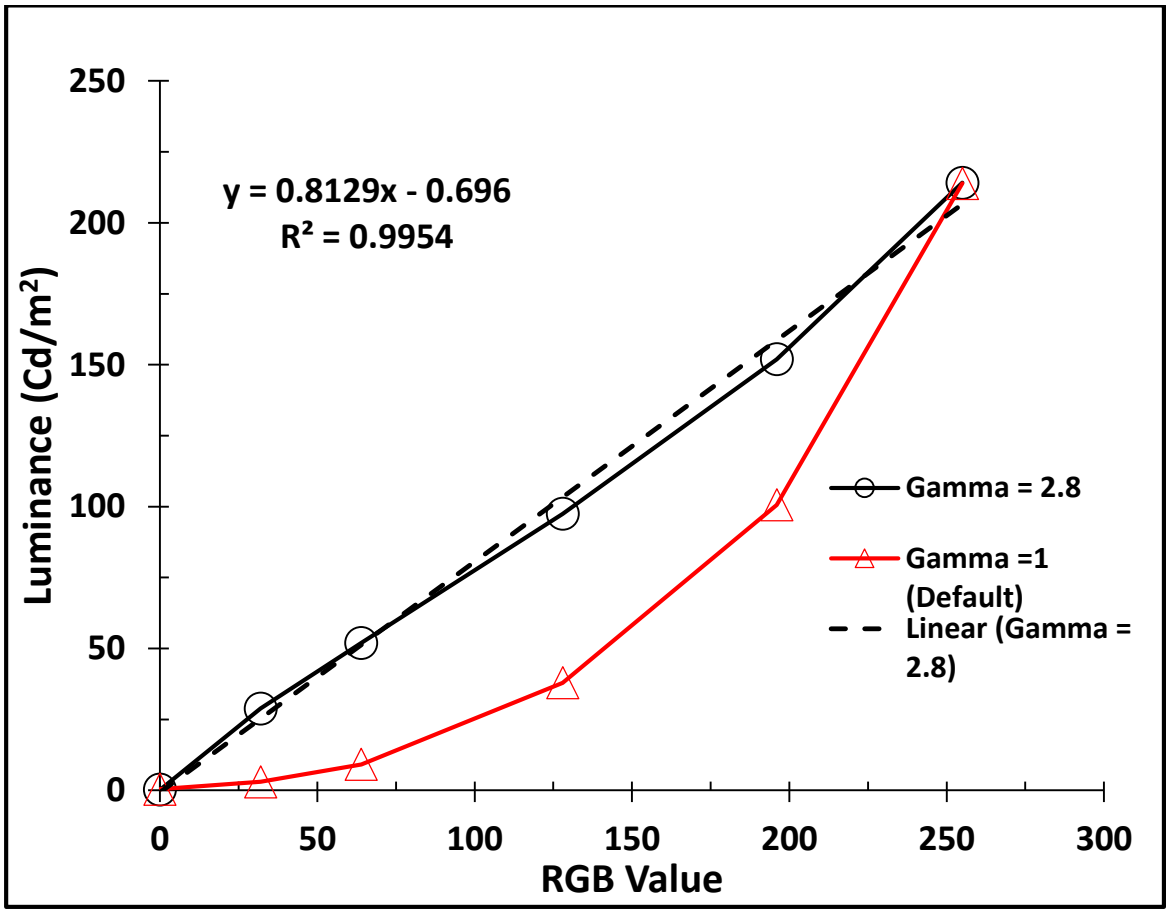

6.2 IR-MP1: Overlap Region Computation

As discussed in **CHAPTER II**, the 2 IR-MP1 images from the follow-up testing (supra-threshold screening) are registered using the dual bootstrapping algorithm (and

affine transformation). The test grid from the follow-up test (test # 2) is replotted on the baseline IR-image using MATLAB and based on the affine coefficients. The average absolute offset was computed in a cohort of 4 CFL subjects (6 follow-up test image pairs) using the formula described below. The 4 CFL subjects (MD 1 - 4 are part of CFL cohort S1-S33, listed in **Table 3-1** of Chapter III).

Average Absolute Offset (in X and Y) = $\sum|X_B - X_F|/N$; $\sum|Y_B - Y_F|/N$

Where, X_B, Y_B = X and Y coordinates of test point in baseline testing.

X_F, Y_F = X and Y coordinates of test point in follow-up testing.

N= Number of test points in the sampling array.

Subject Code	Avg. Abs. X Offset (arc min)	Avg. Abs. Y Offset (arc min)
MD1a / S3	13.11	7.82
MD1b / S3	3.05	6.47
MD2a / S4	1.46	2.60
MD2b / S4	6.90	4.03
MD3 / S2	13.84	8.73
MD4 / S1	10.49	1.59
Mean (n=6)	**8.14**	**5.21**
S.D	**5.19**	**2.90**
Median	**8.69**	**5.25**

Using the deg-to-pixel conversion factor of 15.19 provided by MP-1.

1 IR image pixel ≈ 3.95 arc min. Overlap region: Mean ± 2SD (Offset)

Thus, the overlap region extends ~18.5 and 11 arc min horizontally and vertically on each side of the test spot. **Thus the overlap region is: ~37x22 arc min or ≈ 8x5 IR image pixels.**

6.3 Supra-threshold Screening: Targets Missed

Subject Code	Total Locations Screened	Targets missed on Screening	
		Test # 1	Test # 2
S1	28	0	6
S2	67	8	11
S3	73	7	12
S4	50	4	5
S5	67	0	0
S6	33	3	2
S7	37	0	0
S8	41	25	30
S9	37	26	25
S10	55	6	24
S11	29	13	25
S12	36	7	5
S14	23	0	0
S15	41	2	3
S16	33	25	31

S18	57	7	1
S19	67	4	2
S20	94	41	59
S22	57	45	46
S23	77	6	38
S25	37	19	29
S26	62	39	32
S27	39	13	21
S28	62	31	40
S29	73	50	56
S30	31	0	0
S31	44	5	2
S32	62	3	3
S33	56	0	0

6.4 MS-nonMS locations – All Subjects

Images are listed below in order of subject codes for all the 22 CFL subjects with either AMD/STGD first and then the 7 CFL subjects with miscellaneous diagnoses. Note that subjects who showed zero MS or zero nonMS locations are also listed. The full-sized IR images are from baseline (Test #1, exported from NIDEK MP-1) of the supra-threshold screening at the PRL. The inset on top left corner in each image is the zoomed test grid, where the identification and labeling of MS and nonMS locations on the replotted test grid

was done using MATLAB after registering the IR image pairs using a dual bootstrapping algorithm, GDB-ICP. (Also, See methods **CHAPTER III**)

Note: In some of the images below, there is a tendency for the subject to fixate towards the fovea (the center of cloud of cyan fixation dots seems to drift from the word-PRL towards the fovea). This is perhaps due to the fact that the PRL for large targets (like the circular fixation target used during the screening of the word-fixation PRL) can be shifted toward the vestigial fovea, perhaps as the result of filling-in (Pratt, Ohara, Woo, & Bedell, 2014). Another potential explanation is that the tendency to drift towards foveal fixation is perhaps contingent on the duration of CFL and longstanding cases of CFL may be less likely exhibit this behavior.

Legend for all images: Blue Squares: Test locations from Test #1

Blue Filled Squares: Undetected target locations from Test # 1 (Dotted square: Overlap region)

Red Squares: Test locations from Test #2

Red Thicker Outline Squares: Undetected target locations from Test # 2.

Labeling of MS and nonMS (yellow) locations is also shown.

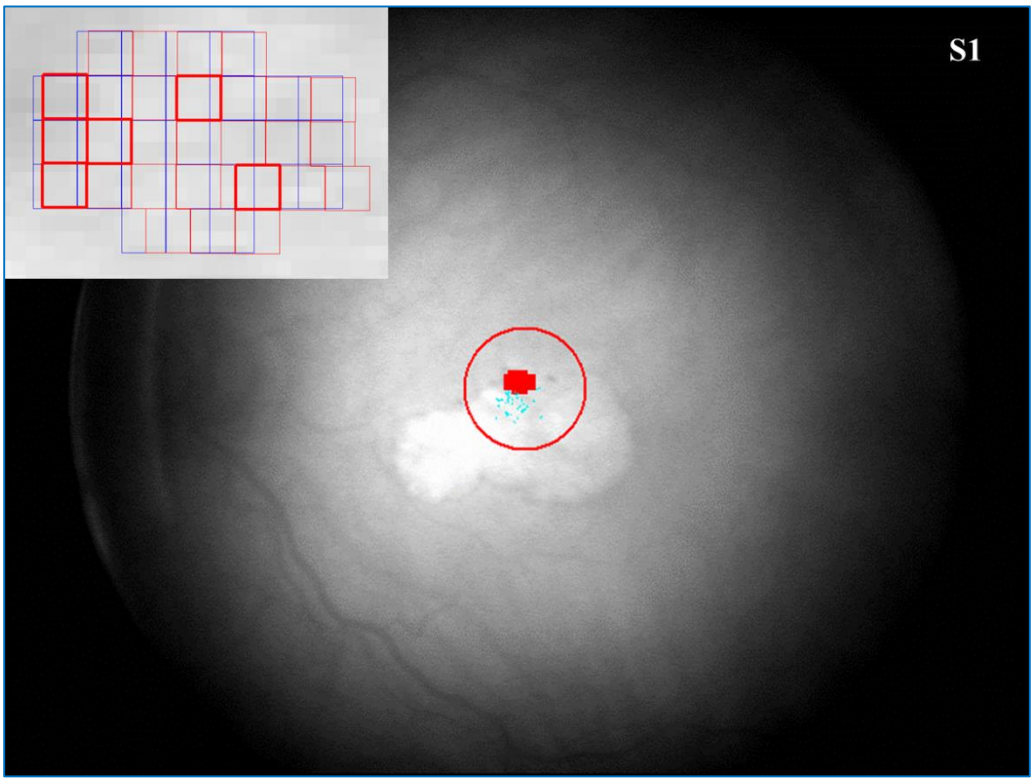
S1

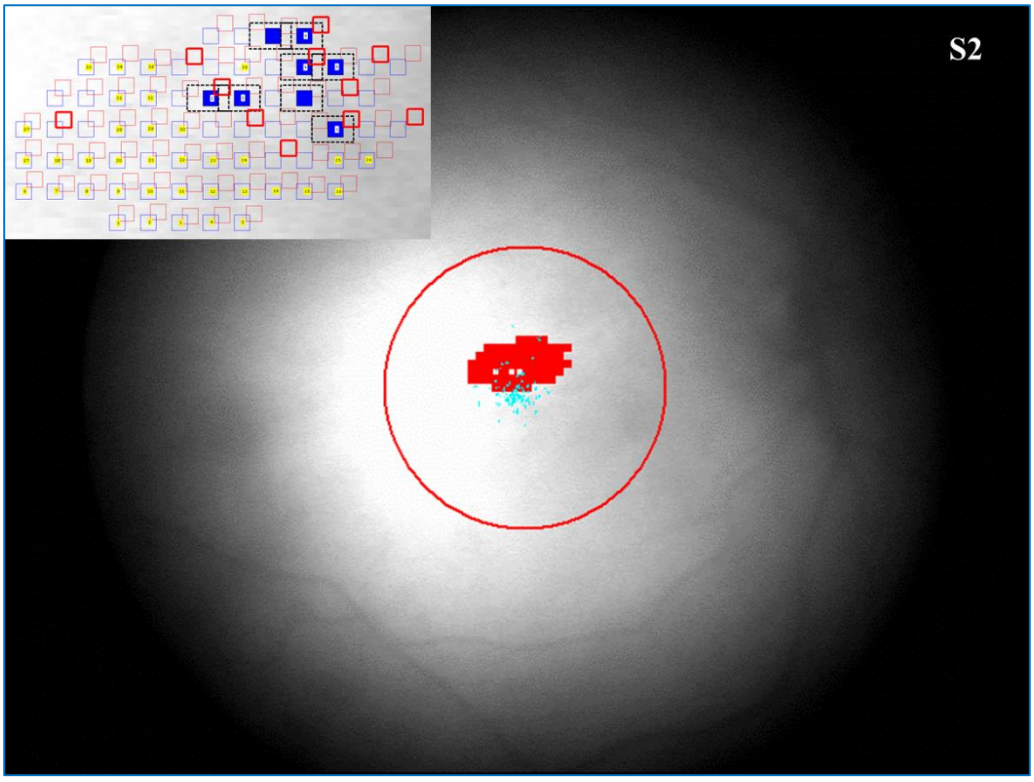
S2

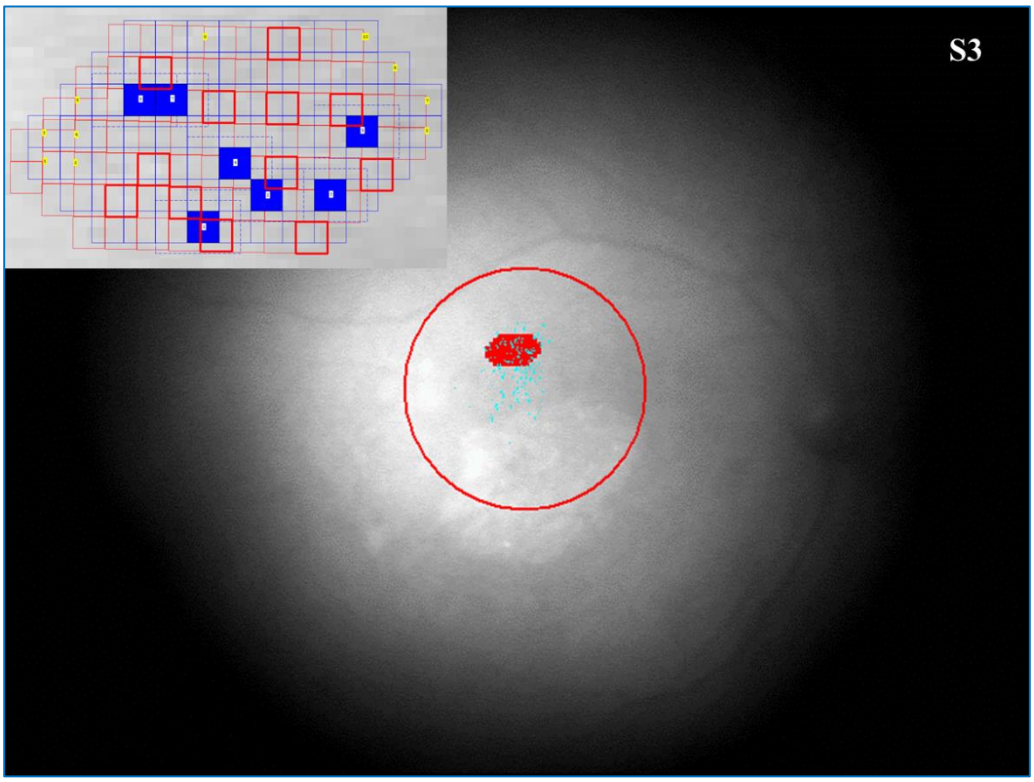
S3

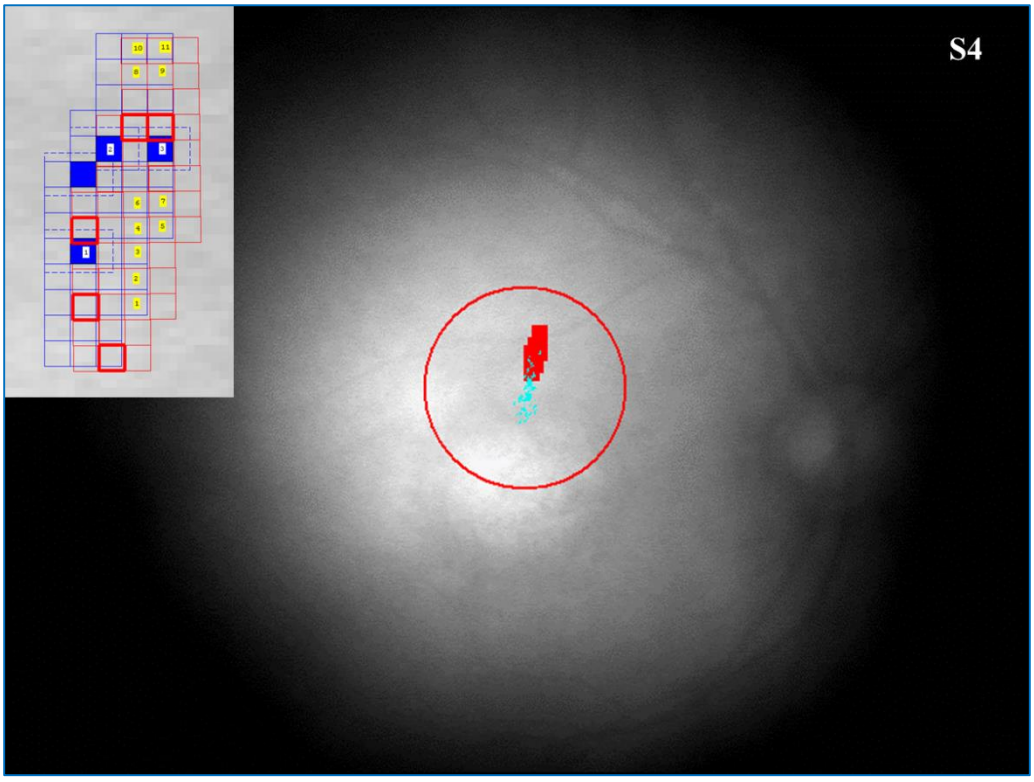
S4

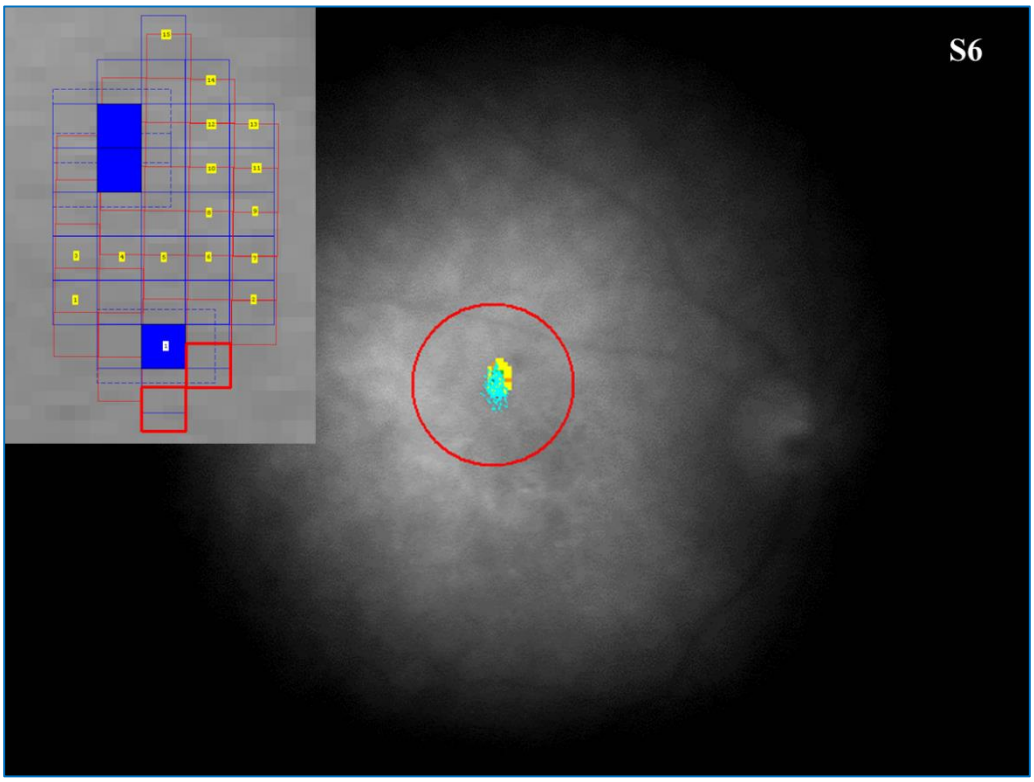
S6

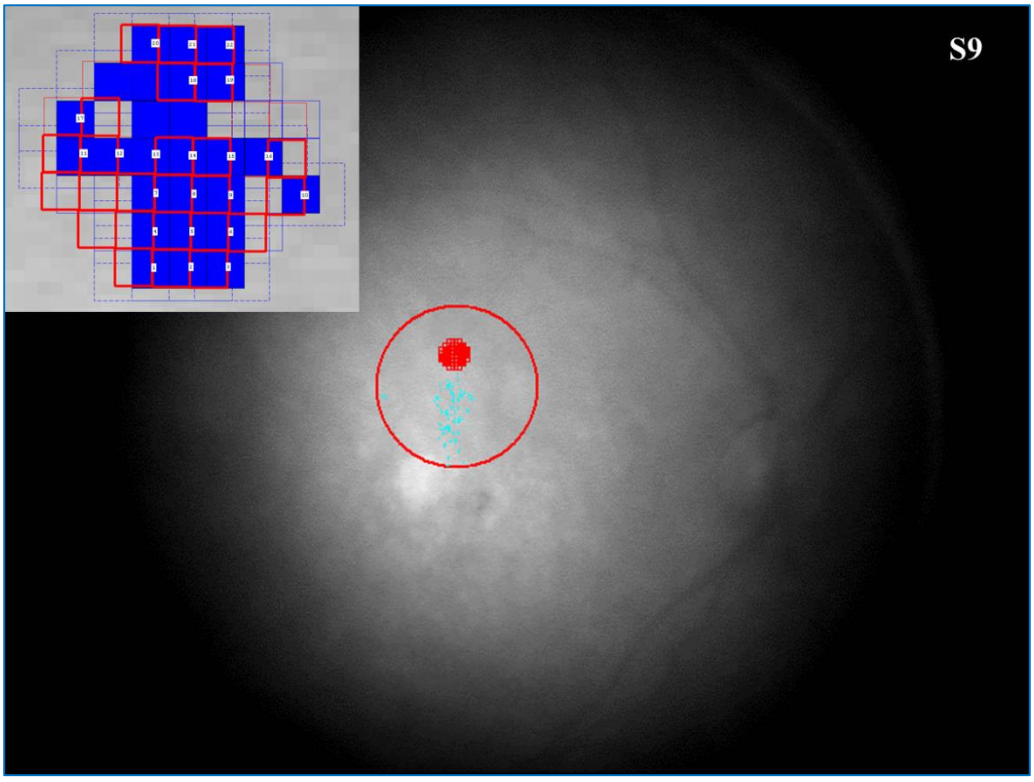
S9

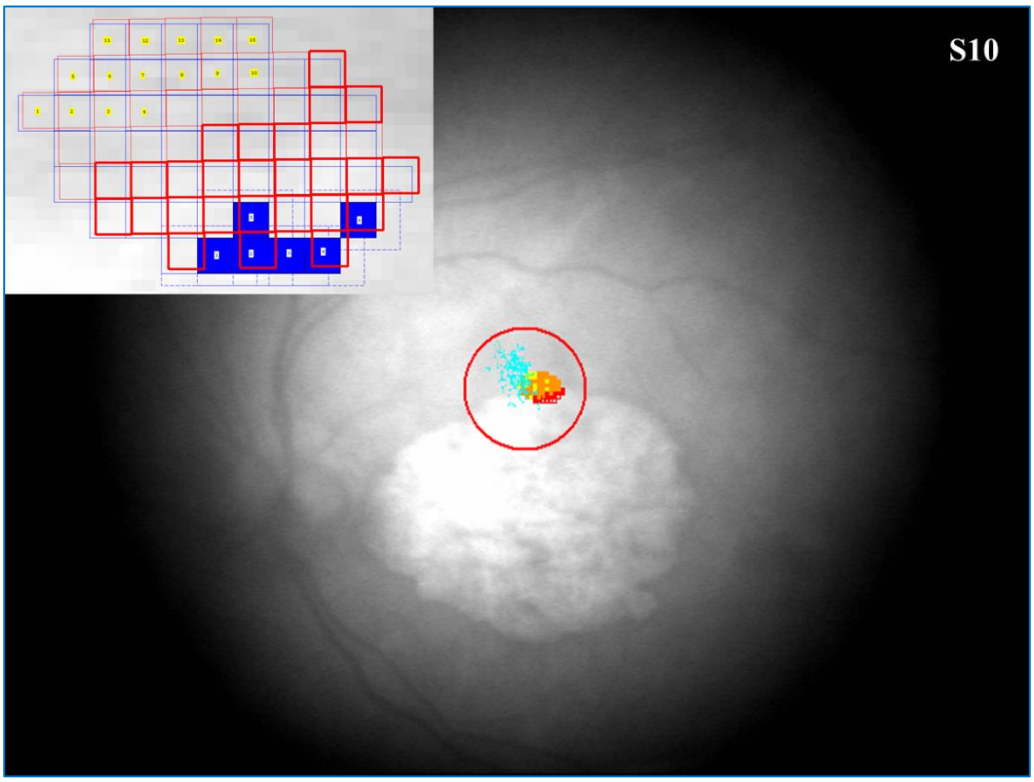
S10

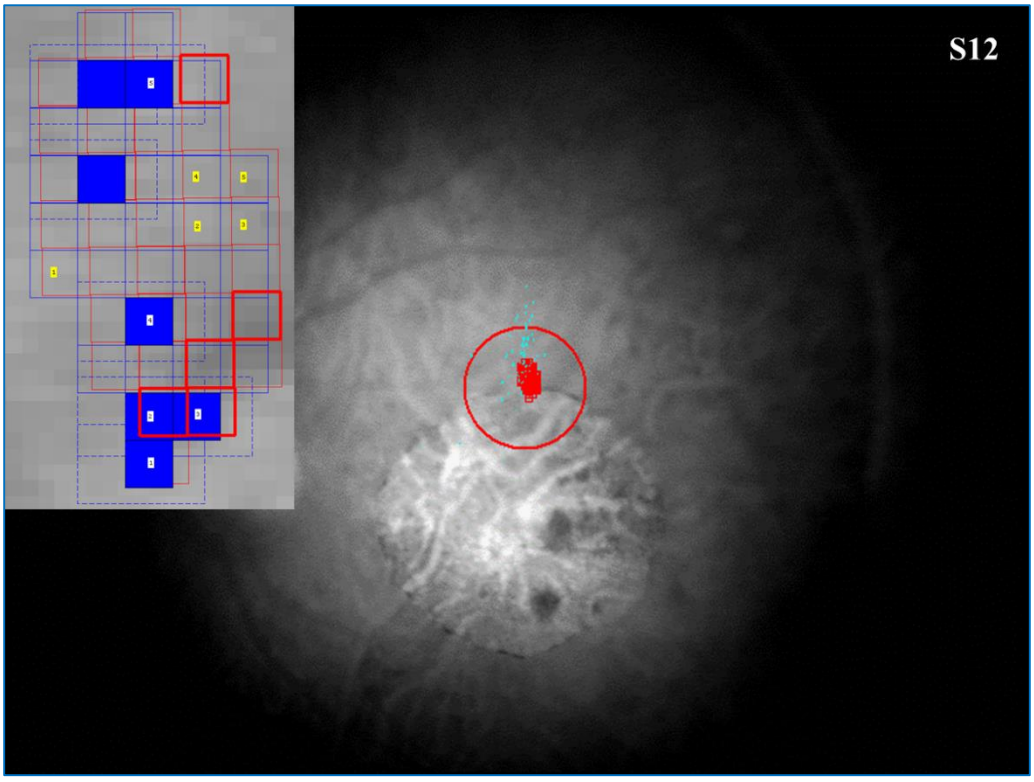
S12

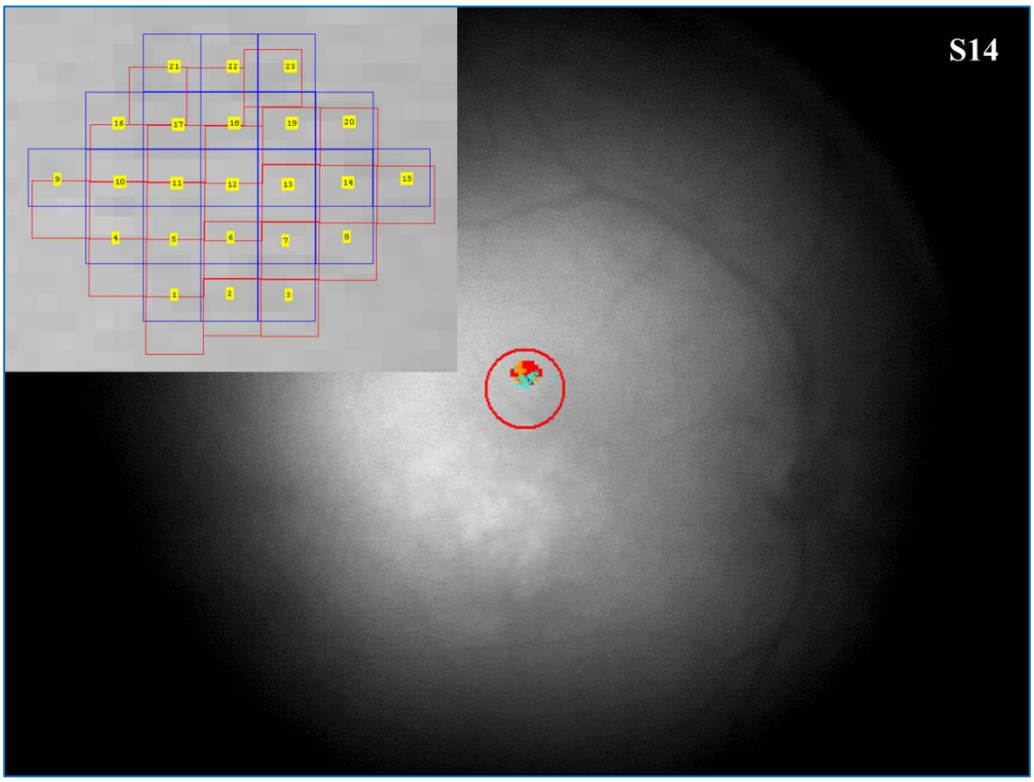
S14

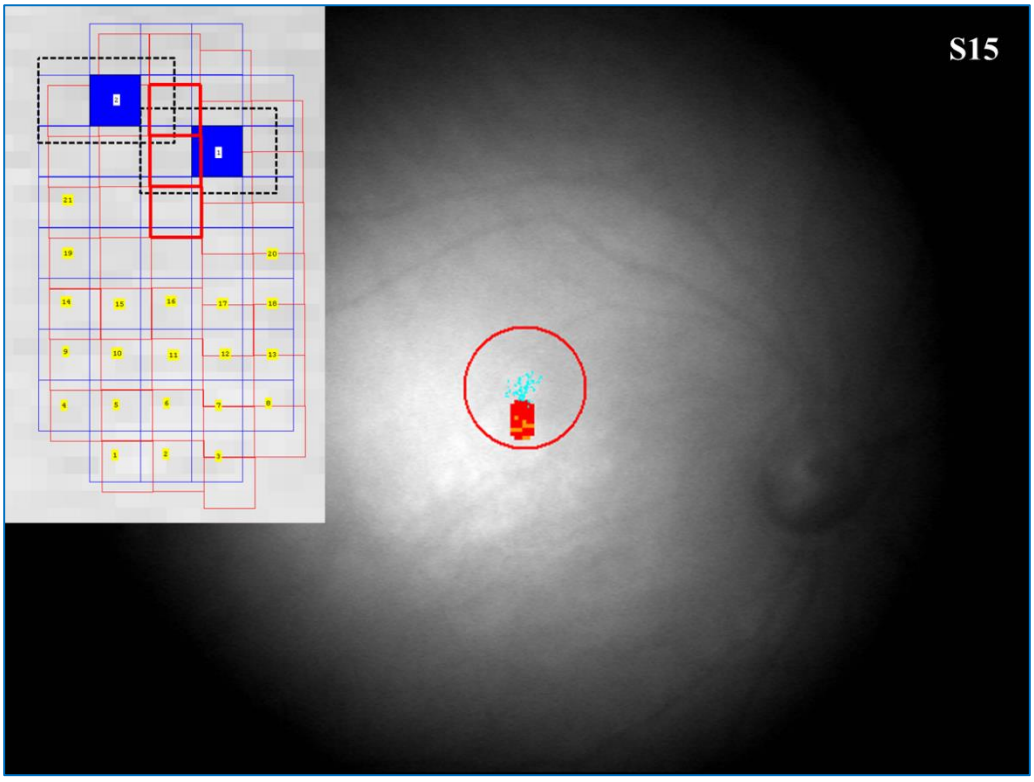
S15

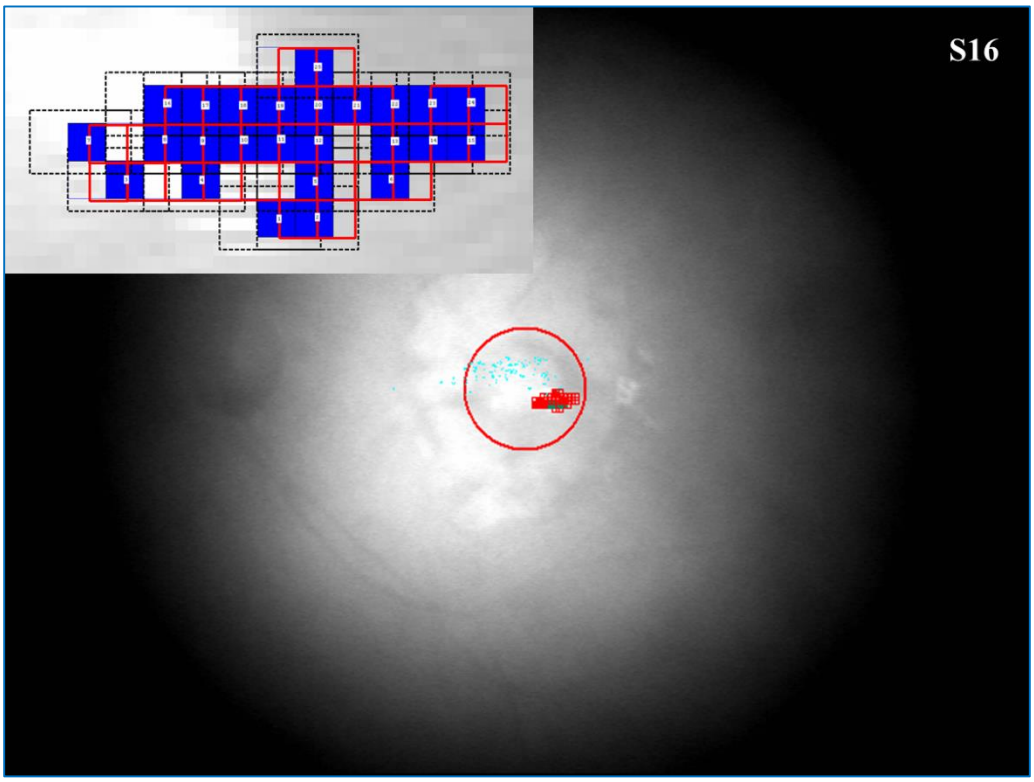
S16

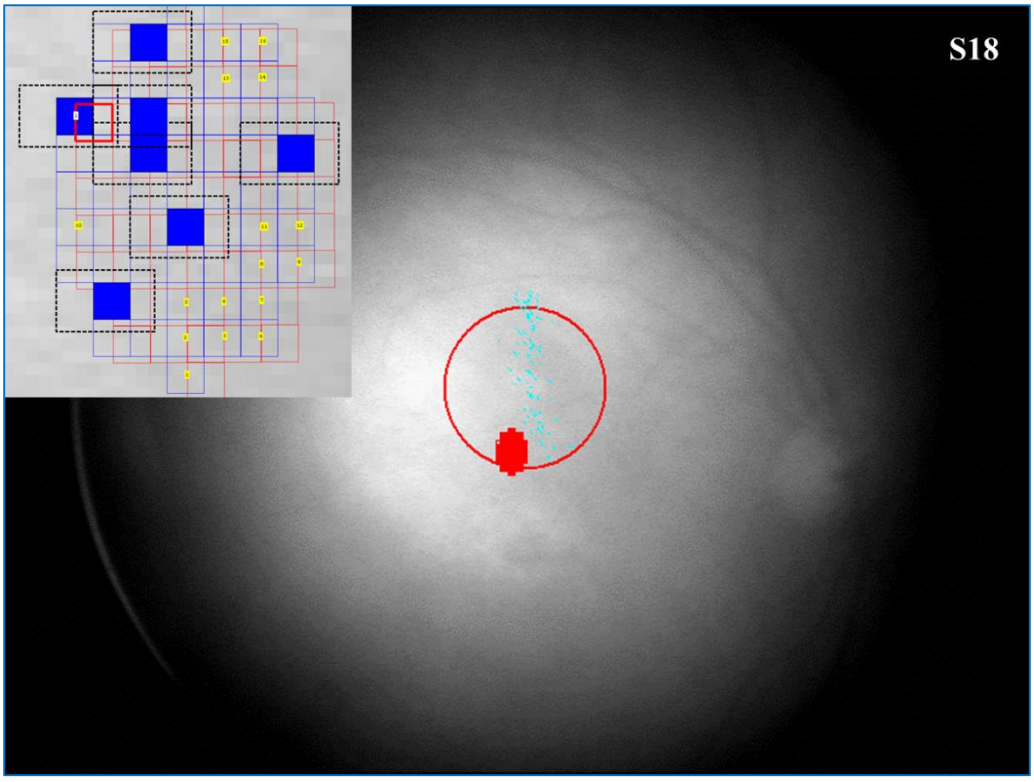
S18

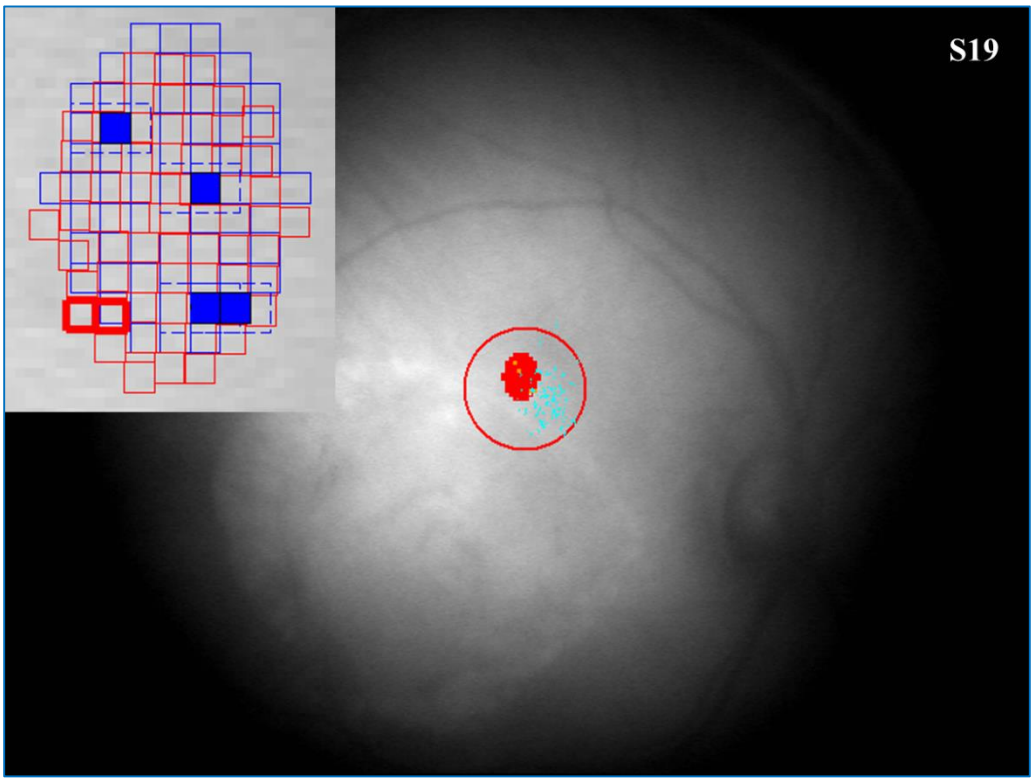
S19

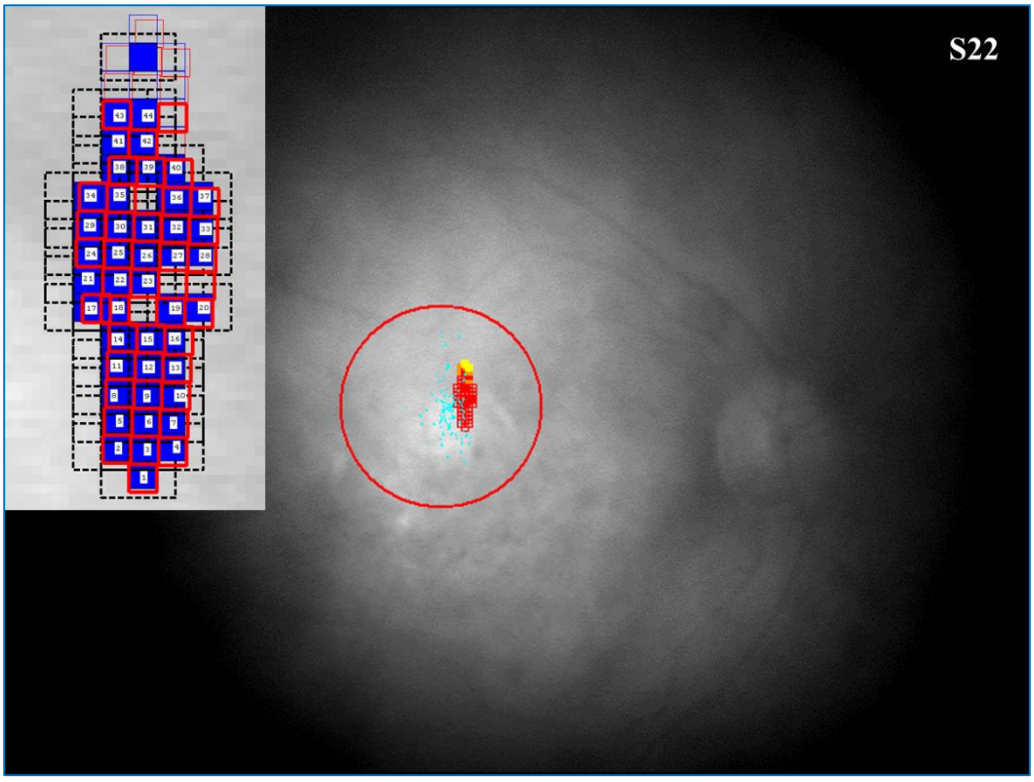
S22

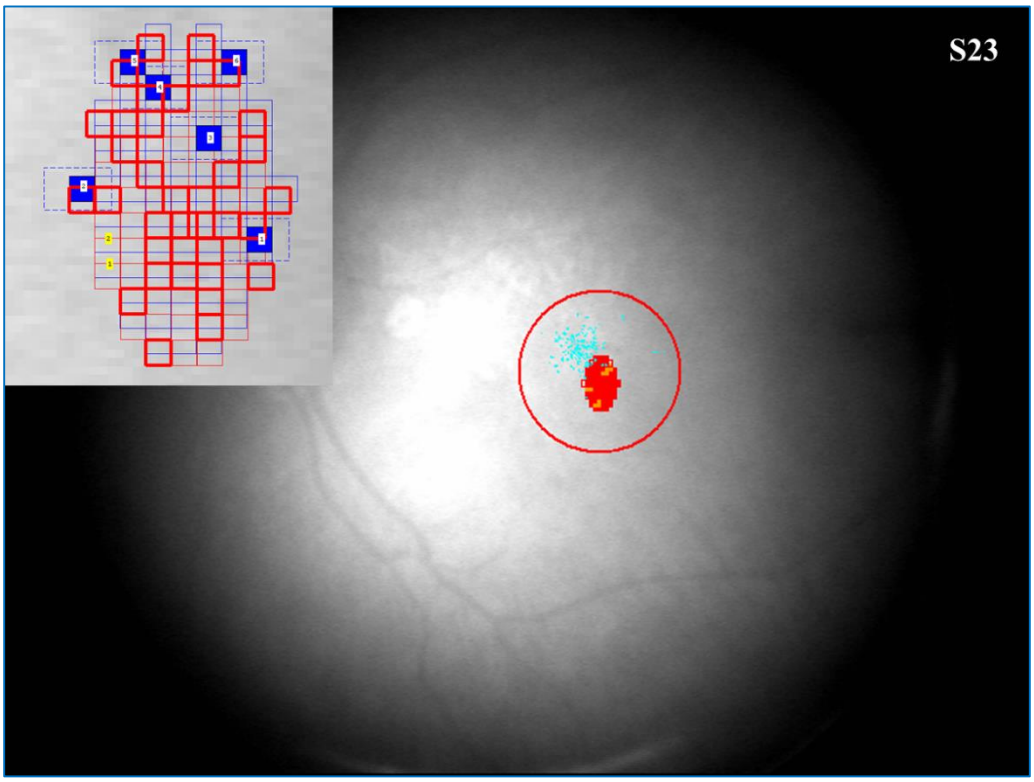
S23

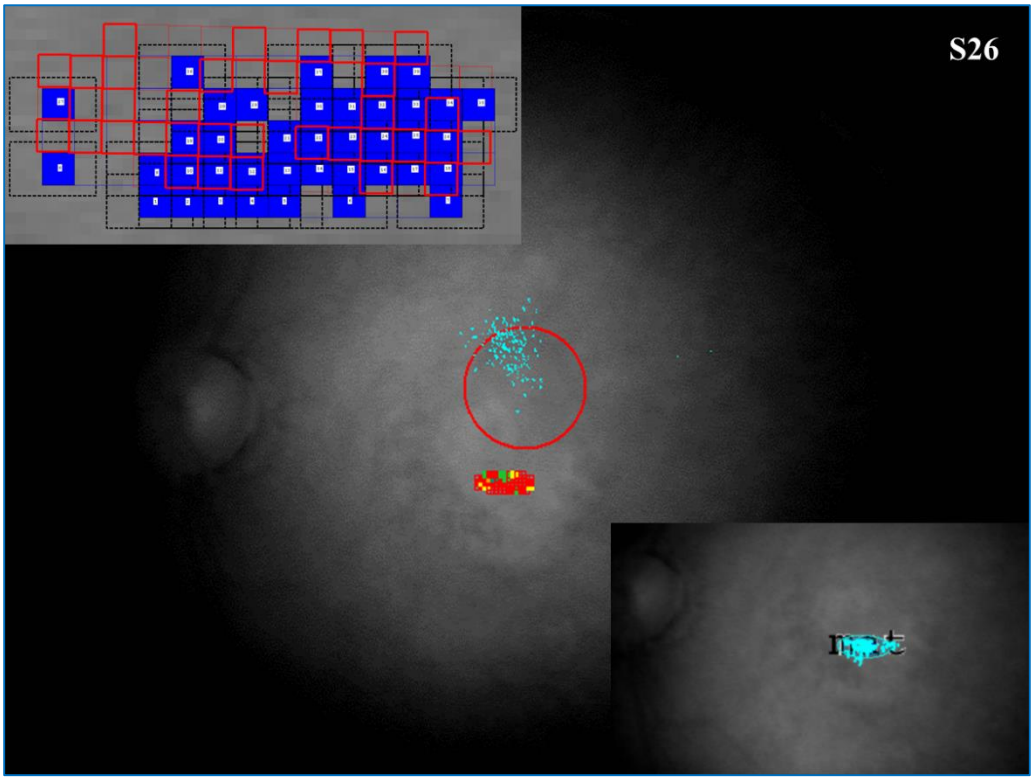
S26

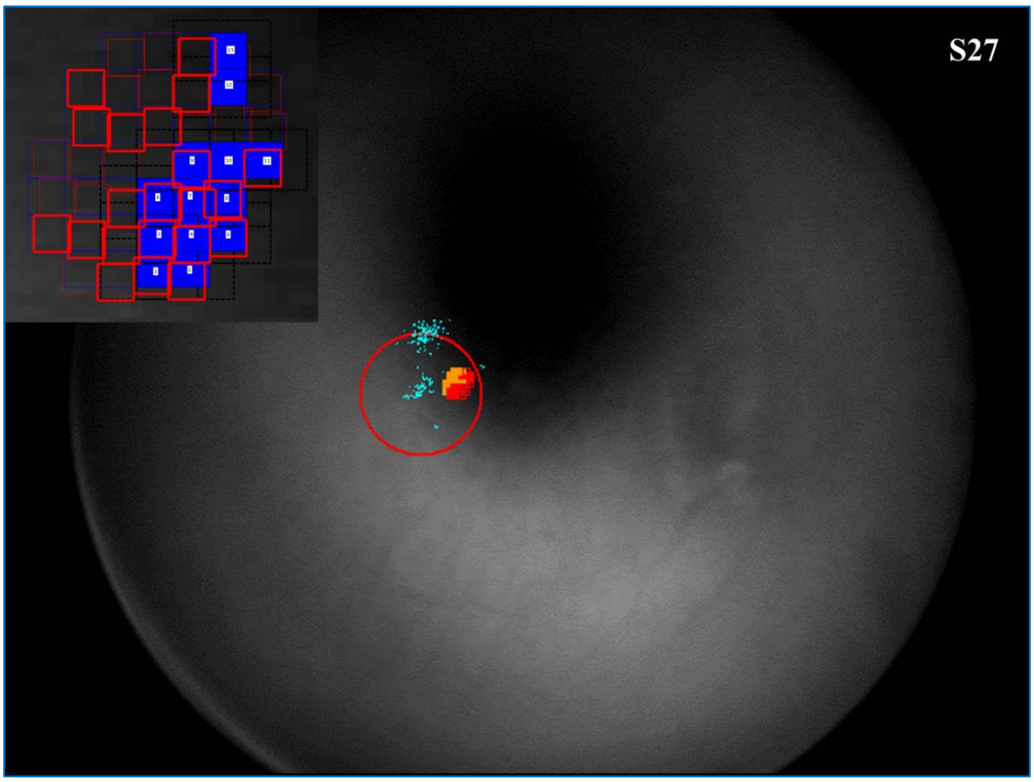
S27

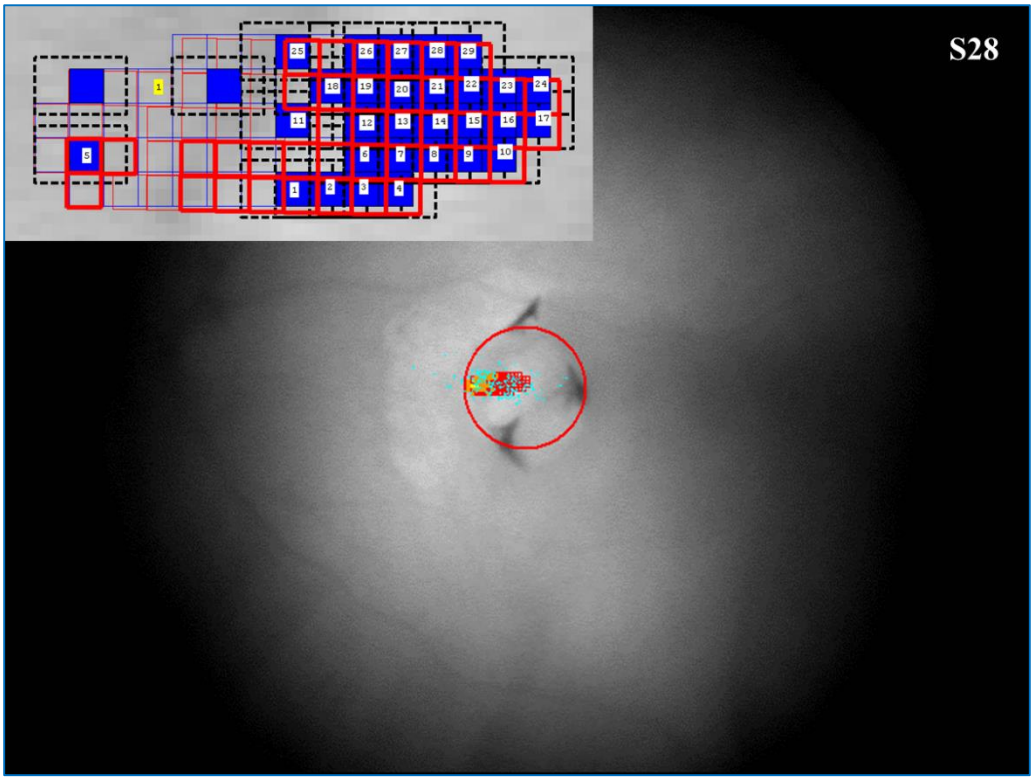
S28

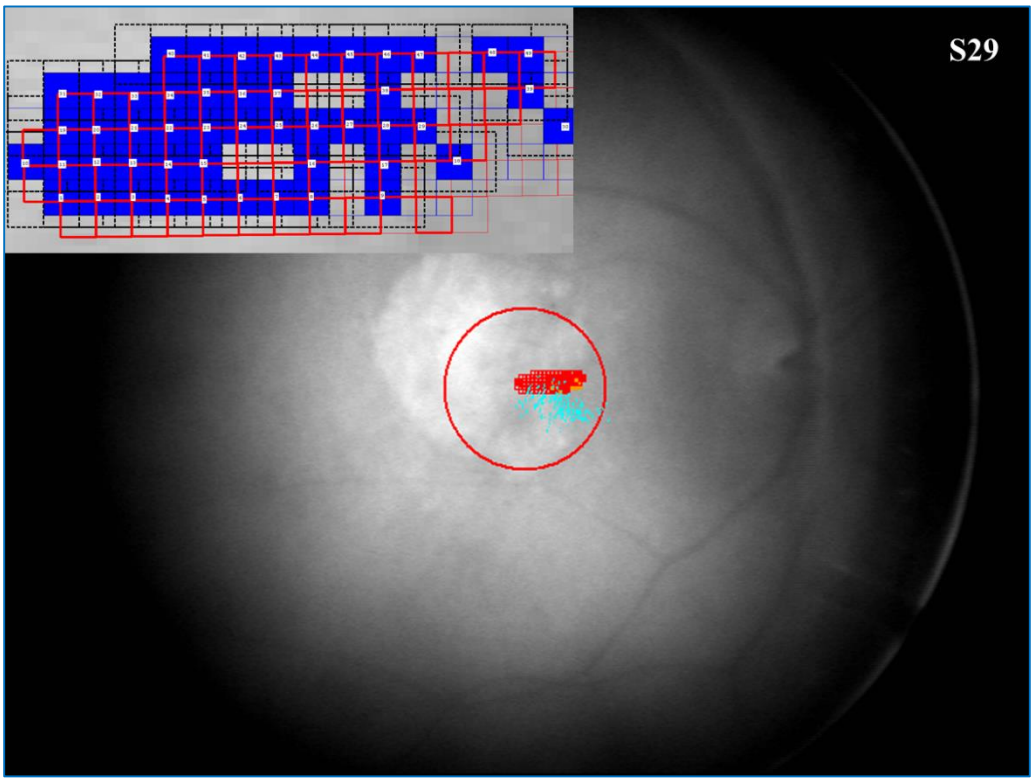
S29

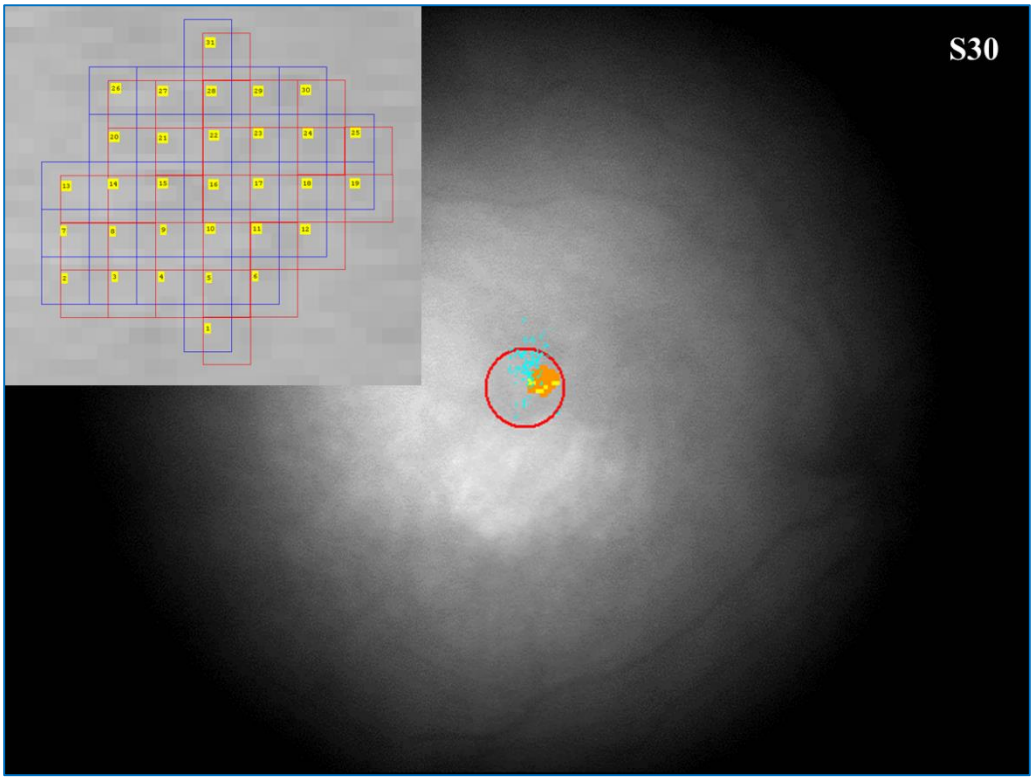
S30

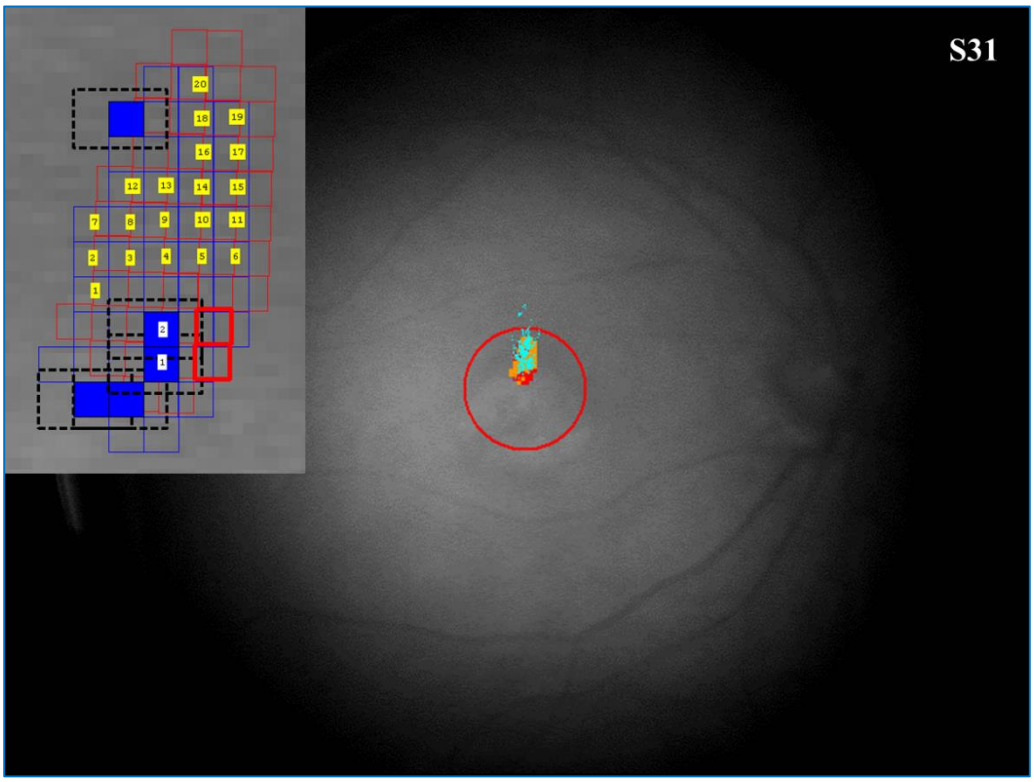
S31

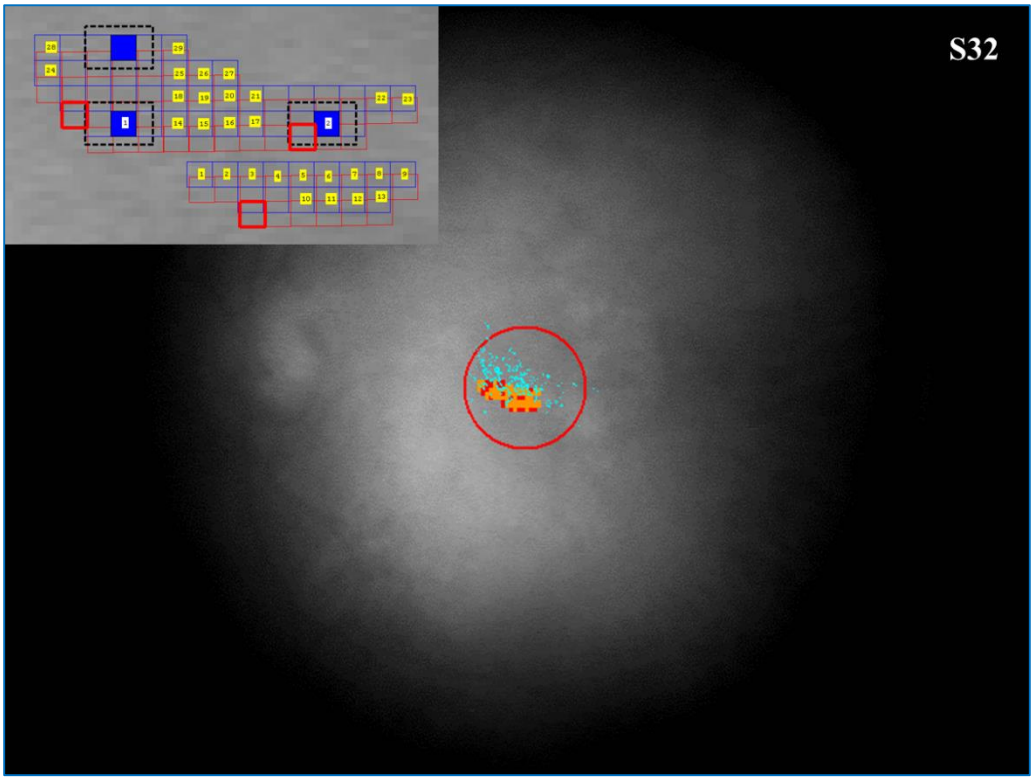
S32

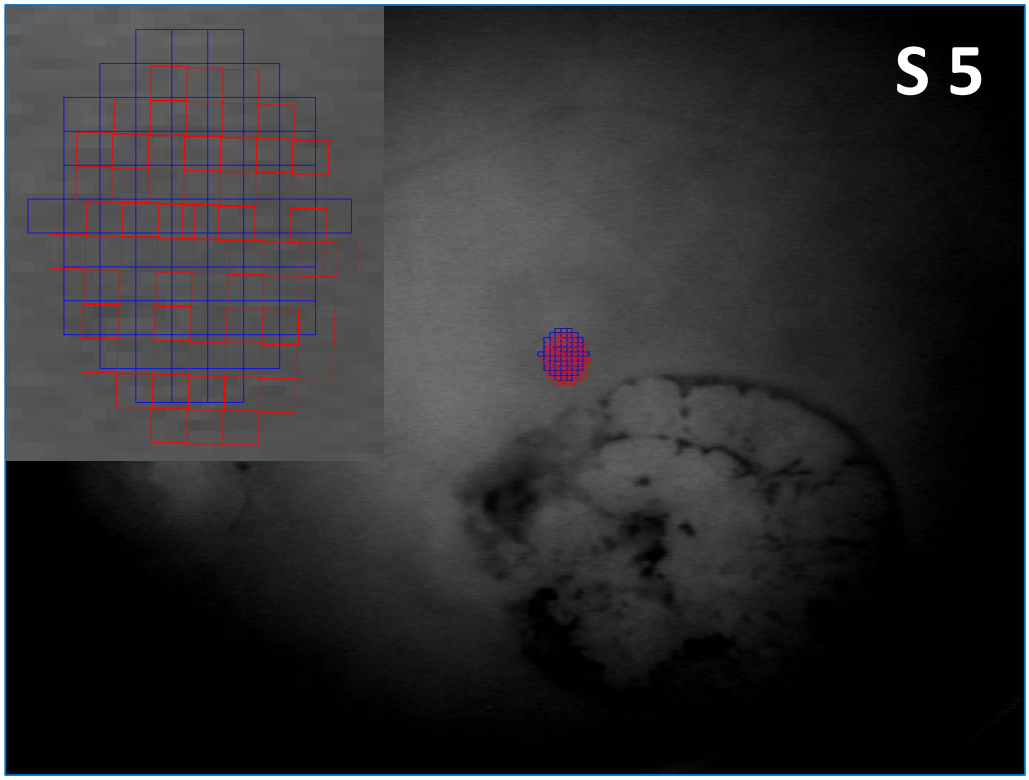
S 5

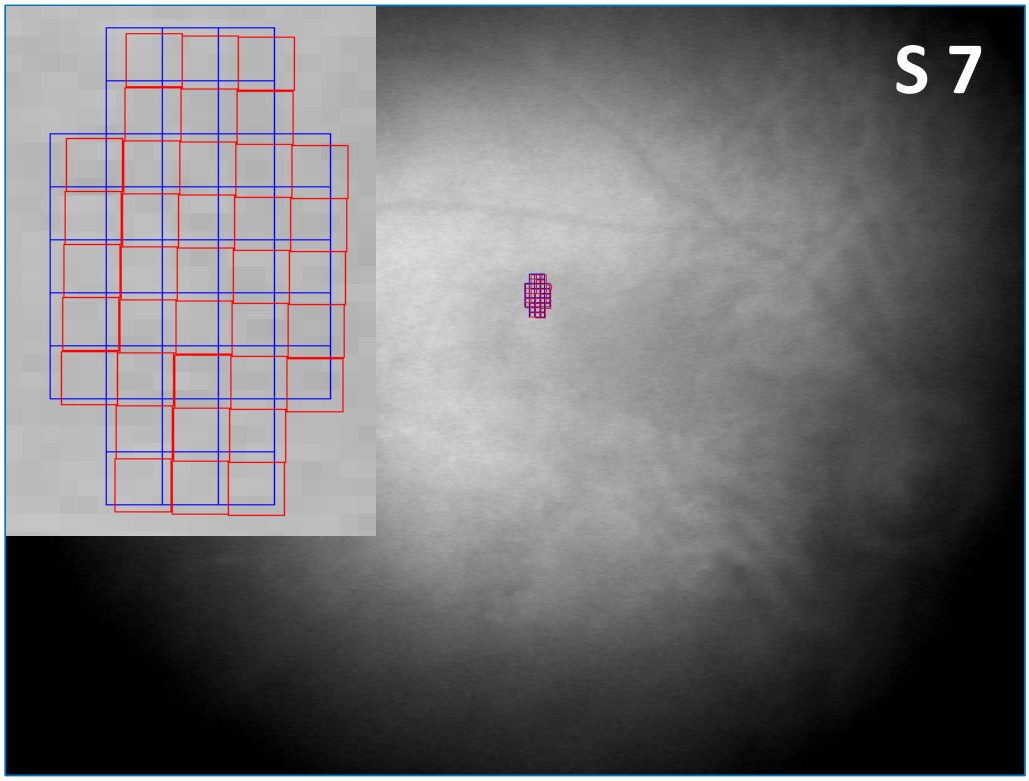
S 7

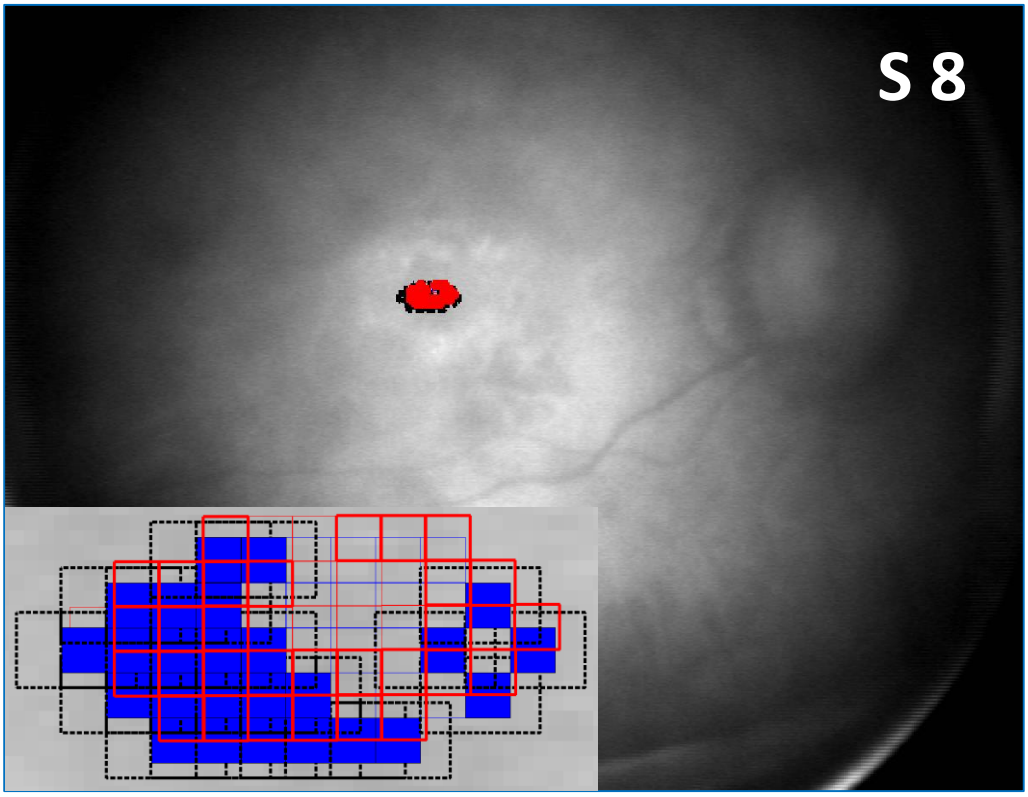
S 8

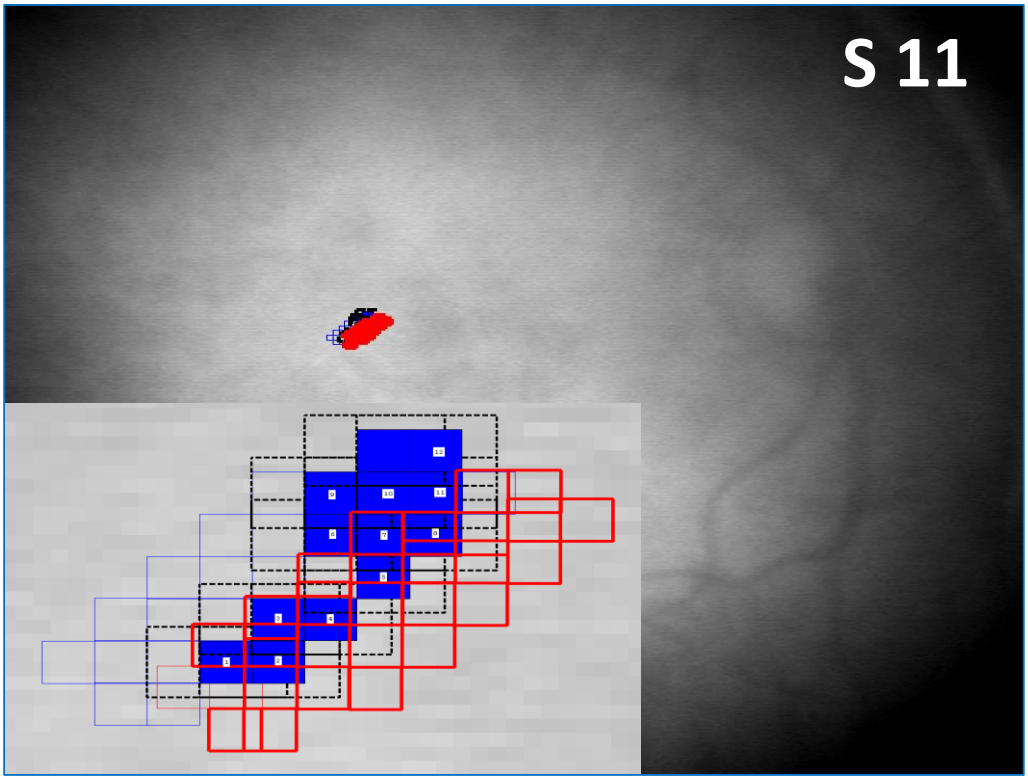
S 11

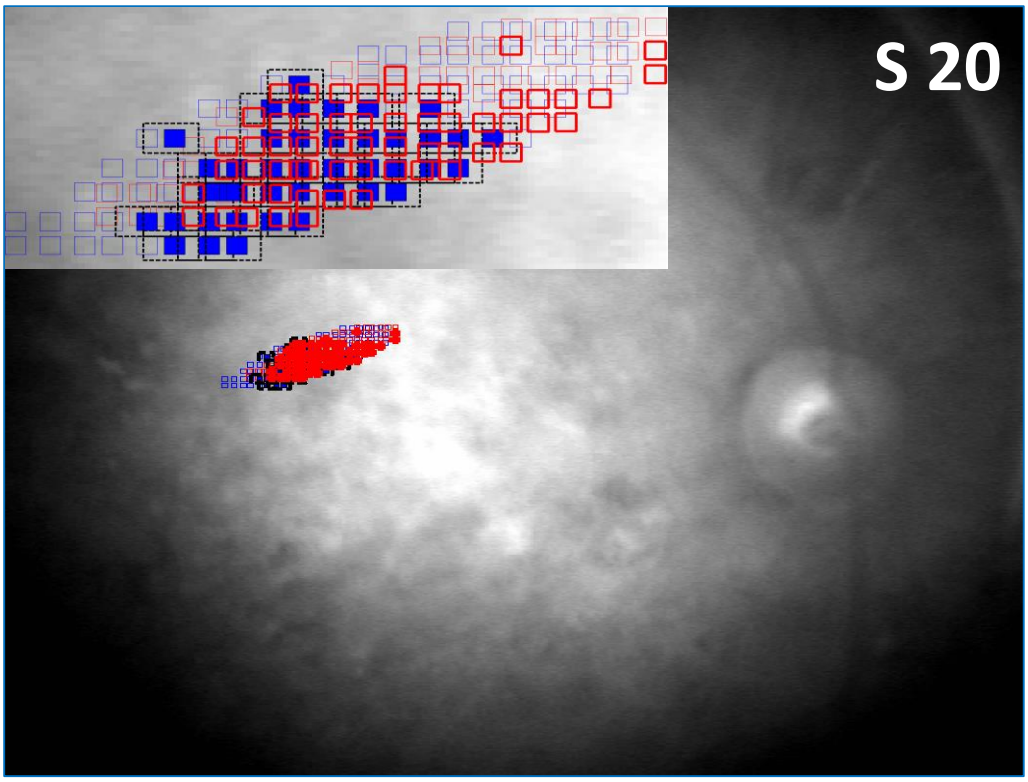
S 20

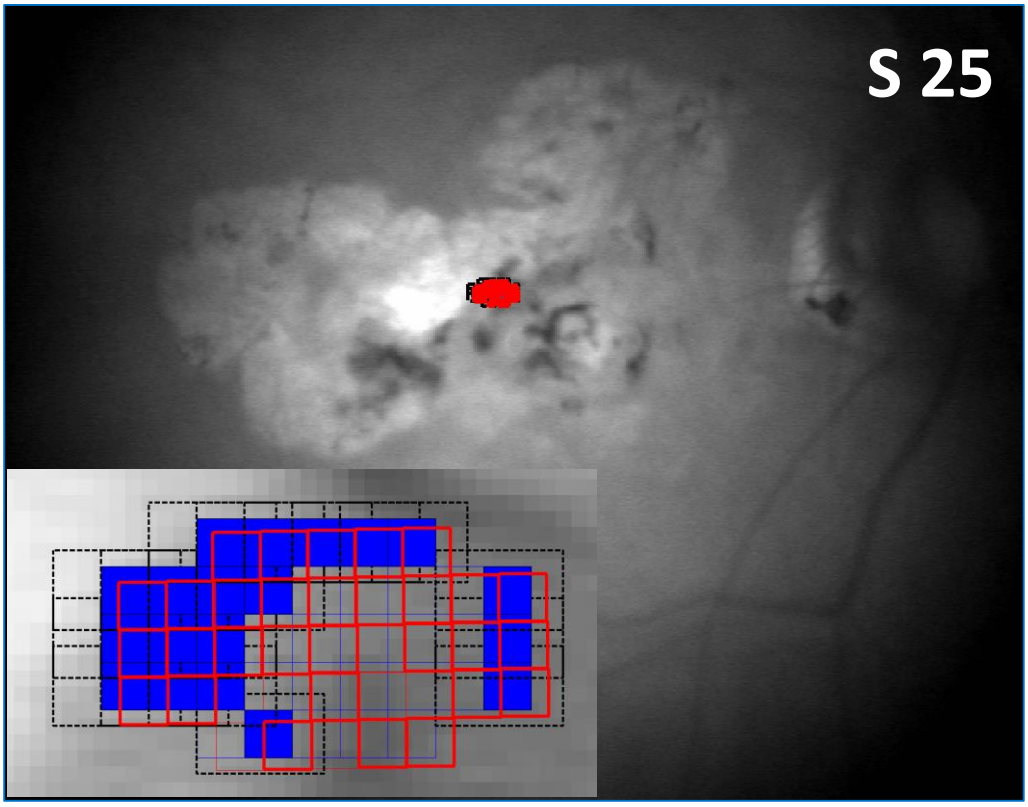
S 25

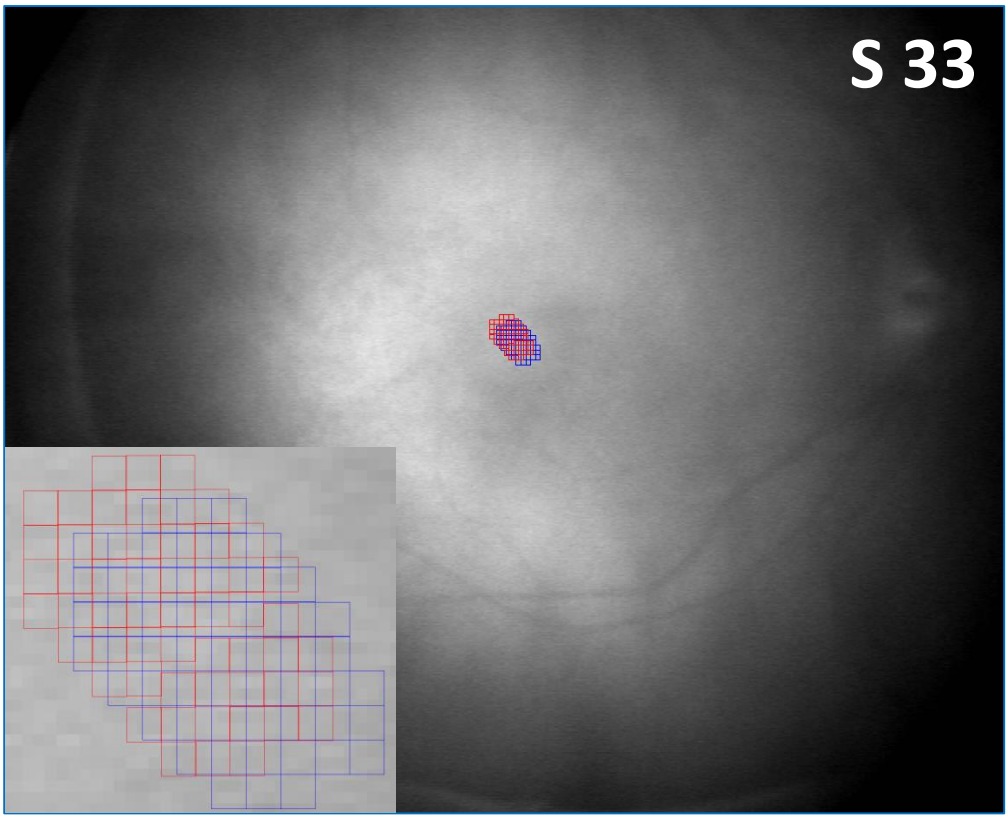
S 33

6.5 Computation of ROI in OCT scan image

The region of interest corresponds to the locations in the OCT scan image that either had overlapping locations where the observer failed to detect the test spot during baseline and follow-up screening (MS locations) or where the test spot was detected on both screening tests (nonMS locations). Locations were classified as MS/nonMS from a pair of supra-threshold screening tests using a Goldmann Size II (nominally 13 arc min) test spot presented in a NIDEK MP1. As discussed in **CHAPTER III** methods, an affine transformation was used to map the locations from IR-MP1 image coordinates to those of the IR-SLO-Spectralis image coordinates. The registration was assessed by a psychophysical method of constant stimuli.

Subject Code	Diagnosis	Offset Direction	Slope	Slope SE	Bias	Absolute Bias	Bias SE
S4	STGD	Vertical	3.935	2.266	0.272	0.272	2.988
S26	STGD	Vertical	2.529	0.014	-1.869	1.869	1.057
S16	AMD	Vertical	3.987	2.266	-0.201	0.201	2.988
S29	AMD	Vertical	1.975	0.005	0.456	0.456	0.994
					Mean	**0.700**	
					SD	**0.787**	
S4	STGD	Horizontal	1.816	0.005	0.874	0.874	1.992
S26	STGD	Horizontal	5.382	3.321	0.060	0.060	3.066

S16	AMD	Horizontal	5.402	3.321	-0.001	0.001	3.125
S29	AMD	Horizontal	4.593	2.641	-2.371	2.371	2.991
					Mean	**0.826**	
					SD	**1.104**	

The table lists (all values in pixels) the slope and the bias of the cumulative Gaussian fit to the psychometric function plotted for the examiner's evaluation for the direction of the image offset. The variance (in arc min) was computed from the SD of the absolute bias using the conversion factor of 51.2 pixels/deg. The variances from the registration error are: 0.85 and 1.67 arc min sq. (See Col. 2 in table below) respectively in vertical and horizontal direction.

Direction	**IR-SLO Registration Error – Variance**	**Uncompensated FEMs Variance**	**Sqrt (Sum of Variances)**	**Test Target Size**	**Sum**
	(arc min Sq.)	(arc min Sq.)	(arc mins)	(arc mins)	(arc mins)
V	0.850	22.373	4.819	13	17.819
H	1.674	18.063	4.443	13	17.443

Given that a 15 deg scan in the OCT spans 768 OCT image pixels and a 20 deg scan spans 1024 image pixels, we know that each OCT image pixel is 1.172 arc min. From this pixel-to-visual-angle conversion we derive that 17.82 and 17.44 arc min correspond to 14.8 and 15.2 OCT image pixels in the vertical and horizontal directions. Thus, the ROI corresponding to a size II test spot after accounting for 2 sources of variance, was ~14 OCT image pixels.

6.6 OCT Image Segmentation – Special Cases

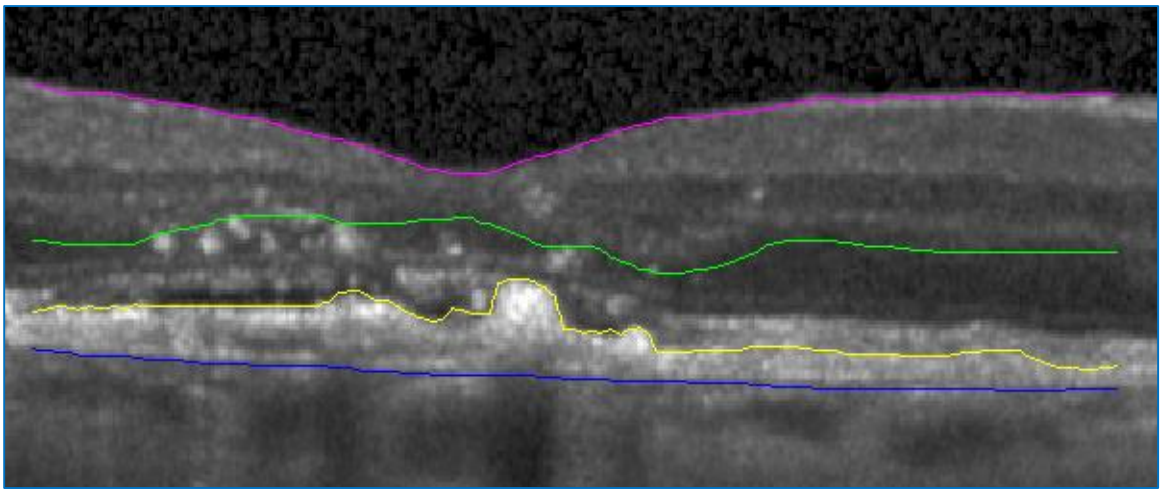

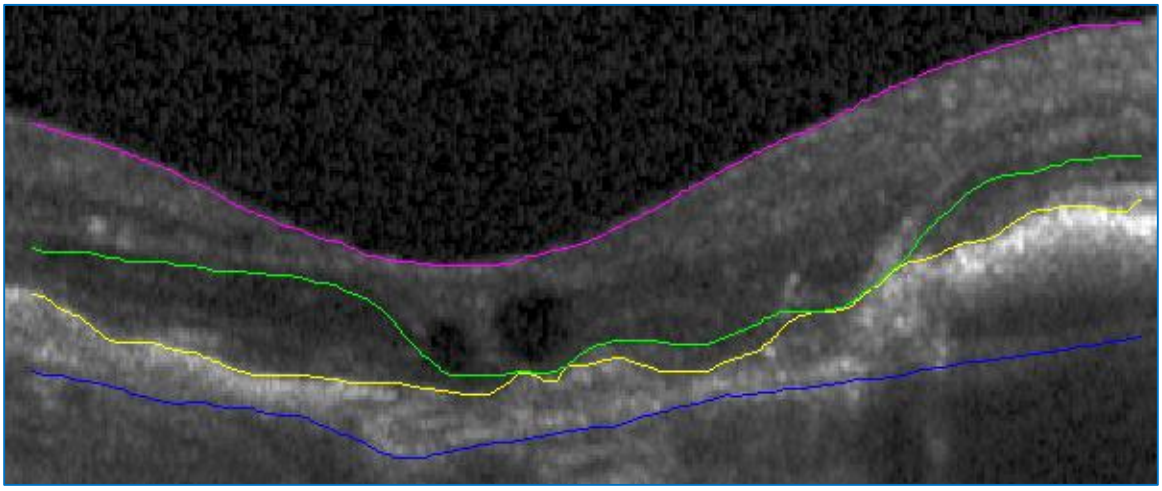

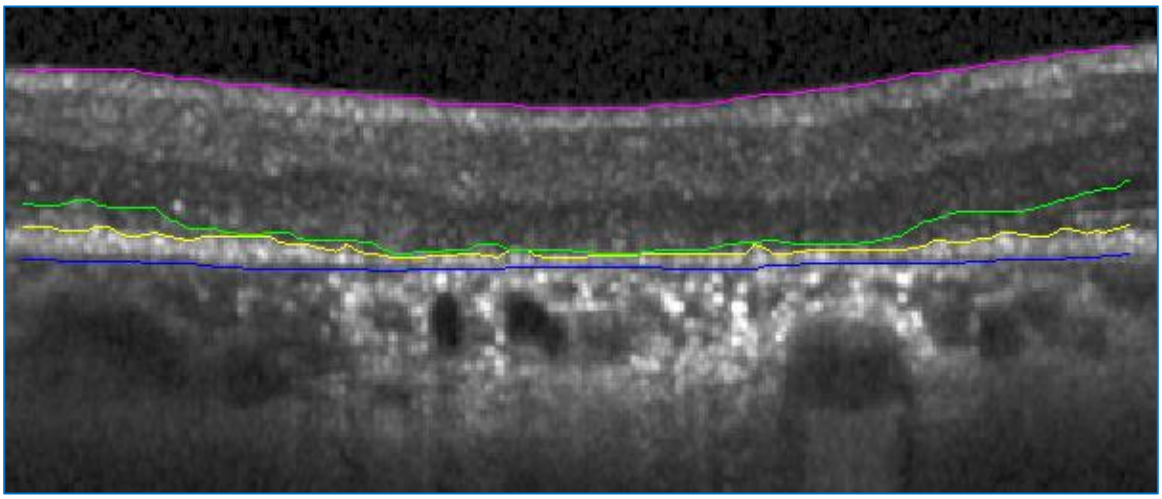

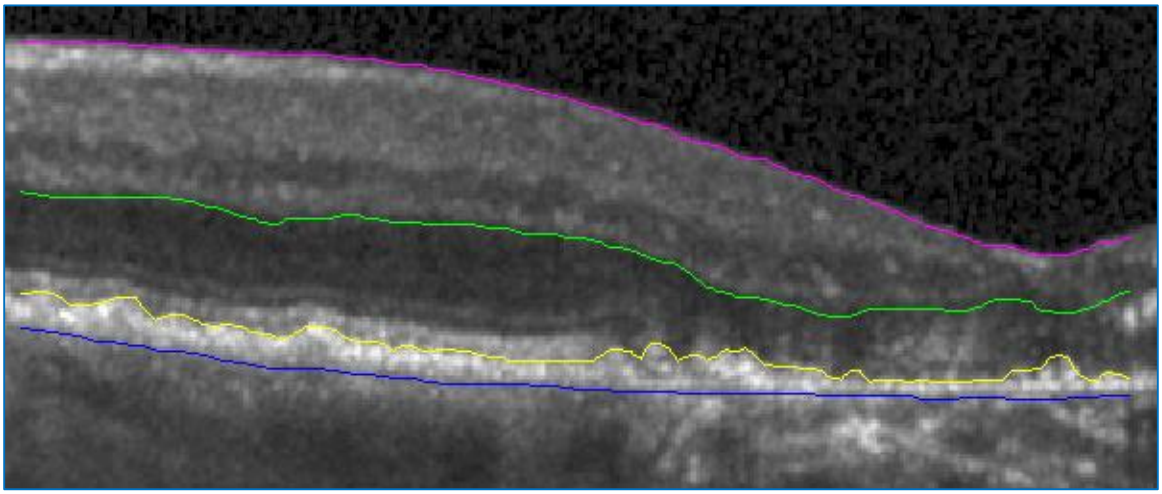

OCT scan descriptions from top:

Scan 1: S2 (AMD). Note how RPE-BM includes the sub-foveal drusen (yellow trace). The hyper reflective material (suspected to be migrated RPE) was included within PL boundaries (green)

Scan 2: S28 (AMD). RPE shows pigment epithelium detachment (right end of the segmented region). The outer margin of RPE-BM complex was still marked (blue) at the

base of the presumed BM location and the inner margin (yellow) was marked around the elevated RPE borders. Also note the PL margin wraps around the circular shadow regions.

Scan 3: S22 (STGD). Note the apparent total thinning of the photoreceptor layer and how the PL margin (green) almost hugs the RPE inner margin (yellow). The RPE thinning also causes enhancement of the signal in the underlying choroid region.

Scan 4: S32 (AMD). Note how the hyper-reflective band above the inner margins of the RPE (yellow) is either absent or merges with RPE layer. In the latter case, it was included as part of the RPE layer. Also note how the contour of the PL margin (green) is similar to that of ILM. The contour of other layers served as the guide when the margin of layer being marked was unclear, especially for PL marking.

6.7 Thickness Ratios and SDs for all Layers

Legend for tables below:

Rows 2-3: For scans from MS locations.

Rows 5-6: For scans from nonMS locations.

Column 3: Average thickness for the RPE-BM layer

Column 4: Average thickness for the Photo-receptor and Outer nuclear layer (PL)

Column 5: Average thickness for the total retinal layers (TRL)

S2		RPE-BM	PL	TRL
MS	AVG	18.95	28.25	66.45
N=6	SD	2.58	3.31	5.19
NonMS	AVG	17.88	20.48	81.72
N=36	SD	4.66	6.47	5.33
	Ratio	1.06	1.38	0.81

S3		RPE-BM	PL	TRL
MS	AVG	10.51	19.02	70.02
N=7	SD	1.08	2.47	0.95
NonMS	AVG	11.88	21.36	71.22
N=10	SD	2.66	4.14	1.17
	Ratio	0.88	0.89	0.98

S4		RPE-BM	PL	TRL
MS	AVG	10.15	18.46	77.11
N=3	SD	0.55	0.78	0.32
NonMS	AVG	9.18	18.61	76.97
N=11	SD	0.66	1.41	1.14
	Ratio	1.11	0.99	1.00

S6		RPE-BM	PL	TRL
MS	AVG	6.71	8.65	71.68
N=1	SD	N	N	N
NonMS	AVG	8.29	9.82	72.64
N=15	SD	1.90	2.49	1.10
	Ratio	0.81	0.88	0.99

S10		RPE-BM	PL	TRL
MS	AVG	5.02	11.32	66.86
N=6	SD	0.77	2.73	1.42
NonMS	AVG	10.96	19.14	73.93
N=15	SD	1.66	2.45	0.87
	Ratio	0.46	0.59	0.90

S12		RPE-BM	PL	TRL
MS	AVG	6.08	11.66	62.90
N=5	SD	1.36	7.78	5.61
NonMS	AVG	8.08	20.71	69.04
N=5	SD	0.37	1.78	1.95
	Ratio	0.75	0.56	0.91

S15		RPE-BM	PL	TRL
MS	AVG	11.97	19.00	70.69
N=2	SD	4.53	0.19	1.22
NonMS	AVG	8.57	14.87	65.55
N=21	SD	0.96	3.42	2.09
	Ratio	1.40	1.28	1.08

S18		RPE-BM	PL	TRL
MS	AVG	9.66	24.23	73.65
N=1	SD	N	N	N
NonMS	AVG	9.78	18.21	72.65
N=16	SD	0.68	2.56	1.11
	Ratio	0.99	1.33	1.01

S23		RPE-BM	PL	TRL
MS	AVG	17.12	24.48	66.21
N=6	SD	2.41	4.12	8.01
NonMS	AVG	15.68	24.03	77.50
N=2	SD	0.87	0.72	1.43
	Ratio	1.09	1.02	0.85

S28		RPE-BM	PL	TRL
MS	AVG	14.03	9.92	57.80
N=29	SD	5.55	9.11	6.58
NonMS	AVG	8.62	31.23	59.79
N=1	SD	N	N	N
	Ratio	1.63	0.32	0.97

S31		RPE-BM	PL	TRL
MS	AVG	10.23	8.07	56.08
N=2	SD	0.44	2.45	2.11
NonMS	AVG	9.54	15.38	66.78
N=22	SD	0.74	2.01	4.08
	Ratio	1.07	0.52	0.84

S32		RPE-BM	PL	TRL
MS	AVG	12.01	37.18	96.10
N=2	SD	2.15	1.34	4.37
NonMS	AVG	9.39	38.35	95.23
N=29	SD	1.67	2.74	4.14
	Ratio	1.28	0.97	1.01

S8		RPE-BM	PL	TRL
MS	AVG	8.78	5.84	36.20
N=25	SD	0.85	1.84	3.72
NonMS	AVG	7.68	8.53	28.79
N=1	SD	N	N	N
	Ratio	1.14	0.69	1.26

S20		RPE-BM	PL	TRL
MS	AVG	11.07	9.30	81.64
N=34	SD	5.61	8.95	5.04
NonMS	AVG	10.25	24.02	91.60
N=15	SD	5.86	9.15	5.23
	Ratio	1.08	0.39	0.89

S25		RPE-BM	PL	TRL
MS	AVG	29.15	32.85	80.35
N=19	SD	18.08	8.75	14.13
NonMS	AVG	65.98	17.68	98.22
N=1	SD	N	N	N
	Ratio	0.44	1.86	0.82

Note that S8, S20 and S25 had miscellaneous diagnoses that lead to CFL.

Subjects with zero nonMS location and who were matched with other CFL subjects:

Subjects with zero nonMS location are: S9, S11, S22, S26, S27 and S29, who were matched with S4, S2, S3, S18, S2, S2, respectively, for computing the MS/nonMS thickness ratios.

S9		RPE-BM	PL	TRL
MS	AVG	11.06	10.04	69.64
N=22	SD	2.12	4.26	1.38
S4				
NonMS	AVG	9.18	18.61	76.97
N=11	SD	0.66	1.41	1.14
	Ratio	1.20	0.54	0.90

S11		RPE-BM	PL	TRL
MS	AVG	16.04	6.27	73.45
N=12	SD	4.51	5.32	1.85
S2				
NonMS	AVG	17.88	20.48	81.72
N=36	SD	4.66	6.47	5.33
	Ratio	0.90	0.31	0.90

S22		RPE-BM	PL	TRL
MS	AVG	5.82	6.14	54.46
N=44	SD	1.87	5.87	7.18
S3				
NonMS	AVG	11.88	21.36	71.22
N=10	SD	2.66	4.14	1.17
	Ratio	0.49	0.29	0.76

S26		RPE-BM	PL	TRL
MS	AVG	9.37	7.89	32.31
N=39	SD	1.87	2.70	3.20
S18				
NonMS	AVG	9.78	18.21	72.65
N=16	SD	0.68	2.56	1.11
	Ratio	0.96	0.43	0.44

S27		RPE-BM	PL	TRL
MS	AVG	15.79	18.99	55.62
N=13	SD	2.83	4.37	9.20
S2				
NonMS	AVG	17.88	20.48	81.72
N=36	SD	4.66	6.47	5.33
	Ratio	0.88	0.93	0.68

S29		RPE-BM	PL	TRL
MS	AVG	6.86	13.34	67.00
N=49	SD	2.25	7.11	8.46
S2				
NonMS	AVG	17.88	20.48	81.72
N=36	SD	4.66	6.47	5.33
	Ratio	0.38	0.65	0.82

6.8 CPS (MN Read) and BCEA: All Subjects

Subject Code	CPS (MN Read)	1 SD BCEA (deg^2)		
	(logMAR)	Test 1	Test 2	Test 3
S1	0.7	0.2	0.26	0.16
S2	0.8	0.48	15.18	2.31
S3	1.3	1.12	1.69	1.31
S4	1	0.57	0.51	0.63
S5	1.15	0.69	0.88	0.85
S6	0.95	0.39	0.34	0.32
S7	1.2	0.84	2.94	1.01
S8	0.8	0.04	0.25	0.53
S9	1.1	1.89	1.16	1.12
S10	1.15	0.36	0.66	0.71
S11	1.22	0.82	0.61	1.9
S12	1.25	2.55	1.1	0.59
S14	1.1	0.25	0.3	0.51
S15	1.27	0.46	0.45	--
S16	1.4	1.12	2.61	0.62
S18	1.07	3.53	1.51	1.97
S19	1.1	1.55	2.59	2.58
S20	1	7.78	4.4	17.02
S22	1.3	2.21	1.39	2.07
S23	0.8	1.05	1.22	0.41

S25	1.2	0.29	0.41	0.47
S26	1.07	0.54	0.89	1.24
S27	1.15	0.26	0.52	0.45
S28	1.175	0.8	0.76	0.42
S29	0.85	0.98	0.65	4.61
S30	1.2	1.22	0.77	0.97
S31	0.875	0.48	0.66	0.47
S32	1.175	1.96	1.61	2.34
S33	0.95	1.21	1.86	3.5
Average	**1.08**	**1.23**	**1.54**	**1.37**
Median	**1.10**	**0.82**	**0.80**	**0.91**
SD	**0.18**	**1.49**	**2.72**	**1.21**

Note that S2 sometimes uses two preferred word fixation loci, which accounts for the very large BCEA on fixation test 2. Multiple PRLs account also for the large BCEA for S20 on fixation test 3.

6.9 Scatter plot: Max RS (MN Read) vs BCEA

The relationship was NOT significant either with or without the outlier (r = -0.140, t (27) = 0.733, p = 0.47 and r = -0.197, t (26) = 1.026, p = 0.314).

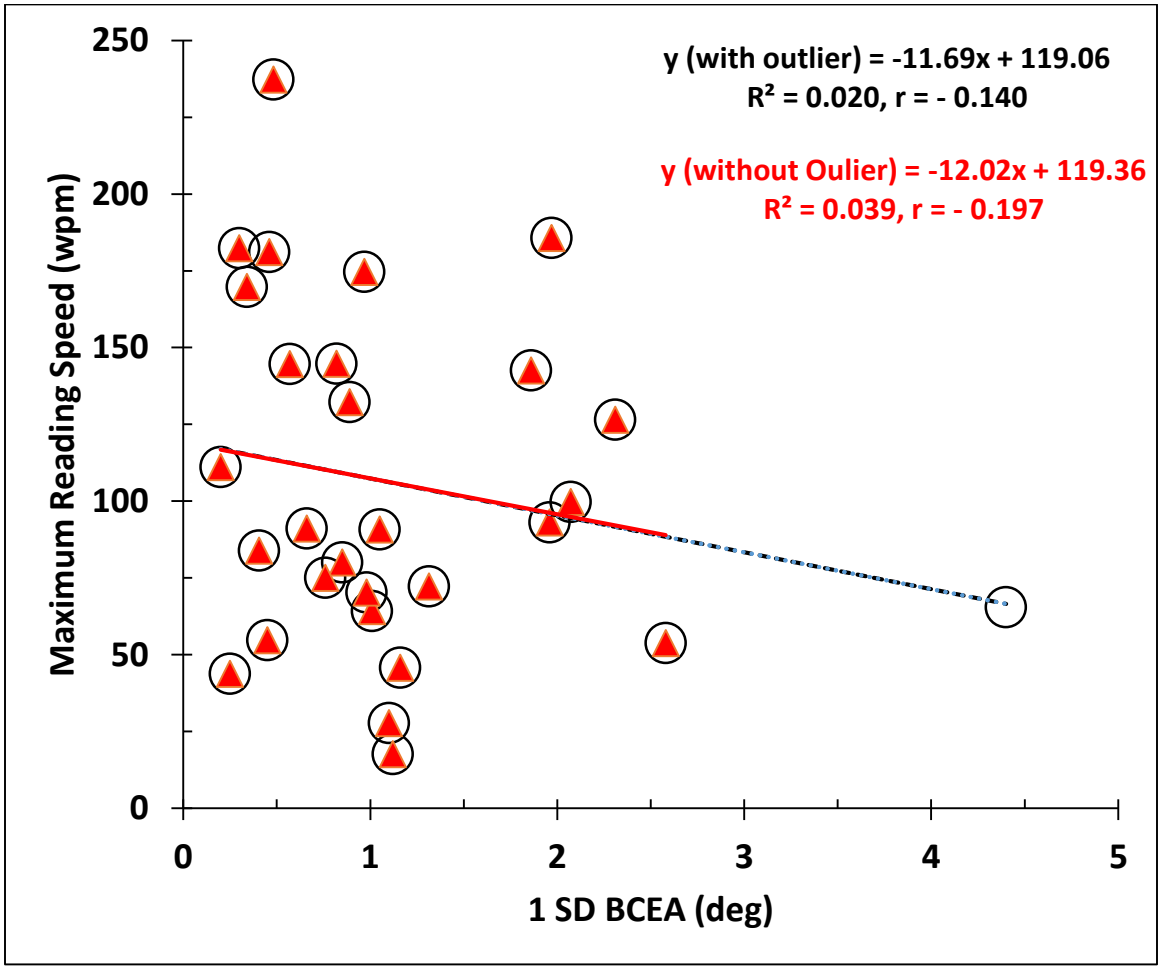

6.10 Scatter plot: Max. RS (MN Read) vs Eccentricity

The relationship was NOT significant (r = -0.232, t (27) = 1.238, p = 0.227).

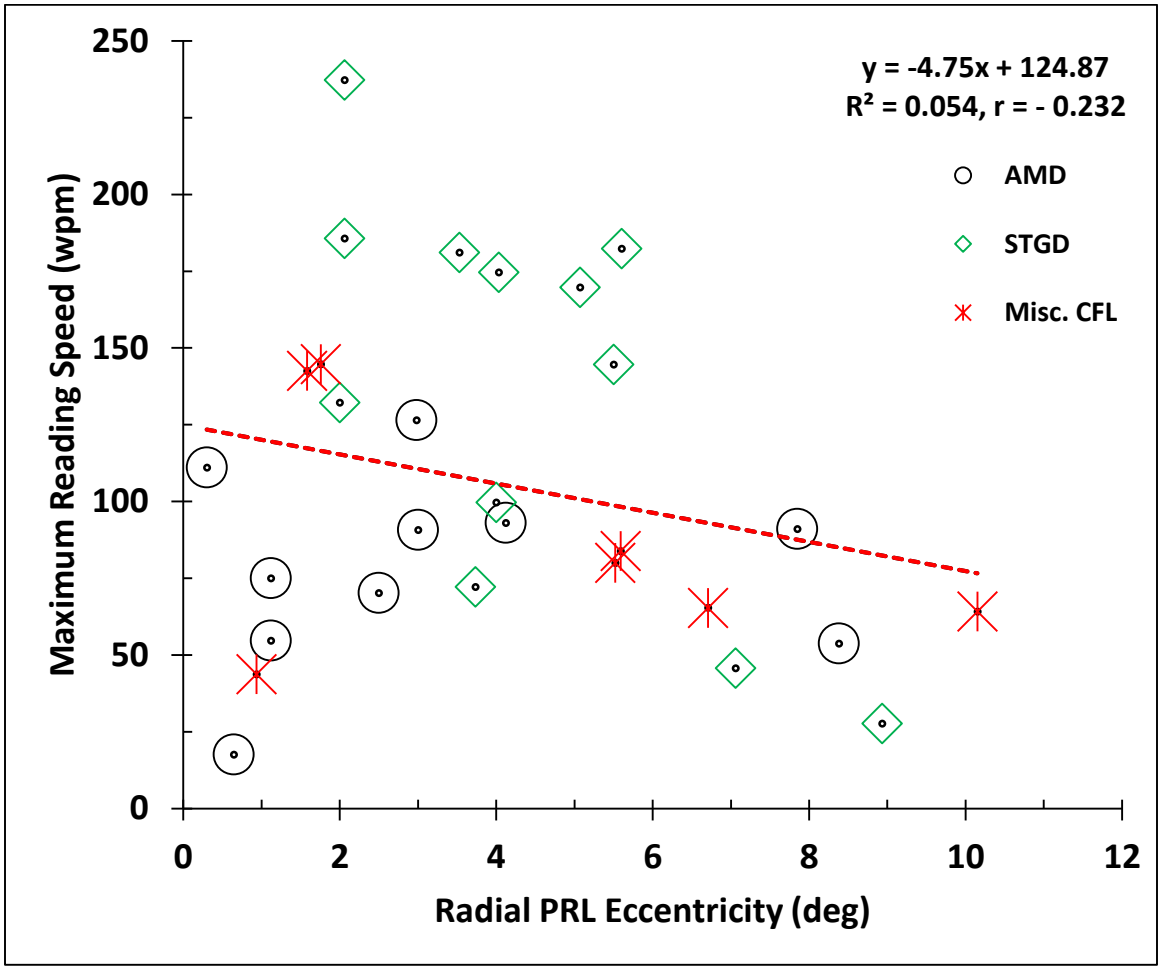

6.11 Scatter plot: Reading Acuity (MN Read) vs Eccentricity

The relationship was significant (r = +0.383, t (27) = 2.157, p = 0.040).

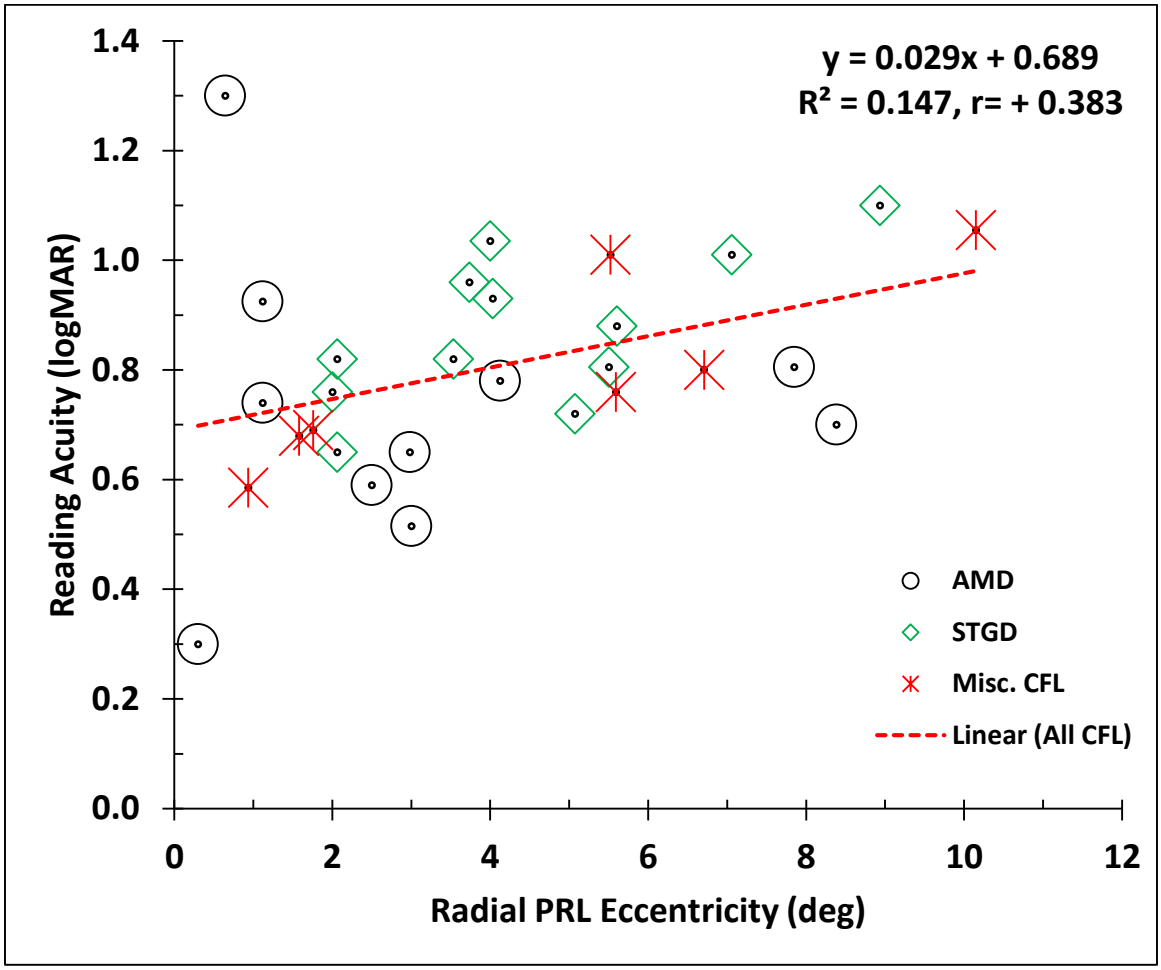

6.12 Scatter plot: CPS vs Reading Acuity (MN Read)

The relationship was significant ($r = +0.826$, $t(27) = 7.618$, $p = 3 \times 10^{-8}$).

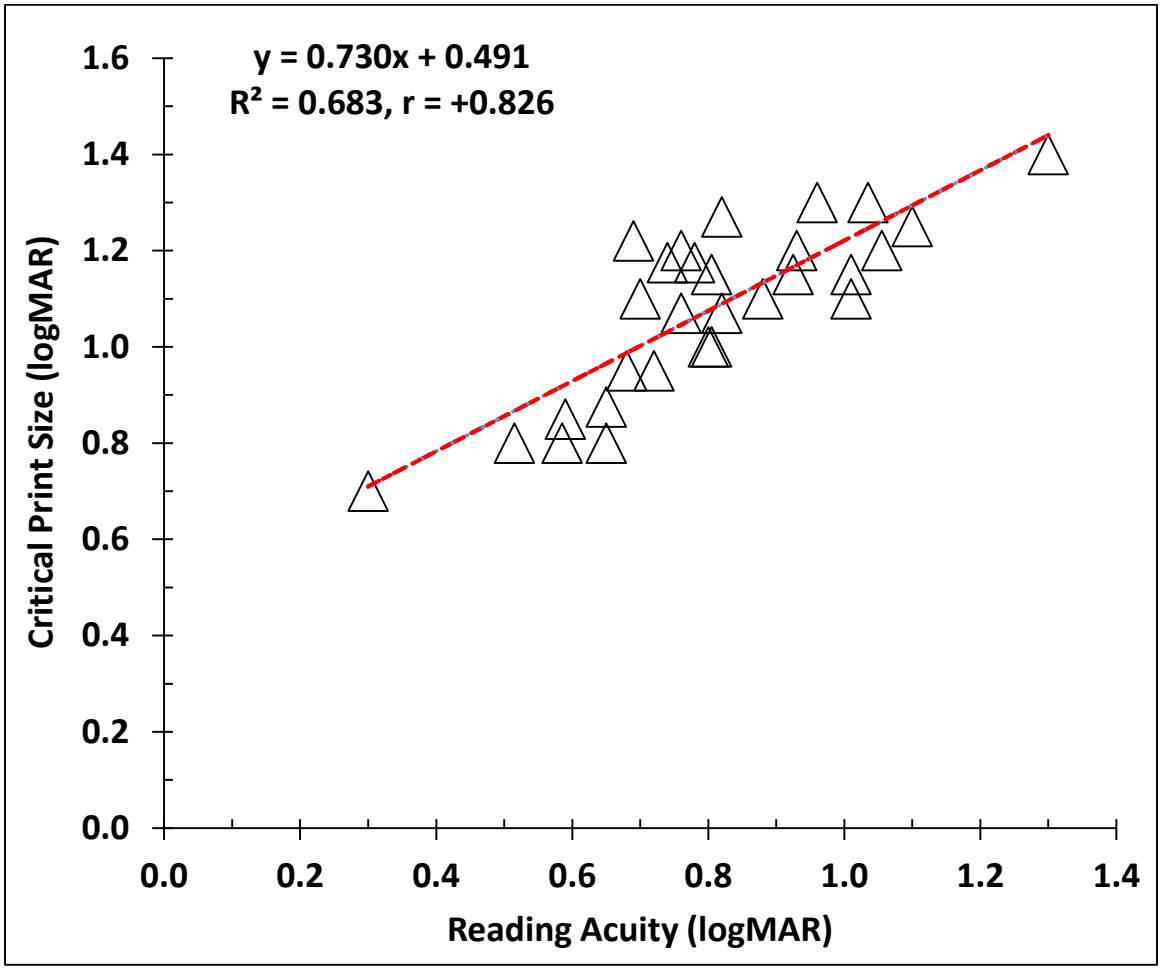

6.13 Scatter plot: Max. RS (MN Read) vs Age

The relationship was significant (r= -0.508, t (27) = 3.067, p = 0.0049).

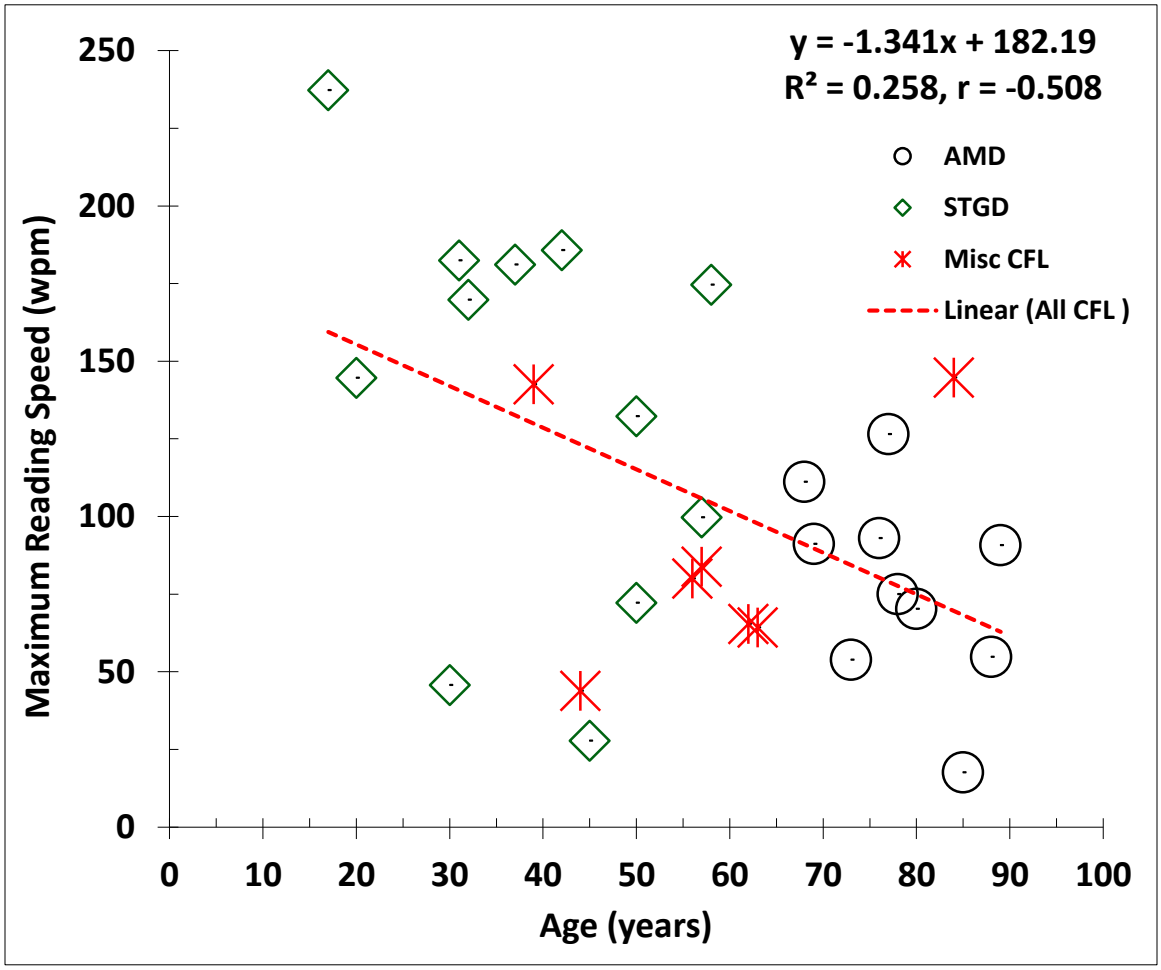

6.14 Scatter plot: % MS vs Age

The relationship was NOT significant (r= +0.237, t (27) = 1.269, p = 0.215).

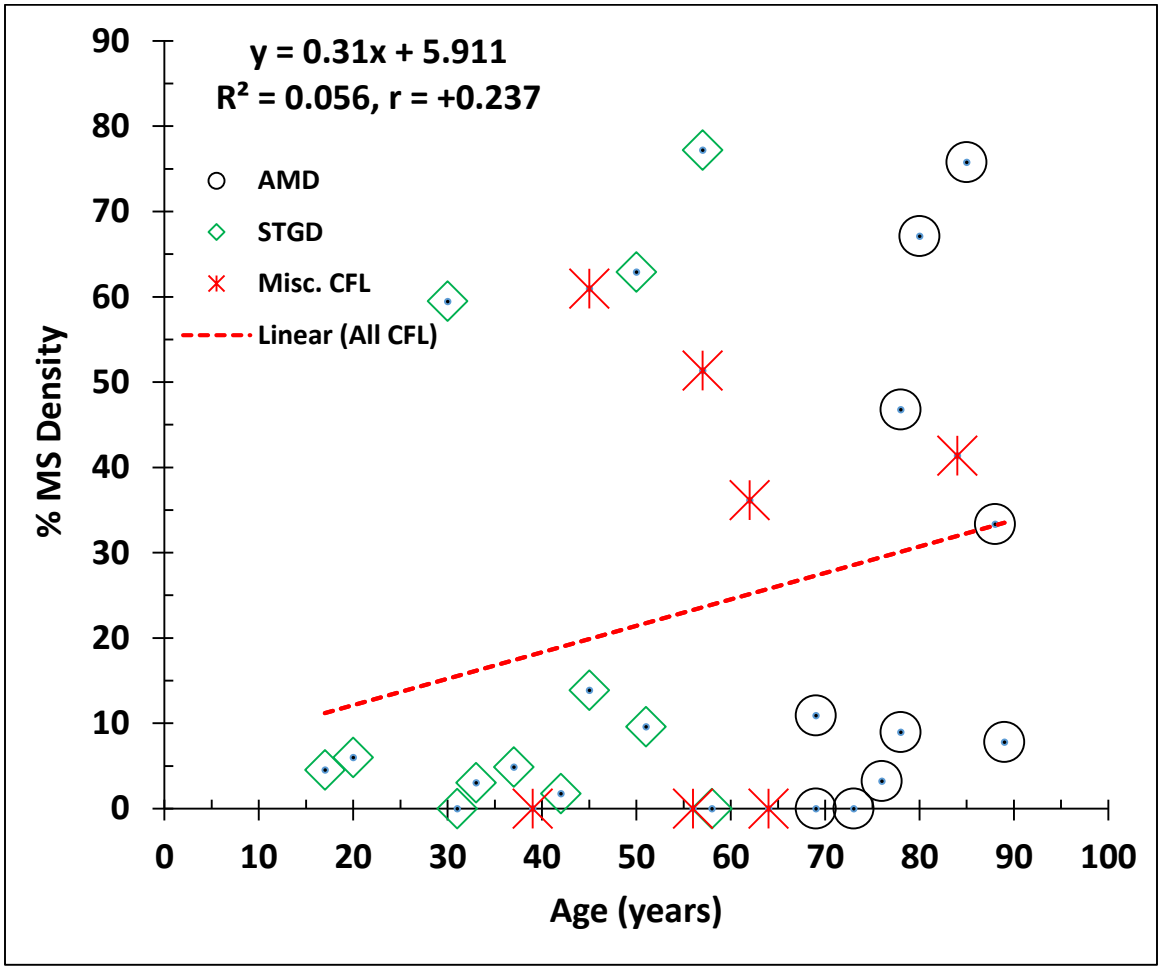

6.15 Scatter plot: BCEA vs % MS

The relationship was NOT significant (r= -0.066, t (26) = 0.339, p = 0.737).

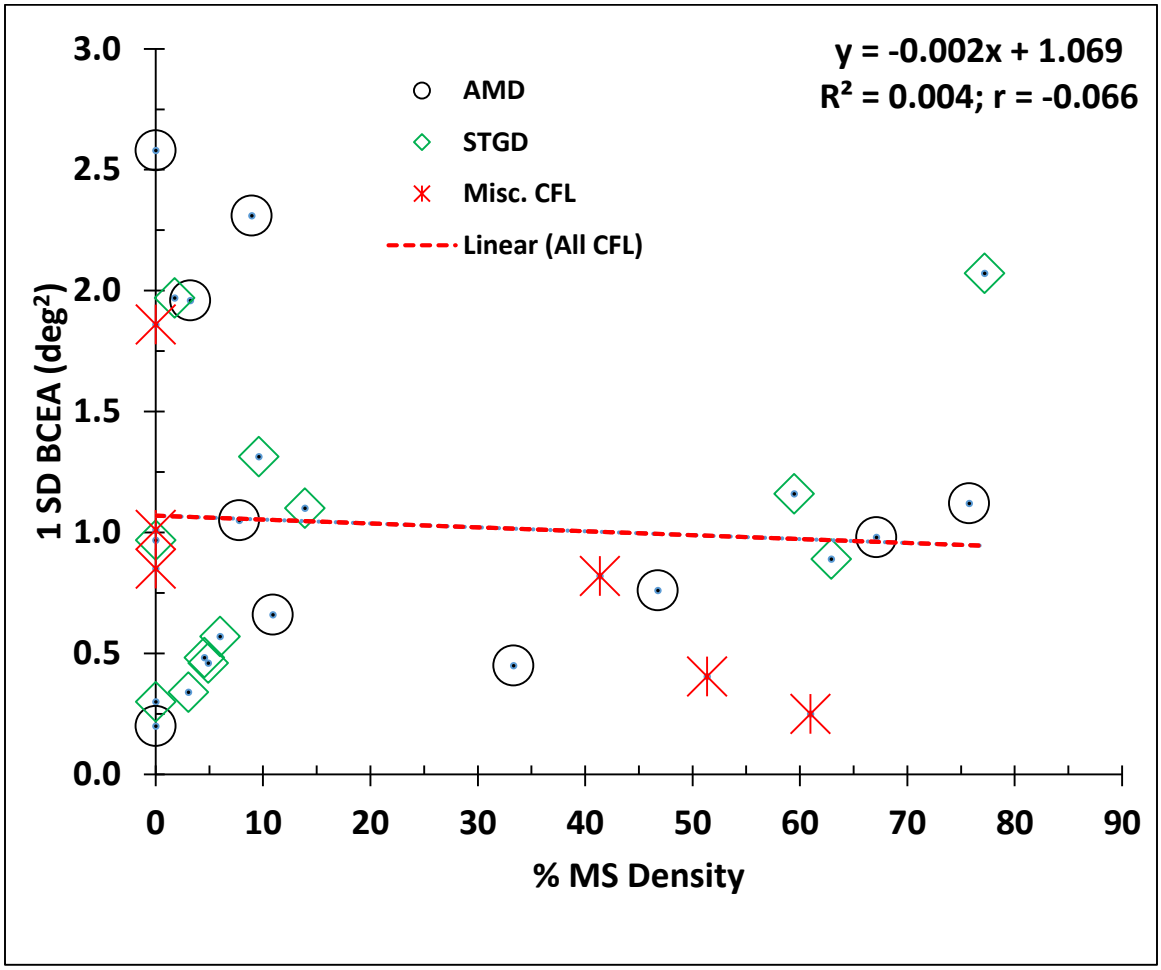

6.16 PRL Meridian and Polar Angle

Subject Code	Test Eye	Diagnosis	PRL Meridian (Retinal)	Radial Eccentricity (°)	Polar Angle (°)
S1	OS	AMD	Nasal	0.30	181.07
S2	OD	AMD	Infero-Nasal	2.98	322.55
S3	OD	STGD	Superior	3.73	97.70
S4	OD	STGD	Superior	5.50	91.60
S5	OS	CRD	Superior	5.52	95.19
S6	OD	STGD	Superior	5.07	77.47
S7	OD	Plaq. Mac	Superior	10.15	84.23
S8	OD	CRD	Temporal	0.94	119.52
S9	OD	STGD	Superior	7.06	91.96
S10	OS	AMD	Supero-Nasal	7.85	110.51
S11	OD	Mac Hole	Superior	1.76	75.18
S12	OS	STGD	Superior	8.93	104.29
S14	OD	STGD	Superior	5.60	74.47
S15	OD	STGD	Superior	3.53	74.40
S16	OS	AMD	Infero-Nasal	0.65	307.98
S18	OD	STGD	Superior	2.06	75.96
S19	OD	AMD	Superior	8.38	72.65
S20	OD	Plaq. Mac.	Supero-Temporal	6.71	116.57
S22	OD	STGD	Superior	4.00	90.00
S23	OS	AMD	Inferior	3.00	270.00

S25	OD	MMD/Toxo	Infero-Temporal	5.59	206.57
S26	OS	STGD	Inferior	2.00	270.00
S27	OD	AMD	Supero-Nasal	1.12	63.43
S28	OS	AMD	Supero-Temporal	1.12	63.43
S29	OD	AMD	Nasal	2.50	0.00
S30	OD	STGD	Superior	4.03	82.87
S31	OD	STGD	Superior	2.06	75.96
S32	OS	AMD	Nasal	4.12	165.96
S33	OD	Cone Dys	Inferior	1.58	251.57
			Minimum	**0.30**	
			Maximum	**10.15**	
			Median	**3.73**	
			Mean	**4.06**	

Note that the retinal eccentricity and the meridian of the PRL were calculated from the results of each examination by assuming a foveal location that is 15.5° temporal and 1.5° below the center of each patient's optic disc (Rohrschneider, 2004).

For computing the polar angle, a PRL to the right of the estimated foveal location (i.e., nasal retina in the right eye and temporal retina in the left eye) was designated as having a meridian of zero. Superior and inferior on the retina were designated as the 90° and 270° meridians, respectively.

6.17 Supra-threshold Screening: Normally-sighted Subjects

Age	Eye	Radial Ecc. (°)	Retinal Meridian	Roughly Matches With	Total Locations Screened	Sampling Density(°)	Not Seen	Not Seen	% MSs
							Test #1	Test #2	
68	OS	6	Infero-Nasal	S25	36	0.2	1	0	0
71	OS	2	Supero-Temporal	S11	30	0.2	2	0	0
27	OS	6	Superior	S5	68	0.2	0	0	0
29	OD	4	Supero-Temporal	S3	75	0.2	1	1	0
61	OS	4	Nasal	S32	65	0.2	1	0	0
69	OD	7	Supero-Temporal	S20	95	0.3	4	1	1.05
56	OD	3	Infero-Nasal	S2	68	0.4	0	0	0
31	OS	8	Superior	S10	55	0.2	0	1	0
				Total	**492**		**9**	**3**	

Note that of the 8 subjects screened only one of them had an overlapping MS (in 1 location out of 95 locations screened, ~1.05%).

6.18 Supra-threshold Screening: Relative Scotomas

Code	Diagnosis	Screening Luminance	Total Locations	Not Seen #1	Not Seen #2
		(dB)	Screened		
S3	STGD	4	73	2	2
S4	STGD	6	50	10	17
S5	Cone-rod Dys	5	67	0	1
S6	STGD	5	33	1	1
S7	Plaq. Mac	5	37	1	0
S11	Macular Hole	4	29	15	28
S12	STGD	5	36	10	9
S14	STGD	7	23	0	0
S15	STGD	7	41	5	9
S18	STGD	5	57	6	10
S19	AMD	3	67	4	2
S31	STGD	5	44	15	15
S32	AMD	5	62	19	15

The screening for relative scotomas with a luminance level that is +5 dB brighter than median sensitivity around PRL was done in 13 of the 29 subjects with CFL. This was asides the screening with the brightest test spots (0 dB screening), and the luminance of the test spots used for this screening is listed in column 3.

7. REFERENCES

Acton, J. H., Smith, R. T., Greenberg, J. P., & Greenstein, V. C. (2012). Comparison between MP-1 and Humphrey visual field defects in glaucoma and retinitis pigmentosa. *Optometry and Vision Science*, *89*(7), 1050–1058.

Acton, J. H., Smith, R.T, Hood, D. C., & Greenstein, V. C. (2012). Relationship between retinal layer thickness and the visual field in early age-related macular degeneration. *Investigative Ophthalmology and Visual Science*, *53*(12), 7618–7624.

Ambati, J., & Fowler, B. J. (2012). Mechanisms of age-related macular degeneration. *Neuron*, *75*(1), 26–39.

American Academy of Ophthalmology - Retina/Vitreous Panel. (2015). *Preferred Practice Pattern Guidelines. Age-Related Macular Degeneration*. (S. Garratt, Ed.) (Jan 2015). San Francisco, CA.: American Academy of Ophthalmology. Retrieved from www.aao.org/ppp

Amore, F. M., Fasciani, R., Silvestri, V., Crossland, M. D., de Waure, C., Cruciani, F., & Reibaldi, A. (2013). Relationship between fixation stability measured with MP-1 and reading performance. *Ophthalmic and Physiological Optics*, *33*(5), 611–617.

Bach, M. (1996). The Freiburg visual acuity test- Automatic measurement of visual acuity. *Optometry and Vision Science*, 73(1), 49-53.

Bagiella, E., Sloan, R. P., & Heitjan, D. F. (2000). Mixed-effects models in psychophysiology. *Psychophysiology*, *37*(1), 13–20.

Bedell, H. E., Pratt, J. D., Krishnan, A., Kisilevsky, E., Brin, T. A., Gonzalez, E. G., … Tarita-Nistor, L. (2015). Repeatability of Nidek MP-1 fixation measurements in patients with bilateral central field loss. *Investigative Ophthalmology and Visual Science*, *56*(4), 2624–2630.

Bek, T., & Lund-Andersen, H. (1989). The influence of stimulus size on perimetric detection of small scotomata. *Graefe's Archive for Clinical and Experimental Ophthalmology*, *227*, 531–534.

Bellmann, C., Feely, M., Crossland, M. D., Kabanarou, S. A., & Rubin, G. S. (2004). Fixation stability using central and pericentral fixation targets in patients with age-related macular degeneration. *Ophthalmology*, *111*(12), 2265–2270.

Bindewald, A., Bird, A. C., Dandekar, S. S., Dolar-Szczasny, J., Dreybaupt, J., Fitzke, F. W., … Wolf, S. (2005). Classification of fundus autofluorescence patterns in early age-related macular disease. *Investigative Ophthalmology and Visual Science*, *46*(9), 3309–3314.

Bouma, H. (1973). Visual interference in the parafoveal recognition of initial and final letters of words. *Vision Research*, *13*(4), 767–782.

Brainard, D. H. (1997). The psychophysics toolbox. *Spatial Vision*, *10*, 443–446.

Bressler, N. M., & PHP-Research-Group. (2005). Preferential hyperacuity perimeter (PreView PHP) for detecting choroidal neovascularization study. *Ophthalmology*, *112*(10), 1758–1765.

Bullimore, M. A., Bailey, I. L., & Wacker, R. T. (1991). Face recognition in age-related maculopathy. *Investigative Ophthalmology and Visual Science*, *32*(7), 2020–2029.

Cacho, I., Dickinson, C. M., Smith, H. J., & Harper, R. A. (2010). Clinical impairment measures and reading performance in a large age-related macular degeneration group. *Optometry and Vision Science*, *87*(5), 344–349.

Calabrese, A., Bernard, J. B., Faure, G., Hoffart, L., & Castet, E. (2014). Eye movements and reading speed in macular disease: The shrinking perceptual span hypothesis requires and is supported by a mediation analysis. *Investigative Ophthalmology and Visual Science*, *55*(6), 3638–3645.

Castet, E., & Crossland, M. (2012). Quantifying eye stability during a fixation task : A review of definitions and methods. *Seeing and Perceiving*, *25*, 449–470.

Chen, F. K., Patel, P. J., Xing, W., Bunce, C., Egan, C., Tufail, A. T., … Da Cruz, L. (2009). Test-retest variability of microperimetry using the Nidek MP1 in patients with macular disease. *Investigative Ophthalmology and Visual Science*, *50*(7), 3464–3472.

Cheong, A. M. Y., Legge, G. E., Lawrence, M. G., Cheung, S. H., & Ruff, M. A. (2007). Relationship between slow visual processing and reading speed in people with macular degeneration. *Vision Research*, *47*(23), 2943–2955.

Cheong, A. M. Y., Legge, G. E., Lawrence, M. G., Cheung, S. H., Ruff, M. A., & Otr, L. (2008). Relationship between visual span and reading performance in age-related macular degeneration. *Vision Research*, *48*(4), 577–588.

Cherici, C., Kuang, X., Poletti, M., & Rucci, M. (2012). Precision of sustained fixation in trained and untrained observers. *Journal of Vision*, *12*(6), 1–31.

Chiang Lee, K. Y., Tomidokoro, A., Sakata, R., Konno, S., Mayama, C., Saito, H., … Araie, M. (2010). Cross-sectional anatomic configurations of peripapillary atrophy evaluated with spectral domain-optical coherence tomography. *Investigative Ophthalmology and Visual Science*, *51*(2), 666–671.

Chiu, S. J., Izatt, J. a., O'Connell, R. V., Winter, K. P., Toth, C. a., & Farsiu, S. (2012). Validated automatic segmentation of AMD pathology including drusen and geographic atrophy in SD-OCT images. *Investigative Ophthalmology and Visual Science*, *53*(1), 53–61.

Chung, S. T. L., Mansfield, J. S., & Legge, G. E. (1998). Psychophysics of reading. XVIII. The effect of print size on reading speed in normal peripheral vision. *Vision Research*, *38*(19), 2949–2962.

Chung, S. T. L., & Tjan, B. S. (2010). Spatial frequency and contrast properties of reading in central and peripheral vision. *Journal of Vision*, *9*(9), 1–29.

Cideciyan, A. V., Swider, M., Aleman, T. S., Sumaroka, A., Schwartz, S. B., Roman, M. I., … Jacobson, S. G. (2005). ABCA4-associated retinal degenerations spare structure and function of the human parapapillary retina. *Investigative Ophthalmology and Visual Science*, *46*(12), 4739–4746.

Crossland, M. D., Crabb, D. P., & Rubin, G. S. (2011). Task-specific fixation behavior in macular disease. *Investigative Ophthalmology and Visual Science*, *52*(1), 411–416.

Crossland, M. D., Culham, L. E., Kabanarou, S. A., & Rubin, G. S. (2005). Preferred retinal locus development in patients with macular disease. *Ophthalmology*, *112*(9), 1579–1585.

Curcio, C. A., Owsley, C., & Jackson, G. R. (2000). Spare the rods, save the cones in aging and age-related maculopathy. *Investigative Ophthalmology and Visual Science*, *41*(8), 2015–2018.

de Jong, P. T. V. M. (2006). Age-related macular degeneration. *The New England Journal of Medicine*, *355*(3), 1474–1485.

Deubel, H., Schneider, W. X., & Bridgeman, B. (2002). Transsaccadic memory of position and form. *Progress in Brain Research*, *140*, 165–180.

Dimitrov, P. N., Robman, L. D., Varsamidis, M., Aung, K. Z., Makeyeva, G. A., Guymer, R. H., & Vingrys, A. J. (2011). Visual function tests as potential biomarkers in age-related macular degeneration. *Investigative Ophthalmology and Visual Science*, *52*(13), 9457–9469.

Dinc, U. A., Yenerel, M., Gorgun, E., & Oncel, M. (2008). Assessment of macular function by microperimetry in intermediate age-related macular degeneration. *European Journal of Ophthalmology*, *18*(4), 595–600.

Ditchburn, R., & Ginsborg, B. L. (1953). Involuntary eye movements during fixation. *Journal of Physiology*, *119*, 1–17.

Dockeray, F. C. P. W. (1910). The span of vision in reading and the legibility of letters. *The Journal of Educational Psychology*, *1*(3), 123–131.

Dorey, C. K., Wu, G., Ebenstein, D., Garsd, A., & Weiter, J. (1989). Cell loss in the aging retina - Relationship to lipofuscin accumulation and macular degeneration. *Investigative Opthalmology and Visual Science*, *30*(8), 1691–1699.

Elliott, D. B., Trukolo-Ilic, M., Strong, J. G., Pace, R., Plotkin, A., & Bevers, P. (1997). Demographic characteristics of the vision-disabled elderly. *Investigative Ophthalmology and Visual Science*, *38*(12), 2566–2575.

Falkenberg, H. K., Rubin, G. S., & Bex, P. J. (2007). Acuity, crowding, reading and fixation stability. *Vision Research*, *47*(1), 126–135.

Fantes, F. E., & Anderson, D. R. (1989). Clinical histologic correlation of human peripapillary anatomy. *Ophthalmology*, *96*(1), 20–25.

Fine, E. M., & Rubin, G. S. (1999). Reading with simulated scotomas: Attending to the right is better than attending to the left. *Vision Research*, *39*(5), 1039–1048.

Fishman, G. A., Farbman, J. S., & Alexander, K. R. (1991). Delayed rod dark adaptation in patients with Stargardt's disease. *Ophthalmology*, *98*(6), 957–962.

Fleckenstein, M., Issa, P. C., Helb, H. M., Schmitz-Valckenberg, S., Finger, R. P., Scholl, H. P. N., … Holz, F. G. (2008). High-resolution spectral domain-OCT imaging in geographic atrophy associated with age-related macular degeneration. *Investigative Ophthalmology and Visual Science*, *49*(9), 4137–4144.

Fletcher, D. C., & Schuchard, R. A. (1997). Preferred retinal loci relationship to macular scotomas in a low-vision population. *Ophthalmology*, *104*(4), 632–638.

Fletcher, D. C., Schuchard, R. A, & Renninger, L. W. (2012). Patient awareness of binocular central scotoma in age-related macular degeneration. *Optometry and Vision Science*, *89*(9), 1395–1398.

Fletcher, D. C., Schuchard, R. A., & Gale, W. (1999). Relative locations of macular scotomas near the PRL: Effect on low vision reading. *Journal of Rehabilitation Research and Development*, *36*(4), 356–364.

Forster, K. I. (1970). Visual perception of rapidly presented word sequences of varying complexity. *Perception & Psychophysics*, *8*(4), 215–221.

Fujita, K., & Yuzawa, M. (2003). Preferred retinal locus in patients with age-related macular degeneration. *Nippon Ganka Gakkai Zasshi*, *107*(10), 602–606.

Garvin, M. K., Abràmoff, M. D., Wu, X., Russell, S. R., Burns, T. L., & Sonka, M. (2009). Automated 3-D intraretinal layer segmentation of macular spectral-domain optical coherence tomography images. *IEEE Transactions on Medical Imaging*, *28*(9), 1436–1447.

Geller, A. M., Paul, S. A., & Green, D. G. (1992). Effect on grating identification of sampling with degenerate arrays. *Journal of Optical Soceity of America A*, *9*(3), 472–477.

Goodrich, G.L. (1977). Training eccentric viewing. *Journal of Visual Impairment and Blindness*, *71*(9), 377–381.

Hartmann, K. I., Bartsch, D. U., Cheng, L., Kim, J. S., Gomez, M. L., Klein, H., & Freeman, W. R. (2011). Scanning laser ophthalmoscope imaging stabilized microperimetry in dry age-related macular degeneration. *Retina*, *31*(7), 1323–1331.

Helmholtz, H. (1925). *Helmholtz's Treatise on Physiological Optics.* (J.P.C. Southall, Ed.) *Electronic Edition: 2001 - University of Pennsylvania* (Special Ed, Vol. III). Wisconsin: Optical Soceity of America. Retrieved from URL: http//psych.upenn.edu/backuslab/helmholtz

Hogg, R. E., & Chakravarthy, U. (2006). Visual function and dysfunction in early and late age-related maculopathy. *Progress in Retinal and Eye Research*, *25*(3), 249–276.

Huang, W. C., Cideciyan, A. V., Roman, A. J., Sumaroka, A., Sheplock, R., Schwartz, S. B., … Jacobson, S. G. (2014). Inner and outer retinal changes in retinal degenerations associated with ABCA4 mutations. *Investigative Ophthalmology and Visual Science*, *55*(3), 1810–1822.

Iwama, D., Tsujikawa, A., Ojima, Y., Nakanishi, H., Yamashiro, K., Tamura, H., … Yoshimura, N. (2010). Relationship between retinal sensitivity and morphologic changes in eyes with confluent soft drusen. *Clinical and Experimental Ophthalmology*, *38*(5), 483–488.

Jackson, G. R., Scott, I. U., Kim, I. K., Quillen, D. A., Iannaccone, A., & Edwards, J. G. (2014). Diagnostic sensitivity and specificity of dark adaptometry for detection of age-related macular degeneration. *Investigative Ophthalmology and Visual Science*, *55*(3), 1427–1431.

Jonas, J. B., Budde, W. M., & Panda-Jonas, S. (1999). Ophthalmoscopic evaluation of the optic nerve head. *Survey of Ophthalmology*, *43*(4), 293–320.

Juola, J. F., Ward, N. J., & Mcnamara, T. (1982). Visual search and reading of rapid serial presentations of letter strings , words , and text. *Journal of Experimental Psychology: General*, *111*(2), 208–227.

Kleiner, M., Brainard, D., Pelli, D., Ingling, A., Murray, R., & Broussard, C. (2007). What's new in Psychtoolbox-3 ? *ECVP-30*.

Kleiner, R. C., Enger, C., & Fine, S. L. (1988). Contrast sensitivity in age-related macular degeneration. *Archives of Ophthalmology*, *106*, 55–57.

Kosnik, W., Fikre, J., & Sekuler, R. (1986). Visual fixation stability in older adults. *Investigative Ophthalmology and Visual Science*, *27*(12), 1720–1725.

Krishnan, A., & Bedell, H. E. (2014). Sensitivity around the word-fixation PRL in subjects with central field loss. *Optometry and Vision Science*, *91*, E–Abstract 145066.

Kumar, G., & Chung, S. T. L. (2014). Characteristics of fixational eye movements in people with macular disease. *Investigative Opthalmology and Visual Science*, *55*(8), 5125-5133.

Kwon, M., Nandy, A. S., & Tjan, B. S. (2013). Rapid and persistent adaptability of human oculomotor control in response to simulated central vision loss. *Current Biology*, *23*(17), 1663–1669.

Landa, G., Su, E., Garcia, P. M. T., Seiple, W. H., & Rosen, R. B. (2011). Inner segment-outer segment junctional layer integrity and corresponding retinal sensitivity in dry and wet forms of age-related macular degeneration. *Retina*, *31*(2), 364–370.

Lee, W., Nõupuu, K., Oll, M., Duncker, T., Burke, T., Zernant, J., … Allikmets, R. (2014). The external limiting membrane in early–onset stargardt disease. *Investigative Ophthalmology and Visual Science*, *55*(10), 6139–6149.

Legge, G. E., Ahn, S. J., Klitz, T. S., & Luebker, A. (1997). Psychophysics of reading XVI. The visual span in normal and low vision. *Vision Research*, *37*(14), 1999–2010.

Legge, G. E., & Kersten, D. (1987). Contrast discrimination in peripheral vision. *Journal of the Optical Society of America A*, *4*(8), 1594–1598.

Legge, G. E., Mansfield, J. S., & Chung, S. T. L. (2001). Psychophysics of reading XX. Linking letter recognition to reading speed in central and peripheral vision. *Vision Research*, *41*, 725–743.

Legge, G. E., Ross, J. A., Isenberg, L. M., & LaMay, J. M. (1992). Psychophysics of reading XII. Clinical predictors of low-vision reading speed. *Investigative Ophthalmology and Visual Science*, *33*(3), 677–687.

Legge, G. E., Rubin, G. S., & Luebker, A. (1987). Psychophysics of reading V. The role of contrast in normal vision. *Vision Research*, *27*(7), 1165–1177.

Legge, G. E., Rubin, G. S., Pelli, D. G., & Schleske, M. M. (1985). Psychophysics of reading II. Low vision. *Vision Research*, *25*(2), 253–265.

Levi, D. M. (2008). Crowding—An essential bottleneck for object recognition: A mini-review. *Vision Research*, *48*(5), 635–654.

Levi, D. M., Sharma, V., & Klein, S. A. (1997). Feature integration in pattern perception. *Proceedings of the National Academy of Sciences USA*, *94*(October), 11742–11746.

Lim, L., Mitchell, P., Seddon, J., Holz, F. G., & Wong, T. (2012). Age-related macular degeneration. *Lancet*, *379*, 1728–1738.

Lima, V. C., Prata, T. S., De Moraes, C. G. V, Kim, J., Seiple, W., Rosen, R. B., … Ritch, R. (2010). A comparison between microperimetry and standard achromatic perimetry of the central visual field in eyes with glaucomatous paracentral visual-field defects. *British Journal of Ophthalmology*, *94*(1), 64–67.

Liu, L., & White, J. (2010). Early age-related macular degeneration impairs tolerance to stimulus degradation. *Optometry and Vision Science*, *87*(8), 532–542.

Loftus, G., Kaufman, L., Nishimoto, T., & Ruthruff, E. (1992). *Eye Movements and Visual Cognition: Effects of visual degradation on eye-fixation duration, perceptual processing and long-term visual memory*. (K. Rayner, Ed.). New York: Springer NY.

Longhin, E., Convento, E., Pilotto, E., Bonin, G., Vujosevic, S., Kotsafti, O., & Midena, E. (2013). Static and dynamic retinal fixation stability in microperimetry. *Canadian Journal of Ophthalmology*, *48*(5), 375–380.

Macedo, A. F., Crossland, M. D., & Rubin, G. S. (2011). Investigating unstable fixation in patients with macular disease. *Investigative Ophthalmology and Visual Science*, *52*(3), 1275–1280.

Maia-lopes, S., Silva, E. D., Fa, M., Reis, A., Faria, P., & Castelo-branco, M. (2008). Evidence of widespread retinal dysfunction in patients with stargardt disease and morphologically unaffected carrier relatives. *Investigative Ophthalmology and Visual Science*, *49*(3), 1191–1199.

Mansfield, J. S., Legge, G. E., Luebker, A., & Cunningham, K. (1994). *MNREAD Acuity Charts. Minnesota Laboratory for Low-Vision Reserarch*. Minneapolis: Lighthouse Low Vision Products. Retrieved from http://gandalf.psych.umn.edu/groups/gellab/MNREAD/mnread.pdf

Martinez-Conde, S., Macknik, S. L., & Hubel, D. H. (2004). The role of fixational eye movements in visual perception. *Nature Reviews Neuroscience*, *5*(3), 229–240.

Mcculloch, D. L., Loffler, G., Colquhoun, K., Bruce, N., Dutton, G. N., & Bach, M. (2011). The effects of visual degradation on face discrimination. *Ophthalmic and Physiological Optics*, *31*(3), 240–248.

McMahon, T., Hansen, M., & Viana, M. (1991). Fixation characteristics in macular disease. *Investigative Ophthalmology and Visual Science*, *32*(3), 567–574.

Midena, E., Radin, P. P., & Convento, E. (2006). *Perimetry and the Fundus: An Intoduction to Microperimetry.* (E. Midena, Ed.) (First). SLACK.

Midena, E., Vujosevic, S., & Cavarzeran, F. (2010). Normal values for fundus perimetry with the microperimeter MP1. *Ophthalmology*, *117*(8), 1571–1576.

Midena, E., Vujosevic, S., Convento, E., Manfre, A., Cavarzeran, F., & Pilotto, E. (2007). Microperimetry and fundus autofluorescence in patients with early age-related macular degeneration. *British Journal of Ophthalmology*, *91*(11), 1499–1503.

NIDEK Technologies. (2010). *Microperimeter MP1: Operator's Manual*. *NIDEK* (Vol. 27.2.0). Italy: NIDEK Technologies Srl.

NIH/NEI. Age related macular degeneration. Retrieved January 1, 2016, from https://nei.nih.gov/eyedata/amd

Ortiz, C., Jiménez, J. R., Pérez-ocón, F., & Castro, J. J. (2010). Retinal-image quality and contrast-sensitivity function in age-related macular degeneration. *Current Eye Research*, *35*(8), 757–761.

Owsley, C., Jackson, G. R., Cideciyan, A. V., Huang, Y., Fine, S. L., Ho, A. C., … Jacobson, S. G. (2000). Psychophysical evidence for rod vulnerability in age-related macular degeneration. *Investigative Ophthalmology and Visual Science*, *41*(1), 267–273.

Parodi, M. B., Iacono, P., Triolo, G., La Spina, C., Zucchiatti, I., Cicinelli, M. V., … Bandello, F. (2015). Morpho-functional correlation of fundus autofluorescence in Stargardt disease. The *British Journal of Ophthalmology*, 99, 1354-1359.

Pascolini, D., & Mariotti, S. P. (2011). Global estimates of visual impairment: 2010. *The British Journal of Ophthalmology*, *96*(5), 614–618.

Pelli, D. G., & Robson, J. G. (1988). The design of a new letter chart for measuring contrast sensitivity. *Clinical Vision Science*, *2*(3), 187–199.

Pelli, D. G., Tillman, K. A., Freeman, J., Su, M., Berger, T. D., & Majaj, N. J. (2007). Crowding and eccentricity determine reading rate. *Journal of Vision*, *7*(2), 20.1–36.

Plank, T., Rosengarth, K., Schmalhofer, C., Goldhacker, M., Brandl-Ruhle, S., & Greenlee, M. W. (2014). Perceptual learning in patients with macular degeneration. *Frontiers in Psychology*, *5*(OCT), 1–14.

Pratt, J. D., Ohara, J., Woo, S., & Bedell, H. E. (2014). Fixation locus in patients with bilateral central scotomas for targets that peceptually fill in. *Optometry and Vision Science*, *91*(3), 312–321.

Rayner, K. (1975). The perceptual span and peripheral cues in reading. *Cognitive Psychology*, *7*, 65–81.

Rayner, K., & Bertera, J. H. (1979). Reading without a fovea. *Science*, *206* (4417), 468–469.

Rayner, K., Pollatsek, A., & Schotter, E. R. (2012). *Word Identification and Eye Movements*. (A. F. Healy, R. W. Proctor, & Weiner Irving B, Eds.) (Second). Hoboken, New Jersey: John Wiley & Sons Inc.

Regan, D., & Neima, D. (1983). Low-contrast letter charts as a test of visual function. *Ophthalmology*, *90*(10), 1192–1200.

Reinhard, J., Messias, A., Dietz, K., MacKeben, M., Lakmann, R., Scholl, H. P. N., … Trauzettel-Klosinski, S. (2007). Quantifying fixation in patients with Stargardt disease. *Vision Research*, *47*(15), 2076–2085.

Richter-Mueksch, S., Vécsei-Marlovits, P. V, Sacu, S. G., Kiss, C. G., Weingessel, B., & Schmidt-Erfurth, U. (2007). Functional macular mapping in patients with vitreomacular pathologic features before and after surgery. *American Journal of Ophthalmology*, *144*(1), 23–31.

Rogala, J., Zangerl, B., Assaad, N., Fletcher, E. L., Kalloniatis, M., & Nivison-Smith, L. (2015). In vivo quantification of retinal changes associated with drusen in age-related macular degeneration. *Investigative Ophthalmology and Visual Science*, *2014*, 36–38.

Rohrschneider, K. (2004). Determination of the location of the fovea on the fundus. *Investigative Ophthalmology and Visual Science*, *45*(9), 3257–3258.

Rohrschneider, K. (2007). *Essentials in Ophthalmology: Medical Retina*. (F. G. Holz & R. F. Spaide, Eds.). Springer Berlin Heidelberg.

Rohrschneider, K., Bültmann, S., Springer, C., Youssri, A. I., Miller, J. W., Xiao, Q., … Lihua, Y. (2008). Use of fundus perimetry (microperimetry) to quantify macular sensitivity. *Progress in Retinal and Eye Research*, *27*(5), 536–548.

Rohrschneider, K., Springer, C., Bültmann, S., & Völcker, H. E. (2005). Microperimetry-Comparison between the micro perimeter 1 and scanning laser ophthalmoscope-fundus perimetry. *American Journal of Ophthalmology*, *139*(1), 125–134.

Rubin, G. S., & Legge, G. E. (1989). Psychophysics of reading VI. The role of contrast in low vision. *Vision Research*, *29*(1), 79–91.

Rubin, G. S., & Turano, K. (1994). Low vision reading with sequential word presentation. *Vision Research*, *34*(13), 1723–1733.

Sansbury, R., Skavenski, A., Haddad, G., & Steinman, R. (1973). Normal fixation of eccentric targets. *Journal of the Optical Soceity of America*, *63*(5), 612–614.

Scherlen, A., Bernard, J., Calabrese, A., & Castet, E. (2008). Page mode reading with simulated scotomas : Oculo-motor patterns. *Vision Research*, *48*, 1870–1878.

Schuchard, R. A., Naseer, S., & De Castro, K. (1999). Characteristics of AMD patients with low vision receiving visual rehabilitation. *International Journal of Conflict Management*, *36*(4), 294–302.

Schuman, S. G., Koreishi, A. F., Farsiu, S., Jung, S., Izatt, J. A., & Toth, C. A. (2009). Photoreceptor layer thinning over drusen in eyes with age-related macular degeneration imaged in vivo with spectral-domain optical coherence tomography. *Ophthalmology*, *116*(3), 488–496.

Scullica, L., & Falsini, B. (2001). Diagnosis and classification of macular degenerations: An approach based on retinal function testing. *Documenta Ophthalmologica*, *102*(3), 237–250.

Seiple, W., Holopigian, K., Szlyk, J. P., & Greenstein, V. C. (1995). The effects of random element loss on letter identification: Implications for visual acuity loss in patients with retinitis pigmentosa. *Vision Research*, *35*(14), 2057–2066.

Seiple, W., Rosen, R. B., Castro-Lima, V., & Garcia, P. (2012). The physics and psychophysics of microperimetry. *Optometry and Vision Science*, *89*(8), 1182–1191.

Seiple, W., Rosen, R. B., & Garcia, P. M. T. (2013). Abnormal fixation in individuals with age-related macular degeneration when viewing an image of a face. *Optometry and Vision Science*, *90*(1), 45–56.

Shima, N., Markowitz, S. N., & Reyes, S. V. (2010). Concept of a functional retinal locus in age-related macular degeneration. *Canadian Journal of Ophthalmology*, *45*(1), 62–66.

Smith, R. T., Chan, J. K., Busuoic, M., Sivagnanave, V., Bird, A. C., & Chong, N. V. (2006). Autofluorescence characteristics of early, atrophic, and high-risk fellow eyes in age-related macular degeneration. *Investigative Ophthalmology and Visual Science*, *47*(12), 5495–5504.

Smith, W., Assink, J., Klien, R., Mitchell, P., Klaver, C., Klien, B., & de Jong, P. T. V. M. (2001). Risk factors for age-related macular degeneration. *Ophthalmology*, *108*(4), 697–704.

Sperling, G. (1960). The information available in brief visual presentations. *Psychological Monographs*, *74*(11), 1–29.

Springer, C., Bültmann, S., Völcker, H. E., & Rohrschneider, K. (2005). Fundus perimetry with the Micro Perimeter 1 in normal individuals: Comparison with conventional threshold perimetry. *Ophthalmology*, *112*(5), 848–854.

Steinman, R. M. (1965). Effect of target size, luminance, and color on monocular fixation. *Journal of the Optical Society of America*, *55*(9), 1158-1165.

Sullivan, B., Jovancevic-misic, J., Hayhoe, M., & Sterns, G. (2008). Use of multiple preferred retinal loci in Stargardt's disease during natural tasks: A case study. *Ophthalmic and Physiological Optics*, *28*(2), 168–177.

Sulzbacher, F., Kiss, C., Kaider, A., Eisenkoelbl, S., Munk, M., Roberts, P., … Schmidt-Erfurth, U. (2012). Correlation of SD-OCT features and retinal sensitivity in neovascular age-related macular degeneration. *Investigative Ophthalmology and Visual Science*, *53*(10), 6448–6455.

Sunness, J. S., Applegate, C. A., Haselwood, D., & Rubin, G. S. (1996). Fixation patterns and reading rates in eyes with central scotomas from advanced atrophic age-related macular degeneration and Stargardt disease. *Ophthalmology*, *103*(9), 1458–1466.

Sunness, J. S., & Steiner, J. N. (2008). Retinal function and loss of autofluorescence in stargardt disease. *Retina*, *28(6)*, 794–800.

Taylor, S. E. (1965). Eye Movements in Reading : Facts and Fallacies Published by : American Educational Research Association Stable URL : http://www.jstor.org/stable/1161646. *American Educational Research Journal*, *2*(4), 187–202.

Thaler, L., Schütz, A. C., Goodale, M. A., & Gegenfurtner, K. R. (2013). What is the best fixation target? The effect of target shape on stability of fixational eye movements. *Vision Research*, *76 (2013)*, 31–42.

Thomas, M. G., Gottlob, I., McLean, R. J., Maconachie, G., Kumar, A., & Proudlock, F. A. (2011). Reading strategies in infantile nystagmus syndrome. *Investigative Ophthalmology and Visual Science*, *52*(11), 8156–8165.

Timberlake, G. T., Mainster, M. A., Peli, E., Augliere, R. A., Essock, E. A., & Arend, L. E. (1986). Reading with a macular scotoma. I. Retinal location of scotoma and fixation area. *Investigative Ophthalmology and Visual Science*, *27*(7), 1137–1147.

Timberlake, G. T., Mainster, M. A., Webb, R. H., Hughes, G. W., & Trempe, C. L. (1982). Retinal localization of scotomata by scanning laser ophthalmoscopy. *Investigative Ophthalmology and Visual Science*, *22*(1), 91–97.

Timberlake, G. T., Sharma, M. K., Grose, S. A, Gobert, D. V, Gauch, J. M., & Maino, J. H. (2005). Retinal location of the preferred retinal locus relative to the fovea in scanning laser ophthalmoscope images. *Optometry and Vision Science* , *82*(3), 177–185.

Timberlake, G, & Ward, W. (2013). Optical attachment for binocular imaging with the Scanning Laser Ophthalmoscope (SLO) (abstract). *Investigative Ophthalmology and Visual Science*, *54*(15), 2182.

Trauzettel-Klosinski, S. (2011). *Rehabilitative techniques*. (C. Kennard & R.J. Leigh, Eds.) *Handbook of Clinical Neurology* (1st ed., Vol. 102). Elsevier B.V.

Von Noorden, G., & Mackensen, G. (1962). Phenomenology of eccentric fixation. *American Journal of Ophthalmology*, *53*(4), 642-660.

Vujosevic, S., Midena, E., Pilotto, E., Radin, P. P., Chiesa, L., & Cavarzeran, F. (2006). Diabetic macular edema: Correlation between microperimetry and optical coherence tomography findings. *Investigative Ophthalmology and Visual Science*, *47*(7), 3044–3051.

Vukicevic, M., Le, A., & Baglin, J. (2010). A simplified method identifying the trained retinal locus for training in eccentric viewing. *Journal of Visual Impairment and Blindness*, *90*(9), 555–561.

Walsh, D. V, & Liu, L. (2014). Adaptation to a simulated central scotoma during visual search training. *Vision Research*, *96*, 75–86.

Wang, Y., Wilson, E., Locke, K. G., & Edwards, A. O. (2002). Shape discrimination in age-related macular degeneration. *Investigative Ophthalmology and Visual Science*, *43*(6), 2055–2062.

White, J. M., & Bedell, H. E. (1990). The oculomotor reference in humans with bilateral macular disease. *Investigative Ophthalmology and Visual Science*, *31*(6), 1149–1161.

Whittaker, S. G., Budd, J., & Cummings, R. W. (1988). Eccentric fixation with macular scotoma. *Investigative Ophthalmology and Visual Science*, *29*(2), 268–278.

Wiecek, E. K., Jackson, M. Lou, & Bex, P. J. (2015). Binocular microperimetry with simulated asymmetric bilateral scotomas (abstract). *Investigative Ophthalmology and Visual Science*, *56*(7), 549.

Winther, C., & Frisen, L. (2015). New rarebit vision test captures macular deficits hidden to acuity tests. *Acta Ophthalmologica*, *93*, 481–485.

Woo, S., & Bedell, H. E. (2006). Beating the beat: Reading can be faster than the frequency of eye movements in persons with congenital nystagmus. *Optometry and Vision Science*, *83*(8), 559–571.

Woods, R. L., Vera-Diaz, F. A., Lichtenstein, L., & Peli, E. (2007). Spatial alignment of microperimeters (abstract). *Investigative Ophthalmology and Visual Science*, *48*(5), 144.

Yang, G., Stewart, C. V., Sofka, M., & Tsai, C. L. (2007). Registration of challenging image pairs: Initialization, estimation, and decision. *IEEE Transactions on Pattern Analysis and Machine Intelligence*, *29*(11), 1973–1989.

Yarbus, A. L. (1967). *Eye movements and vision*. (B. Haigh & L. Riggs, Eds.) *Academy of Sciences of the USSR*. New York: Plenum Press.

Yehoshua, Z., & Rosenfeld, P. J. (2012). Strategies for following dry age-related macular degeneration. *Ophthalmic Research*, *48* (SUPPL. 1), 6–10.

Yu, D., Cheung, S., Legge, G. E., & Chung, S. T. L. (2007). Effect of letter spacing on visual span and reading speed. *Journal of Vision*, *7*(2), 1–10.